

Multichannel Near Infrared Spectroscopy to
monitor cerebral oxygenation in infants and
children supported in extracorporeal membrane
oxygenation (ECMO)

Maria D. Papademetriou

A thesis submitted to
University College London
for the degree of
Doctor of Philosophy

Supervised by
Professor Clare E. Elwell
Dr. Ilias Tachtsidis

Department of Medical Physics and Bioengineering
University College London

2011

Declaration

I, Maria D. Papademetriou, declare that the work presented in this thesis is my own, and where information has been derived from other sources, those sources are credited.

Abstract

Extracorporeal membrane oxygenation is a life support system for infants and children with intractable cardiorespiratory failure. The risk for developing neurological injuries in this group of patients is considerable. The causes are multifactorial and are not yet fully understood. Induction of ECMO involves ligation of the major neck vessels – common carotid artery and internal jugular vein – which may cause lateralised cerebrovascular injury. Physiologic changes such as hypoxia, hypotension and hypercarbia associated with ECMO can disrupt cerebral autoregulation.

Near infrared spectroscopy (NIRS) offers the advantage of continuous non invasive means of monitoring cerebral oxygenation at the bedside. To date, NIRS systems used clinically are single or dual channel systems and do not allow evaluation of the status of cerebral circulation in the extended cerebral regions.

This work involves the development of a multichannel NIRS system for use in paediatric cardiothoracic intensive care with specific application on patients supported on extracorporeal circulation. A novel flexible neonatal cap was designed and constructed to accommodate an array of sources and detectors that provide measurements of multisite cerebral oxygenation from 12 channels. Multimodal data collection (systemic and ECMO circuit parameters) simultaneous with multichannel NIRS was established to allow monitoring of multisite cerebral oxygenation and haemodynamics.

A novel method of analysis, wavelet cross-correlation, was generated to study the concordance between multisite oxyhaemoglobin concentration (HbO_2) and mean arterial pressure (MAP) as a means to investigate regional variations in cerebral circulation and assess cerebral autoregulation. Group data of 6 patients showed statistically significant differences in WCC between right and left hemispheres during sequential changes in ECMO circuit blood flow. WCC between HbO_2 and MAP provides a useful method to investigate the dynamics of cerebral autoregulation during ECMO. Modest manipulations of ECMO flows are associated with regional changes in cerebral autoregulation which may potentially have an important bearing on clinical outcome.

Acknowledgements

First I would like to thank my supervisor Prof Clare Elwell. Her guidance and support throughout the past years have been nothing but inspirational. I feel privileged to have her as a supervisor and be part of her high standard multidisciplinary academic group. I feel lucky to know her as a person as she is an extraordinary personality. I am particularly grateful for her constant encouragement and strength during the process of writing this thesis.

Special thanks go to Dr Ilias Tachtsidis for sharing his valuable knowledge and expertise in the field. I am grateful for his long enlightening and constructive discussions; discussions, which generated interesting ideas some of which were implemented in this work. I appreciate that fact that he was always available when needed.

I am indebted to Dr Aparna Hoskote for her important role as my clinical supervisor. Her contribution is highly recognised and appreciated. I would also like to thank Prof Martin Elliott for sharing his knowledge on the clinical aspects of the project and for his help in initiating the project. I would also like to express my gratitude to the ECMO coordinators, ECMO nurses, and to the consultants in Cardiac Intensive Care Unit of Great Ormond Street Hospital. Special thanks go to Dr Timothy Thiruchelvam for willingly acting as a deputy when Dr Hoskote was not in the unit.

Many thanks to Dr Atsushi Maki for acting as the project coordinator between Hitachi Medical Ltd and UCL and for his great hospitality when visiting the Hitachi's headquarters in Japan. Thanks to Dr Hirabayashi for exchanging ideas on the neonatal cap design and optical holders.

Special thanks to Dr Marina Hughes for providing the MRI scans. I would also like to thank Glaudio Capelli and Giovanni Biglino for producing the 3D

reconstructions of the scans and Martin Watmough for providing the rapid prototyping of the dummy heads.

I am grateful to my colleagues Dr Terence Leung, Dr Anna Blasi, Dr Murad Banaji for exchanging knowledge at different stages and different aspects of the project.

I would like acknowledge and thank Panayiota Ellina for sharing her expertise in photoshop.

Finally I would like to thank my beloved parents, Ermioni and Demetris for their endless love, affection, emotional support, their constant encouragement and for always acting as a safety net.

Last but not least I am truly indebted to my beautiful sister Sophia for all her help, all the effort, the support, for always being there for me. She is truly exceptional and it is through her that I gained the strength needed to complete this thesis.

This work has been supported by Hitachi Medical Ltd.

Table of Contents

ABSTRACT	3
ACKNOWLEDGEMENTS	4
TABLE OF CONTENTS	7
LIST OF FIGURES	13
LIST OF TABLES	19
LIST OF ACRONYMS	21
Chapter 1	25
INTRODUCTION	25
1.1 Motivation and objectives.....	25
1.2 Thesis Overview.....	26
Chapter 2	29
BASIC HUMAN ANATOMY AND PHYSIOLOGY	29
2.1 Blood circulation in healthy humans.....	29
2.1.1 Functional anatomy of the heart.....	29
2.1.2 Arterial blood pressure.....	31
2.1.3 Oxygen transport to tissue.....	33
2.1.4 Neonatal circulation.....	36
2.1.4.1 Fetal circulation.....	36
2.1.4.2 Fetal Hemoglobin.....	37
2.1.4.3 Circulatory changes at birth.....	38
2.2 Cerebral Circulation	39
2.2.1 Basic anatomy of the human brain.....	41
2.2.2 Cerebral Blood Flow (CBF).....	43
2.2.2.1 Cerebral Autoregulation.....	44

2.2.2.2 Blood gases and cerebral blood flow	46
2.2.3 Cerebral haemodynamic oscillations.....	47
Chapter 3	51
NEAR INFRARED SPECTROSCOPY: THEORY AND INSTRUMENTATION.....	51
3.1 Light propagation in tissue.....	51
3.1.1 Light Absorption	52
3.1.2 Absorbing compounds in tissue.....	54
3.1.3 Light Scattering	57
3.1.4 Models of light transport in tissue	59
3.1.5 The modified Beer-Lambert Law	61
3.2 Types of instrumentation	64
3.2.1 Continuous wave systems	65
3.2.2 Time-domain systems.....	65
3.2.3 Frequency Domain systems	66
3.2.4 Dual-Channel near infrared spectrometer NIRO 200.....	66
3.2.4.1 Spatially Resolved Spectroscopy	67
3.2.4.2 Tissue Oxygenation Index (TOI).....	69
3.2.5 Multichannel Optical topography ETG-100	70
3.2.5.1 Other multichannel optical systems.....	72
Chapter 4	75
EXTRACORPOREAL CIRCULATION IN INFANTS AND CHILDREN	75
4.1 Extracorporeal membrane oxygenation (ECMO)	75
4.1.1 The ECMO circuit.....	76
4.1.2 Physiology of ECMO.....	77
4.1.2.1 Cannulation	77
4.1.2.2 Oxygen delivery in ECMO	78
4.1.2.3 Blood flow and oxygenation.....	78
4.1.2.4 Pulsatility in blood flow.....	80
4.1.2.5 Weaning from ECMO.....	81
4.2 Cardiopulmonary bypass for repair of congenital heart defects.....	81
4.2.1 Congenital cardiovascular Defects	82
4.2.1.2 Hypothermia.....	83

4.3 Neurological morbidity on ECMO	85
4.4 Neurological monitoring on extracorporeal circulation	88
4.4.1 Electroencephalographic monitoring	88
4.4.2 Transcranial Doppler	89
4.4.3 Near infrared spectroscopy.....	90
4.4.3.1 Near Infrared Spectroscopy on ECMO patients.....	91
4.4.3.2 NIRS in neonates with congenital heart diseases.....	93
4.4.3.3 Concluding Remarks	94
Chapter 5	116
CEREBRAL AND PERIPHERAL OXYGENATION IN CHILDREN SUPPORTED ON ECMO FOR CARDIO-RESPIRATORY FAILURE	116
5.1 Introduction	116
5.2 Protocol	118
5.3 Instrumentation	119
5.4 Subjects.....	122
5.5 Cerebral and Peripheral tissue oxygenation during various ECMO phases	124
5.5.1 Cannulation	124
5.5.2 Weaning	125
5.5.3 CO ₂ challenge	126
5.5.4 Temperature challenge.....	126
5.6 Spectral Analysis	132
5.6.1 Power spectral density.....	132
5.6.1.1 Methods	132
5.6.1.2 Results	132
5.6.2 Coherence.....	140
5.6.2.1 Methods	140
5.6.2.2 Results	140
5.7 Discussion.....	143
Chapter 6	148
MULTICHANNEL NEAR INFRARED SPECTROSCOPY TO MEASURE REGIONAL CEREBRAL OXYGENATION IN INFANTS AND CHILDREN SUPPORTED ON ECM..	148
6.1 Introduction	148

6.2 Methods.....	149
6.2.1 Instrumentation	149
6.2.2 Neonatal cap design and construction	151
6.2.3 Protocol	156
6.2.4 Patients	156
6.2.3 Data rejection	156
6.2.4 Data analysis.....	157
6.3 Results	157
6.3.1 Flow changes	160
6.3.2 Weaning	163
6.4 Discussion and Conclusions.....	178
Chapter 7	180
WAVELET CROSS-CORRELATION TO INVESTIGATE REGIONAL VARIATION IN CEREBRAL OXYGENATION IN INFANTS SUPPORTED ON ECMO.....	180
7.1 Introduction	180
7.2 Methods.....	185
7.2.1 Subjects	185
7.2.2 Instrumentation	186
7.2.3 Data Analysis	188
7.3 Results	193
7.3.1 Wavelet cross-correlation (WCC)	193
7.3.1.1 Alterations in the ECMO flows.....	193
7.3.1.2 Weaning	199
7.3.2 Synchronisation index (γ)	203
7.3.2.1 Alteration in ECMO flows.....	203
7.3.2.2 Weaning	208
7.4 Discussion.....	212
7.5 Conclusions.....	215
Chapter 8	215
CONCLUSIONS AND FURTHER WORK	215
8.1 Introduction	215
8.2 Summary and Concluding work of this thesis	216

8.3 Further work.....	220
REFERENCES.....	223

List of Figures

Figure 2.1: The cross section of a human heart.....	30
Figure 2.2: Description of the phases constituting a cardiac cycle.....	31
Figure 2.3: Pressure waves at different sites in the arterial tree.....	32
Figure 2.4: Average values and normal ranges for systolic and diastolic arterial blood pressure according to birth weight in newborn infants.....	33
Figure 2.5: Oxygen dissociation curve.....	34
Figure 2.6: The influence of pH, pCO ₂ and temperature on the oxygen dissociation curve.....	35
Figure 2.7: Fetal circulation.....	38
Figure 2.8: Arteries of the neck and head	40
Figure 2.9: Origins of the blood vessels that form the arterial circle.....	40
Figure 2.10: Major veins of the head	41
Figure 2.11: Divisions of the brain	42
Figure 2.12: Lobes of the brain	42
Figure 2.13: Coverings of the brain	42
Figure 2.14: The skull of a term neonate.	43
Figure 2.15: Head circumference charts for girls and boys from birth to 18 years...43	
Figure 2.16: The cerebral autoregulation curve.	45
Figure 2.17: Effect of pCO ₂ (left) and pO ₂ (right) on cerebral blood flow.....	46
Figure 2.18: An example measurement showing the existence of systemic influence on the ΔHbO_2 signal.....	48
Figure 3.1: Light absorption in a non scattering medium.....	52
Figure 3.2: Absorption spectrum of pure water.	54
Figure 3.3: Spectrum of pork fat in the NIR	55
Figure 3.4: Specific absorption spectra of HbO ₂ and HHb in the NIR.....	56

Figure 3.5: The difference absorption spectrum between the oxidised and reduced forms of cytochrome oxidase.	56
Figure 3.6: Attenuation of light through a scattering medium.	57
Figure 3.7: Schematic illustrating the scattering phase function $f(\hat{s}, \hat{s}')$	58
Figure 3.8: Predicted relationship of attenuation as a function of absorption coefficient.	63
Figure 3.9: Types of measurements techniques used in near infrared spectroscopy systems	64
Figure 3.10: NIRO-200 probe schematic.	67
Figure 3.11: Schematic diagram of the lock in amplifier system used in the Hitachi ETG-100 system	71
Figure 3.12: ETG-100 OT 3x3 configuration for bilateral monitoring.	72
Figure 4.1: Illustration of the ECMO circuit.	77
Figure 4.2: Haemodynamics and gas exchange changes during VA ECMO.	79
Figure 4.3: Haemodynamics and gas exchange changes during VV ECMO.	80
Figure 4.4: Whole body oxygen Consumption as a function of temperature	84
Figure 5.1: Schematic diagram of the instrumentation used when monitoring using the dual-channel NIRO-200 system.	120
Figure 5.2: Illustrating the sequence followed for obtaining simultaneous collection of systemic, ECMO parameters and with optical parameters from the dual-channel NIRS system NIRO-200.	121
Figure 5.3: HbO ₂ (red), HHb (blue), HbT (black) and TOI (green) data for the brain and leg of patient D4 monitored during cannulation	127
Figure 5.4: HbO ₂ (red), HHb (blue), HbT (black) and TOI (green) data for the brain and leg of patient D1 monitored during reduction in ECMO circuit flows	128
Figure 5.5: HbO ₂ (red), HHb (blue), HbT (black) and TOI (green) in the brain and leg of patient D1 monitored during ECMO “trial off” period.	129
Figure 5.6: HbO ₂ (red), HHb (blue), HbT (black) and TOI (green) data for the brain and leg of patient D8 during changes in pCO ₂	129
Figure 5.7: HbO ₂ (red), HHb (blue), HbT (black) and TOI (green) data for the brain and leg of VA ECMO patient D8 during changes in temperature	131
Figure 5.8: PSDs in the brain (blue) and leg (pink) of patient D1	135

Figure 5.9: (a) HbO ₂ data in the brain and leg for patient D4 monitored during reductions in the ECMO flows. (b) Corresponding PSDs in the brain (blue) and leg (pink).....	136
Figure 5.10: (a) HbO ₂ data in the brain and leg for patient D3. (b) Corresponding PSDs in the brain (blue) and leg (pink).....	137
Figure 5.11: (a) HbO ₂ data in the brain and leg for patient D5. (b) Corresponding PSDs in the brain (blue) and leg (pink).....	137
Figure 5.12: (a) HbO ₂ data in the brain and leg for patient D6. (b) Corresponding PSDs in the brain (blue) and leg (pink).....	138
Figure 5.13: PSDs in the brain (blue) and leg (pink) of patient D7.....	138
Figure 5.14: PSDs in the brain (blue) and leg (pink) of patient D2.....	138
Figure 5.15: Power ratio as a function of ECMO flow in the brain and leg for the 7 ECMO patients monitored during ECMO flow changes	139
Figure 5.16: Comparison between the strength of oscillations in the brain and leg.....	139
Figure 5.17: Temporal variation in cerebral HbD and peripheral HbD along with MAP for patient D8.....	141
Figure 5.18: Coherence function between cerebral HbD and MAP for patient D8 at initial 100% ECMO flow.....	142
Figure 6.1: Illustrating the sequence followed for obtaining simultaneous collection of systemic, ECMO parameters and with optical parameters collected with ETG-100.....	151
Figure 6.2: Source (S) – Detector (D) configuration used allowing measurements of haemoglobin concentration to be obtained from a total of 12 channels.....	152
Figure 6.3: The neonatal optical fibres and holders.....	153
Figure 6.4: 3D reconstructions of MRI scans from the radiology archives of GOS Hospital.....	152
Figure 6.5: ETG-100 neonatal cap on a dummy head.....	154
Figure 6.6: The neonatal cap in use.....	155
Figure 6.7: Multisite brain oxygenation and haemodynamics of Patient 4 during flow changes.....	164
Figure 6.8: Mean absolute changes in haemoglobin concentrations across the 12-channels and systemic parameters for Patient 4	165

Figure 6.9: Multisite brain oxygenation and haemodynamics of Patient 5 during flow changes.....	166
Figure 6.10: Mean absolute changes in haemoglobin concentrations across the 12-channels and systemic parameters for Patient 5	167
Figure 6.11: Multisite brain oxygenation and haemodynamics of Patient 6 during flow changes.....	168
Figure 6.12: Mean absolute changes in haemoglobin concentrations across the 12-channels and systemic parameters Patient 6	169
Figure 6.13: Multisite brain oxygenation and haemodynamics of Patient 7 during flow changes.....	170
Figure 6.14: Mean absolute changes in haemoglobin concentrations across the 12-channels and systemic parameters for Patient 7	171
Figure 6.15: Multisite brain oxygenation and haemodynamics of Patient 8 during flow changes.....	172
Figure 6.16: Mean absolute changes in haemoglobin concentrations across the 12-channels and systemic parameters Patient 8	173
Figure 6.17: Multisite brain oxygenation and haemodynamics of Patient 10 during flow changes.....	174
Figure 6.18: Mean absolute changes in haemoglobin concentrations across the 12-channels and systemic parameters for Patient 10	175
Figure 6.19: Multisite brain oxygenation and haemodynamics of Patient 9 during weaning	176
Figure 6.20: Mean absolute changes in haemoglobin concentrations across the 12-channels and systemic parameters between showing the effect of clamping the cannulae for Patient 9 during weaning	177
Figure 7.1: Schematic diagram showing the sequence followed during alterations in the ECMO flows.....	185
Figure 7.2: (a) Real and Imaginary part of the Morlet wavelet (b) the Morlet Wavelet with dilations, contraction and translations.....	189
Figure 7.3: Wavelet cross-correlation and synchronisation index between signals with the same frequency content (signals 1 &2), same frequency content but out of phase (signals 1 & 3), and signals with different frequency content (signals 1 & 4).	191

Figure 7.4: Wavelet cross-correlation between MAP and HbO ₂ for two ECMO patients.	193
Figure 7.5: Group wavelet cross-correlation between MAP and HbO ₂ within scale band $a_i = 5 < a < 20$ ($f_{ai} = 0.25 \text{ Hz} < f_a < 1 \text{ Hz}$)	1975
Figure 7.6: Group wavelet cross-correlation between MAP and HbO ₂ within scale band $a_{ii} = 20 < a < 40$ ($f_{a_{ii}} = 0.13 \text{ Hz} < f_a < 0.25 \text{ Hz}$).....	197
Figure 7.7: Group wavelet cross-correlation between MAP and HbO ₂ within scale band $a_{iii} = 20 < a < 40$ ($f_{a_{iii}} = 0.06 \text{ Hz} < f_a < 0.13 \text{ Hz}$)	198
Figure 7.8: Wavelet cross-correlation between MAP and HbO ₂ within scale band $a_i = 5 < a < 20$ ($f_{ai} = 0.25 \text{ Hz} < f_a < 1 \text{ Hz}$) for patient 9 during weaning	200
Figure 7.9: Wavelet cross-correlation between MAP and HbO ₂ within scale band $a_{ii} = 20 < a < 40$ ($f_{a_{ii}} = 0.13 \text{ Hz} < f_a < 0.25 \text{ Hz}$) for patient 9 during weaning	201
Figure 7.10: Wavelet cross-correlation between MAP and HbO ₂ within scale band $a_{iii} = 40 < a < 80$ ($f_{a_{iii}} = 0.06 \text{ Hz} < f_a < 0.13 \text{ Hz}$) for patient 9 during weaning.....	202
Figure 7.11: Synchronisation index, γ , as a function of scale at baseline and minimum flows.	203
Figure 7.12: Group synchronisation index, γ , between MAP and HbO ₂ within scale band $a_i = 5 < a < 20$ ($f_{ai} = 0.25 \text{ Hz} < f_a < 1.0 \text{ Hz}$).	205
Figure 7.13: Group synchronisation index, γ , between MAP and HbO ₂ within scale band $a_{ii} = 20 < a < 40$ ($f_{ai} = 0.13 \text{ Hz} < f_a < 0.25 \text{ Hz}$).....	206
Figure 7.14: Group synchronisation index, γ , between MAP and HbO ₂ within scale band $a_{iii} = 40 < a < 80$ ($f_{ai} = 0.06 \text{ Hz} < f_a < 0.13 \text{ Hz}$).....	207
Figure 7.15: Synchronisation index between MAP and HbO ₂ within scale band $a_i = 5 < a < 20$ ($f_{ai} = 0.25 \text{ Hz} < f_a < 1 \text{ Hz}$) for patient 9 during weaning	209
Figure 7.16: Synchronisation index between MAP and HbO ₂ within scale band $a_{ii} = 20 < a < 40$ ($f_{a_{ii}} = 0.13 \text{ Hz} < f_a < 0.25 \text{ Hz}$) for patient 9 during weaning.....	210
Figure 7.17: Synchronisation index between MAP and HbO ₂ within scale band $a_{iii} = 40 < a < 80$ ($f_{a_{iii}} = 0.06 \text{ Hz} < f_a < 0.13 \text{ Hz}$) for patient 9 during weaning	211

List of Tables

Table 2.1: Respiration rate and heart rate in infants and children.	48
Table 3.1: List of main commercially available CW single or dual channel near infrared spectroscopy systems.....	67
Table 3.2: List of main multichannel optical systems.....	74
Table 4.1: NIRS monitoring in patients with congenital heart diseases.....	96
Table 4.2: NIRS monitoring in ECMO patients.....	110
Table 5.1: List of ECMO patients monitored using the dual channel NIRO-200 system.....	123
Table 5.2: COH scores for patient D8.....	142
Table 5.3: Oscillations in the ECMO patients monitored with the dual-channel system.....	143
Table 6.1: Demographics of ECMO patients included in the multichannel NIRS study.	158
Table 6.2: List of patients included in the multichannel study showing useful channels after data rejection.....	159
Table 3: List of patients monitored with the multichannel system during alterations in the ECMO flows.	160
Table 7.1: Demographics of the patients used in the WCC analysis	187
Table 7.2: Active channels and flow periods used in the group analysis of the six ECMO patients monitored during alterations in the ECMO flows.....	187

List of Acronyms

ABP	arterial blood pressure
ADC	analogue-to-digital converter
ASD	arterial septal defects
ASO	arterial switch operation
AV valves	artioventricular valves
BP	blood pressure
CA	circulatory arrest
CaBF	Cerebral artery blood flow
CBF	cerebral blood flow
CBFV	Cerebral blood flow velocity
CDH	Congenital diaphragmatic hernia
cCyt.aa₃	Cytocrome oxydase
CHD	congenital heart defects
CICU	cardiac intensive care unit
CMRO₂	cerebral metabolic activity
CNS	central nervous system
CO	cardiac output
CO₂	carbon dioxide
COH	Coherence
CPB	cardiopulmonary bypass
CPP	cerebral perfusion pressure
CPR	cardiopulmonary resuscitation
CSF	cerebrospinal fluid
CT	Computerised tomography
CVP	central venous pressure

CVR	cerebrovascular resistance
CW	continuous wave
CWT	Continuous wavelet transform
CytOx	oxidised cytochrome
DH	deep hypothermia
DHCA	deep hypothermia circulatory arrest
DO₂	systemic oxygen delivery
DPF	differential pathlength factor
DQ	developmental quotient
ECLS	extracorporeal life support
ECMO	extracorporeal membrane oxygenation
EDV	end-diastolic volume
EEG	Electroencephalography
FD	frequency-domain
FDS	frequency domain systems
FM	frequency multiplexing
GOSH	Great Ormond Street Hospital
H₂CO₃	carbonic acid
HbD	HbO ₂ -HHb, cerebral intravascular oxygenation
HbO₂	Oxyhaemoglobin
HbT	total haemoglobin
HF	high frequency
HHb	Deoxyhaemoglobin
HLHS	hypoplastic left heart syndrome
HR	heart rate
ICP	intracranial pressure
ICU	intensive care unit
IJV	internal jugular vein
IVC	Inferior vena cava
JVP	Jugular venous pressure
LCaBF	left common carotid artery blood flow
LF	low frequency
LV	left ventricle

MAP	mean arterial pressure
MAS	Meconium aspiration syndrome
MCA	middle cerebral artery
MBBL	modified Beer-Lambert law
MBFV	mean blood flow velocity
MRI	Magnetic resonance imaging
NIR	near infrared
NIRS	near infrared spectroscopy
O₂	oxygen consumption
OD	optical density
OMM	optical multichannel monitoring
OR	operating room
OT	optical topography
PA	pulmonary artery
pCO₂	partial carbon dioxide pressure
PFC	persistent fetal circulation
PMDF	photon measurement density function
pO₂	partial oxygen pressure
PRx	Pressure reactivity index
PSD	power spectral density
PVR	pulmonary vascular resistance
RCCA	right common carotid artery
RIJV	right internal jugular vein
RLFP	regional low flow cerebral perfusion
RR	respiration rate
RTE	radiative transfer equation
RTV	Room temperature vulcanisation
RV	right ventricle
SaO₂	arterial saturation at the arterial cannula
SpO₂	oxygen saturation
SRS	spatially resolved spectroscopy
SV	stroke volume
SVC	Superior vena cava

SvO₂	venous saturation
TAPVR	total anomalous pulmonary venous return
TCD	Transcranial Doppler
TD	Time domain
TDS	time domain systems
TGA	transposition of the great arteries
TOI	tissue oxygenation index
TOF	Time of flight
TOS	tissue oxygen saturation
TPSF	temporal point spread function
ULF	ultralow frequency
VA ECMO	veno-arterial ECMO
VHF	very high frequency
VLF	very low frequency
VO₂	oxygen consumption
VSD	ventricular septal defects
VV ECMO	veno-venous ECMO
WCC	Wavelet cross-correlation

Chapter 1

INTRODUCTION

1.1 Motivation and objectives

The risk of neurological injury for infants and children with cardiac and/or acute respiratory defects undergoing surgical procedures which involve the use of extracorporeal circulation is considerable. Extracorporeal circulation may refer to either mechanical life support, such as extracorporeal membrane oxygenation (ECMO), or cardiopulmonary bypass (CPB) for the repair of congenital cardiac defects (CHD). The causes for neurological injuries in these patients are multifactorial and include preoperative brain malformations, perioperative hypoxemia and low cardiac output states, and brain injury occurring during patient's recovery. Extracorporeal life support in the form of extracorporeal membrane oxygenation (ECMO) importantly influences neurological outcome, the causes of which are not yet fully understood. Alterations in cerebral blood flow, reoxygenation injury, thromboembolism, and loss of pulsatility have been described as possible underlying pathomechanisms. With increasing overall survival, the understanding of the impact of long term neurologic sequelae on quality of life is crucial. Therefore, developing improved monitoring techniques for early detection of neurologic injury is highly significant and would both allow intervention on individual patients and drive refinements in strategies to reduce risk.

Near infrared spectroscopy (NIRS) offers the advantage of a continuous, non invasive means of monitoring cerebral oxygenation at the bedside. In the 1970s Jobsis demonstrated that transmittance measurements of near-infrared radiation could be used to monitor the degree of oxygenation of certain metabolites. Consequently, the diagnostic potential of optical methods was established, and since then there is an increasingly widespread use and development of clinical near infrared spectroscopy (NIRS). The use of NIRS in cardiopulmonary bypass (CPB) for infants suffering from CHD was introduced in the 1990s. To date, even though many centres have used this monitoring technique on patients with CHD, there is minimum literature on the use of this technique on ECMO patients. Furthermore, the primary focus in almost all the NIRS studies so far has been on absolute changes in tissue oxygen saturation – a number representing the percentage of oxygenated haemoglobin in the field of view. In addition, all the commercially available systems have only two channels, thus are not able to measure cerebral oxygenation in all regions of the brain.

The main objective of my work was the development of a multichannel NIRS system and its use in an intensive care environment to monitor infants and children supported on ECMO. In conjunction with the system development, my work aims to develop analysis tools to assess regional variations in cerebral circulation and cerebral autoregulation during different ECMO phases. My work, which is described extensively in this thesis, forms the initial stages of a project whose long term aim is the real time assessment of regional dynamic cerebral autoregulation and establishment of a cerebral autoregulation index that will potentially aid clinical management.

1.2 Thesis Overview

Chapter 2 gives an overview of the basic human anatomy and physiology. It includes a description of blood circulation, from the function of the human heart to oxygen transport to tissue. The chapter focuses on cerebral circulation with a brief description of brain anatomy and an extensive discussion on cerebral blood flow including cerebral autoregulation.

An introduction to the physics of optics of near infrared spectroscopy (NIRS) is given in *chapter 3*. The chapter also provides a description of the main NIRS instrumentation. It describes the dual channel NIRO-200 spectroscopy system (Hamamatsu Photonics KK) used for data collection as part of this work and lists other main commercially available dual channel systems. The development and clinical application of a commercial multichannel system (ETG-100, Hitachi Medical Systems) forms the main part of this work and the hardware, operation and function of it are also presented in this chapter. An outline of the main multichannel NIRS systems available commercially and developed prototypes is also provided.

Chapter 4 depicts the clinical background to the project providing a description of the physiology and pathophysiology of extracorporeal circulation, in the form of extracorporeal membrane oxygenation (ECMO), in infants and children with cardio-respiratory failure. An overview of the physiology of cardiopulmonary bypass for congenital heart defects is also presented. Neurological morbidity on ECMO is discussed and non invasive methods of neurological monitoring are outlined. An extensive literature review on the use of NIRS technology on infants and children placed on ECMO and CPB for CHD is also provided.

The work carried out with the dual channel NIRS system (NIRO-200) is thoroughly discussed in *Chapter 5*. This chapter describes and discusses the use of a dual channel NIRS system to study cerebral and peripheral oxygenation in infants and children supported on ECMO. The induction of the instrumentation in the intensive care unit, data collection, as well as the clinical protocol are presented. The spectral analysis in the Fourier domain in terms of power spectral density and coherence for peripheral and cerebral oxygenation are described, and the results are presented and discussed.

Chapter 6 portrays the induction and use of the multichannel NIRS, optical topography system, ETG-100, in neonatal cardiac intensive care to study patients supported on ECMO. The development of the multichannel system for clinical use and application is described. An analytical illustration is given of the design and construction of a novel flexible neonatal cap incorporating an array of sources and detectors such that oxygenation measurements can be obtained from 12 channels. Results obtained with the multichannel system are shown along with systemic and

ECMO circuit parameters obtained simultaneously. Absolute changes in chromophore concentrations, systemic and ECMO variables are presented for each patient individually and discussed.

Chapter 7 focuses on the results obtained from the multichannel NIRS, ETG-100, system and presents in detail a novel method of spectral analysis based on wavelets. The analysis method uses wavelet-cross correlation (WCC) to investigate the relation between MAP and HbO₂ as a means of assessing cerebral autoregulation in neonates supported on ECMO during alterations in the ECMO flows and during weaning off ECMO. The method was also used as a means of assessing regional variations during these procedures. The results are presented and discussed extensively.

A summary of the thesis, conclusions and further work are outlined in *chapter 8*.

Chapter 2

BASIC HUMAN ANATOMY AND PHYSIOLOGY

2.1 Blood circulation in healthy humans

The cardiovascular system consists of the pulmonary circuit and the systemic circuit. The pulmonary circuit consists of arteries and veins that transport blood from the right ventricle of the heart to the lungs and back to the right atrium of the heart. Oxygenated blood leaving the heart enters the major arteries of the body; it then travels through arterioles to capillaries transporting oxygen and nutrients to all organs and tissues. Deoxygenated blood then travels through the venules and veins before returning to the right atrium of the heart.

2.1.1 Functional anatomy of the heart

The heart contains four muscular chambers-the right and left atria and the right and left ventricles (figure 2.1). The right atrium receives blood from the superior vena cava and passes it to the right ventricle through the right atrioventricular (tricuspid) valve. From the right ventricle, blood flows through the pulmonary semilunar valve into the pulmonary trunk. The pulmonary trunk branches to form the

right and left pulmonary arteries, which conduct blood to the gas exchange tissues of the lung. From there, blood flows through pulmonary veins into the left atrium. The left atrium empties blood into the left ventricle through the left atrioventricular (mitral) valve. Then the blood passes to the aorta through the aortic semilunar valve which supplies blood to the systemic circuit.

Figure removed for copyright purposes

Figure 2.1: The cross section of a human heart. Deoxygenated blood from the vena cava enters the right atrium, passes to the right ventricle and then to the lungs via the pulmonary arteries. Blood rich in oxygen enters the left atrium via the pulmonary veins and passes to the left ventricle and aorta which supply blood to the systemic circuit. (Martini 2006).

A complete heartbeat consists of contraction (systole) and relaxation (diastole) of the heart chambers and is given the term cardiac cycle. The phases of the cardiac cycle – arterial systole, arterial diastole, ventricular systole, and ventricular diastole - are shown in figure 2.2. The amount of blood pumped out a single ventricle during a single beat is called the stroke volume (SV).

Figure removed for copyright purposes

Figure 2.2: Description of the phases constituting a cardiac cycle. One heart beat or one full cardiac cycle lasts about 500 msec in infants and 800 msec in adults. (Martini 2006).

2.1.2 Arterial blood pressure

Blood flows because of a pressure gradient. The progressive fall in pressure as blood passes through the circulatory system is directly related to resistance. Although pumping of the heart causes fluctuations in aortic blood pressure the mean pressure remains almost constant. The greatest drop in pressure occurs across the arterioles where resistance to blood flow is greatest. Pressure waves at different sites in the arterial tree are shown in figure 2.3. Systolic, diastolic, and mean arterial pressures (MAP) are the three blood pressure (BP) values typically reported; to interpret a BP reading, all 3 must be evaluated. Systolic and diastolic BP are the pressures at the highest and lowest points of the arterial waveform, respectively. Mean arterial pressure is the average pressure during the entire cardiac cycle and integrates the area under the arterial pressure waveform. The value of MAP depends on the shape and size of the pressure-wave contour. If a MAP value is not available from a monitor, different formulas are available for estimating it. These formulas estimate MAP by

making assumptions about the shape of the arterial pressure waveform (for example, adding one third of the pulse pressure value to the diastolic value) (Stebor and Short 2005). Systolic and diastolic pressure values in newborns are shown in figure 2.4.

The principal determinant of the arterial blood pressure is the volume of blood in the arteries. Arterial blood volume is directly proportional to blood pressure. Cardiac output and peripheral resistance are directly proportional to blood volume and are therefore the two major factors influencing blood pressure. Cardiac output is the amount of blood that flows out of the heart per unit time (Cardiac output (CO) = stroke volume (SV) x heart rate (HR)) (Martini 2006).

Mechanical, neural and chemical factors regulate the strength of the heartbeat and therefore of the stroke volume. The heart rate is influenced by the autonomic nervous system, circulating hormones and the venous return. Blood viscosity affects peripheral resistance. For a detail description of the factors affecting arterial blood pressure the reader is referred to (Martini 2006, Thibodeau and Patton 2007a).

Figure removed for copyright purposes

Figure 2.3: Pressure waves at different sites in the arterial tree. With transmission of the pressure wave into the distal aorta and large arteries, the systolic pressure increases and the diastolic pressure decreases. The quoted pressure values are for adults (Smith and Kampine 1990b).

Figure removed for copyright purposes

Figure 2.4: Average values (dashed lines) and normal ranges (solid lines) for (a) systolic and (b) diastolic arterial blood pressure according to birth weight in newborn infants. (Vermold et al. 1981)

2.1.3 Oxygen transport to tissue

Exchange of gases in the lungs takes place between alveolar air and blood flowing through lung capillaries. Oxygen from the alveolar air enters the blood stream by diffusing down its pressure gradient and carbon dioxide molecules exit the blood out into the alveolar air. The amount of oxygen absorbed across the lung in the process of pulmonary gas exchange is exactly equal to the amount of oxygen consumed by peripheral tissues during metabolism regardless of the status of pulmonary function.

Systemic oxygen delivery (DO_2) is the amount of oxygen delivered to peripheral tissues each minute or the product of arterial oxygen content times cardiac output (CO). DO_2 is controlled by cardiac output (CO), haemoglobin concentration, haemoglobin saturation, and dissolved oxygen in that order. The normal value for DO_2 is 4-5 times oxygen consumption (VO_2) regardless of the patient size (Levick 2003). When VO_2 changes, secondary to variations in metabolism, DO_2 readjusts by increasing or decreasing CO to maintain the normal DO_2/VO_2 ratio. Since the oxygen content of normal arterial blood is the same for all ages and sizes of patients (20 cc O_2 /dl), variations in oxygen delivery for patients of different size and metabolic activity are caused by variations in CO (Levick 2003). The oxygen content is rarely measured directly for clinical applications, and it is standard practice to describe

blood oxygenation in terms of P_{aO_2} (partial pressure of oxygen in arterial blood) or haemoglobin saturation.

The chief constituent of the erythrocyte is haemoglobin (Hb). Haemoglobin is a quaternary protein containing four *heme* groups each of which contains an iron atom (Fe). An oxygen molecule can combine with the iron atom within each *heme* group to form oxyhaemoglobin (HbO_2), the primary oxygen carrier. Each gram of haemoglobin can unite with 1.34 ml of oxygen so that the exact amount of oxygen in the blood depends mainly on the amount of haemoglobin present (Smith and Kampine 1990b). Normally the concentration of haemoglobin is 15 g/dl of whole blood (Levy and Pappano 2007). If blood is exposed to a sufficiently high oxygen pressure so that 100% of Hb is combined with oxygen to form HbO_2 , it is “fully saturated” with an “oxygen capacity” of 20.1 ml/dl of blood or 20.1 vol % (Thibodeau & Patton 2007a).

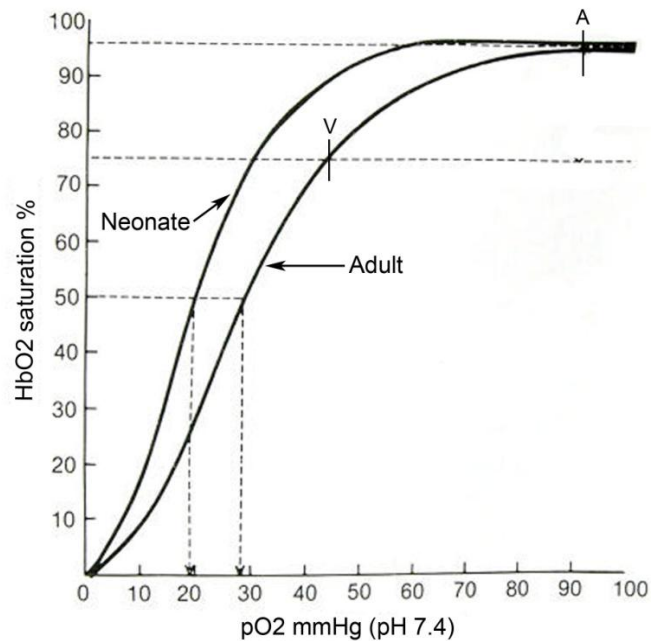


Figure 2.5: Oxygen dissociation curve showing the relationship between partial pressure of oxygen (pO_2) and the percentage of oxyhaemoglobin (HbO_2) saturation of the blood. In adults, in the alveoli of the lungs (A) the pO_2 is about 100 mm hg, which results in 97% HbO_2 saturation. in the mixed venous blood returning from the tissues, the pO_2 has fallen to about 40 mm Hg and the HbO_2 saturation is approximately 75% (V). In neonates the curve is shifted to the left due to the greater oxygen affinity of the neonatal haemoglobin. (adapted from Smith & Kampine 1990b)

Figure removed for copyright purposes

Figure 2.6: The influence of pH, pCO₂ and temperature on the oxygen dissociation curve. Small shifts of the curve to the right which occur in the tissues because of lower pH, higher pCO₂, and higher temperature, tend to lessen the affinity of Hb for oxygen and assist ion release of oxygen to the tissues.(Smith & Kampine 1990b)

The amount of oxygen with which each unit of Hb will actually combine is dependent primarily on the partial pressure of oxygen (pO₂) to which the Hb is exposed. This relationship is defined by the oxygen dissociation curve (figure 2.5). In the alveoli of the lungs, where the pO₂ is normally at a high level, the blood will be about 97% saturated, i.e., 97% of Hb is combined with O₂ (A in figure 2.5). After the blood has given up some of its oxygen in the tissues and reached the large veins (mixed venous blood), its pO₂ value would have decreased to about 40 mm Hg, V as indicated in figure 2.5, at this pO₂ the blood will be only about 75% saturated with oxygen. Since mixed venous blood haemoglobin saturation reflects the DO₂/VO₂ ratio, it is the most important indicator for managing critically ill patients. While oxygen content is determined primarily by the pO₂, it is also influenced to a lesser

extent by other factors such as pH, pCO₂, and blood temperature. A decrease in pH or an increase in any of the other three factors will produce a “shift to the right” in the oxyhaemoglobin dissociation curve (figure 2.6). The result is that at the same pO₂, less O₂ will be bound to the Hb and consequently more released to the tissues, which results in less affinity of Hb for O₂. Conversely, an increase in pH or decrease in pCO₂ and blood temperature will have the opposite effect (i.e. the dissociation curve will shift to the left so there is greater affinity of haemoglobin for oxygen). Furthermore, the upper “plateau” portion of the curve suggests that large changes in pO₂ will have relatively little effect on HbO₂ saturation than would ordinarily be the case. On the other hand, in the capillaries, where the pO₂ falls sharply, as represented by the steep portion of the curve, the tissues have the advantage of being able to pick up a large supply of oxygen with only a small decrease in pO₂.

2.1.4 Neonatal Circulation

One of the most interesting aspects of circulatory development reflects the differences between the life of an embryo or fetus and that of an infant. Throughout embryonic and fetal life, the lungs are collapsed; yet after delivery, the newborn infant must be able to extract oxygen from inspired air rather than across the placenta.

2.1.4.1 Fetal circulation

Fetal circulation is shown in figure 2.7. Deoxygenated fetal blood is conducted to the placenta via a pair of umbilical arteries, which arise from the internal iliac arteries and enter the umbilical cord. Blood returns from the placenta in the single umbilical vein, bringing oxygen and nutrients to the developing fetus. The umbilical vein drains into the ductus venosus, a vascular connection to an intricate network of veins within the developing liver. The ductus venosus collects blood from the veins of the liver and from the umbilical vein and empties into the inferior vena cava (IVC). The IVC also drains blood returning from the lower trunk and extremities. On reaching the heart, blood is effectively divided into two streams by the edge of the interatrial septum: (1) one stream passes into right atrium where it is joined by blood

from the superior vena cava (SVC) which is blood returning from the myocardium and upper parts of body, and (2) a larger stream is shunted to the left atrium through the foramen ovale (lying between IVC and left atrium) (Murphy 2005). The foramen ovale, or interatrial opening, is associated with a long flap that acts as a valve. Although the interatrial and interventricular septa develop early in the fetal life, the interatrial partition remains functionally incomplete until birth. Blood can flow freely from the right atrium to the left atrium, but any backflow will close the valve and isolate the two chambers. Thus blood can enter the heart at the right atrium and bypass the pulmonary circuit. During diastole, blood enters the right atrium and flows into the right ventricle, but it also passes into the left atrium through the foramen ovale. About 25% of the blood arriving at the right atrium bypasses the pulmonary circuit in this way (Martini et al. 2006). Blood flowing through the foramen ovale and into left atrium passes into the left ventricle where it is ejected into the ascending aorta. This relatively oxygen rich blood passes predominantly to the head and upper extremities. A second short-circuit exists between the pulmonary and aortic trunks. This connection, the ductus arteriosus, consists of a short, muscular vessel. Because of the large pulmonary vascular resistance over 90% of the blood leaving the right ventricle passes through the ductus arteriosus and enters the systemic circuit rather than continuing to the lungs.

2.2.4.2 Fetal Haemoglobin

Fetal haemoglobin is the main oxygen transport protein in the fetus during the last seven months of development in the uterus and in the newborn until roughly 6 months old (Murphy 2005). Functionally, fetal haemoglobin differs most from adult haemoglobin in that it is able to bind oxygen with greater affinity than the adult form, giving the developing fetus better access to oxygen from the mother's bloodstream. In newborns, fetal haemoglobin is nearly completely replaced by adult haemoglobin by approximately the twelfth week of postnatal life. Fetal haemoglobin's affinity for oxygen is substantially greater than that of adult haemoglobin (Murphy 2005). As a result, the oxygen saturation curve is left-shifted for fetal haemoglobin in comparison to the same curve in adult haemoglobin (figure 2.5).

Figure removed for copyright purposes

Figure 2.7: Fetal circulation (Murphy 2005)

2.2.4.3 Circulatory changes at birth

At birth, when the infant takes the first breath, the lungs expand, and so do the pulmonary vessels. There is therefore, a dramatic fall in the pulmonary vascular resistance and blood rushes into the pulmonary vessels. The increase in pulmonary blood flow leads to a large rise in pulmonary venous return to the left atrium. The left atrial pressure therefore exceeds the right atrial pressure. This reversal of pressure gradient across the atria allows the flap of the foramen ovale to push against the atrial septum and the atrial shunt is effectively closed. Although the initial closure of the foramen ovale occurs within minutes to hours of birth, anatomical closure by tissue proliferation takes several days. As a result, all blood from the right atrium now passes into the right ventricle. The ductus arteriosus constricts due to the high partial pressure of oxygen. The process is usually complete within 2 days after birth. Other changes over several weeks include a reduction in the thickness of the walls of right ventricle and the muscle layer of the pulmonary arterioles.

Under certain circumstances, the newborn may revert back to a fetal-type circulation, a pathophysiological state termed Persistent Fetal Circulation (PFC) (Thibodeau and Kevin 2007). In the presence of certain stimuli, such as hypoxia, hypercarbia and acidosis, the pulmonary arterioles will constrict and lead to an increase in Pulmonary Vascular Resistance (PVR). The increase in PVR favours a right to left shunt and the foramen ovale and ductus arteriosus subsequently remain patent. In the absence of a placenta for gas exchange, it is clear that this scenario can lead to a catastrophic outcome in the newborn. There are two categories of congenital heart disease (acyanotic and cyanotic) that result from structural, valvular and vascular abnormalities (see chapter 4).

2.2 Cerebral Circulation

The brain takes up 2% of total body weight but it receives 15% of cardiac output (Martini 2006). Oxygen and glucose utilisation are also high compared to other organs. Figure 2.8 depicts the arterial structure in the brain. The vascular anatomy is unusual in that multiple potential collateral channels exist to supply the high blood flow and metabolism. Since the brain is contained within the rigid skull, cerebral blood volume must be tightly controlled to prevent elevation of intracranial pressure (ICP).

Blood in the brain is supplied by four major brain arteries, two carotid and two vertebral arteries. The carotid arteries contribute about 80% of the total perfusion and are therefore more important (Thibodeau & Patton 2007b). The common carotid arteries ascend deep in the tissue of the neck and they can usually be located by pressing gently along either side of the windpipe until a strong pulse can be felt. Each common carotid artery divides into an external and internal carotid artery (figure 2.8). The external carotid arteries supply blood to the neck, esophagus, pharynx, larynx, lower jaw and face. The internal carotid arteries enter the skull through the carotid canals of the temporal bones, delivering blood to the brain. The internal carotid arteries normally supply the arteries of the anterior half of the cerebellum. The vertebral arteries fuse to form the basilar artery which is interconnected with the carotid arteries to form a ring-shaped anastomosis, the circle

of Willis (figure 2.9). The circle of Willis helps to balance the blood pressure in the anterior and posterior regions and helps to protect the brain against further damage should one of these arteries become occluded. The venous return from the brain is accomplished through the superficial cerebral veins, deep cerebral veins and cerebral venous sinuses and they collectively drain to the internal jugular vein (figure 2.10).

Figure removed for copyright purposes

Figure 2.8: Arteries of the neck and head (Martini 2006)

Figure removed for copyright purposes

Figure 2.9: Origins of the blood vessels that form the arterial circle (Thibodeau and Patton 2007b)

Figure removed for copyright purposes

Figure 2.10: Major veins of the head (Thibodeau & Patton 2007b)

2.2.1 Basic anatomy of the human brain

The brain, in conjunction with the spinal cord, forms part of the central nervous system (CNS). It consists of four main regions, the cerebral hemispheres, the diencephalons, the brain stem and the cerebellum (figure 2.11). The cerebral hemispheres are covered by an outer layer of grey matter, approximately 5mm thick (adults), known as the cerebral cortex. The surface of the cerebral hemispheres is highly convoluted consisting of ridges called sulci and deeper ridges called fissures, increasing the surface area of the cortex. The fissures separate the hemispheres into lobes (figure 2.12).

The brain is protected by several layers: the scalp, skull, various membranes (meninges) and the cerebrospinal fluid (CSF). A cross section of the brain illustrating its protective layers is shown in figure 2.13. Pia matter covers the surface of the cortex tightly. The arachnoid mater, surrounds the pia matter loosely, without following the contour of the cortex. The space in between pia and arachnoid matter, namely subarachnoid space, is filled with the CSF and contains the blood vessels that serve the brain.

Figure 2.14 shows the skull of a term neonate. The plates of the skull are not fused and fontanelles exist, composed of fibrous tissue rather than bone. The skull is soft and thinner than in an adult, and therefore likely to transmit near infrared (NIR) light more readily than the adult skull. The face-to-cranium ratio is 1 to 8 rather than

1 to 2 in the adult. Skull sizes and shapes vary between infants of the same gestational age, including the effects of illness and deformities. A plot of head circumference with age is shown in figure 2.15.

Figure removed for copyright purposes

Figure 2.11: Divisions of the brain (Thibodeau & Patton 2007b)

Figure removed for copyright purposes

Figure 2.12: Lobes of the brain (Martini 2006)

Figure removed for copyright purposes

Figure 2.13: Coverings of the brain (Thibodeau & Patton 2007b)

Figure removed for copyright purposes

Figure 2.14: The skull of a term neonate (Hall-Craggs 1995).

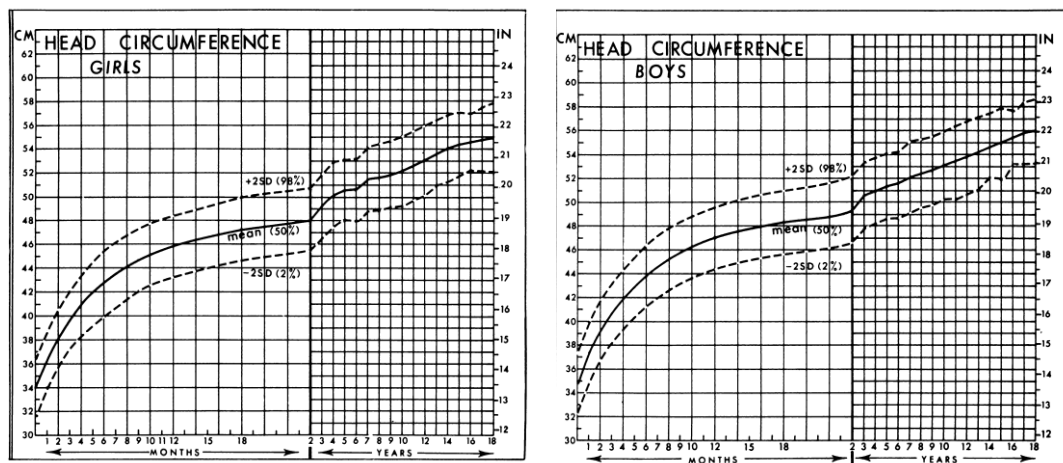


Figure 2.15: Head circumference charts for girls and boys from birth to 18 years (Nellhaus 1968).

2.2.2 Cerebral Blood Flow (CBF)

As in other vascular beds, the volume of inflow of blood to the brain depends upon the interplay of the various factors which on one hand determine the perfusion or effective head pressure and, on the other, the resistance to blood flow offered by the vessels. Cerebral blood flow can be expressed as being directly proportional to the cerebral perfusion pressure (CPP) and inversely proportional to the cerebrovascular resistance (CVR) (Steiner and Andrews 2006).

The simplest way of expressing CPP is to consider it as the net head of pressures forcing blood through the cerebral vessels and it is therefore the difference between the mean arterial (MAP) and jugular venous (JVP) pressures (Czosnyka and Pickard 2004). In some tissues there is a third pressure to consider and this is the pressure external to the blood vessels because if high this pressure can restrict flow through the tissue. Such a situation exists in the brain where the external pressure is the intracranial pressure (ICP). Consequently, $CPP = MAP - ICP$ (if ICP is higher than JVP) or $CPP = MAP - JVP$ (if JVP is higher than ICP) (Walters 1998). Because JVP is very small, it is often disregarded and perfusion pressure is assumed to be equivalent to mean arterial pressure (MAP).

2.2.2.1 Cerebral Autoregulation

A characteristic feature of the cerebral circulation while the brain is in a resting state, is its ability to maintain total and regional blood flows relatively constant over a wide range of arterial blood pressures (Busija and Heistad 1984). The independence of cerebral blood flow from arterial blood pressure typically is called cerebral autoregulation (Busija 1993). The brain maintains its blood flow largely, but not completely, constant by vasodilation during decreases and vasoconstriction during increases in perfusion pressure. The resulting autoregulation curve, as depicted schematically in figure 2.16, thus represents a steady state relationship (Kuschinsky 1996). Autoregulation is the process which maintains CBF constant over a wide range of arterial blood pressure (60-140 mmHg in adults) (Edvinsson 1993). However, there are certain limits beyond which the autoregulatory system fails; this results in cerebral oedema if the pressure exceeds approximately 140mmHg (adults) and cerebral ischemia due to lack of flow if the pressure falls below about 60mmHg. In infants and children there is an incomplete understanding the limits of cerebral autoregulation (Brady et al. 2010b). The range of autoregulation and its upper limit is thought to be changing with gestational age and it can range from 45 mmHg to 100 mmHg at 33 and 47 weeks gestational age, respectively (Ramaekers et al. 1990). Blood flow in the brain is often better regulated than in most other organs. The arterial vessel wall allows its diameter to expand

about 4-fold, resulting in a 256-fold change in blood flow to suit the arterial pressure variation. Total absence of autoregulatory mechanisms would result in a flow-pressure relationship that would be concave to the pressure axis because of the elasticity of the vasculature (Purves 1972). In such a situation, an increase in perfusion causes a passive distension of the cerebral vessels.

Figure removed for copyright purposes

Figure 2.16: The cerebral autoregulation curve. Cerebral blood flow is constant under a wide range of mean arterial pressures (Kuschinsky 1996).

A number of mechanisms have been suggested to explain the nature of autoregulation: i) the myogenic mechanism in which the arterioles and small arteries constrict or dilate as an intrinsic response to an increase or decrease in the transmural pressure gradient, ii) the metabolic mechanism in which changes in the metabolic microenvironment are thought to be responsible for the vasomotor response, and iii) the neurogenic mechanism in which perivascular nerves have been proposed to play a role in the cerebral autoregulation. For more details on the mechanisms of autoregulation the reader is referred to (Edvinsson 1993) and (Kuschinsky 1996).

The assessment of cerebral autoregulation is important for rational clinical management of specific conditions. In adults, these include severe head injury, acute ischemic stroke or subarachnoid haemorrhage, which are known to abolish

autoregulation. Preterm infants and infants and children supported on extracorporeal circulation, either in the form of mechanical support (i.e. ECMO) or CPB, are patient groups where impairment of cerebral autoregulation is also evident. The risk factors associated with loss of cerebral autoregulation in ECMO patients are discussed in chapter 4. A major aim of the work included in this thesis is the development of novel methods of analysis to assess cerebral autoregulation in infants supported on ECMO. Hence, the subject of cerebral autoregulation, including a detailed description of existing and novel methods of assessing cerebral autoregulation is presented in chapter 7.

2.2.2.2 Blood gases and cerebral blood flow

The cerebral arteriolar response to CO_2 , pH and O_2 can also alter the blood flow significantly. The response of these vessels to CO_2 is the strongest and it is generally accepted that CBF is increased by a raised arterial pCO_2 and a lowered arterial pO_2 . In contrast, CBF is decreased by a lowered arterial pCO_2 . Figure 2.17 shows the response of cerebral circulation to changes in pCO_2 and pO_2 .

Figure removed for copyright purposes

Figure 2.17: Effect of pCO_2 (left) and pO_2 (right) on cerebral blood flow. The steepest part of the pCO_2 is near 40 mm Hg, indicating a high sensitivity of CBF to pCO_2 at physiological levels. At normal pO_2 levels of 80 to 120 mm Hg, the effect of CBF is practically nil. (Smith and Kampine 1990a)

Effects of CO₂

The changes of CBF with variations of the arterial pCO₂ are basically mediated by concomitant changes in the pH of the brain tissue. The highly diffusible nature of CO₂ evades the blood brain barrier causing changes in the pH of the perivascular fluid (CSF). When CO₂ is dissolved into water it forms a weak acid, called carbonic acid (H₂CO₃), and the topical application of low-pH solutions induces vasodilation. Therefore, an increased arterial pCO₂ (or hypercapnia) provokes an increase in the size of pial arteries. CO₂ exerts its cerebrovascular effects by modulating extracellular pH in the immediate vicinity of the smooth muscle cells.

Effects of O₂

In contrast to effects of altering pCO₂, a decrease in arterial pO₂ leads to an increase in CBF whereas an increase of arterial pO₂ beyond the normal values has no effect. Hypoxia, or inhalation of low oxygen partial pressure, causes dilation of the pial arteries, whereas hyperoxia, or high oxygen partial pressure, causes a moderate vasoconstriction.

2.2.3 Cerebral haemodynamic oscillations

The presence of haemodynamic oscillations in the brain have been studied widely by different techniques, such as laser Doppler flowmetry (Hudetz et al. 1992), transcranial Doppler sonography (Zhang et al. 1998) and near infrared spectroscopy (NIRS) (Obrig et al. 2000). In general, these oscillations can be characterised as *fast* (originating from heart rate (HR) (1-2.7Hz) and respiratory rate (RR) (0.2-0.5Hz) (table 3.1)) and *slow* (<0.1Hz) spontaneous periodic oscillations. The use of NIRS in detecting oscillations in a wide range of frequencies (0.1-5Hz) was established by Chance et al. (1993). Elwell and coworkers (Elwell et al. 1999) demonstrated the presence of RR and HR in NIRS signals in human adults (figure 2.18). Similarly, oscillations related to RR and HR have also been observed in neonates (Roche-Labarbe et al. 2007).

Figure removed for copyright purposes

Figure 2.18: An example measurement showing the existence of systemic influence on the ΔHbO_2 signal (Elwell et al. 1999). Respiratory and cardiac oscillation are shown by the nasal airflow and pulse waveforms, respectively. These oscillations are reflected in the HbO_2 signal.

Table 2.1: Respiration rate and heart rate in infants and children.

Age	Respiration rate Breaths per minute	Heart rate	
		High Beats per minute	Low Beats per minute
Birth-1 year	30-36	160	100
1-3 years	24-40	150	90
3-6 years	22-34	140	80
6-12 years	18-30	130	70
12-18 years	12-16	120	60

The origin of the slow spontaneous periodic oscillations is unclear. They occur without any overt stimulus (spontaneity), they can be differentiated from other oscillatory phenomena (slowness) such as the HR and RR cycles, and they are altered by pharmacological and pathological conditions (modulability) (Obrig et al. 2000). NIRS studies have revealed slow oscillations of the haemoglobin oxygenation state of infants (Livera et al. 1995). Taga et al. demonstrated, with the use of a NIRS multichannel optical topography system, that spatially synchronised slow oscillations of haemoglobin oxygenation state exist throughout the occipital cortex of neonates (Taga et al. 2000). The presence of slow spontaneous oscillations may be more significant in the oxyhaemoglobin signal measured by NIRS, rather than in the

deoxyhaemoglobin (or total haemoglobin) signal (Elwell et al. 1999, Obrig et al. 2000). Also, hypercapnia may attenuate these oscillations (Obrig et al. 2000).

Chapter 3

NEAR INFRARED SPECTROSCOPY: THEORY AND INSTRUMENTATION

3.1 Light propagation in tissue

In the 1970s Jobsis demonstrated that transmittance measurements of near-infrared radiation could be used to monitor the degree of oxygenation of certain metabolites (Jobsis 1977). Consequently, the diagnostic potential of optical methods was established, and since then there is an increasingly widespread use and development of clinical near infrared spectroscopy (NIRS).

Near infrared spectroscopy offers a safe, non-invasive means of monitoring cerebral and peripheral oxygenation. The technique has its basis on the fact that biological tissue is relatively transparent in the near infrared (NIR) region of the spectrum (600-1000nm). However, human tissue contains a variety of substances (or chromophores) with well defined absorption spectra at NIR wavelengths. Chromophores, whose concentration remains constant with time include, water, melanin, and bilirubin. Conversely, chromophores, such as oxygenated haemoglobin (HbO_2), deoxyhaemoglobin (HHb), and oxidised cytochrome oxidase (CytOx), have concentrations in tissue which are strongly linked to tissue oxygenation and

metabolism. When chromophores in tissue are present in sufficient quantities, they can contribute significant attenuation to measurements of transmitted light. Light interaction with tissue involves scatter and absorption; the amount of each depending upon the type of tissue illuminated and the wavelength of incident light.

3.1.1 Light Absorption

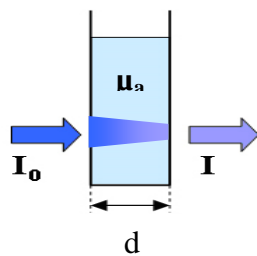


Figure 3.1: Light absorption in a non scattering medium.

The quantitative relationship between light absorption in a non-scattering, absorbing medium dissolved in a non-absorbing solution and the thickness of the medium was firstly determined by Bourger in 1729 and then by Lambert in 1760. They demonstrated that when light with intensity I is incident on a medium with successive layers of thickness δd the same fraction (dI) of the incident intensity I is absorbed

(figure 3.1). The mathematical expression is known as Lambert-Bouguer:

$$\frac{dI}{I} = -\mu_a \cdot \delta d \quad (3-1)$$

where μ_a is a constant known as the absorption coefficient, usually expressed in cm^{-1} . The absorption coefficient, μ_a , represents the probability of a photon being absorbed per unit length of travel. The reciprocal, $1/\mu_a$, is called the absorption pathlength. Integration of the above expression gives:

$$I = I_0 e^{-\mu_a d} \quad (3-2)$$

Alternatively, the above expression can be expressed in base 10 logarithms:

$$I = I_0 10^{-kd} \quad (3-3)$$

where k is known as the extinction coefficient, expressed in cm^{-1} . In 1852 Beer determined that the absorption coefficient of an absorbing compound is linearly dependent to its concentration c when dissolved in a non-absorbing solution:

$$\mu_a = a \cdot c \quad (3-4)$$

where a is the specific absorption coefficient measured in $\text{molar}^{-1} \cdot \text{cm}^{-1}$ (Beer 1852). Substituting for μ_a in the Lambert-Bouguer law gives what is known as the Beer-Lambert law:

$$I = I_0 e^{-a \cdot c \cdot d} \quad \text{or} \quad I = I_0 10^{-\varepsilon \cdot c \cdot d} \quad (3-5)$$

where ε is the specific extinction coefficient, usually expressed in units of $\text{molar}^{-1} \cdot \text{cm}^{-1}$.

The absorbance, A , of a medium (in optical density (OD)) is defined as the \log_{10} ratio of the incident and transmitted intensities:

$$\begin{aligned} A &= \log_{10} \left(\frac{I_0}{I} \right) \\ &= \varepsilon \cdot c \cdot d \end{aligned} \quad (3-6)$$

In a solution containing a mixture of n absorbing compounds, the total absorbance is the sum of the individual extinction coefficients multiplied by the distance d

$$\begin{aligned} A &= (k_1 + k_2 + \dots + k_n) \cdot d \\ &= (\varepsilon_1 c_1 + \varepsilon_2 c_2 + \dots + \varepsilon_n c_n) \cdot d \end{aligned} \quad (3-7)$$

The Beer-Lambert law assumes a monochromatic and perfectly collimated beam, and that the sum of the transmitted and absorbed light equals the incident light. Therefore, it does not take into account losses due to reflection at the surface of the medium and most importantly scattering of light.

3.1.2 Absorbing compounds in tissue

Biological tissue can be approximated as a homogeneous mixture of compounds, whose overall light absorption in tissue, at a given wavelength, depends on the type and concentration of the present chromophores. Each chromophore has its own distinctive absorption spectrum. The chromophores of interest for NIRS are those whose absorption characteristics vary with oxygenation status. However, chromophores whose concentration is likely to remain constant still contribute to the total loss of light in tissue. It is therefore important to look at the wavelength spectrum over which useful physiological information can be revealed from both types of tissue chromophores.

Figure removed for copyright purposes

Figure 3.2: Absorption spectrum of pure water over the range 200-2000nm and 650-1000nm (Elwell 1995).

Water

The content of water in the in humans varies with tissue type, gender and age. In the neonatal brain water comprises 90% by mass, whereas in the adult skeletal muscle is around 74% (Woodard and White 1986). It is therefore considered to be the dominant tissue chromophore in spectroscopic measurements. The extinction spectrum of water is shown in figure 3.2. It can be seen that there is a relatively low absorption region between 600 and 900 nm. Beyond 900nm the absorption increases rather rapidly and peaks around 970nm followed by a minor trough and a more pronounced increase at longer wavelengths. The “window” transparency in the

region of low absorbance allows NIR spectroscopic measurements through several centimetres of tissue to be made.

Lipids

Lipids are present in subcutaneous tissue and constitute about 2.6% in newborns, 6.1% in infants (18 months), and 11.6% in children (3-18 years) and adults (Cope 1991). The extinction spectrum of lipids is similar to that of water (figure 3.3). However, the water content is much higher than lipids in the human brain and absorption in the later can be considered negligible. As with water, lipids are treated as a static absorption with a fixed concentration through the duration of measurements.

Figure removed for copyright purposes

Figure 3.3: Spectrum of pork fat in the NIR from 650 to 1000 nm. (van der Zee 1992)

Haemoglobin

Haemoglobin is carried in the red blood cells, or erythrocytes, and constitutes 40-50% of the total blood volume, the balance being plasma (Marieb 1998). Haemoglobin consists of four haem groups each of which contains an iron atom in its ferrous (Fe^{+2}) form. Iron atoms in haemoglobin physically bind to oxygen molecules to form oxy-haemoglobin (HbO_2). The de-oxygenated form, when the oxygen molecules separate from the iron atoms in the body tissue, is known as de-oxyhaemoglobin (HHb). The sum of HbO_2 and HHb give the total haemoglobin (HbT) in the body, which gives a good approximation of the blood volume. Arterial blood is about 98% oxygen saturated and has a bright red colour, whereas venous

blood is about 70% oxygenated and has a purple colour. Figure 3.4 shows the absorption spectra of HbO₂ and HHb in the NIR region of the spectrum. The two absorption spectra differ significantly, hence the visible colour difference between venous and arterial blood. It can be seen that the two spectra cross at about 800nm, the isobestic point. Making simultaneous spectroscopic measurements at a minimum of two wavelengths around the isobestic point allows HbO₂ and HHb to be monitored separately.

Figure removed for copyright purposes

Figure 3.4: Specific absorption spectra of HbO₂ and HHb in the NIR. (Cope 1991)

Figure removed for copyright purposes

Figure 3.5: The difference absorption spectrum between the oxidised and reduced forms of cytochrome oxidase. (Cope 1991)

Cytochrome Oxidase

Cytochrome oxidase (CytOx) is the terminal enzyme in the cellular respiratory chain, and is located in the mitochondrial membrane. The absorption spectrum of CytOx depends on its redox state which in turn depends on the availability of oxygen in the cells. The absorption spectrum of CytOx in its oxidised state shows a broad peak around 830nm. This peak is not present in its reduced state. This makes it possible to make inferences on the availability of oxygen in the cellular level by measuring the difference between the oxidised and reduced forms of CytOx (figure 3.5). Although the magnitude of the absorption coefficient is similar to haemoglobin, the concentration of CytOx in tissue is low relative to that of haemoglobin, thus making it difficult to determine its absorption spectrum (Tachtsidis et al. 2007).

3.1.3 Light Scattering

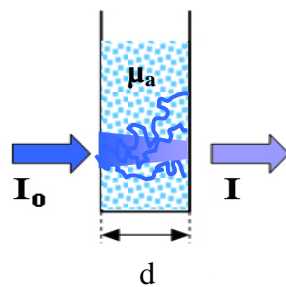


Figure 3.6: Attenuation of light through a scattering medium.

Light scattering in tissue arises due to refractive index mismatch at a cellular (microscopic) scale. The highest contribution to scattering results from refractive index variations between the cell membranes and organelles within each cell. This can be attributed to the fact that they account for a large proportion of the solid content of tissue.

Conversely, red blood cells account for approximately 2% of the solid content and their contribution to scattering is considered to be low (Cope 1991). Scattering is the dominant mechanism in light propagation through tissue. Even for thin, sub-millimetre, sections of tissue, injected photons are likely to be scattered several times before they reach the boundary. As a consequence a coherent, collimated input laser beam will be effectively incoherent and isotropic after traversing a few millimetres of tissue. Even though it has a dominant effect in light attenuation, scattering effects do not change over time and they are thus considered to be negligible when calculating the changes in chromophores concentrations.

Scattering deflects photons from their path, increasing their pathlength when traversing tissue and subsequently increasing their probability of being absorbed (figure 3.6). The scatter coefficient μ_s , for a medium containing a single type of scattering component, represents the probability of a photon being scattered per unit length of travel and can be defined as:

$$I = I_0 \exp(-\mu_s d) \quad (3-8)$$

where I is the non-scattered light after traversing a non-absorbing sample of thickness d . The scattering pathlength, $1/\mu_s$ is the average distance a photon travels between consecutive scattering events. In a simplistic model the path of single photon can be approximated to be the linear combination of scattering and absorption:

$$\mu_t = \mu_s + \mu_a \quad (3-9)$$

The above expression is valid in the ideal case of a single scattering event within a medium. In reality, there are many systems, such biological tissue, for which the assumption that the particles are independent of one another is invalid and multiple scattering becomes important.

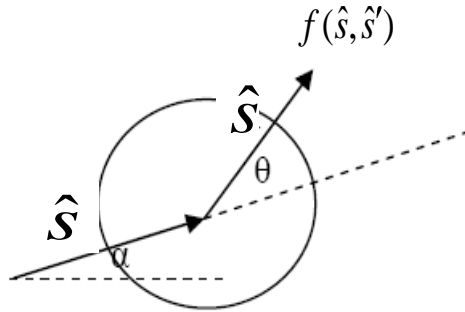


Figure 3.7: Schematic illustrating the scattering phase function $f(\hat{s}, \hat{s}')$

When a photon that is incident along a direction described by the unit vector \hat{s} experiences a scattering event, the angular probability of it being scattered into the direction \hat{s}' is given by the normalised phase function $f(\hat{s}, \hat{s}')$. This is illustrated in figure 3.7. For random, soft tissues it can be assumed that the probability distribution is a function of the angle between the incident and scattered photon only, and does not depend on the angle of incidence relative to the scatterer. Hence, the phase function can be conveniently expressed as a function of the cosine of the scattering

angle $\hat{s} \cdot \hat{s}' = \cos\theta$. When measuring light scattered many times by biological tissue, the precise form of the phase function is less relevant and can be represented by g , the mean cosine of the scattering angles or anisotropy factor:

$$g = \int_{4\pi} p(\theta) \cos\theta d\hat{s} \quad (3-10)$$

For $g = 1$, all radiation travels along the forward incident direction, and for $g = 0$ scattering is entirely isotropic. Scattering in human tissue is strongly forward directed with typically in the range $0.69 \leq g \leq 0.99$ (Cheong et al. 1990). Despite this forward scattering, typical values of the scattering coefficient ensure that photons travelling through a few millimetres of tissue quickly lose all of their directionality and thus become isotropically distributed. Therefore, it is often appropriate to assume isotropic scattering where the scattering coefficient has been reduced by a factor $(1-g)$:

$$\mu'_s = \mu_s(1-g) \quad (3-11)$$

where μ'_s is the transport scattering coefficient or effective number of “isotropic” scatterers per unit length. Hence, the expression for the transport attenuation coefficient becomes:

$$\mu'_t = \mu'_s + \mu_a \quad (3-12)$$

3.1.4 Models of light transport in tissue

The time-dependent diffusion equation is an approximation of the radiative transfer equation (RTE) and is one of the most widely used analytical models of light transport through highly turbid media (Arridge et al. 1992). In the RTE wave phenomena such as polarisation and interference, and particle properties such as inelastic collisions are ignored. Consequently, the RTE is the expression of the balance of energy inside a volume element of the scattering medium. The equation describes the behavior of the energy radiance $I(\vec{r}, t, \hat{s})$, i.e., the energy, moving in the direction \hat{s} , per unit of solid angle, per unit of time, and per unit of area normal to the \hat{s} direction:

$$\frac{1}{c} \frac{\partial I(\vec{r}, t, \hat{s})}{\partial t} + \hat{s} \cdot \nabla I(\vec{r}, t, \hat{s}) + (\mu_a + \mu_s) I(\vec{r}, t, \hat{s}) = \mu_s \int_{4\pi} f(\hat{s}, \hat{s}') I(\vec{r}, t, \hat{s}) d^2 \hat{s} + S(\vec{r}, t, \hat{s}) \quad (3-13)$$

where c is the speed of light inside the diffusing medium, μ_s and μ_a are the scattering and absorption coefficients, respectively. $S(\vec{r}, t, \hat{s})$ is the source term, and $f(\hat{s}, \hat{s}')$ is the scattering phase function. The terms on the left of the RTE represent change of the energy radiance in time, change in energy flow, loss due to absorption and scattering, respectively and they balance with the terms on the right, gain due to scattering sources and gain due to radiation sources.

The RTE is a complicated equation and it is almost impossible to obtain analytical solutions. The diffusion equation

$$\frac{1}{c} \frac{\partial \Phi(\vec{r}, t)}{\partial t} - D \nabla^2 \Phi(\vec{r}, t) + \mu_a \Phi(\vec{r}, t) = S(\vec{r}, t) \quad (3-14)$$

where c is the speed of light in the medium, $\Phi(\vec{r}, t)$ the photon fluence rate,

$$\Phi(\vec{r}, t) = \int_{4\pi} I(\vec{r}, t, \hat{s}) d\hat{s} \quad (3-15)$$

D the diffusion coefficient,

$$D = \frac{1}{3(\mu_a + (1-g)\mu_s)} \quad (3-16)$$

and $S(\vec{r}, t)$ the photon source is an analytical approximation to the RTE used to describe photon migration through highly diffusing media. The approximation is valid when scatter dominates over absorption ($\mu_s \gg \mu_a$) when detected light is effectively diffuse (i.e. when the source detector separation $d \gg 1/\mu_s'$).

Analytical solutions to the diffusion equation exist in the form of Greens functions for various simple geometries including a slab (Contini et al. 1997, Patterson et al. 1989). For semi-infinite half-space geometry, the solution of the diffusion equation for an impulse (δ -function) is expressed as:

$$R(\vec{r}, t) = (4\pi Dc)^{-3/2} \cdot \frac{1}{\mu_s'} \cdot t^{-5/2} \cdot \exp(-\mu_a \cdot c \cdot t) \cdot \exp\left(-\frac{r^2 + \mu_s'^{-2}}{4Dvt}\right) \quad (3-17)$$

where R is the intensity of the reflected light at a distance r , t is the time from the impulse input, μ_a and μ_s' are the absorption and transport scattering coefficients respectively.

3.1.5 The modified Beer-Lambert Law

The attenuation of NIR light in tissue is a result of both scattering and absorption. Scattering causes approximately 80% of the total attenuation and the remaining 20% is due to absorption. Attenuation is defined as the log (base 10) ratio of the incident to remitted (reflected or transmitted) intensities

$$A = \log_{10} \left(\frac{I_0}{I} \right) \quad (3-18)$$

where I_0 is the incident intensity and I reflected or transmitted intensity. Since attenuation is defined in the same way as absorbance, in the case of a non-scattering medium, it can be equated with the Beer-Lambert law (equation 3-6) (Delpy et al. 1988). However, in the case of multiple scattering and absorption, the loss of light due to scattering and the increased optical pathlength as a result of scatter need to be incorporated to the existing attenuation equation. The attenuation in inhomogeneous layers of tissue can be approximated by a modified Beer-Lambert law (MBBL) to include an additional pathlength factor due to the effect of multiple scattering (Delpy et al. 1988):

$$A = \log_{10} \left(\frac{I_0}{I} \right) = \varepsilon \cdot c \cdot d \cdot B + G \quad (3-19)$$

where B is the dimensionless differential pathlength factor (DPF) that accounts for photons extended pathlength and G is the geometry and scattering dependent term that accounts for scattering and other boundary losses. The product ($d \cdot B$) is known as the “differential pathlength” or “effective optical pathlength”, and has the units of length (cm).

The scattering component G is generally unknown and is highly dependent on the measurement geometry making it difficult to obtain absolute value of attenuation as a function of chromophore concentrations. However, under the assumption that G does

not change during the measurement period, it is possible to determine changes in attenuation. Therefore, the MBLL can be expressed as:

$$\Delta A = \Delta C \cdot \varepsilon \cdot d \cdot B \quad (3-20)$$

Consequently, changes of light absorption at multiple wavelengths are mainly due to changes in chromophore concentration. In classical spectroscopy, HbO₂ and HHb are the two common parameters of interest and changes in their concentrations can be obtained by solving equation 3-20 at a minimum of two wavelengths. If the number of wavelengths exceeds the numbers of chromophores under interest, the accuracy of the calculation can be improved by using a multi-linear regression to fit each chromophore spectrum (Cope 1991). Therefore, equation 3-20 can be expanded to account for the number of chromophores (j) measured and to form a set of simultaneous equations:

$$\Delta A_{(i)} = \left(\Delta C_{(i,j)} \cdot \varepsilon_{(i,j)} + \Delta C_{(i,j)} \cdot \varepsilon_{(i,j)} \right) dB \quad (3-21)$$

where i corresponds to each of the wavelengths and j to each of the chromophores. When solving for HbO₂ and HHb the above equation can be rewritten as

$$\Delta A_{(i)} = \left(\Delta HbO_2 \cdot \varepsilon_{HbO_2(i)} + \Delta HHb \cdot \varepsilon_{HHb(i)} \right) dB \quad (3-22)$$

or expressed as a matrix

$$\begin{bmatrix} \Delta HbO_2 \\ \Delta HHb \end{bmatrix} = \begin{bmatrix} \varepsilon_{HbO_2(\lambda_1)} & \varepsilon_{HHb(\lambda_1)} \\ \varepsilon_{HbO_2(\lambda_2)} & \varepsilon_{HHb(\lambda_2)} \end{bmatrix}^{-1} \cdot \begin{bmatrix} \Delta A_{(\lambda_1)} \\ \Delta A_{(\lambda_2)} \end{bmatrix} \cdot dB \quad (3-23)$$

The dimensions of a matrix depend on the number of chromophores of interest.

The MBLL conversion matrix above requires the input of the optical pathlength which is the product of the optode spacing and the Differential pathlength factor (DPF). The DPF is an estimate of the additional distance the photons have to travel due to scattering. In highly scattered media, such as tissue, the DPF is not only strongly dependent upon the scattering coefficient μ_s but is also a weaker function of the absorption coefficient μ_a . The relationship between μ_a and DPF can be demonstrated using theoretical data generated using a diffusion equation model of attenuation as a function of μ_a in a scattering and non-scattering medium (Delpy and Cope 1997). The attenuation of light as a function of μ_a for a certain thickness and for four different scattering coefficients is shown in figure 3.8. The differential pathlength can be determined by the gradient of the slope. The figure shows that the

differential pathlength increases with increasing scattering coefficient and decreases with absorption coefficient. The fact that attenuation is not zero at zero absorption can be accounted by light scattering at the boundary. Since μ_a and μ_s are wavelength dependent, the DPF is also dependent upon the wavelength used. The changes in attenuation caused by changes in chromophore concentrations are small compared to the large constant background and the DPF can therefore be assumed to be constant for a given tissue (Franceschini and Boas 2004). It has been suggested that the absorption dependent variation in optical pathlength in physiological measurements in the NIR region is often lower than 15% with a typical value of approximately 5% (Elwell 1995).

Figure removed for copyright purposes

Figure 3.8: Predicted relationship of attenuation as a function of absorption coefficient for four different values of scattering coefficient (Delpy & Cope 1997)

The optical pathlength of photons can be determined using Time domain systems (TDS) (Schmidt 1999) or Frequency domain systems (FDS) (Duncan et al. 1993). Duncan et al (1995) have reported an age dependence of DPF from a study of 283 subjects and suggested the following relationship (Duncan et al. 1995):

$$DPF_{780} = 5.13 + 0.07A_y^{0.81} \quad (3-24)$$

DPF_{780} is the calculated DPF at 780nm and A_y is the age of the subject in years.

3.2 Types of instrumentation

Several review papers provide a description of the main recently developed NIRS instrumentation (Ferrari et al. 2004, Wolf et al. 2007). In general, near infrared spectroscopy and imaging systems can be categorised into three different measurement techniques: continuous wave (CW), frequency-domain (FD), and time-domain (TD) systems.

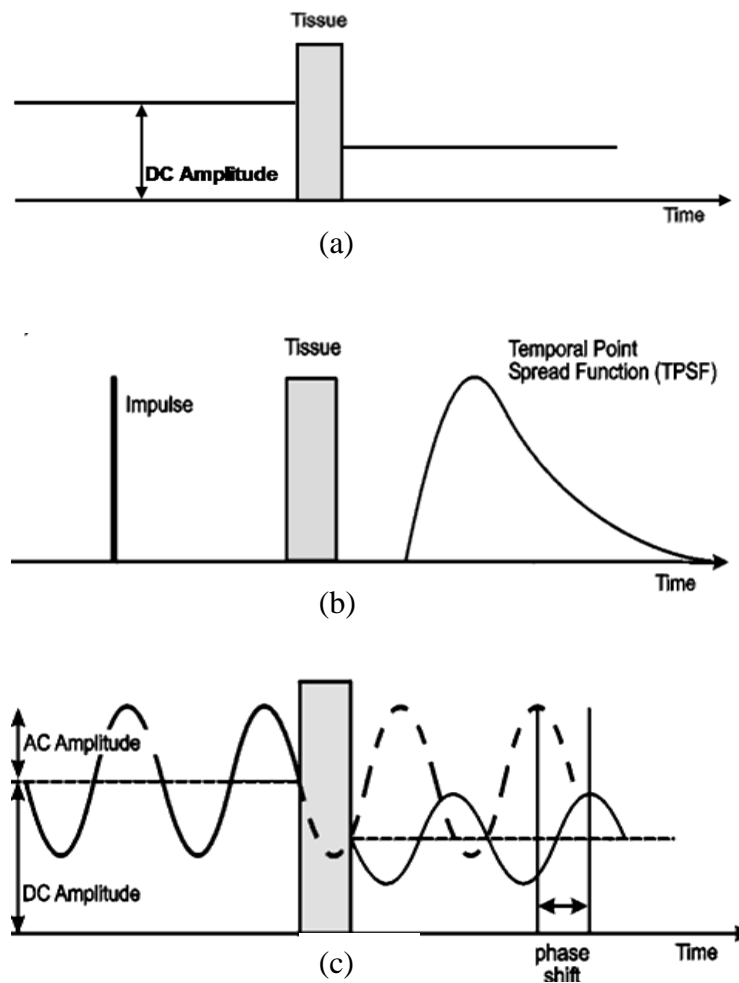


Figure 3.9: Types of measurements techniques used in near infrared spectroscopy systems. (a) Continuous wave measurement technique, (b) Time domain measurement technique, (c) Frequency domain measurement technique (Hebden et al. 1997).

3.2.1 Continuous wave systems

CW systems emit light continuously and provide a simple approach to measure intensity attenuation (figure 3.9a). A drawback of this type of system is the higher sensitivity to tissue immediately below the optodes, due to the so called photon measurement density function (PMDF) which typically has a banana-like shape (Arridge 1995). Measurements of intensity are not sufficient to separate the effects of absorption and scatter at a single wavelength. In general, these systems use the modified Beer-Lambert law to derive the relative changes in haemoglobin concentration and absolute concentration of the chromophores cannot be obtained. Consequently, CW instruments rely on the assumptions that changes in light intensity result from absorption changes in tissue and that scattering remains constant throughout the measurement. Furthermore, the actual photon pathlength cannot be measured using this method but it can be estimated from simulations and earlier studies (see section 3.1.5). However, CW systems are compact, relatively inexpensive and have fast acquisition rate when compared to TD and FD systems. Sections 3.2.4 and 3.2.5 give a detail description of the dual-channel CW NIRO-200 and the multichannel CW ETG-100 systems which are used in the research carried out as part of this PhD.

3.2.2 Time-domain systems

TD systems use laser sources to emit pulses of light, in the order of picoseconds. The emerging intensity is detected as a function of time by fast photon counting detectors. In other words, TD systems measure the times of flight (TOF) of photons through tissue, providing a temporal distribution known as the Temporal Point Spread Function (TPSF) (figure 3.9b). The photon optical pathlength can then be calculated using the mean transit time of the scattered photons and the velocity of light in tissue ($d=vt$). Absolute absorption and scattering coefficients, and therefore absolute haemoglobin concentrations, can be calculated from the TPSF by using a model of the light transport in tissue (Arridge et al. 1992). As one of the early development of a TD system, MONSTIR-UCL is an optical tomography system that uses 32 time-resolved detectors to generate a sequence of 3D brain images from the

light transmitted across layers of tissue (Schmidt 1999). TD systems use expensive electronics and even though their photon counting detectors are highly sensitive detecting the whole TPSF can be slower compared to other techniques.

3.2.3 Frequency Domain systems

FD systems use radio-frequency (few hundreds of MHz) intensity modulated light sources. The detected signal is compared to a reference signal and the phase shift and modulated amplitude decay are recorded, in addition to the attenuated light intensity. FD systems record both the amplitude and phase which allows absorption and scatter to be separated. The phase shift can then be used to measure the optical pathlength, thereby allowing real-time computation of the absolute haemoglobin concentrations. Determination of the DPF in this way allows for an estimate of the depth resolution which is of great relevance in differentiating between extra- and intra-cerebral changes in the measured parameters. These systems are still relatively inexpensive and have fast image acquisition (but lower than CW) they are however limited by the finite number of modulated frequencies which can be used.

3.2.4 Dual-Channel near infrared spectrometer NIRO 200

NIRO 200 (Hamamatsu Photonics KK) is a dual channel, continuous wave near infrared spectrometer which measures changes in HbO₂ and HHb concentrations by utilising the MBL. Furthermore, the NIRO 200 consists of PIN silicon photodiode segmented into two and uses spatially resolved spectroscopy (SRS), described in section 4.2.1, to give an absolute value of tissue oxygen saturation as a percentage, namely Tissue Oxygenation Index (TOI) (Al Rawi et al. 2001, Suzuki et al. 1999). TOI is the ratio of oxygenated to total haemoglobin concentrations.

This NIRS system uses laser diodes as light sources emitting at 3 wavelengths (778, 809 and 850nm). Light from the sources is sequentially pulsed and emitted through optical fibres which are built into the probe holder. It penetrates and propagates through tissue, where it gets absorbed and diffused. It is then detected as a function of distance by the segmented photodiode (figure 3.10). The distance

between the source and the midpoint of the detector is 4cm. Other commercially available single or dual- channel CW systems are listed in Table 1.

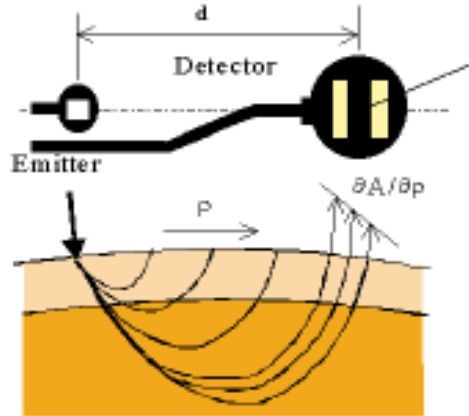


Figure 3.10: NIRO 200 probe schematic (modified from (Suzuki et al.1999)).

Table 3.1: List of main commercially available CW single or dual channel near infrared spectroscopy systems

Name of instrument	Company	Webside
FORE-SIGHT	Casmed, USA	www.casmed.com
INVOS 5100	Somanetics, USA	www.somanetics.com
NIRO-300	Hamamatsu, Japan	www.hamamatsu.com
NIRO-200	Hamamatsu, Japan	www.hamamatsu.com
NIRO-100	Hamamatsu, Japan	www.hamamatsu.com
NIRO-100NX	Hamamatsu, Japan	www.hamamatsu.com
OM-220	Shimadzu, Japan	www.shimadzu.co.jp
EQUANOX	NONIN, USA	www.nonin.com
NIMO	NIROX, Italy	www.nirox.it
ODISsey	ViOptix, Inc., USA	www.viOptix.com

3.2.4.1 Spatially Resolved Spectroscopy

Spatially resolved spectroscopy (SRS) is a NIRS technique used to derive an absolute value for mixed venous oxygen saturation. The technique is based in the solution of the diffusion approximation equation for semi-infinite half-space geometry (equation 3-17). For a continuous wave (cw) system, the light intensity,

$I(\vec{r})$, can be expressed as the integral of the reflected intensity, $R(\vec{r}, t)$, over time. Hence, light attenuation is defined as the negative log of $I(\vec{r})$:

$$A(\vec{r}) = -\log_{10} \int_0^{\infty} R(\vec{r}, t) dt \quad (3-25)$$

By differentiating $A(\vec{r})$ with respect to \vec{r} and substituting for $R(\vec{r}, t)$ in equation 3-17 we obtain:

$$\frac{\partial A}{\partial r} = \frac{1}{\ln 10} \cdot \left(\sqrt{3 \cdot \mu_a \cdot \mu_s'} + \frac{2}{r} \right) \quad (3-26)$$

By measuring $\partial A / \partial r$ at different wavelengths, we can obtain a value for the product $\mu_a \cdot \mu_s'$ using the above equation. If we assume that μ_s' is constant with respect to wavelength in the NIR region, then we can replace μ_s' with a constant k and obtain a value for the relative absorption coefficients $k\mu_a$. However, in reality μ_s' decreases slightly with respect to wavelength λ (Matcher et al. 1995) and an additional term can be added to express μ_s' :

$$\mu_s' = k(1 - h\lambda) \quad (3-27)$$

where h is the normalized slope of μ_s' with wavelength λ , which is fairly constant among tissue types and subjects (Matcher et al. 1996, Suzuki et al. 1999). Therefore, equation 3-26 can be rewritten as:

$$k\mu_{a(\lambda)} = \frac{1}{3(1-h\lambda)} \cdot \left(\ln 10 \frac{\partial A(\lambda)}{\partial r} - \frac{2}{r} \right)^2 \quad (3-28)$$

Substituting equation 3-4 in the above expression we get:

$$\begin{bmatrix} kHbO_2 \\ kHHb \end{bmatrix} = \mathbf{\mu}_{i,j}^{-1} \begin{bmatrix} k\mu_a(\lambda_1) \\ k\mu_a(\lambda_2) \\ k\mu_a(\lambda_3) \end{bmatrix} \quad (3-29)$$

where $\lambda_1, \lambda_2, \lambda_3$ are the 3 wavelengths of the system. If we assume k is constant then an index, namely tissue oxygenation index (TOI) representing the ration between oxygenated haemoglobin and total haemoglobin can be obtained:

$$TOI = \frac{kHbO_2}{kHbO_2 + kHHb} \times 100 \quad (3-30)$$

3.2.4.2 Tissue Oxygenation Index (TOI)

As described in the section above TOI refers to the ratio between the concentration of oxy-haemoglobin and the concentration of total haemoglobin in the tissue illuminated by the source of the probe. However, the area under the field of view is a multi-compartmental system consisting of arteries, arterioles, capillaries, venules and veins with a typical arterial: venous volume ratio of 1:3 (25% arterial and 75% venous) (An and Lin 2002). Assuming that $[HbO_2]_{art}$ and $[HbO_2]_{ven}$ is the oxyhaemoglobin concentration (in mmolar) of the arterial and venous compartments, respectively, and V_a and V_v the arterial and venous blood volume per unit mass of tissue (in L/g), respectively, then the total oxygenated haemoglobin per unit mass of tissue (in mmoles/g) can be represented by (Tachtsidis 2005):

$$[HbO_2] = V_a [HbO_2]_{art} + V_v [HbO_2]_{ven} \quad (3-31)$$

and the total haemoglobin per unit mass of tissue (in mmoles/g) by:

$$[HbT] = (Hb \cdot 10^2) \cdot MW_{Hb} \cdot (V_a + V_v) \quad (3-32)$$

where Hb is the concentration of haemoglobin in blood (in g/dL), assumed constant in all compartments and MW_{Hb} is the molecular weight of haemoglobin (mmoles/g). Then, by substituting equations (3-31) and (3-32) in the TOI expression we get:

$$TOI = \frac{\frac{V_a}{V_v} [HbO_2]_{art} + [HbO_2]_{ven}}{(Hb \cdot 10^2) \cdot MW_{Hb} (1 + \frac{V_a}{V_v})} \times 100 \% \quad (3-33)$$

Therefore, TOI depends on both the arterial:venous volume ratio and their relative oxygenations. It is, however, more sensitive to venous oxygenation than arterial oxygenation. By considering the definitions of arterial oxygen saturation ($S_aO_2 = [HbO_2]_{art} / [HbT]_{art}$) and venous oxygen saturation ($S_vO_2 = [HbO_2]_{ven} / [HbT]_{ven}$), equation (3-33) can be rewritten as:

$$TOI = S_aO_2 \cdot \frac{V_a}{V_a + V_v} + S_vO_2 \cdot \frac{V_v}{V_a + V_v} \quad (3-34)$$

Considering the definition of the Fick equation (Purves 1972):

$$S_vO_2 = S_aO_2 - \frac{CMRO_2}{k \cdot CBF \cdot [Hb \cdot 10^{-2}]} \quad (3-35)$$

where $CMRO_2$ is the oxygen consumption (in ml of Oxygen/min), k is the oxygen combining power of Hb (~1.306 ml of Oxygen/g of Hb) and CBF is cerebral blood flow (in ml/min) and Hb is the haemoglobin (in g of Hb/dL of blood), equation (3-34) becomes (Tachtsidis et al. 2008):

$$TOI = SaO_2 - \frac{V_v}{V_v + V_a} \cdot \frac{CMRO_2}{k \cdot CBF \cdot [Hb \cdot 10^{-2}]} \times 100 \% \quad (3-36)$$

The above equation shows that TOI depends directly on the arterial:venous volume ratio and $CMRO_2$, and indirectly on CBF. Therefore an increase in TOI can be caused by: (i) venous constriction resulting from minor decrease in venous blood pressure (BP), (ii) arterial dilation caused by a minor decrease in arterial blood pressure (ABP) or a rise in arterial partial pressure of carbon dioxide (pCO₂), (iii) a decrease in $CMRO_2$ or (iv) an increase in CBF. Conversely, a decrease in TOI can be caused by: (i) venous dilation resulting from minor increase in venous BP, (ii) arterial vasoconstriction caused by minor increase in ABP or decrease in pCO₂, (iii) an increase in $CMRO_2$ or (iv) a decrease in CBF.

3.2.5 Multichannel Optical topography ETG-100

The Hitachi ETG-100 was the first commercial optical topography system. It was mainly designed for functional activation studies, and it has been used to study the activity of healthy brain and cerebral pathologies in adults, infants and newborns (Koizumi et al 2005; Koizumi et al 2003). The Hitachi ETG-100 system has a maximum number of 18 optodes, 10 sources and 8 detectors. It uses laser diodes emitting at 2 wavelengths in the NIR region, 780 and 830 nm, and avalanche photodiodes as detectors (Kawaguchi et al. 2001, Yamashita et al. 1999). The power of each laser diode is fixed to about 1.5 mW for each wavelength. A schematic diagram of the system configuration is shown in figure 3.11. Each laser diode is modulated at a different frequency between 1 to 8.7 kHz (chosen as to avoid any overlap in their harmonic frequencies). NIR light at the two different wavelengths reaches the skin of the scalp through a set of optical fibres. The reflected light is transmitted via optical fibres to the detecting photodiodes. Frequency lock-in amplifiers are used to distinguish signals from the different source-detector pairs. Each lock-in amplifier is fed with a reference signal locked to the modulation

frequency of the appropriate light source. This method, known as frequency multiplexing (FM), allows all of the sources to be illuminated simultaneously, so that an image can be obtained more quickly. An analogue-to-digital converter (ADC) is used to digitise the signal which can be shown in the monitor of the incorporated PC in real time. A disadvantage of this system is the relatively short monitoring period which depends on the system's capacity depending on the data acquisition rate. A sampling period of 0.1s allows for a monitoring period of 50min which might be sufficient for functional activation studies but can be insufficient for clinical applications.

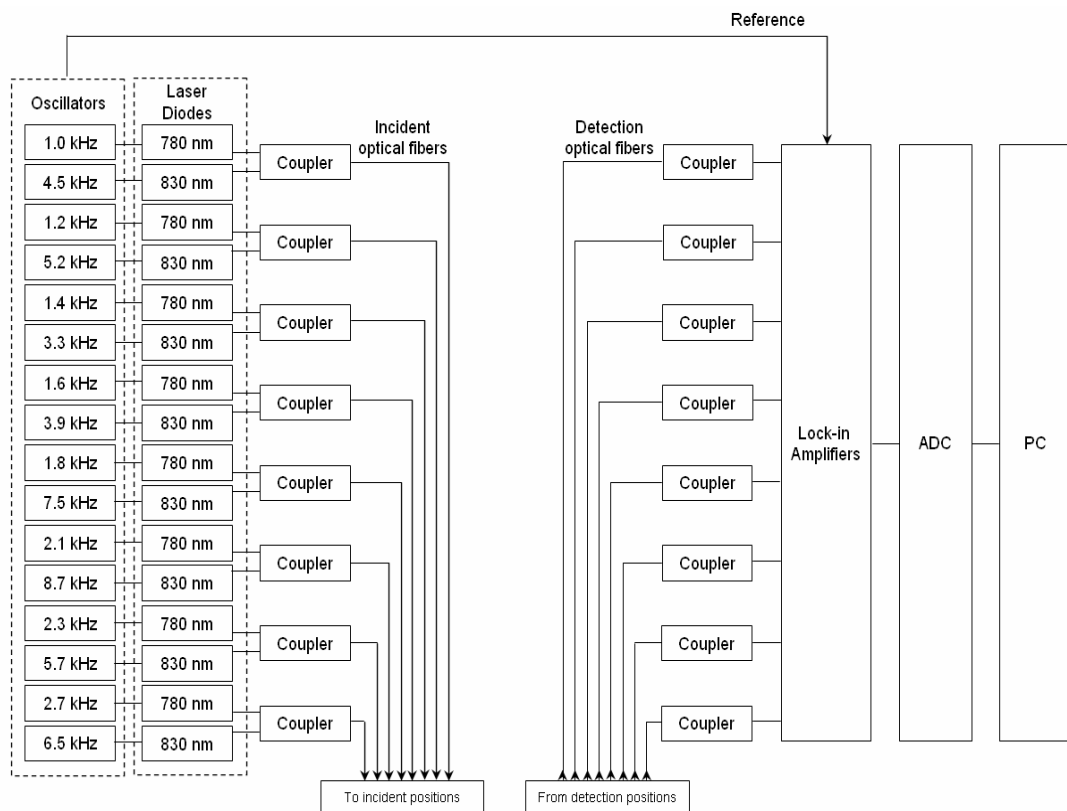


Figure 3.11: Schematic diagram of the lock in amplifier system used in the Hitachi ETG-100 system (Yamashita et al. 1999)

The ETG-100 optical topography (OT) system uses the continuous wavelength (CW) approach to acquire multi-site HbO₂, HHb and HbT concentrations simultaneously (Kawaguchi et al. 2001, Yamashita et al. 1999). The multichannel system does not give information on tissue oxygen saturation. Three standard measurement channel configurations are provided: A two-piece 3x3 configuration

usually used for bilateral monitoring, a 4x4 and a 3x5 configurations. Figure 3.12 illustrates the 3x3 configuration. The illumination (in red) and detection (in blue) fibres are arranged alternately in a lattice configuration to maximise the channel density with a fixed separation distance of 30 mm. This configuration allows a maximum of 24 different measurement locations covering an estimated scalp area of 6 by 6 cm on each hemisphere.

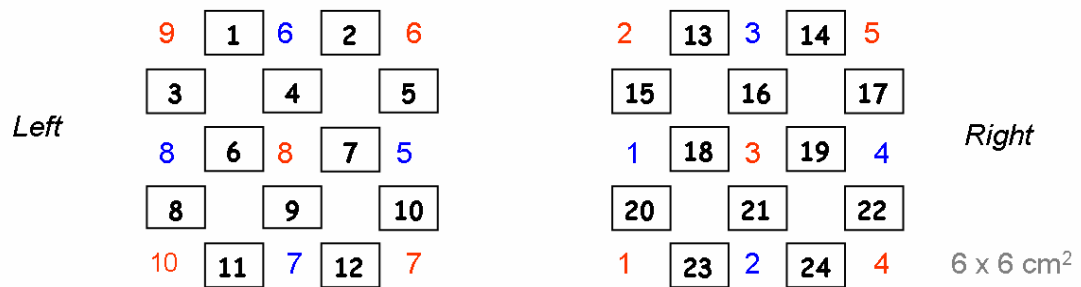


Figure 3.12: ETG-100 OT 3x3 configurations for bilateral monitoring. Sources are shown in red, detectors in blue and the channels are shown in squares.

The more recent optical topography systems developed by Hitachi use a greater number of source-detector pairs and can obtain measurements from 48 and 120 channels, ETG-4000 and ETG-7000, respectively. A more important advantage of these systems over the ETG-100 system is that the intensities of the lasers can be controlled automatically.

3.2.5.1 Other multichannel optical systems

Various multichannel optical systems for have been developed in various research laboratories. Table 2 lists main multichannel optical topography and tomography systems available commercially and developed prototypes. Optical topography enables two dimensional mapping of the brain activity from the light reflectance technique while optical tomography employs the light transmittance technique to interrogate deep brain tissue and to generate series of brain-slice images (i.e. tomographic map).

A CW optical topography system was developed at University College London that employs 32 laser diodes (16 at 770nm and 16 at 850nm) and 16 avalanche

photodiodes. The system uses software incorporating fast Fourier transforms to demultiplex multiple source signals which are modulated at different frequencies in parallel. This allows for a more flexible, smaller, and less complex system than is achievable using traditional hardware demodulation techniques, such as lock-in amplifiers. A range of different optical fiber arrays can be used with only minor changes being needed to the software. Furthermore, the probe array of this system is comprised of multiple source-detector separations. By using multiple distances a range of depths can be covered resulting in improved depth resolution and spatial accuracy. In addition to the frequency multiplexed scheme, the system can also operate in a time multiplexed scheme, which involves illuminating individual laser sources in turn for a short period. Although this has the disadvantage of reducing the image acquisition rate, the overall signal to noise ratio of the data is increased as there is less background light contributing shot noise to the measurement.

Similar to the UCL optical topography system, the CW4 and CW5 systems (developed at Photon Migration Lab, Massachusetts General Hospital and TechEn Inc.) are frequency multiplexed where the detected signals are demultiplexed using Fourier transformations.

Among the currently commercially available multichannel optical systems are the Dynot (NIRx Medical technologies) and the Imagent (ISS, Inc.). The NIRx system uses a time multiplexed scheme, where the sources are illuminated sequentially, which decreases the frame rate but has the advantage of increasing the dynamic range. The ISS system is unique in quantifying the optical properties of biological tissues since it employs the FD technique. Another commercially available system is the optical multichannel monitoring (OMM) system, developed by Shimadzu Corporation. This is a TD system with up to 16 light sources and 16 detectors and an expanded detection dynamic range for measurements with various transmitter-receiver distances. Simultaneous multi-distance measurements are useful to distinguish depth resolution.

Table 3.2: List of main multichannel optical systems

	Name of instrument	Type	parameters measured	max. # of channels	technical referene	company/institution (website)
Topography	ETG 100	CW	HbO ₂ , HHb, HbT (changes)	24	(Yamashita et al. 1999)	Hitachi, Japan (www.hitachi.med)
	ETG-4000	CW	HbO ₂ , HHb, HbT (changes)	52	Plichta et al 2006	Hitachi, Japan (www.hitachi.med)
	ETG-7000	CW	HbO ₂ , HHb, HbT (changes)	120	Koizumi et al 2003	Hitachi, Japan (www.hitachi.med)
		CW	HbO ₂ , HHb, HbT (changes)	20	(Everdell et al. 2005)	UCL, London (www.
	Imagent	FDS	HbO ₂ , HHb, HbT (absolute value), SO ₂ , μ a, μ s, DPF	128	Zhang et al 2005	ISS, USA (www.iss.com) Artinis, The Netherlands
	OXYMON	CW	HbO ₂ , HHb, HbT (changes)	96	van der Sluijs et al 1998	(www.artinis.com)
Tomography	Dynot	CW	HbO ₂ , HHb, HbT (changes)	32	Schmitz et al 2005	NIRx, USA (www.nirx.net)
	CW4, CW5	CW	HbO ₂ , HHb, HbT (changes)	4 or 58	(Franceschini et al. 2006)	TechEn, Inc., USA (www.nirsoptix.com)
	MONSTIR	TDS	HbO ₂ , HHb, HbT (absolute value), SO ₂ , μ a, μ s, DPF	32	Schmitz et al 2000	UCL, London (www.
	OMM-2001	TDS	HbO ₂ , HHb, HbT (absolute value), SO ₂ , μ a, μ s, DPF	42	(Oda et al. 2003)	Shimadzu, Japan (www.med.shimadzu.co.jp)
	OMM-3000	TDS	HbO ₂ , HHb, HbT (absolute value), SO ₂ , μ a, μ s, DPF	64		Shimadzu, Japan (www.med.shimadzu.co.jp)

Chapter 4

EXTRACORPOREAL CIRCULATION IN INFANTS AND CHILDREN

4.1 Extracorporeal membrane oxygenation (ECMO)

The history and evolution of paediatric cardiac mechanical support is interrelated to the history of cardiopulmonary bypass CPB. In CPB the heart/lung machine is used in the operating room (OR) to provide total support of the heart and lungs. However, when the heart/lung machine is used with extrathoracic cannulation for respiratory and/or cardiac support, the technique is called extracorporeal membrane oxygenation (ECMO).

Reports of the first patients supported for several days by bedside extracorporeal devices began to appear in the literature in the 1970s. Early trials of ECMO were marked by both success and failure. In 1976 Bartlett and coworkers (Bartlett et al. 1976) reported the first neonatal ECMO survivor, who was appropriately named “Esperanza” (“Hope”). This marked the new era of bedside CPB and presented the opportunity to treat intractable cardiorespiratory failure in a population with little hope of survival.

The indications for paediatric ECMO support can be divided into two groups, (a) patients with cardiac failure following open heart surgery and (b) patients with respiratory and/or cardiac failure due to a spectrum of diseases, including myocarditis, cardiomyopathy, arrhythmia, pulmonary hypertension, meconium aspiration syndrome, congenital diaphragmatic hernia (Karl et al. 2006). Therefore, there are two principal modes of ECMO support: veno-arterial (VA) ECMO bypasses both the heart and lungs and is thus the appropriate type of ECMO for patients with circulatory failure, and veno-venous (VV) ECMO provides only respiratory support (Karimova and Goldman 2006). Survival to discharge rates of patients treated with ECMO for short-term cardiac support are in the range 40-80%, depending on the patient's diagnosis and underlying pathophysiology (Zwischenberger and Barlett 2005).

4.1.1 The ECMO circuit

Figure 4.1 shows a typical ECMO circuit. The circuit comprises of venous (1) and arterial (2) cannulae, pump (3), membrane oxygenator (4), heat exchanger (5), bridge (6), venous saturation probe (7), and flow and arterial saturation probe (8). In VA ECMO surgeons insert cannulae in the right common carotid artery (RCCA) and right internal jugular vein (RIJV). Venous blood drains from the patient by gravity and is then pumped through a membrane oxygenator for O₂ and CO₂ exchange. The oxygenated blood then passes through a countercurrent heat exchanger, where it is warmed to the desired temperature before emptying from the arterial cannula into the aorta. The ECMO bridge allows circulation when the patient is clamed off ECMO (i.e. arterial and venous cannulae are clamped off). Venous and arterial saturation as well as flow and hematocrit are continuously monitored by the probes on the venous and arterial cannulae. VV ECMO bypasses only the lungs and in this case the patient has only one double lumen cannula inserted into the RIJV. ECMO circuits may incorporate either a roller head pump or a centrifugal pump. A two headed roller pump compresses the cannula, thereby pushing the blood through the circuit, and a centrifugal pump uses a high speed rotating device that pulls the blood into the pump and then accelerates it radially outwards.

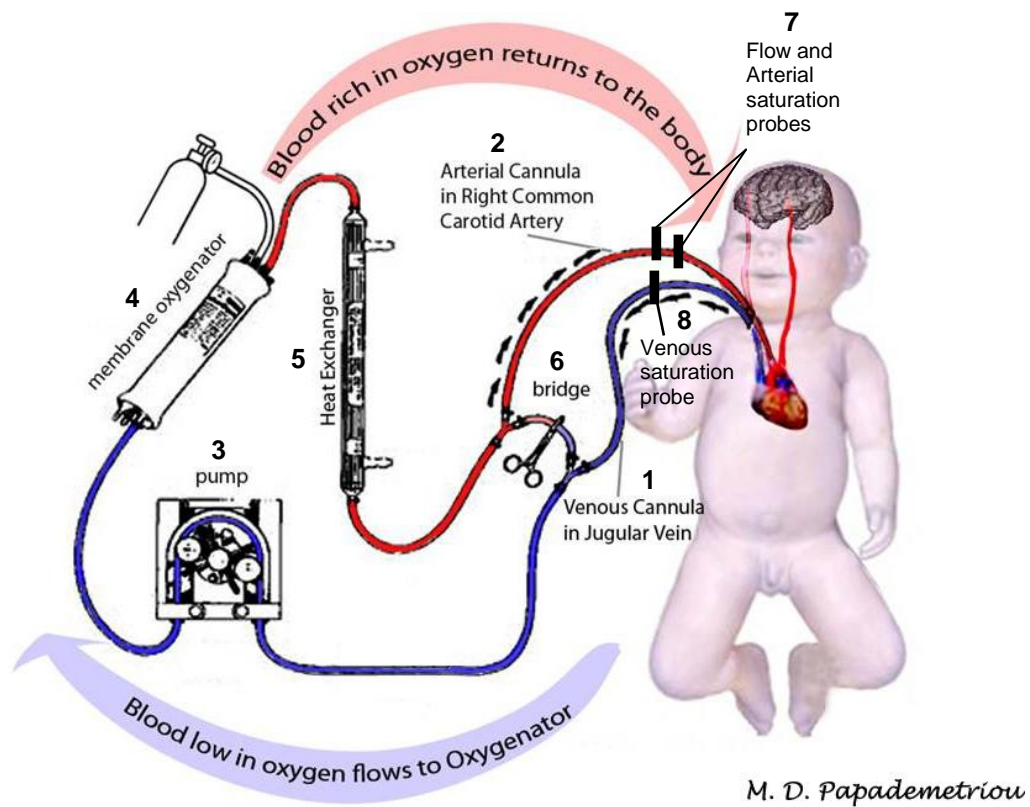


Figure 4.1: Illustration of the ECMO circuit. Deoxygenated blood leaves the patient through the venous cannula inserted in the jugular vein (1), passes through the membrane oxygenator (4) where it gets oxygenated and flows back to the patient through the arterial cannula which is inserted in the right common carotid artery (2).

4.1.2 Physiology of ECMO

4.1.2.1 Cannulation

In contrast to conventional CPB, ECMO cannulation takes place in the intensive care unit (ICU). In VA ECMO the cannulation procedure begins by the surgeon dissecting the right side of the neck to expose RCCA and RIJV. After exposing the RCCA the surgeon pulls the artery out and places clamps distal and proximal to the right atrium. It then ligates the artery and inserts the arterial cannula securing it with stitches. The same thing is then carried out with the RIJV. The clamps are then removed first from the RCCA and then from RIJV and the patient is on ECMO.

4.1.2.2 Oxygen delivery in ECMO

During extracorporeal life support (ECLS), oxygen delivery is controlled by the combination of blood oxygenation in the membrane lung, flow through the extracorporeal circuit, oxygen uptake through the native lung and CO through the native heart.

The size of the ECMO circuit and extracorporeal flow rate are set so that there will be no gas exchange across the native lung. Under this assumption, in VV bypass, PaO₂ and oxygen saturation will be identical to the values in the mixed venous blood. Because of the nature of VV bypass, this saturation will never be higher than 95% and typically will be closer to 80%. Improvement in native lung function results in increasing arterial oxygenation and the amount of native lung function during VV bypass can be identified as the difference between venous and arterial saturation.

In VA bypass, the perfusate blood is typically 100% saturated. When the lung is not functioning the left ventricular ejected blood is identical to the right atrial blood, typically with saturation of 75%. The systemic oxygen content is determined by the following formula: Systemic O₂ content = Perfusate O₂ content x (ECC flow/Total flow) + LV blood O₂ content x (lung flow/total flow), where ECC is the extracorporeal circuit flow and LV is left ventricle (Bartlett et al 2005). Thus, during VA bypass, an increase in systemic PaO₂ may be indicative of improving lung function at constant flows, decreasing native CO at constant extracorporeal flow, or increasing extracorporeal flow at constant native CO.

4.1.2.3 Blood flow and oxygenation

The total systemic arterial blood flow is the sum of ECMO pump output and left heart output. ECMO pump output is increased to maintain adequate mean arterial pressure (>40 mm Hg for the infant) and mixed venous saturation (SvO₂>60%) (Barlett 2006). Similarly, the arterial oxygen saturation is the weighted average of ECMO blood and left heart blood saturations. In the beginning of the ECMO treatment, when the patient's lungs and/or heart are at their most critical state, ECMO pump flow is the principal, or the only, component contributing to systemic

arterial flow and oxygen saturation. Later in the course, the patient's lungs and/or heart start recovering, taking over the ECMO pump, thus the left heart blood is assumed to contribute to a greater proportion in the arterial blood flow. This is reflected in an improving arterial wave contour on the monitor.

Figure removed for copyright purposes

Figure 4.2: Haemodynamics and gas exchange changes during VA ECMO (Barlett 2006).

Figure 4.2 shows the physiology in haemodynamics and gas exchange during a VA bypass. This example depicts trends in oxygen consumption (VO_2), arterial saturation (SaO_2) and venous saturation (SvO_2) when several changes occur in the ECMO circuit (ECC flow), such as flow reduction, blood transfusion, oxygenator failure, weaning (Barlett 2006). It also shows what happens to these trends when the patient undergoes clinical conditions, such as seizures and bleeding. Initiation of ECMO is associated with an increase in SaO_2 and SvO_2 . ECMO flow can then be adjusted accordingly so as to maintain SaO_2 over 95% and SvO_2 around 75%. In this case, a decrease in flow is associated with a decrease in SvO_2 . Seizures are associated with an increase in VO_2 which causes a decrease in SvO_2 , due to an increase in oxygen extraction. Bleeding is linked with a decrease in venous return and therefore a decrease in systemic blood flow, projected as a decrease in SvO_2 . Transfusion allows return of flow to normal. However, if excess transfusion volume is given at a constant ECMO flow, the extra blood volume results in an increase in patient lung flow, causing systemic hypoxemia (decrease in SaO_2) when the lungs are not functioning properly, followed by venous hypoxemia. An increase in ECMO flow would compensate for this. In the case of oxygenator failure, a drop in arterial

and then venous saturation is expected. Weaning from ECMO involves the progressive decrease in ECMO flow while maintaining normal arterial and venous saturation during constant VO_2 .

Figure removed for copyright purposes

Figure 4.3: Haemodynamics and gas exchange changes during VV ECMO (Barlett 2006).

Similarly, figure 4.3 shows haemodynamic and gas exchange changes for VV ECMO cannulation during the same events as VA bypass above. Unlike VA bypass, SaO_2 and SvO_2 are nearly the same during VV bypass. Changes related to increased VO_2 , bleeding and transfusion reflect SaO_2 and SvO_2 in the same fashion. Weaning from VV ECMO follows the same pattern as VA ECMO.

4.1.2.4 Pulsatility in blood flow

The effect of VA on systemic perfusion is reflected in the pulse contour and pulse pressure. The extracorporeal pump creates a flow that is essentially non-pulsatile. Consequently, as more blood is routed through the extracorporeal circuit, the systemic arterial pulse contour becomes flatter, then intermittent, and then stops all together when total bypass is reached. Typically, VA ECLS is run at about 80% of normal resting CO, which allows 20% or more of the blood to pass through the lungs and left heart, resulting in a diminished but discernible pulse contour. The discussion concerning pulsatile and non-pulsatile flow has been the subject of much research. As long as total blood flow and is adequate and mean arterial pressure remains within the cerebral autoregulatory range (see chapter 2), fluctuations in the

pump flow are not physiologically important and do not result in significant changes in cerebral blood flow.

4.1.2.5 Weaning from ECMO

One of the greatest challenges of cardiac ECMO is determining the point of which there has been adequate ventricular recovery to allow for a trial of weaning from mechanical support.

During weaning the ECMO flow is gradually reduced over a period of 1-2 hours until the lowest safe flow is achieved. If flow reduction does not cause inadequate mean arterial pressure and/or oxygen saturation, the arterial and venous cannulae are clamped off and the pump is left to re-circulate via the bridge. The patient is considered to be off ECMO support and is usually tried off ECMO for a period of 1-3 hours before a decision about decannulation is made. During this time the cannulae are flushed regularly, by removing the clamps and allowing blood to be flushed in the patient. This is done in order to avoid clotting in the cannulae. If the patient is deemed to have failed the trial off ECMO, as indicated by unstable haemodynamics and/or signs of inadequate tissue oxygen delivery, then full ECMO support is recommenced.

4.2 Cardiopulmonary bypass for repair of congenital heart defects

Cardiopulmonary bypass (CPB) is a form of extracorporeal circulation consisting primarily of a pump, a venous reservoir and an oxygenator. During CPB, deoxygenated venous blood returning from the body to the heart is drained out of the circulation via venous cannulae into the artificial extracorporeal circuit. Typically, the blood collects in a reservoir, from which it is pumped through an oxygenator and heat exchanger before being returned to the patient, usually via an arterial cannula placed in the ascending aorta, thereby eliminating the need for blood to go through the heart or lungs (Jones and Elliott 2004). The overall principle and objective is to

provide a bloodless operative field enabling good surgical exposure with prevention of end organ function. The safe conduct of CPB in the neonate and infant requires a comprehensive understanding of the physiologic alterations associated with CPB. These variables include circuit design, hemodilution, altered perfusion, degree of hypothermia, acid-base management.

4.2.1 Congenital cardiovascular Defects

Congenital heart defects result from abnormal cardiac development or inappropriate connections between the heart and major arteries and veins. Heart defects are among the most common birth defects and are the leading cause of birth defect-related deaths. They can be put into four major categories:

- i) Septal defects: defects in the interatrial septum (Arterial septal defects (ASD)) or the interventricular septum (ventricular septal defects (VSD)), allowing blood to flow from the left side of the heart to the right, reducing the heart's efficiency.
- ii) Obstruction defects: Obstruction defects occur when heart valves, arteries, or veins are abnormally narrow or blocked. Common obstruction defects include pulmonary valve stenosis, aortic valve stenosis, and coarctation of the aorta.
- iii) Cyanosis: called such because they result in cyanosis, a bluish-grey discoloration of the skin due to a lack of oxygen in the body. Such defects include persistent truncus arteriosus, total anomalous pulmonary venous connection, tetralogy of Fallot, transposition of the great vessels, and tricuspid atresia.
- iv) Hypoplasia: failure of the right ventricle or the left ventricle to develop adequately, leaving only one side of the heart capable of pumping blood to the body and lungs. Hypoplasia of the heart is rare but is the most serious form of CHD; it is called hypoplastic left heart syndrome when it affects the left side of the heart and hypoplastic right heart syndrome when it affects the right side of the heart.

For a more detail description of CHD the reader is referred to (Lissauer and Clayden 2001). Congenital heart diseases can be surgically corrected by placing the patient on cardiopulmonary bypass (CPB). Recovery from cardiac surgery may include placing the patient on extracorporeal membrane oxygenation (ECMO). The most serious congenital heart defects associated with neurodevelopmental dysfunction are transposition of the great arteries (TGA) and hypoplastic left heart syndrome (HLHS). Treatments of these two congenital conditions involve complicate surgical techniques which include hypothermia and circulatory arrest and can potentially lead to neurological complications.

4.2.1.2 Hypothermia

The principle clinical effect of hypothermia is the reduction in metabolic rate and molecular movement (Jaggers and Ungerleider 2006). Figure 2.9 shows the relationship between whole body oxygen consumption and body temperature. As body temperature decreases both basal and functional cellular metabolism are reduced. Therefore, hypothermia allows a reduction in flow rates and facilitates surgical exposure by reducing the amount of blood returning to the heart through collateral vessels.

Three methods of CPB are used: (1) mild hypothermia (30 to 34 °C), (2) moderate hypothermia (25 to 30°C), and (3) deep hypothermia (15 to 22°C), depending on the needs of low flow and the duration of aortic cross-clamp (Jones & Elliott 2004). Recommendations for optimal pump flow rates for children are based on the body surface area and maintaining efficient organ perfusion as determined by arterial blood gases, acid-base balance, and whole body oxygen consumption during CPB. Normothermic flow rates for children are based on body weight (table 2.1).

Also, the use of hypothermia is mandatory for brain protection when prolonged periods of circulatory arrest are utilized. In the brain the most important determinant of cerebral blood flow (CBF) is cerebral metabolic activity ($CMRO_2$) with regional and total CBF increasing or decreasing to match fluctuations in the metabolic demands of a region. Cerebral metabolism is reduced 5-7% for each degree Celsius reduction in temperature with a smaller but corresponding reduction in CBF (Stump et al. 1999).

Figure removed for copyright purposes

Figure 4.4: Whole body oxygen Consumption as a function of temperature (Jaggers & Ungerleider 2006)

While in moderate hypothermia cerebral autoregulation is preserved, during deep hypothermic conditions autoregulation of cerebral blood flow is lost and cerebral blood flow seems to be more directly correlated with mean arterial blood pressure. At deep hypothermia, cellular metabolism is so low and membrane fluidity is reduced to such a large extent that cellular basal metabolic needs and cellular membrane integrity can be maintained for a relatively long period of time and this is probably why the clinical outcomes following periods of deep hypothermia circulatory arrest (DHCA) seem to be unaffected by arrest durations below 45 min at 18 °C (Wypij et al. 2003). The maximum duration of DHCA is unknown. It is logical that the period should be as short as possible but long enough to accomplish satisfactory surgical repair. Increased periods of DHCA are associated with increased brain injury (Jones & Elliott 2004).

Neurologic injury in Cardiopulmonary bypass for congenital heart defects

The neonate or infant with congenital heart disease constitutes a patient at risk for neurologic impairment. This risk seems to have three elements: (1) pre-existing risk associated with various congenital heart lesions, (2) injury induced by CPB and the various CPB strategies that can be employed by the surgical team, and (3) injury sustained during the “vulnerable” period after exposure to CPB.

In children, the most prominent acute complications are focal and generalized seizures, intracranial haemorrhage, and spinal cord infarction. The chronic or late sequelae of cardiac surgery include learning disorders, cerebral palsy, gait disorders, seizures, and learning disorders (Tasker 2006). Global cerebral hypoperfusion may result from a variety of problems, such as incorrect cannulae placement, prolonged cardiopulmonary bypass, or inadequate perfusion pressure in the perioperative period.

The most effective means of protecting the brain from cardiopulmonary bypass induced injury is hypothermia. The periods or events of particular concern, when the brain is at increased risk of neurologic insult, are the active cooling period; the period of low-flow cardiopulmonary bypass or total circulatory arrest; and the period during weaning and separation from cardiopulmonary bypass. Deep hypothermic circulatory arrest can have significant effects on intracranial haemodynamics via effects on cerebral blood flow and intracranial pressure. These changes may occur both during the surgical procedure and for a significant period after surgery, with the consequence of changes or disruption in normal cerebral oxygenation and metabolism, and ensuing ischemia (Greeley et al. 1989, Taylor et al. 1992). In comparison with deep hypothermic circulatory arrest, low-flow cardiopulmonary bypass may, theoretically, maintain some cerebral blood flow (Bellinger et al. 2003). However, at the extreme of the low-flow state, the effects of the two techniques on cerebral blood flow are indistinguishable (Tasker 2006).

4.3 Neurological morbidity on ECMO

Since the first use in neonates in 1974, extracorporeal membrane oxygenation (ECMO) has been a life-saving technology for newborns. Most patients are placed on ECMO due to severe hypoxemia from respiratory failure or decreased oxygen delivery from cardiac failure. ECMO has been used to treat a variety of cardio-respiratory problems, including meconium aspiration syndrome (MAS), persistent pulmonary hypertension of the neonate (PPHN), congenital diaphragmatic hernia (CDH), sepsis, and cardiac anomalies. Severe respiratory failure has been a major cause for return hospitalization and late deaths, but mortality has remained specific to

the primary diagnosis prior to ECMO. For example, ECMO patients with the diagnosis of CDH or total anomalous pulmonary venous return (TAPVR) have about 50% mortality while the diagnosis of MAS has a mortality of about 5% (Van Meurs et al. 2005b). For all diagnoses, the mortality for newborns placed on ECMO is about 20% according to the ELSO registry (Van Meurs et al. 2005a). Even though ECMO therapy has significantly improved outcome in the newborn, morbidity and mortality associated with brain injury is considerable for this population.

Multiple factors increase the risk of intracranial injury in infants undergoing ECMO. The reported frequency of abnormal neuroimaging has ranged from 28% to 52%, depending on the neuroimaging techniques and methods of classification (Bulas and Glass 2005). Patients placed on ECMO as a group have experienced significant pre ECMO haemodynamic instability and have been potentially exposed to hypoxia, hypotension, alkalosis, hypercarbia, and profound acidosis (Graziani et al. 1997a, Von Allmen and Ryckman 1991). Several physiologic changes, including asphyxia, hypoxia and hypercarbia, can all disrupt cerebral autoregulation leaving the cerebral microcirculations vulnerable to alterations in systemic blood pressure. Loss of autoregulation in an already injured brain in the presence of systemic heparinisation, such as occurs with ECMO, can result in cerebral haemorrhage (Short et al. 1994a). Hypotension before or during ECMO may result in cerebral ischemia. Liem and coworkers demonstrated changes on ECMO including increased cerebral blood volume, loss of autoregulation, reactive hypoperfusion and hemodilution (Liem et al. 1995a).

In addition, a risk for cerebral injury is introduced by the various aspects of the ECMO procedure itself. The ECMO run exposes the patient to carotid artery and jugular vein ligation, heparinisation, coagulopathy and hypertension, all of which can predispose to neurologic complications (Weber et al. 1996). In addition, alteration of blood flow dynamics can similarly affect cerebral blood flow. There has been concern that ligation of the carotid artery may cause lateralised cerebrovascular injury. Hunter et al in their study of cerebral blood flow using laser Doppler flowmetry in newborn lambs, showed that carotid ligation caused a transient (60 seconds) decrease of CBF in the right cerebral cortex (Hunter et al. 2004). Several early studies noted an increase in injuries to the right hemisphere in infants who

underwent ligation of the right carotid artery (Hahn et al. 1992, Hofkosh et al. 1991, Mendoza et al. 1991). Graziani et al used magnetic resonance angiography and demonstrated asymmetric cerebrovascular response to carotid ligation of the right versus left middle cerebral artery but they report no selective or greater injury to the right hemisphere as compared with the left (Graziani et al. 1997b). Whether or not the neuroimaging data sufficiently support increased structural vulnerability to the right hemisphere in ECMO treated neonates, some evidence of increased right hemisphere vulnerability is present at a functional level. The preliminary question, however, is whether there is sufficient neurospecificity in the neonate in regard to neuropsychological or motor functions. Selective deficits in receptive and expressive language, visual/motor integration, and behaviour problems have been identified in early childhood following unilateral brain injury during the perinatal period (Bulas & Glass 2005).

Given the relatively high rate of neuroimaging abnormality among ECMO-treated neonates, neurodevelopmental outcome studies have been important in defining the functional impact. There is growing concern that infants with congenital diaphragmatic hernia (CDH) treated with ECMO have a worse neurological outcome when compared to infants that were not treated with ECMO and other non-CDH ECMO-treated patients (Khan and Lally 2005). Stolar et al. found that 89% for infants treated with ECMO for indications other than CDH were cognitively normal. In contrast, only 60% of infants with CDH treated with ECMO had a normal cognitive outcome (Stolar 1996). McGahrn et al. showed a survival rate of 75% among infants with CDH that were treated with ECMO, of which 67% exhibited signs of neurological compromise (McGahren et al. 1997). Based on these findings it has been suggested that the poor neurological outcome maybe a function of the severity of the illness, although independent ECMO factors could not be excluded.

Numerous investigators have reported on the neurodevelopmental outcome of the ECMO patient and consistently report Bayley scores in the normal range in the first 2 years of life. Fewer studies of ECMO survivors at older ages have been performed. Glass et al. reported that by 5 years of age, mean IQ scores remain in the normal range, but are lower than controls. Approximately 15% of ECMO survivors at age of 5 had a major handicap, most commonly mental retardation, while <5% had severe

or profound impairment. Nevertheless, 50% of ECMO survivors have an increased risk of learning and behavioural problems when compared to normal controls (Bulas & Glass 2005). As a result of these deficits, ECMO survivors are vulnerable to academic and psychosocial difficulties.

Neuroprotective strategies are adopted on ECMO which include mild hypothermia (Horan et al. 2004). Mild hypothermia has been studied in the context of perinatal asphyxia and cardiac arrest and long term neurological outcome is as yet not studied in children. Hypercarbia increases cerebral blood flow and can increase cerebral oxygenation but can cause cerebral hyperaemia. In addition, it is a systemic vasodilator and can improve cardiac output and systemic oxygenation.

4.4 Neurological monitoring on extracorporeal circulation

The most serious complications of the ECMO patient have been neurological complications (e.g. learning disorders, motor dysfunction, and cerebral palsy). During the ECMO course, frequent neurological examinations should be performed and real-time neurologic monitoring should be an integral part of neuroprotective strategies for paediatric patients on extracorporeal circulation. Ideally, monitoring should allow easy, reliable, and reproducible detection of adverse neurologic events. Several monitoring modalities such as electroencephalograph, transcranial Doppler and near infrared spectroscopy are available.

4.4.1 Electroencephalographic monitoring

Electroencephalography (EEG) examines the electrical activity of the brain. The standard EEG records up to 16 channels and was used repeatedly to investigate cortical function during and after ECMO. Post-ECMO EEG was used as a predictor of neurodevelopmental outcome in ECMO survivors but it was shown that EEG abnormalities had no correlation with neurodevelopmental outcome (Kumar et al. 1999). EEG studies during ECMO, if highly correlated with later definitive neuroimaging, might be used to affect the acute clinical care (Gannon et al. 2001). However, described pathological findings lack clinical relevance or are found to be

poorly predictive for permanent neurological impairment (Goodman et al. 2001, Graziani et al. 1994, Trittenwein et al. 2006).

EEG has also been used in cardiac surgery during CPB and deep hypothermia and it has been shown that it can predict the risk of clinical seizures (Lozano and Mossad 2004). However, seizure activity on CPB has little predictive value for later neurologic outcome in neonates (Hoffman 2006). EEG has also been used as a rough guide to anesthetic depth and can be used to determine electrocerebral silence before using DHCA .

EEG is non invasive, continuous and portable but there are several considerations limiting its use during extracorporeal circulation. EEG slowing is not specific for ischemia or hypoxia and does not differentiate among the effects of anesthetics, hypothermia, hypoglycemia, hemodilution, PCO₂ changes or extreme hypotension.

4.4.2 Transcranial Doppler

Transcranial Doppler ultrasound (TCD) is another non invasive technique that can be used for neuromonitoring. TCD measures velocities in the proximal segment of the middle cerebral artery (MCA), which provides 70% of blood flow to the ipsilateral cerebral hemisphere. As such, TCD may facilitate detection of cerebral ischemia.

TCD has rarely been used on ECMO patients but has been used in several studies during congenital heart surgery. Weber *et al* (1994) have used TCD to investigate the effects of venous occlusion on cerebral blood flow during ECMO and concluded that cephalic venous drainage may help prevent the neurological complication of ECMO by maintaining normal cerebral blood flow. TCD also showed slight but significant differences in BFV between right and left MCA (Graziani et al. 1994). TCD has been used extensively in paediatric cardiac surgery to examine cerebral physiology in response to CPB, hypothermia, low-flow bypass, RLFP to the brain and DHCA (Andropoulos et al. 2003a, Hillier et al. 1991). A unique contribution of TCD stems from the detection of high-intensity transient signals, which signify embolic phenomena (O'Brien et al. 1997).

TCD allows noninvasive, continuous monitoring of acute changes in blood flow velocity caused by perfusion changes and therefore cannula malposition can be quickly identified (Rodriguez et al. 2000). However, the validity of blood flow velocity measurements as a surrogate of cerebral blood flow relies on the assumption that the diameter of the MCA remains constant. CBFV is dependent on the diameter of the blood vessel, whereas cerebral blood flow depends on the cerebral vascular resistance, which changes in response to changes in CO₂, temperature, cerebral perfusion pressure, and bypass flow. Reproducibility varies with transducer position. TCD velocities reveal trends on changes in CBF and not absolute values. Prospective studies addressing the association between cerebral blood flow velocity abnormalities measured by TCD and neurologic outcome are necessary.

4.4.3 Near infrared spectroscopy

Near infrared spectroscopy (NIRS) is a noninvasive optical technique that can measure oxyhaemoglobin and deoxyhaemoglobin concentrations and can determine cerebral oxygen saturation. For a detailed description of NIRS systems and their operation the reader is refer to chapter 3 of this thesis.

To date there are three commercially available NIRS systems; (1) NIRO (Hamamatsu Photonics, Japan), (2) INVOS, (Somanetics Corp., Troy MI) and (3) FORE-SIGHT (CAS medical systems, Bradford CT). All three systems use source and segmented photodetector pairs to perform spatially resolved spectroscopy and obtain an absolute value for tissue oxygen saturation as a percentage. The major difference between the NIRO system and the rest is that it provides additional information related to the concentrations of oxy- and deoxy-haemoglobin. The NIRO system uses differential spectroscopy to obtain relative changes in the concentrations of the two chromophores making it possible to identify whether changes in oxygen saturation result from changes in blood volume or changes in oxygen consumption. An increase/decrease in blood volume causes an increase/decrease in total haemoglobin concentration which in return causes a change in oxygen saturation. Changes in oxygen consumption are reflected by changes in oxy- and deoxy-

haemoglobin concentrations in opposite directions so that the total haemoglobin concentration stays the same.

This section reviews the application of NIRS systems in neonatal and paediatric patients supported on ECMO and in neonatal patients undergoing cardiopulmonary bypass procedures for the correction of congenital cardiac defects. Tissue oxygen saturation measured by the various NIRS systems is referred to by different acronyms in the literature depending on the system used. For the purpose of this chapter a general term is given to tissue oxygen saturation namely tissue oxygen saturation (TOS).

4.4.3.1 Near Infrared Spectroscopy on ECMO patients

The first study on ECMO patients using NIRS was reported in 1995 by Liem et al. They investigated cerebral oxygenation in relation to changes in some physiologic variables during induction of ECMO in 24 newborn infants. The patients were monitored from cannulation until 60 minutes after starting ECMO and haemodynamic parameters such as heart rate (HR), mean arterial blood pressure (MAP), oxygen and carbon dioxide partial pressures (pO_2 and pCO_2), and arterial saturation (SaO_2) were also measured simultaneously. They found that carotid ligation causes a decrease in oxyhaemoglobin concentration (HbO_2) and increase in deoxyhaemoglobin concentration (HHb), while jugular ligation showed no changes. Also, HbO_2 , SaO_2 , pO_2 and MAP showed significant increase 60 minutes after starting ECMO compared to precannulation values. These were related to an increase in mean blood flow velocity (MBFV) and cerebral blood volume (CBV) which may result from loss of autoregulation, reactive hypoperfusion and haemodilution. They also report a positive correlation of total haemoglobin concentration (HbT) with MAP and negative correlation with pO_2 (Liem et al. 1995a).

The effects of right carotid artery ligation and variations in ECMO flow on regional cerebral oxygenation index were investigated by Ejike et al. They used a dual channel NIRS system placing the probes on the right and left frontal hemispheres. Their study demonstrated no relationship between ECMO flow and TOS changes. A brief period of cerebral oxygen desaturation of the right frontal

region at the time of right carotid ligation was seen in patients examined during cannulation. Right sided TOS remained depressed for 17-45 mins. Following this depression in TOS on the right, there was a transient increase in TOS above baseline observed in both hemispheres. Periods of “trailing off” ECMO were not related to any change in TOS in either hemisphere (Ejike et al. 2006).

Van Heijst et al use NIRS to study oxygenation and haemodynamics in left and right cerebral hemispheres during induction of VA ECMO in 10 newborn infants. They demonstrated that RCCA ligation causes a decrease in oxyhaemoglobin concentration and an increase in deoxyhaemoglobin concentration which were reversed 60 minutes after initiation of ECMO. Right internal jugular vein (RIJV) ligation caused no changes. Although the results suggest a potential ischemic period after right common carotid artery (RCCA) ligation, there was no difference in NIRS parameters between the right and left cerebral hemispheres (Van Heijst et al. 2004).

Another study, neonates were monitored with NIRS before, during, and after cannulation for ECMO to determine the direct effects of ligation of the main vessels in the neck in cerebral oxygenation (Fenik and Rais-Bahrami 2009). They observed a decrease in TOS for most subjects during ECMO surgery (ligation of RCCA and RIJV), and gradual increase in TOS for the first hours of ECMO.

NIRS was also used in an animal study to investigate the cause of the haemodynamic changes occurring during opening of the bridge in VA ECMO infants, demonstrating significant decrease in mean arterial blood pressure with associated decreases in cerebral oxygenation and peripheral arterial saturation. The cerebral haemodynamic changes were found to be related to an arteriovenous shunt over the bridge that may contribute to the occurrence of cerebral ischemia and/or intracranial haemorrhages (Van Heijst et al. 2001).

Rais-Bahrami et al compared cerebral TOS obtained using NIRS with venous saturation in 17 VV ECMO neonates and showed a high level of agreement between the two (Rais-Bahrami et al. 2006).

4.4.3.2 NIRS in neonates with congenital heart diseases

The use of NIRS technology for the monitoring of the cerebral oxygenation and haemodynamics during congenital heart surgery was first reported in 1991 by Greeley et al (Greeley et al. 1991). Since then, the application of NIRS has gained increasing interest. Several review articles capture the widespread acceptance of NIRS in the field of neonatal and paediatric cardiac surgery (Andropoulos et al. 2004a, Chakravarti et al. 2008, Hirsch et al. 2009, Hoffman 2006, Lozano and Mossad 2004, Williams and Ramamoorthy 2007). A comprehensive publication list of the application of NIRS in neonates with CHD preoperatively, intraoperatively and postoperatively is shown in table 4.1.

NIRS has been used preoperatively to study the indication of hypoxia-ischemia in patients with CHD prior to cardiac surgery (Ramamoorthy et al. 2002). A comparison of cerebral TOS between healthy patients and patients with CHD has shown that cerebral TOS varies with anatomy and arterial saturation (Kurth et al. 2001). It has been shown that cerebral TOS in patients with acyanotic lesions is similar to healthy subjects, in contrast with cyanotic patients where cerebral TOS was decreased. In addition, Toet et al. have shown that lower TOS obtained prior to arterial switch operation are related with lower DQ (developmental quotient) (Toet et al. 2005).

NIRS has also been used intraoperatively to evaluate the effects of various operative techniques on cerebral oxygenation and metabolism. In an attempt to identify vulnerable periods for the development of neurologic injury, Daubeney et al (1998) used NIRS on patients undergoing CPB with or without deep hypothermia circulatory arrest (DHCA). They showed that the onset of bypass caused an increase in TOS. Furthermore, during circulatory arrest TOS decreased with rate of decay influenced by temperature at onset of arrest. Reperfusion caused an immediate increase in TOS followed by a decrease during rewarming. Discontinuation of bypass caused a precipitous decrease in TOS (Daubeney et al. 1998). Hoffman et al used NIRS during the Norwood procedure with DHCA and showed that TOS was maintained during regional cerebral perfusion at prebypass levels with DH. However, after rewarming and separation from CPB, TOS was lower compared with prebypass (Hoffman et al. 2004). Tobias et al report the use of NIRS during DHCA

and showed that TOS increases after cooling on CPB, while after the onset of DHCA an incremental decrease in TOS with an average rate of 0.9% per min is obtained (Tobias et al. 2009).

NIRS technique has also been used to examine brain oxygenation during regional low-flow cerebral perfusion (RLFP), a technique whereby the brain is perfused via the right innominate artery to provide unilateral cerebral perfusion during CHD surgeries involving aortic arch reconstruction. Bilateral NIRS has been used to examine correlation between right and left hemispheres (Andropoulos et al. 2004a, Hofer et al. 2005). Also NIRS has been used to study the impact of acid-base management (pH-stat vs. α -stat) during CPB on cerebral oxygenation (Sakamoto et al. 2004).

The use of NIRS postoperatively has been employed by several groups. Phelps et al used NIRS to study cerebral oxygenation in patients with hypoplastic left heart syndrome (HLHS) after the Norwood procedure to relate cerebral oxygenation with the risk of adverse outcome (Phelps et al. 2009). Li et al sought to quantitatively define the effects of stepwise increase in arterial carbon dioxide tension on systemic oxygen transport and cerebral and splanchnic circulation after the Norwood procedure (Li et al. 2008). In addition, NIRS was used in postoperative CHD patients to study the relationship between TOS and central venous oxygenation and it was found that even though they correlate, interchangeability is precluded due to wide limits of agreement (McQuillen et al. 2007b, Nagdyman et al. 2004).

4.4.3.3 Concluding Remarks

NIRS due to its unique qualities, including non invasive, continuous and real time measurement of cerebral oxygenation, has gained increasing use as a monitoring technique in neonatal and paediatric cardiothoracic care. The continued desire to mitigate the neurologic complications associated with this group of patients and its surgical intervention is laudable.

The significant variability in NIRS measurements, temporally and between individual patients, precludes the establishment of absolute threshold values.

Furthermore, the wide heterogeneity in anatomy and physiology in CHD and ECMO patients results in varying baseline levels of oxygenation. Caution must be exercised in extrapolating regional measurements to global findings. Therefore, it is important to look at trends in NIRS signals rather than relying on a single marker such as tissue oxygen saturation.

Alterations in regional oxygen saturation may reflect local changes and not necessarily indicate global hypoperfusion. The clinically commercially available NIRS systems monitor TOS in only a small tissue volume of the frontal cerebral cortex; other areas of the cortex and deeper structures in the brain are not assessed by these systems. The development of a multichannel NIRS system that will allow global monitoring of cerebral oxygenation to be used clinically in neonatal and paediatric cardiac patients should be highly beneficial.

Although clinical evidence suggests a correlation between low cerebral oxygen saturations and adverse neurologic outcome, additional prospective outcome data in infants and children using this modality are necessary. As additional studies are performed and as technologic advancements are made, NIRS will continue to provide important insights into the haemodynamics and pathophysiology of neonates and children, and will likely find its way into routine clinical practice.

Table 4.1: NIRS monitoring in Patients with congenital heart diseases (modified from (Hirsch et al. 2009))

Author	Device	Patient Population	Total Number	Objectives	Results
Anesthesia					
(LeBlanc et al. 2000)	NIRO	Elective ASD or VSD with (n=11) or without (n=13) propofol	24	Effect of propofol on the redox status of Cytaa3 and neurologic complications	Prpofol has similar effects on Cytaa3 as hypothermia; no gross neurologic complications
(Nagdyman et al. 2008)	NIRO/INVOS	children with congenital heart defects	31	Compared two different near-infrared spectrophotometers: TOS measured using NIRO 200 and INVOS 5100 with venous oxygen saturation in the jugular bulb (SjO ₂) and central venous oxygen (SvO ₂) from the superior caval vein (SVC) during elective cardiac catheterization in children.	Cerebral TOS measured with NIRO and SjO ₂ were significantly correlated (r = 0.56, P < 0.0001), as well as NIRO TOS and SvO ₂ with r = 0.74 (P < 0.0001). Cerebral TOS measured with INVOS and SjO ₂ showed a significant correlation (r = 0.83, P < 0.0001) and INVOS TOS and SvO ₂ showed excellent correlation with r = 0.93 (P < 0.0001).
Coarctation repair					
(Berens et al. 2006)	INVOS	Aortic coarctation repair via left thoracotomy	26	Describe the changes in regional cerebral and somatic TOS with aortic coarctation repair	The decrease in somatic TOS with coarctation repair is less in children than neonates and infants (P<.01), significant increase in cerebral TOS during coarctation repair in children > 1 year
(Azakie et al. 2005)	NIRO	Aortic coarctation repair via left thoracotomy	18	Determine whether aortic occlusion impairs left hemispheric cerebral oxygen balance	Significant decrease in HbO ₂ -HHb between the right and left (P=0.03), significant decrease in HbO ₂ -HHb with nitroprusside (P<0.001)

Table 4.1 (continued)

Deep hypothermia with and without circulatory arrest (CA)

(Kussman et al. 2005)	INVOS	Infant biventricular repair (no arch reconstruction)	62	Evaluate the differences in bihemispheric measurement of TOS during hypothermic CPB. Relationship between cerebral HbO ₂ and Cytaa ₃	No difference between right and left TOS measurements irrespective of CA. Median time to nadir of HbO ₂ during CA was 25 minutes, increased HbT and HbO ₂ above baseline with rewarming (P<.001) with delayed Cytaa ₃ recovery, dissociation between intravascular and mitochondrial oxygenation in patients > 2 weeks
(Greeley et al. 1991)	NIRO	Deep hypothermia with or without CA in neonates and children	15	The effect of CA on CMRO ₂ and oxygenation	HbO ₂ and Cyaa ₃ decreased during CA, CMRO ₂ and Cyaa ₃ remained lower than baseline after CPB with CA but returned to normal in non-CA patients (P < .01)
(Kurth et al. 1992)	NIMS	Neonates undergoing surgery with CA	17	Kinetics of HbO ₂ in neonates during DHCA	HbO ₂ increases during cooling (P < .05), decrease during CA in a curvilinear distribution until a plateau at 40 minutes (P < .001), and returns to baseline with rewarming
(Kurth et al. 1995)	NIMS	Repair of palliation using CA	26	Variation in changes of intraop TOS between neonates, infants, children and are these changes associated with postop neurologic dysfunction	The half life of TOS during CA is longer for neonates > infants > children (P < .001), patients with neurologic complications had less of an increase in TOS on CBP and a significant shorter cooling time pre-CA (P < .05), no significant difference in TOS between groups

Table 4.1 (continued)

(Tobias et al. 2009)	INVOS	Patients with CHD undergoing surgery with DHCA	8	To present data regarding use of a commercially available near infrared spectroscopy monitor during deep hypothermic circulatory arrest in paediatric patients undergoing surgery for congenital heart disease.	The baseline cerebral oxygenation was $63 \pm 11\%$ and increased to $88 \pm 7\%$ after 15 min of cooling to a nasopharyngeal temperature of 17-18°C on cardiopulmonary bypass. In 5 of 8 patients, the cerebral oxygenation value had achieved its peak value (either $\geq 90\%$ or no change during the last 2-3 min of cooling on cardiopulmonary bypass). After the onset of deep hypothermic circulatory arrest, there was an incremental decrease in cerebral oxygenation to a low value of $53 \pm 11\%$. The greatest decrease occurred during the initial 5 min of deep hypothermic circulatory arrest ($9 \pm 3\%$). Over the entire period of deep hypothermic circulatory arrest, there was an average decrease in the cerebral oxygenation value of 0.9% per min (range of 0.5 to 1.6% decline per minute).
(du Plessis et al. 1995)	NIRO	Infant biventricular repair with low flow or CA	63	Relationship between cerebral HbO ₂ and Cytaa ₃	Median time to nadir of HbO ₂ during CA was 25 minutes, increased total HbT and HbO ₂ above baseline with rewarming (P<.001) with delayed Cytaa ₃ recovery, dissociation between intravascular and mitochondrial oxygenation more pronounced in patients > 2 weeks.

Table 4.1 (continued)

Regional low flow perfusion (RLFP)

(Hofer et al. 2005)	INVOS	RLFP for Norwood procedure	10	Correlation of bilateral NIRS monitoring during RLFP with variable flow rates	There was a significant decrease in bilateral TOS and SvO ₂ with decreasing RLFP rates (P < .001). Wide interindividual variation in TOS
(Andropoulos et al. 2004a)	INVOS	RLFP for Norwood procedure or aortic arch reconstruction	19	Correlation of bilateral NIRS monitoring during RLFP adjusted for CBFV with TCD	During RLFP, correlation between hemispheres was poor and only partially returned to baseline after RLFP with the left side always being the lower value
(Hoffman et al. 2004)	INVOS	RLFP for Norwood procedure	9	Relative changes in cerebral and somatic oxygenation during RLFP adjusted for TOS and CBFV	TOS was maintained during RLFP but decreased below baseline after CPB. There was no correlation between cerebral and somatic oxygenation at any time point.
(Andropoulos et al. 2003a)	INVOS	RLFP for Norwood procedure or aortic arch reconstruction	34	Describe the addition of CBFV monitoring by TCD to TOS as a guide to bypass flow during RLFP	Poor correlation between MAP and required CPB flow. 14/34 had TOS greater than 95% during RLFP increasing the risk of hyperperfusion. No outcomes correlation for the addition of CBFV to TOS to guide PB flow.
Table 5.1 (continued)					
(Kilpack et al. 2004)	INVOS	RLFP for Norwood or aortic arch reconstruction	34	Demonstrate maintenance of adequate TOS with RLFP when CPB flow adjusted for TOS and CBFV	No difference in TOS on full flow CPB, RLFP, and resumption of full flow CPB. However, CPB flow was adjusted to maintain value within 10% baseline
Table 4.1 (continued)					
(Andropoulos et al. 2003b)	INVOS	RLFP for Norwood procedure or aortic arch reconstruction	20	Demonstrate the correlation between CBVI based on NIRS and CBFV by TCD	Poor correlation between CBVI and CBFV. Right sided CBFV did not correlate with RLFP flow rate

(Pigula et al. 2001)	INVOS	RLFP for Norwood procedure or aortic arch reconstruction	15	Ability of RLFP to provide subdiaphragmatic somatic circulatory support as measured by somatic NIRS	Abdominal aortic blood pressure, quadriceps blood volume, and quadriceps TOS were significantly greater during RLFP than DHCA ($P < 0.05$)
(Pigula et al. 2000)	INVOS/NIRO	Neonatal aortic arch reconstruction with RLFP (n=6) and neonatal cardiac repair with DHCA (n=6)	12	Experiential report of using NIRS guided RLFP versus DHCA	RLFP flow rate of 20 mL/kg/min maintained baseline values. TOS and CBVI decrease significantly during DHCA but are maintained during RLFP.
Perfusion techniques					
(Han et al. 2004)	INVOS	Repair of ASD or VSD with bloodless (n=18) or blood (n=18) prime	36	Compare the effect of blood versus bloodless CPB prime on TOS	TOS decreases below baseline in both groups at the start of CPB and during rewarming ($P < .001$) with a greater reduction in the bloodless prime group ($P < .01$).
(Sakamoto et al. 2004)	NIRO	CPB in cyanotic patients using alpha-stat (n=19) versus pH-stat (n=21) strategy	40	Evaluate the effect of pH strategies on TOS and SPCC	TOS was significantly lower ($P=0.008$) and the HHb was significantly higher ($p < 0.0001$) with alpha-stat. SPCC was significantly lower with pH-stat ($P < 0.0001$).
(Shaaban et al. 2004)	NIRO	Cold (25°C) (n=9) versus warm (35°C) (n=9) CPB for biventricular repair	18	Compare the effect of cold versus warm CPB in terms of extent of cerebral damage (measured by S100b) and HbO ₂	S100b increased significantly in both groups. No correlation between S100b and NIRS measurements except lowest post-CPB Cytaa ₃ level ($P=0.016$). TOS was significantly impaired during rewarming

Table 4.1 (continued)

(Wardle et al. 1998)	NIRO	Deep hypothermia (15°C) (n=15) versus mild–moderate hypothermia (22–28 °C) (n=15) CPB	30	Investigate the effect of hypothermia and CA on cerebral FOE.	FOE increases with the institution of CPB in cyanotic patients FOE decreases during cooling and only increases during rewarming in the continuous flow group. No significant difference between groups at any time in Cyt _{a3}
(Chow et al. 1997a)	NIRO	CPB using pulsatile and nonpulsatile flow	40	Examine the relationship between pump flow rate and cerebral haemodynamics during pulsatile and nonpulsatile CPB	CBF decreased by 36% per Lm ² /min decrease in pump flow rate regardless of pulsatility
(Kurth et al. 1997)	NIMS	CPB: warm (n=10), hypothermic (25°C) (n=10), hypothermic/low flow (n=9), and hypothermic /low Hct (n=9)	38	Evaluate the effect of perfusate temperature, pump flow rate and Hct on cerebral O ₂ extraction	TOS increases during cooling (P<0.001), TOS increased after CPB was discontinued in the low flow and low Hct group
Intraoperative monitoring (Fenton et al. 2007)	INVOS	Single ventricle stage palliation (n=34) and ductus dependent complete repair (n=12)	46	Determine whether TOS is related to the stage of single ventricle palliation	TOS at the end of the operation was significantly lower in patients who died (P=0.01), TOS decreases significantly after stage 1 palliation (P=0.001) and increases after stage 2 palliation (P=.04). No correlation with neurologic complications
(Murayama et al. 2006)	NIRO	Repair of cyanotic (n=10) and noncyanotic (n=10) heart defects	20	Differences in TOS at the initiation of CPB for cyanotic and noncyanotic heart defects.	Cerebral HbO ₂ , HHb, and HbT decrease and then plateau on CPB. HHb and HbT decreased more markedly in the cyanotic patients (P<0.01).

Table 4.1 (continued)

(Hayashida et al. 2004)	PSA-3N	Noncyanotic CHD repaired with CPB	65	Measure the incidence of cerebral ischemia using bispectral index and NIRS in children having cardiac surgery.	Cerebral ischemia (defined as abrupt decrease in both TOS and bispectral index with acute hypotension) was more common and frequent in children <4 years. TOS was more dependent on arterial pressure in children <4 years. Cerebral ischemia frequency correlated negatively with Hct (P<0.0001). HbO ₂ decrease on CPB with no change in HHb.
(Morimoto et al. 2003)	NIRO	Repair of VSD	16	Examine changes in cerebral oxygenation using NIRS during VSD repair	TOS decreased by >15% in 10/18 patients with cardiac manipulation. TOS increases with the institution of CPB and decays at 0.25%/min at <20°C and 2%/min at >20°C. TOS varied inversely with the rate of cooling (P=0.04)
(Daubeney et al. 1998)	INVOS	Biventricular repair	18	Identify periods of cerebral oxygen supply and demand mismatch using NIRS	Of patients with neurologic changes, significantly more had noteworthy intraop changes that were not intervened on (P=0.003) with significantly fewer of these patients discharged from the hospital within 1 week (P<0.05)
(Austin et al. 1997)	INVOS	CHD repair with CPB	250	Examine the potential benefit of interventions based on intraop neurophysiologic monitoring (TCD, EEG, NIRS) in decreasing postop neurologic complications and length of hospital stay	No relation between arterial oxygen tension and CBF. DBF is associated with CPB flow rate (decreases 4.2 fold per l/m ² /min)
(Chow et al. 1997b)	NIRO	Noncyanotic CHD repaired with CPB	14	Explore the relation between arterial oxygen tension and CBF during CPB	

Table 4.1 (continued)

(Van Bel et al. 1996)	Radiometer	Neonatal and infant CDH repair with CPB	12	Investigate the changes in cerebral haemodynamics and oxygenation during DHCA	CBV decreased significantly with cooling and increased significantly with rewarming ($P < .001$). CBV did not change with pump flow rate of MAP
(Skov and Greisen 1994)	Radiometer	Biventricular cyanotic (n=5) and noncyanotic (n=9) CHD repair with CPB	14	Examine the changes in cerebral $Cyaa_3$ during induction of CPB	In cyanotic patients, the HbT decreased rapidly and then reached a plateau, $Cyaa_3$ decreased and HbO ₂ index increased. There were no significant changes in the noncyanotic patients. The magnitude of the change in $Cyaa_3$ was associated with the magnitude of change on HbT ($P < 0.0001$). Signal noise analysis raised concern about the validity of the results.
(Fallon et al. 1993)	NIRO	Repair of CHD with CPB	13	Use of NIRS to monitor CBF, CBV, and CBVR	CBVF significantly decreased during hypothermic (25°C) bypass
(Redlin et al. 2008)	NIRO	Repair of CHD with CPB	20	Assess the extent to which mixed venous oxygen saturation as a measure for adequacy of perfusion, reflects the oxygenation status of upper and lower body compartments.	Venous oxygen saturation was lower and lactate concentration higher in blood from superior relative to inferior venous line. Mixed venous oxygen saturation correlated with venous oxygen saturation from inferior venous line and tissue oxygenation index of lower limb. No correlation was found between mixed venous oxygen saturation and venous oxygen saturation from superior venous line or cerebral tissue oxygenation index.

Table 4.1 (continued)

(Fallon et al. 1994)	NIRO	Elective CHD repair with CPB	19	Measure the change in CBV associated with changing PaCO ₂ (CBVR) under anaesthesia and during hypothermic CPB	CBVR is preserved under anaesthesia and hypothermic CPB. The relationship between CBV and PaCO ₂ is linear
Intraoperative combined with preoperative/postoperative monitoring					
(McQuillen et al. 2007a)	NIRO	Patients with CHD, preop/postop MRI and intraop NIRS	16	Define the risk factors for preop and postop brain injuries and association with functional cardiac anatomic groups (intraop NIRS was a secondary analysis)	TOI significantly decreased during aortic XC in patients with positive postop MRIs (P=.008)
(Dent et al. 2006)	INVOS	Norwood procedure with RLFP, preop/postop MRI, preop/introp/postop NIRS	22	Preop and postop MRI findings in neonates undergoing a Norwood procedure with RLFP	Prolonged low postop TOS (<45% for >180 minutes) was associated with new or worsening lesions (P=.029) with a positive predictive value of 90% for positive MRI findings
(Toet et al. 2005)	INVOS	Transposition of the great arteries repair with DHCA, preop/intraop/postop NIRS	20	Monitoring NIRS before, during, and after arterial switch operation to evaluate its relation to neurodevelopmental outcomes	Recovery time for the EEG did not correlate with normalisation of the TOS. Complete recovery of the TOS takes 6-72 hours postop. Preop decrease in TOS tended to correlate with decreased Bayley score but was not significant
Monitoring technique					
(Roberts et al. 1998)	NIRO	Repair of CHD with CPB	19	Describe a novel method to measure CBF using indocyanine green tracer with NIRS	11% variation between measurements within individual patients, 73% of the variability was accounted for by pump flow and temperature

Table 4.1 (continued)

Preoperative ICU monitoring

(Takami et al. 2005)	NIRO	CHD patients with increased pulmonary blood flow	8	Evaluate serial changes in oxygenation state in the head and body in patients with increased pulmonary blood	With decreased TOS after the initiation of hypoxia, cerebral and brachial HbO ₂ decreased with an increase in HHb
(Ramamoorthy et al. 2002)	NIM-prototype	Single ventricle neonates	15	Evaluate changes in TOS with inspired 17% FiO ₂ or 3% CO ₂	Significant increase in TOS and MAP with 3% CO ₂ , no change in TOS or MAP with 17% FiO ₂
(Kurth et al. 2001)	NIM-prototype	CHD and normal	110: 91 with CHD, 19 normal	Correlation of TOS and CEo ₂ between CHD patients and normal	TOS was significantly decreased in patients with PDA, TOF, HLHS, PA, SV with shunt and BDG but was the same for VSD, CoA, and Fontan. CEo ₂ was significantly increased for PDS and HLHS. SaO ₂ was correlated with TOS but was not a good substitute (R ² =0.4)

Postoperative ICU monitoring

(McQuillen et al. 2007b)	INVOS	Postop CHD patients	70	Relationship between changes in TOS with changes in regional flank SO ₂ and central SvO ₂ Monitored for 24 hours	Central SvO ₂ was correlated with TOS and flank TOS with wide limits of agreement precluding interchangeability. Changes in PaCO ₂ and MAP were associated with changes in TOS but not flank TOS or SvO ₂ . Changes in SaO ₂ were associated with SvO ₂ but not TOS.
(Mott et al. 2006)	INVOS	Bidirectional Glenn (BDG)	10	Response of TOS to (1) hyperventilation with increased TV, (2) hyperventilation with increased RR, (3) hypoventilation with decreased RR. Monitoring for 4 hours	(1) Increased pH, decreased PCO ₂ , PCO ₂ , as 1; (3) no change in pH, increased PCO ₂ , and increased TOS. Hyperventilation should be avoided in patients with BDG due to potential decrease in TOS.

Table 4.1 (continued)

(Nagdyman et al. 2006)	NIRO	Elevated pulmonary vascular resistance after CPB	13	Examine alterations in cerebral oxygenation in children treated with increasing doses of sildenafil for elevated vascular resistance. Monitored for 1 hour	TOS increased significantly after the first two doses but quickly returned to baseline ($P=.01$), no change with the third dose. There was no correlation between cardiac index and TOS
(Li et al. 2006)	INVOS	Postop Norwood patients	11	Determine if NIRS cerebral and splanchnic monitoring accurately reflects systemic oxygen delivery when compared with direct measurements. Monitored for 72 hours.	TOS correlates with SaO_2 and PaO_2 ($P<0.0001$) with large interindividual variation, TOS correlates with SvO_2 ($P<0.0001$) with no interindividual variation. Overall, large interindividual variability and intraindividual temporal variability.
(Bassan et al. 2005)	NIRO	Postop CHD patients	43	Correlation of NIRS parameters ($HbD = HHb-HbO_2$) with CBFV by TCD; identify pressure-passive cerebral perfusion by simultaneous measurements of HbD and MAP; and associate higher CO_2 levels with pressure passive Measurements at 6 and 20 hours postop.	Significant relationship between change in CBFV and change in HbD ($P<0.0001$), also with change in HbO_2 ($P<0.001$). 13% of patients had disturbed cerebral pressure autoregulation at 6 hours that persisted at 18 hours, high end tidal CO_2 was correlated with pressure passive rather than autoregulated cerebral perfusion ($P<0.001$)
(Tortoriello et al. 2005)	INVOS	Elective postop CHD patients	20	Compare TOS with SvO_2 (oximetry) after paediatric cardiac surgery. Single measurement 6 hours postop	TOS correlated with SvO_2 ($P<0.001$). There was low intrasubject variation with significant intersubject variation; therefore cannot predict absolute values but can follow trends.

Table 4.1 (continued)

(Srinivasan et al. 2009)	INVOS	Postop Norwood patients	80: 40 with standardise management, 40 without standardise management	Study the impact of a standardised management protocol for neonates undergoing NP	Hospital survival (95% vs. 70%, P= 0.003) and survival to S2P (85% vs. 58%, P= 0.006) was better in the group receiving standardise management. By univariate analysis, regional low flow perfusion, gastrostomy usage, and near infrared spectroscopy were associated with improved hospital and survival to S2P.
(Phelps et al. 2009)	INVOS	Postop Norwood patients	50	Determine whether regional cerebral TOS by NIRS technology could predict risk of adverse outcome after the Norwood procedure.	There were 18 adverse events among the 50 subjects. The mean cerebral TOS for the entire cohort at 1 hour, 4 hours, and 48 hours after surgery was 51% +/- 7.5%, 50% +/- 9.4%, and 59% +/- 8.1%, respectively. Mean cerebral TOS for the first 48 postoperative hours of less than 56% was a risk factor for subsequent adverse outcome (odds ratio 11.9, 95% confidence interval: 2.5 to 55.8). Mean cerebral NIRs of less than 56% over the first 48 hours after surgery yielded a sensitivity of 75.0% and a specificity of 79.4% to predict those at risk for subsequent adverse events.

Table 4.1 (continued)

(Chakravarti et al. 2009)	INVOS	Postop CHD patients	23	To determine if a relationship exists between TOS measured at various body locations by NIRS and blood lactate level in children after cardiac surgery.	Cerebral TOS had the strongest inverse correlation with lactate level followed by splanchnic, renal, and muscle TOS ($r = -0.74$, $p < 0.0001$, $r = -0.61$, $p < 0.0001$, $r = -0.57$, $p < 0.0001$, and $r = -0.48$, $p < 0.0001$, respectively). The correlation improved by averaging the cerebral and renal TOS values ($r = -0.82$, $p < 0.0001$).
(Nagdyman et al. 2004)	NIRO	Postop CHD patients	43	Correlation between TOS as a value for regional TOS and global SvO ₂ (right atrial saturation via central line). Single measurement 2 to 3 hours postop.	TOS correlated with SvO ₂ ($P < 0.001$), PaO ₂ ($P = 0.031$), SaO ₂ ($P = 0.027$), SBP ($P = 0.035$), and MAP ($P = 0.042$). There was no correlation with PaCO ₂ , heart rate, and haemoglobin
(Kaufman et al. 2008)	INVOS	Postop CHD patients	20	Splanchnic oximetry, as measured by near-infrared spectroscopy (NIRS), correlates with gastric tonometry as a means of assessing regional (splanchnic) oxygenation and perfusion.	There was strong correlation between the abdominal TOS and pHi ($r = 0.79$; $p < 0.0001$) as well as between abdominal TOS and SvO ₂ ($r = 0.89$; $p < 0.0001$). There was also significant negative correlation between the abdominal TOS and serum lactate ($r = 0.77$; $p < 0.0001$). Correlations between the dorsal lateral (renal) TOS measurements and serum lactate and SvO ₂ were also significant but not as strong.

Table 4.1 (continued)

Post operative circulatory assist device monitoring (Giacomuzzi et al. 2005)	INVOS	HLHS with postop circulatory support	5	rScO ₂ on circulatory support after SV repair	TOS levels dropped significantly after separation from CPB and remained 20% below baseline for 24 hours and did not normalize until 48 hours despite stable SvO ₂ , MAP, and decreasing lactates.
--	-------	--------------------------------------	---	--	--

Table 4.2: NIRS monitoring in ECMO Patients.

Author	Device	Total Number	Objectives	Results
Animal Studies				
(Van Heijst et al. 2001)	Radiometer	8	Investigate the haemodynamic changes occurring during opening of the bridge in VA ECMO	Bridge opening resulted in change of flow direction between venous cannula and bridge and arterial cannula. A bi phasic response with initial decrease and secondary increase occurred in mean arterial blood pressure and mean left carotid artery blood flow. CVP, HHb and CBV increased, whereas HbO ₂ decreased. These effects occurred in each combination of ECMO flow rate and opening time.
(Liem et al. 1996)	Radiometer	12: 6 hypoxemic, 6 normoxemic	To compare the effect of ECMO on cerebral oxygenation and haemodynamics in normoxemic and hypoxemic piglets.	Cannulation procedure resulted in increased CBV, HHb, and left common carotid artery blood flow (LCaBF) in both groups. At 60 and 120 min after starting ECMO, the values of HbO ₂ , CBV, and LCaBF in both groups were significantly higher than precannulation values. In the hypoxemic groups HHb decreased and SaO ₂ increased. Between hypoxemic and normoxemic groups no significant differences in the response of CBV and LCaBF at 60 and 120 min were found. In piglets cannulation for ECMO resulted in cerebral venous congestion and compensated increase in LCaBF. After starting ECMO, the cerebral O ₂ supply increased due to increased arterial O ₂ content. It was accompanied by similar increase of CBV in both groups, probably as a result of hyperperfusion, which seems to be related to the ECMO procedure itself.

Table 4.2 (continued)

(Liem et al. 1995a)	Radiometer	4 groups of 6 piglets: 1.normoxaemia without ECMO, 2.ECMO after normoxaemia, 3.hypoxaemia without ECMO, 4.ECMO after hypoxaemia	To investigate the cerebrovascular response to changes in arterial CO ₂ tension.	Hypercapnia resulted in increased CBV, HbO ₂ and ICP in all groups, while HHb was decreased. Hypocapnia resulted in decreased cerebral HbO ₂ and increased cerebral HHb except in group 3. LCaBF decreased in all groups except group 2. CBV decreased only in groups 2 and 4. No effect on ICP was observed in any of the groups. The other variables showed no important changes either during hypercapnia or hypocapnia. ECMO after hypoxaemia resulted in a greater response of cerebral HbO ₂ and cerebral HHb during hypocapnia. The effect of hypercapnia on CBV while on ECMO was greater than without ECMO.
(Liem et al. 1995b)	Radiometer	12 piglets and 10 newborn infants	investigate changes of cerebral oxygenation and haemodynamics related to opening of the bypass bridge during veno-arterial extracorporeal membrane oxygenation (ECMO)	Opening of the bridge for 10 s in the infants resulted in a significant decrease in MABP, SaO ₂ , and cerebral HbO ₂ , whereas cerebral HHb increased. CBV did not change significantly. In piglets biphasic changes were observed for MABP, CaBF, cerebral HbO ₂ , and CBV, showing an initial decrease followed by a smaller increase. Cerebral HHb and CVP showed reverse biphasic changes. ICP increased but SaO ₂ was unchanged. In all cases heart rate and cCyt.aa ₃ did not change significantly. Opening of the bridge for 1 s resulted in minor changes in only a few variables. In conclusion, opening of the bridge resulted in a decrease of CBV and cerebral O ₂ supply due to a decrease of cerebral blood flow, followed by a compensatory increase of cerebral O ₂ extraction and vasodilatation.

Table 4.2 (continued)

(Tyree et al. 2009)	INVOS	12	Compare brain tissue oxygen tension (PbtO ₂) with cerebral near infrared spectroscopy (NIRS) and mixed venous oxygen saturation (SvO ₂) during venoarterial extracorporeal membrane oxygenation (VA ECMO) in a porcine model.	TOS and SvO ₂ correlated only marginally with PbtO ₂ (R ² =0.32 and R ² =0.26, respectively) while the correlation between TOS and SvO ₂ was significantly stronger (R ² =0.59). Cerebral metabolites and TOS were significantly altered during attenuation of PbtO ₂ , p<0.05). A subset of animals, following exposure to hypoxia, experienced markedly delayed recovery of both TOS and PbtO ₂ despite rapid normalization of SvO ₂ . Upon further analysis, these animals had significantly lower blood pressure (p=0.001), lower serum pH (p=0.01), and higher serum lactate (p=0.02). Additionally, in this subgroup, TOS correlated better with PbtO ₂ (R ² =0.76). These findings suggest that, in our ECMO model, TOS and SvO ₂ correlate reasonably well with each other, but not necessarily with brain PbtO ₂ and that NIRS-derived TOS may more accurately reflect cerebral tissue hypoxia in sicker animals.
Human Studies				
(Van Heijst et al. 2004)	Radiometer	10	Oxygenation and haemodynamics in the left and right cerebral hemispheres were measured during induction of veno-arterial extracorporeal membrane oxygenation (VA-ECMO).	RCCA ligation caused a decrease in HbO ₂ concentration and an increase in HHb concentration. RIJV ligation caused no changes. 60min after the start of VA-ECMO, HbO ₂ concentration and CBV had increased, and HHb concentration had decreased. There were no differences between the hemispheres. Mean CBFV had increased in the left internal carotid artery, and it increased equally in both middle cerebral arteries. Flow direction was reversed in the right internal carotid artery. Three patients had asymmetric cerebral lesions, not related to differences in the measurements between the cerebral hemispheres.
(Rais-Bahrami et al.2006)	FORE-SIGHT	17 veno-venous ECMO with cephalad catheter	Validation of the NIRS system with the cerebral oxygen saturation measured from blood drawn in neonates.	Compared to the reference values, the bias±precision for cerebral TOS was 0.4±5.1% and derived SvO ₂ was 0.6±7.3%

Table 4.2 (continued)

(Liem et al. 1995a)	Radiometer	24	To investigate cerebral oxygenation and haemodynamics in relation to changes in some relevant physiologic variables during induction of ECMO	After carotid ligation, HbO ₂ decreased whereas HHb increased. After jugular ligation, no changes in cerebral oxygenation were found. At 60 minutes after starting ECMO, the values of HbO ₂ , SaO ₂ , tcPO ₂ , and MABP were significantly higher than the precannulation values, whereas the value of HHb was lower. The MBFV was significantly increased in the major cerebral arteries except the right middle cerebral artery, whereas PI was decreased in all measured arteries. Cerebral blood volume, calculated from changes in HbT and HHb, was increased in 20 of 24 infants after starting ECMO. A positive correlation of HbT with MABP and a negative correlation with tcPO ₂ were found.
(Fenik & Rais-Bahrami 2009)	FORE-SIGHT	17	Neonates were monitored with a cerebral oximeter before, during, and after cannulation for ECMO to determine the direct effects of ligation of the right internal jugular vein and right carotid artery on cerebral oxygenation.	12 experienced low cerebral TOS <60% during pre-ECMO surgery, with most exhibiting the lowest TOS values between cannulation to the onset of ECMO. Two subjects received cardiopulmonary resuscitation (CPR) during surgery and experienced very low TOS (5 and 36%). Pulse oximetry was found to be unreliable during CPR because of diminished pulsatile flow. TOS increased above 60% after the onset of ECMO for all subjects and remained stable.
(Ejike et al. 2006)	INVOS	11	Observe the effects of right carotid artery ligation and variations in extracorporeal life support (ECLS) flow on TOS measured using near infrared spectroscopy.	Ligation of the right carotid artery resulted in a 12–25% decrease in TOS from baseline in the right frontal region for a duration ranging from 17 to 45 mins before returning toward baseline. No substantial change in the left frontal region TOS was detected during cannulation. Following this depression in TOS on the right, there was a transient increase above baseline in TOS observed in both hemispheres on initiating ECLS. No correlation between ECLS flow and TOS was found over the 72-hr period. Periods of “trialing off” ECLS were not related to any change in TOS in either hemisphere.

(Papademetriou et al. 2010)	NIRO 200	4	Investigate differences between oscillations in cerebral and peripheral tissue oxygenation during changes in ECMO flow	Spectral analysis in the form of Fourier transforms were used and to identify the presence of oscillations in different frequency bands. Oscillations related to heart rate and respiration rate appeared in both the brain (cerebral) and the leg (peripheral) data. The presence of mechanical oscillations related to the ECMO pump was also identified in both the brain and the leg in patients where a roller pump was used in the ECMO circuit. Slow frequency oscillations related to Mayer-waves were found in the brain and very slow oscillations related to the endothelia were observed in the leg data.
(Papademetriou et al. 2011)	ETG-100	1	To develop a novel multichannel NIRS protocol for providing regional measurements of cerebral oxygenation and haemodynamics	The preliminary results on single VA-ECMO infant identified differences in regional cerebral oxygenation with changes in ECMO flows

Chapter 5

CEREBRAL AND PERIPHERAL OXYGENATION IN CHILDREN SUPPORTED ON ECMO FOR CARDIO-RESPIRATORY FAILURE

5.1 Introduction

Extracorporeal membrane oxygenation (ECMO) is a life support system for neonates, infants and children with intractable cardio-respiratory failure. It is aimed at supporting the heart and/or lungs temporarily whilst giving them a chance to recover. There are 2 forms of ECMO support—venoarterial (VA) ECMO and venovenous (VV) ECMO. Establishing VA ECMO involves cannulation of major vessels in the neck—right common carotid artery (RCCA) and internal jugular vein—and supports both heart and lungs. VV ECMO involves supporting only the lungs and does not involve cannulation of the RCCA. The ECMO system can operate using two types of blood pumps: 1) A centrifugal pump which uses a high speed rotating device that pulls the blood into the pump and then accelerates it radially outwards and 2) a roller pump which compresses the cannula, thereby pushing the blood through the circuit.

As ECMO is used in patients who are otherwise likely to die, the results focus on survival. However, the reported frequency of abnormal neuroimaging in these patients ranges from 28% to 52%, depending on neuroimaging techniques, and is related both to pre-ECMO events and to the ECMO procedure itself (Bulas and Glass 2005). Patients placed on ECMO as a group have experienced a critical period of haemodynamic instability and have been potentially exposed to dangerously low levels of oxygen in blood, low blood pressure and cell dysfunction. Physiologic changes, such as hypoxia, hypotension, and hypercapnia, associated with ECMO can disrupt cerebral autoregulation. In addition, induction of this life support system exposes the patients to manipulations of the major vessels in the neck. Also, the blood needs to be anticoagulated to maintain flow within the circuit adding risk of bleeding in various organs including the brain. Furthermore, procedures on ECMO affect flow in the circuit and these can similarly affect blood flow to the brain, causing alterations in cerebral perfusion and oxygen delivery to the brain. Previous studies in newborn lambs have shown that VA ECMO alters the ability of the cerebral vasculature to respond, resulting in an impairment of cerebral autoregulation (Short et al. 1993). These alterations were minimal in venovenous ECMO animals (Walker et al. 1996). All the above can have adverse effect on the brain function which can cause neurological disability in the long term.

The development and application of monitors to enhance detection and direct treatment of conditions associated with brain injury is considerable. Near infrared spectroscopy (NIRS) offers the advantage of a continuous, non invasive means of monitoring cerebral oxygenation at the bedside. Ejike et al. report the use of NIRS on ECMO patients during ligation of the RCCA and during variations in the ECMO circuit flows (Ejike et al. 2006). They concluded that regional cerebral oxygenation is not primarily affected by alterations in flows but did demonstrate a significant decrease in right sided cerebral oxygenation during ligation. Previous studies using NIRS to evaluate the effects of vessel ligation showed a decrease in oxy-(HbO₂) and increase in deoxy -(HHb) haemoglobin in the right hemisphere (Liem et al. 1995a) and in both hemispheres (Van Heijst et al. 2004).

To date, NIRS studies on ECMO patients have been concentrated on relative and absolute changes in the amplitudes of HbO₂, HHb and TOI signals, related to vessel

ligation and alterations in the ECMO flows. However, spectral analysis on the NIRS signals may allow us to explore the occurrence of cerebral and peripheral oscillations and potentially relate them to ECMO variables. Furthermore, it has been previously shown that spectral analysis of NIRS signals can be used to assess cerebral autoregulation (De Smet et al. 2009, Tsuji et al. 2000, Wong et al. 2008). Cerebral intravascular oxygenation (HbD), measured by NIRS as the difference between HbO₂ and HHb, can be used as CBF surrogate (Tsuji and du Plessis 1998). Hence, cerebral autoregulation can be evaluated by studying the concordance between HbD and mean arterial blood pressure (MAP), assuming no changes in oxygen consumption, in oxygen saturation and in blood volume.

The long-term aim of this study is to use a multichannel NIRS system, optical topography (OT), to investigate global cerebral oxygenation changes in ECMO patients. However initially regional cerebral and peripheral tissue oxygenation were monitored using a dual channel system, with the aim of investigating the relationship between brain and peripheral tissue oxygenation and how these relate to haemodynamic parameters such as MAP.

5.2 Protocol

All VA and VV ECMO candidates admitted in the intensive care unit (CICU) at Great Ormond Street Hospital (GOSH) were eligible to take part in the study.

The study protocol was designed by the clinical team of the cardiac intensive care unit in GOSH. The ECMO patients as a group go through routine procedures that can cause alterations in cerebral blood flow. These include cannulation, weaning the patient off ECMO prior to decannulation and decannulation. The plan was to assess the effects of these routine procedures on cerebral oxygenation. Therefore, the study period included data collection prior to start of **cannulation** until 10 minutes post establishment of full ECMO flows and prior to start of **weaning for decannulation** until 10 minutes post removal of cannulae. In addition we wanted to assess the effect of **altering ECMO circuit flows** on cerebral oxygenation. This intervention was performed on day 1 or 2 of ECMO support when the patient was on stable ECMO flows with minimal native cardiac output. Manipulations of ECMO circuit flows

were carried out by reducing the circuit flows in consecutive steps of 10% of the initial flow every 10-15 minutes and then stepping the flow back to its initial value.

Mild hypothermia is adopted on ECMO as a neuroprotective strategy. The protocol included an assessment of the effect on cerebral oxygenation of a reduction in temperature to 34°C. **Temperature changes** were performed on day 1 or 2 of ECMO support when the patient was on stable ECMO flows. The temperature was decreased consecutively by 1°C, from normal body temperature to 34°C, every 10-15 minutes and subsequently gradually increased back to normal body temperature.

Increasing CO₂ levels in the blood results in increased cerebral blood flow and can increase cerebral oxygenation. A **CO₂ challenge** is therefore a useful test of cerebral response. This response has not yet been studied in patients on ECMO. The protocol included periods of mild hypercapnia induced by changing the flow of the sweep gases through the membrane oxygenator to achieve pCO₂ of 4.5kPa, 6 and 7kPa consecutively.

Ethical approval was obtained from Great Ormond Street Hospital committee on the Ethics of Human Research. Written, informed parental consent was obtained before each study.

5.3 Instrumentation

Acquiring data in an intensive care environment and especially on this critically ill group of patients was particularly challenging. Setting up the instrumentation was a particularly complex task because the space around the bedside is limited but most importantly because bedside management of this type of patients requires intensive nursing, frequent examinations and routine tests.

A dual channel near infrared system (NIRO 200, Hamamatsu Photonics KK) was used to measure changes in HbO₂ and HHb haemoglobin concentrations using the modified Beer-Lambert Law, and tissue oxygenation index (TOI) using spatially resolved spectroscopy (see chapter 3). NIRS data were collected at frequency of 2Hz or 6Hz and were exported in PC with the use of software designed in Matlab. Channel 1 was placed on the forehead (cerebral) and channel 2 on the calf

(peripheral) of the patients. The optodes were held in place using a double sided tape and elastic bandage to eliminate possible drifts in the signal arising from gradual loss of contact between the optode and the skin. For the conversion of the optical attenuation changes to chromophore concentration changes a differential pathlength factor (DPF) of 4.99 was applied when the patient was younger than 1 year old (Duncan et al. 1995). Otherwise, the age dependence equation of DPF was used (see section 4.1.5).

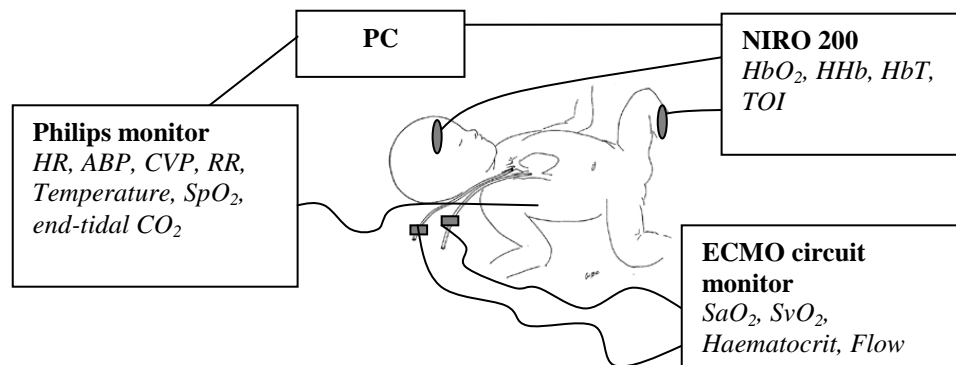


Figure 5.1: Schematic diagram of the instrumentation used. A PC is connected to the Philips monitor via SRS-323 port. Systemic data were collected and exported to the PC via Trendface software. An SD card was used to export the ECMO data for off line analysis. The NIRO-200 was connected to the PC via a SRS-323 port and data were collected via software designed in Matlab..

Figure 5.1 shows a diagram of the instrumentation used. Simultaneous collection of systemic and ECMO circuit parameters was a complicated task. Data exported for off line analysis of these parameters was not being implemented on the intensive care unit. Various methods for exporting the data were investigated; the most straightforward involved using customised software (Trendface, Ixellence GmbH, Germany). The software was installed on a PC and systemic data from the Philips monitors (Intellvue MP70, Philips Medical) were collected through a SRS 323 port. Systemic data; arterial blood pressure (ABP), central venous pressure (CVP), end-tidal CO₂, heart rate (HR), respiration rate (RR), pulse, temperature and arterial oxygen saturation (SaO₂), were continually measured, recorded and displayed in real time at the bedside (Intellvue MP70, Philips Medical). ABP and CVP were obtained invasively, usually from radial artery and femoral vein respectively. SaO₂ was obtained from a pulse oximeter placed on the toe of the patients. ABP, CVP, RR and

end-tidal CO₂ were recorded as continuous waveforms at a frequency of 125Hz (ABP and CVP) and 62.5Hz (RR and end-tidal CO₂). These four parameters were also collected as averaged values at 1Hz. HR, SpO₂, temperature and pulse were also collected at 1Hz.

Parameters related with the ECMO circuit were also collected continually at the bedside (M3 monitoring system, Spectrum Medical Ltd.). These included arterial oxygen saturation measured at the arterial cannula side (SaO₂) and blood flow in the ECMO circuit measured using probes placed at the arterial cannula, venous oxygen saturation (SvO₂) measured using a probe placed on the venous cannula, and haematocrit. An S.D. memory card was used to collect the ECMO circuit parameters by inserting it in the slot of the Spectrum Medical monitor.

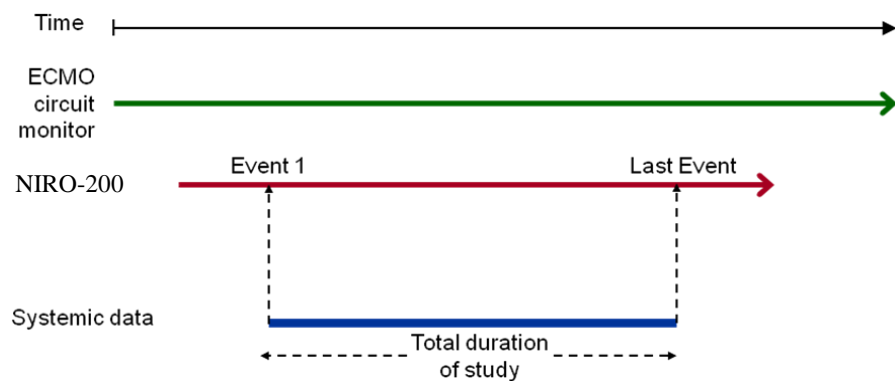


Figure 5.2: Illustrating the sequence followed for obtaining simultaneous collection of systemic, ECMO parameters and with optical parameters from the dual-channel NIRS system NIRO-200.

In order to proceed with data analysis, synchronisation of the time base axes between the three monitors was addressed. Synchronisation between the NIRO data and systemic parameters was achieved by placing an event marker on the NIRO system at the time when the Trendface software started the collection of the systemic data. To synchronise the ECMO circuit parameters with the systemic parameters the clock stamps on the ECMO monitor and Trendface software were used. Figure 5.2 demonstrates the sequence followed for synchronising the data from the three monitors.

5.4 Subjects

A total of 8 ECMO patients, aged between 1 day and 5 years, were monitored during the different ECMO phases as described in the protocol. The patients are listed in table 5.1. This is a rather inhomogeneous group consisting of 7 VA ECMO cases, 3 of which operated on centrifugal pumps and the other 4 on roller pumps, and 1 VV ECMO on roller pump. Even though the aim was to follow the complete protocol with every patient this was not achievable in practice. It was difficult to be present in the intensive care unit at all hours and hence made it particularly difficult to monitor procedures such as cannulation, weaning and decannulation, especially when they these were scheduled at inconvenient hours. However, all 8 patients were monitored during alterations in the ECMO flows. Alterations in the ECMO flows refer to sequential reduction or increase in the ECMO circuit flows from baseline. Flows were reduced/increased in increments of 10% approximately every 10-15. Two patients were monitored during cannulation, 1 patient during weaning “trial off” period, 1 during pCO₂ changes and 1 during temperature changes. The temperature and CO₂ challenges were attempted only once, on different patients. Due to the complex physiology of the ECMO circuit it was particularly difficult to induce changes in both these parameters and these two interventions were later excluded from the protocol.

Table 5.1: List of ECMO patients monitored using the dual channel NIRO-200 system.

Patient ID	Indication for ECMO	Clinical condition	Age	ECMO Type	Cannulation sides	Type of pump	Sampling rate (Hz)	Cannulation	Flow changes	Weaning "trial off"	CO ₂ changes	Temperature changes	Systemic & ECMO circuit parameters
D1	Cardiac - post cardiac surgery	Post TAPVC repair	9 days	VA	RCCA & IJV	Roller	2	-	Yes	Yes	-	-	-
D2	Cardiac - cardiomyopathy	Dilated cardiomyopathy, ventricular tachycardia	5 years	VA	RCCA & IJV & FV	Centrifugal	6	-	Yes	-	-	-	-
D3	Neonatal Respiratory failure	Neonatal hypoxaemic respiratory failure with PPHN	3 days	VV	IJV	Roller	6	-	Yes	-	-	-	-
D4	Cardiac - myocarditis	Parvovirus Myocarditis	1 year	VA	RCCA & IJV	Centrifugal	6	Yes	Yes	-	-	-	-
D5	Cardiac - post cardiac surgery	Post Interrupted Arch/VSD and later Norwood I surgery	5 days	VA	RCCA & IJV	Roller	6	-	Yes	-	-	-	-
D6	Neonatal Respiratory failure	Neonatal hypoxaemic respiratory failure with PPHN	3 days	VA	RCCA & IJV	Roller	6	-	Yes	-	-	-	-
D7	Paediatric Respiratory Failure	RSV broncholitis	3 months	VA	RCCA & IJV	Roller	6	-	Yes	-	-	-	-
D8	Cardiac	Kawasaki disease	6 months	VA	RCCA & IJV	Centrifugal	6	-	Yes	-	Yes	Yes	Yes

5.5 Cerebral and Peripheral tissue oxygenation during various ECMO phases

Varying baseline levels of tissue oxygenation index (TOI) were observed between individual patients. The range of TOI value in both the brain and leg of the patients varied between 55-80% with significant intersubject variability. In addition, variability in the trends of other NIRS parameters (HbO₂, HHb and HbT) were also observed. The small sample size in combination with the diverse population studied made it impractical to formulate group observations by investigating trends or absolute changes in NIRS parameters.

In this section HbO₂, HHb and TOI data obtained during each of the different ECMO phases, cannulation, weaning off ECMO, pCO₂ and temperature challenges, are presented (figures 5.3-5.7).

5.5.1 Cannulation

Monitoring commenced when surgeons begun dissecting the neck and finished when full ECMO was established. Figure 5.3 shows how HbO₂ (red), HHb (blue), HbT (black) and TOI (green) vary in the brain and leg of the patient D1 during the procedure. The dotted lines mark the time when the right common carotid artery (RCCA) was clamped and ligated, right internal jugular vein (RIJV) was clamped and ligated and when all clamps were off and the patient was on ECMO. Clamping the RCCA causes a drop in HbO₂ and an increase in HHb while HbT stays the same, resulting in a drop in TOI. This was observed in both brain and leg. Clamping the RIJV caused an increase in HHb in both brain and leg. When all clamps were off and the patient went on ECMO there was an immediate decrease in HbO₂, HHb and HbT, followed by a decrease in TOI. Then, HbO₂, HbT and TOI in the leg increased and returned to their original values while the same parameters showed an increase in the brain but were still below their original values.

5.5.2 Weaning

The weaning procedure starts by reducing the ECMO circuit flows by 10% approximately every 15 minutes. This is similar to the alteration in the ECMO flows included and described in the protocol above. Figure 5.4 shows NIRS data (HbO₂ (red), HHb (blue), HbT (black) and TOI (green)) in the brain and leg of patient during flow reduction from baseline (100%) flow down to 70% of the baseline flow. The raw data in the brain and leg differ significantly. The leg data showed a gradual decrease followed by a gradual increase in HbO₂ (and HbT) and a gradual increase followed by a gradual decrease in HHb when the flows were reduced from 100% to 90% of baseline flows. A similar pattern was shown when the flows were decreased further to 80%. The increase in HbO₂ when the flows were decreased further to 70% might be an indication that the heart of the patient started to take over. In addition the leg data showed strong very slow oscillations clearly visible when the flow was at 80% of baseline flow. The brain data did not reveal such large changes. However, an increase in HbO₂ was seen when the flows were decreased to 70% of baseline flow.

The weaning procedure, involves reduction of the ECMO circuit flows to minimum, followed by clamping of the arterial and venous cannulae such that blood from the ECMO circuit stops flowing in and out of the patient. The patient is then off ECMO but the ECMO circuit is still connected to the patient with blood circulating through the ECMO circuit bridge. The patient stays connected but off ECMO for several hours in order to verify whether the patient's heart and/or lungs have recovered. This usually called the "trial off" period prior to decannulation. During this period, the arterial and venous cannulae are unclamped and clamped every 15 minutes, "flushing" blood in the patient. This is done in order to prevent blood clotting in the cannulae.

Figure 5.5 shows data collected during ECMO "trial off" period. The dotted lines in the plots represent "flushing" of the cannulae. Flushing the cannulae caused a sharp increase in HbO₂ and decrease in HHb, in both the brain and leg, while HbT increased indicating a rush of blood from the ECMO circuit flowing in the patient. This was reflected as a sharp increase in TOI.

5.5.3 CO₂ challenge

Figure 5.6a shows NIRS data obtained during changes in pCO₂ (HbO₂ (red), HHb (blue), HbT (black) and TOI (green)) in the brain and leg of a patient D8. A change in pCO₂ was achieved by changing the amount of O₂ gas sweep through the membrane oxygenation in the ECMO circuit. In this case, O₂ sweep gas was reduced to 50% of its original value (from 2 lpm to 1 lpm) shown by the first dotted line in the graphs and maintained for about 10 minutes before it was reduced by further 50% (to 0.5 lpm). After 10 minutes the sweep gas was brought back to its original value. During the first reduction pCO₂ was increased from 4.94 kPa to 5.46 kPa, it was then increased further to 7.12 kPa and then brought back to 5.61 kPa (figure 5.6b). An increase in pCO₂ caused a gradual increase in cerebral HbO₂ and HHb, and resulted in a gradual increase in TOI. Furthermore, a decrease in pCO₂ caused a decrease in cerebral HbO₂, HHb and TOI. These changes were not observed in the peripheral oxygenation data.

5.5.4 Temperature challenge

Figure 5.7 shows data collected during the temperature challenge. The dotted lines in the graphs represent a reduction/increase in temperature. Temperature was reduced by 1°C consecutively every 10 minutes and then increased back to original value. A decrease in temperature was associated by a decrease in HbO₂ and TOI and an increase in HHb. Conversely, an increase in temperature caused an increase in HbO₂ and TOI and a decrease in HHb.

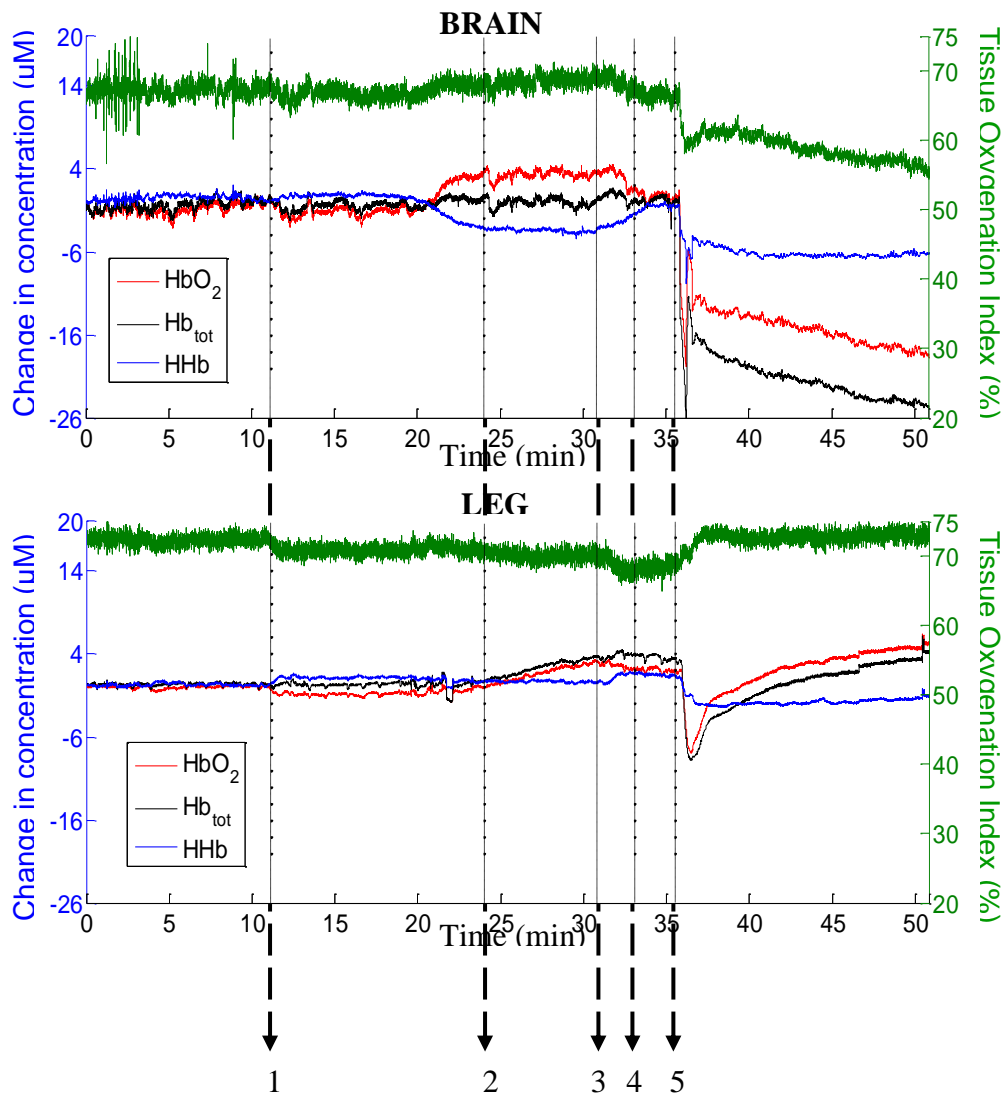


Figure 5.3: HbO_2 (red), HHb (blue), HbT (black) and TOI (green) data for the brain and leg of patient D4 monitored during cannulation. The dotted lines mark events during the cannulation procedure: clamping of the right common carotid artery (RCCA) (1), ligating RCCA (2), clamping of the right internal jugular vein (RIJV) (3), ligating RIJV (4), all clamps removed and patient goes on ECMO support (5).

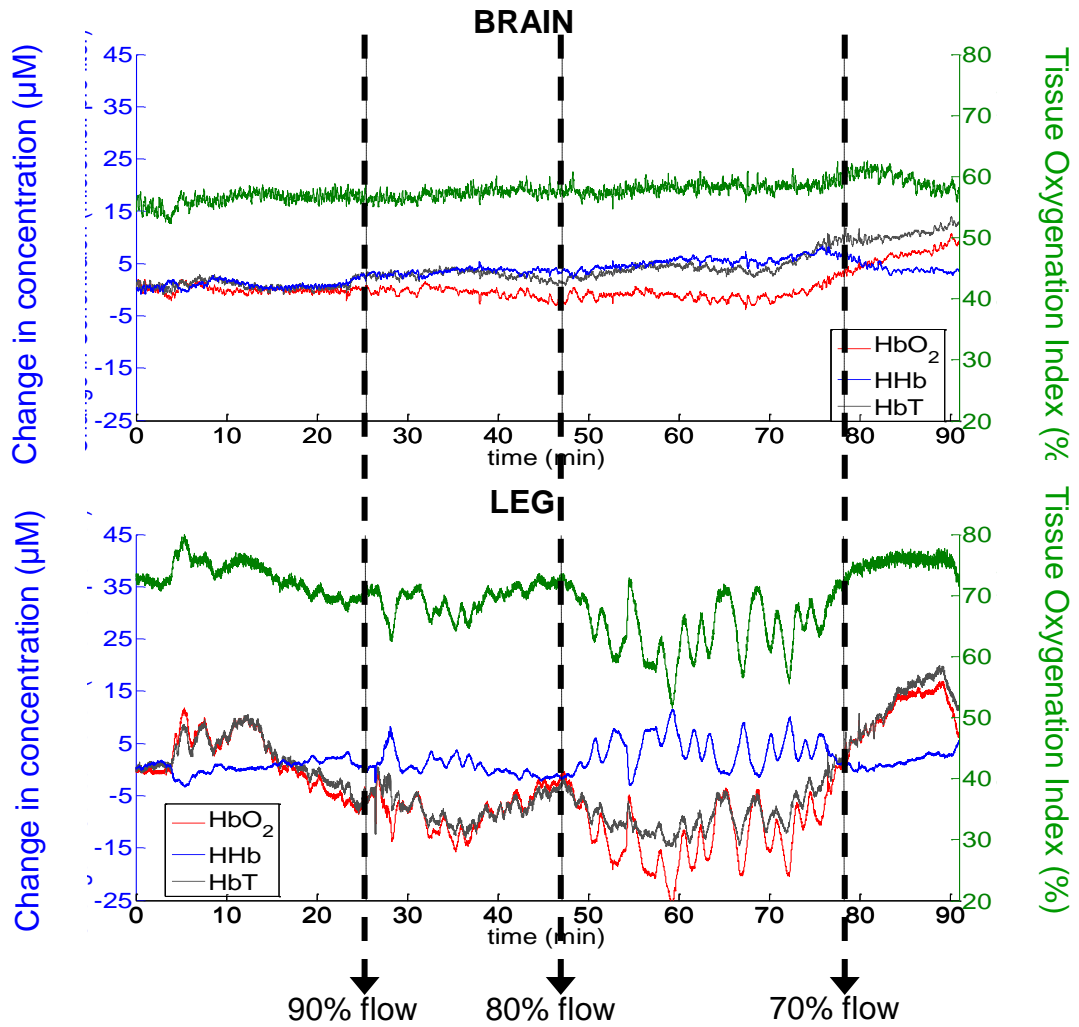


Figure 5.4: HbO₂ (red), HHb (blue), HbT (black) and TOI (green) data for the brain and leg of patient D1 monitored during reduction in ECMO circuit flows. Each reduction in flow is shown by the dotted lines.

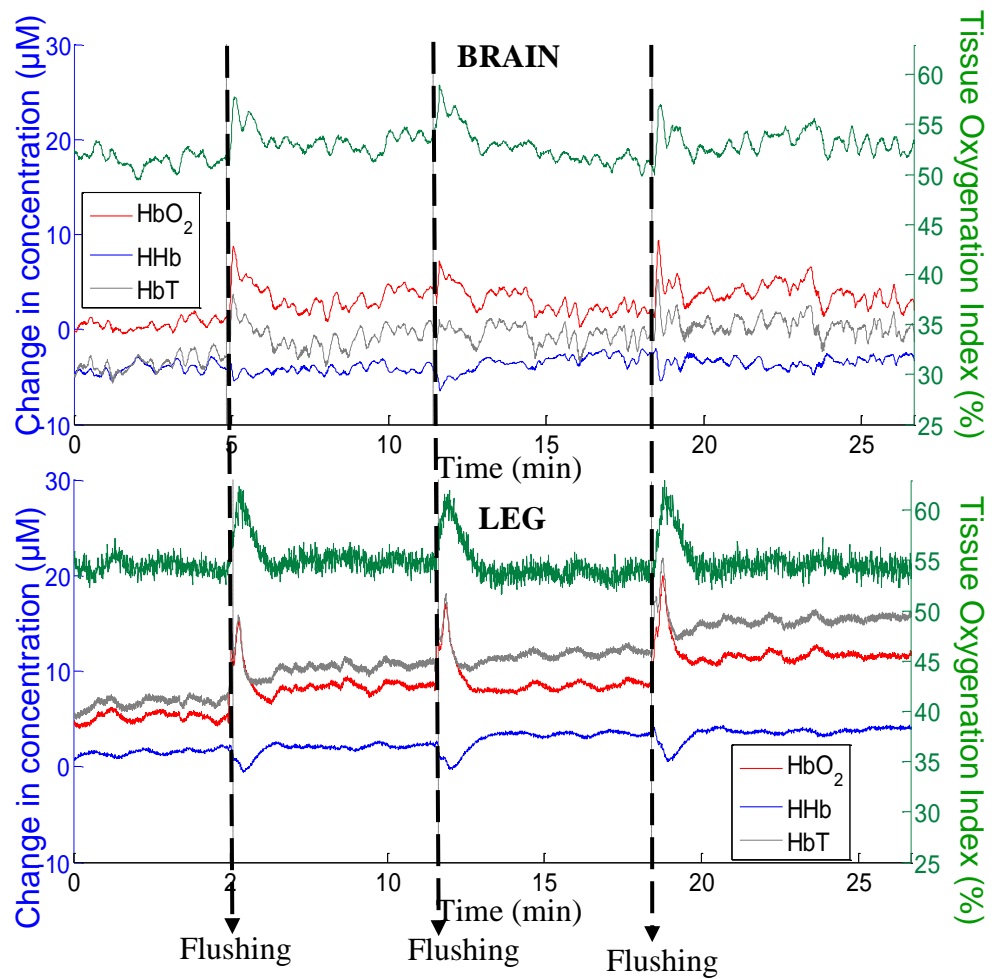


Figure 5.5: HbO₂ (red), HHb (blue), HbT (black) and TOI (green) in the brain and leg of patient D1 monitored during ECMO “trial off” period. Each dotted line represents “flushing” blood in the cannulae.

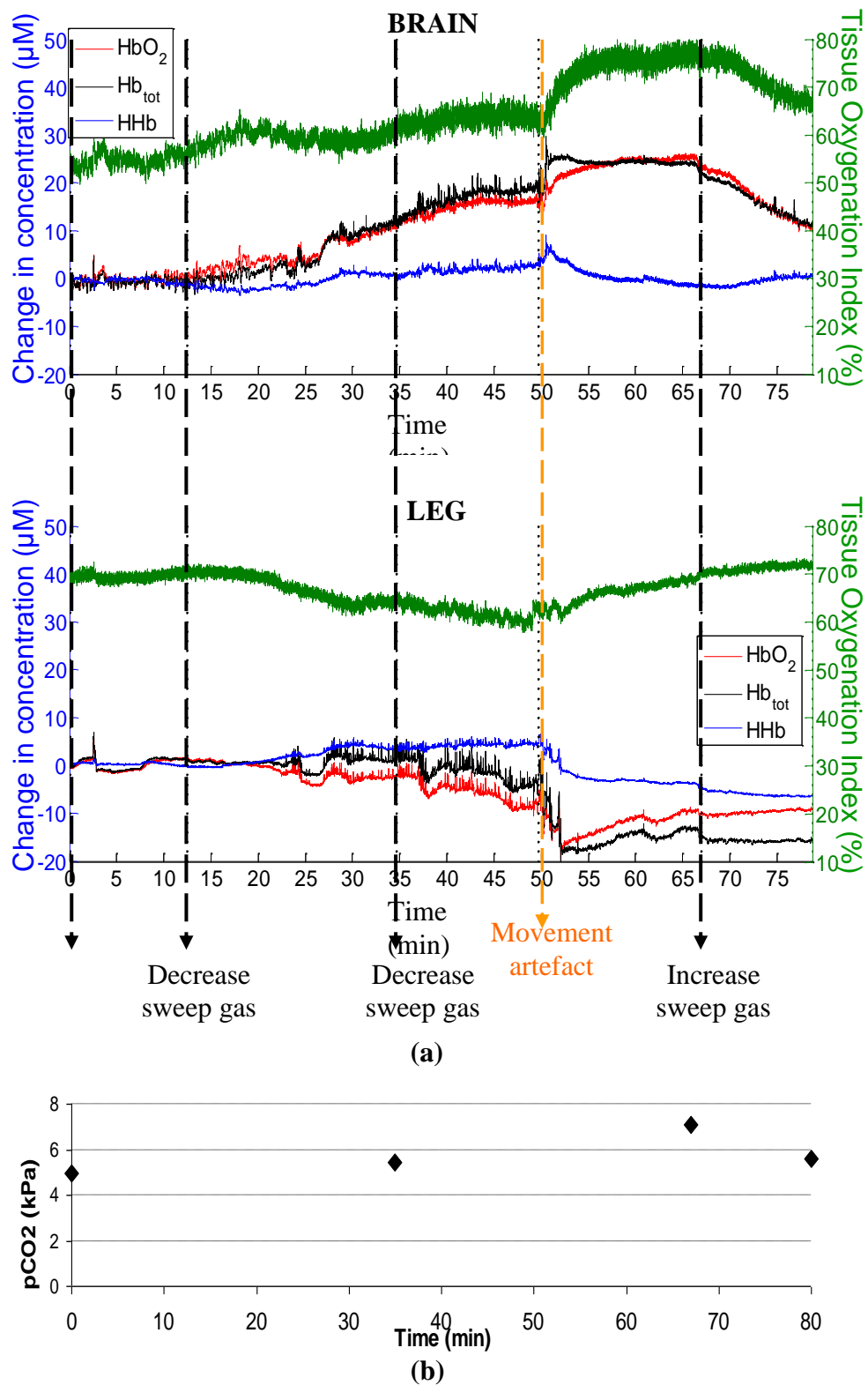


Figure 5.6: (a) HbO_2 (red), HHb (blue), HbT (black) and TOI (green) data for the brain and leg of patient D8 during changes in pCO_2 (b). Each change is shown by the black dotted lines.

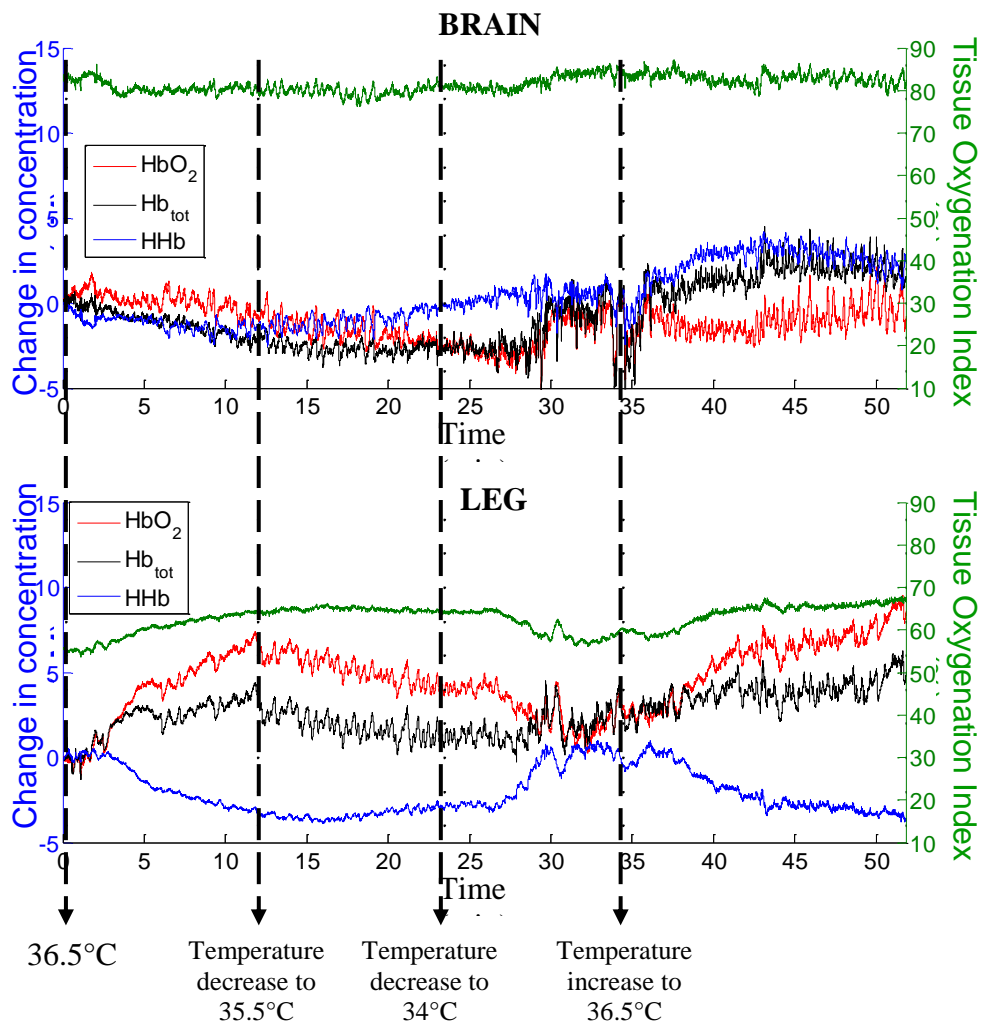


Figure 5.7: HbO₂ (red), HHb (blue), HbT (black) and TOI (green) data for the brain and leg of VA ECMO patient D8 during changes in temperature. Each change is shown by the black dotted lines.

5.6 Spectral Analysis

5.6.1 Power spectral density

5.6.1.1 Methods

Power spectral density analysis was performed on 7 patients monitored during alterations in the ECMO flows (patients D1-D7 on table 5.1). The data were divided into sections each representing each flow period. Power spectral densities (PSD) were obtained for the HbO₂ signal recorded at the two measurement sites. The PSDs were obtained in order to identify the presence of any oscillations occurring in the brain and in the leg and were estimated using Welch's method (Welch 1967). Computations were performed using a scientific software package (Matlab, Mathworks Inc). Four frequency bands were defined (very low (VLF) 0.002-0.25 Hz, low (LF) 0.25-0.5 Hz, high (HF) 0.5-1 Hz and very high (VHF) 1-3 Hz) to extract vasomotion, respiratory, mechanical (or ECMO pump) and cardiac oscillations. The strength of the oscillations between the brain and the leg corresponding to each ECMO circuit flow were compared for the LF band containing respiration rate (RR) and HF band containing any mechanical oscillation from the ECMO pump.

5.6.1.2 Results

Figure 5.8 shows the PSDs of the HbO₂ signal during weaning for patient D1 supported on VA ECMO. The raw HbO₂ data for this patient are shown in figure 5.5. In this case the ECMO flows were reduced sequentially from baseline flow down to 70% of baseline flow by 10% approximately every 10-20 minutes. In this case, a roller pump was used to operate the ECMO circuit. PSD analysis showed the presence of a strong oscillation in the brain and leg that remained constant as the ECMO circuit flow was decreased. This frequency might correspond to the patient's respiration rate (RR). A higher frequency appeared in both the brain and leg that shifted to the left with decreasing ECMO flow. This frequency was twice the frequency of the ECMO roller pump (f_{pump}), which was consistent with the two

headed roller pump. In addition, a very slow oscillation (~ 0.005 Hz) was present only in the leg. The strength of this oscillation appeared to increase as the flow was reduced and is clear even in the time domain (figure 5.5).

Figure 5.9 shows: a) HbO_2 data and b) the corresponding PSDs for patient D4. This patient was supported on a VA ECMO and a centrifugal pump was used to operate the ECMO circuit. The PSDs of this patient showed the presence of two oscillations, one in the LF band corresponding to the patient's RR and the other in the HF band corresponding to the patient's heart rate (HR). There was no indication of the pump frequency. However, oscillations can be observed in the VLF band. In comparison to the previous patient these oscillations occurred around 0.015 Hz and appeared only in the brain and not in the leg.

Figure 5.10 shows HbO_2 data and corresponding PSDs for patient D3 supported on VV ECMO which operated using a roller pump. RR and the HR were present in both brain and leg. Oscillations were also shown around 0.005 Hz which only appeared in the leg data and around 0.05 Hz only appeared in the brain data. The difference between the oscillations in the VLF range can be clearly seen even in the time domain plots (figure 5.10a).

PSD analysis of HbO_2 for patient D5 are shown in figure 5.11. This patient was supported on VA ECMO and the ECMO circuit operated on a roller pump. Oscillations related to the RR and twice the pump frequency (f_{pump}) were observed in both brain and leg data. Slow oscillation around 0.01Hz were only present in the brain. Similarly patient D6 (VA ECMO; roller pump) showed oscillations related to the RR, HR and $2 \times f_{\text{pump}}$ which occurred in both brain and leg (figure 5.12). However, this patient showed the presence of a slow oscillation (0.05Hz) in the leg and not in the brain. PSD analysis of patient D7 (VA ECMO; roller pump) showed the presence of HR oscillations in both the brain and leg, and a slow oscillations (0.05Hz) which appeared only in the brain data (figure 5.13). The pump frequency and RR were not observed in this case.

Spectral analysis was performed on patient D2 undergoing VA ECMO with a centrifugal pump. The PSDs, shown in Figure 5.13 identify the RR and the HR.

Similar to the results of patient 1, the PSD of this patient showed the presence of oscillations (~ 0.005 Hz) in the leg and not in the brain.

In an effort to compare the strength between cerebral and peripheral oscillations, the ratio of the LF and HF powers were obtained as a function of flow change for the brain and leg data of the 7 ECMO patients (figure 5.15). The powers of each band were measured by obtaining the area under the PSD plots for each band. The results are depicted using a colour coded grid shown in figure 5.16 where the LF/HF power in the leg was subtracted from the LF/HF power in the brain. A red colour indicates that the oscillations are stronger in the brain compared to the leg. A blue colour indicates that oscillations in the brain are weaker than in the leg. Comparison between these two bands will give an insight into the strength of the mechanical oscillations caused by the roller pump frequency and potentially compare between the use of a roller and centrifugal pumps. It is worth noting, that in four out of four patients who underwent reductions in flows the oscillations appeared to be weaker in the brain compared to the leg. This type of analysis, on data from a larger population of patients, may be useful in determining whether the level of pulsatility in flow is associated with neurologic dysfunction.

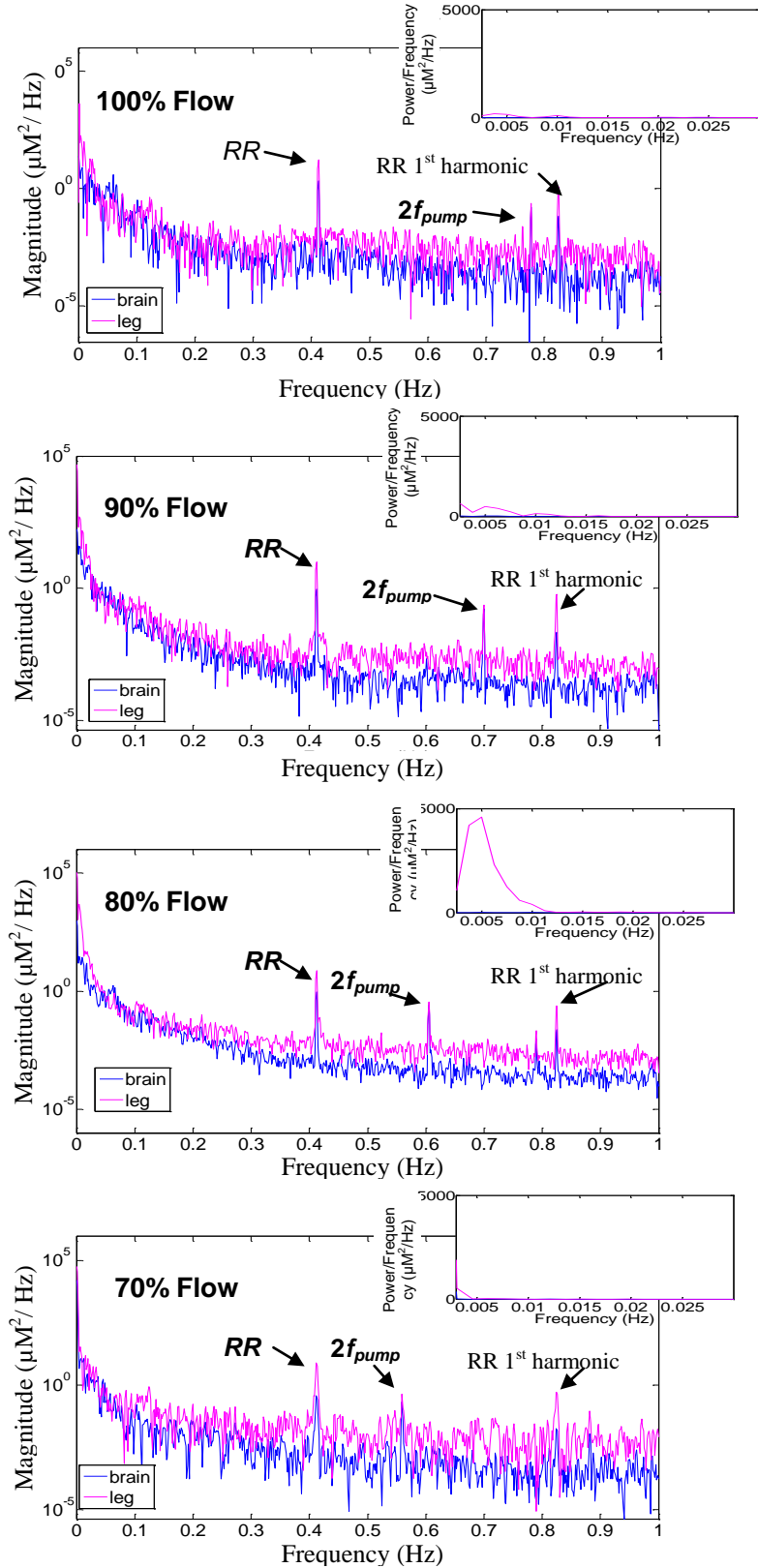


Figure 5.8: PSDs in the brain (blue) and leg (pink) of patient D1 at baseline flow (100% flow), 90%, 80% and 70% of baseline flow. The show the frequencies corresponding to the respiration rate (RR) and twice the pump frequency ($2f_{\text{pump}}$). The inserts show the presence of a slow oscillation in the VLF range of the leg data.

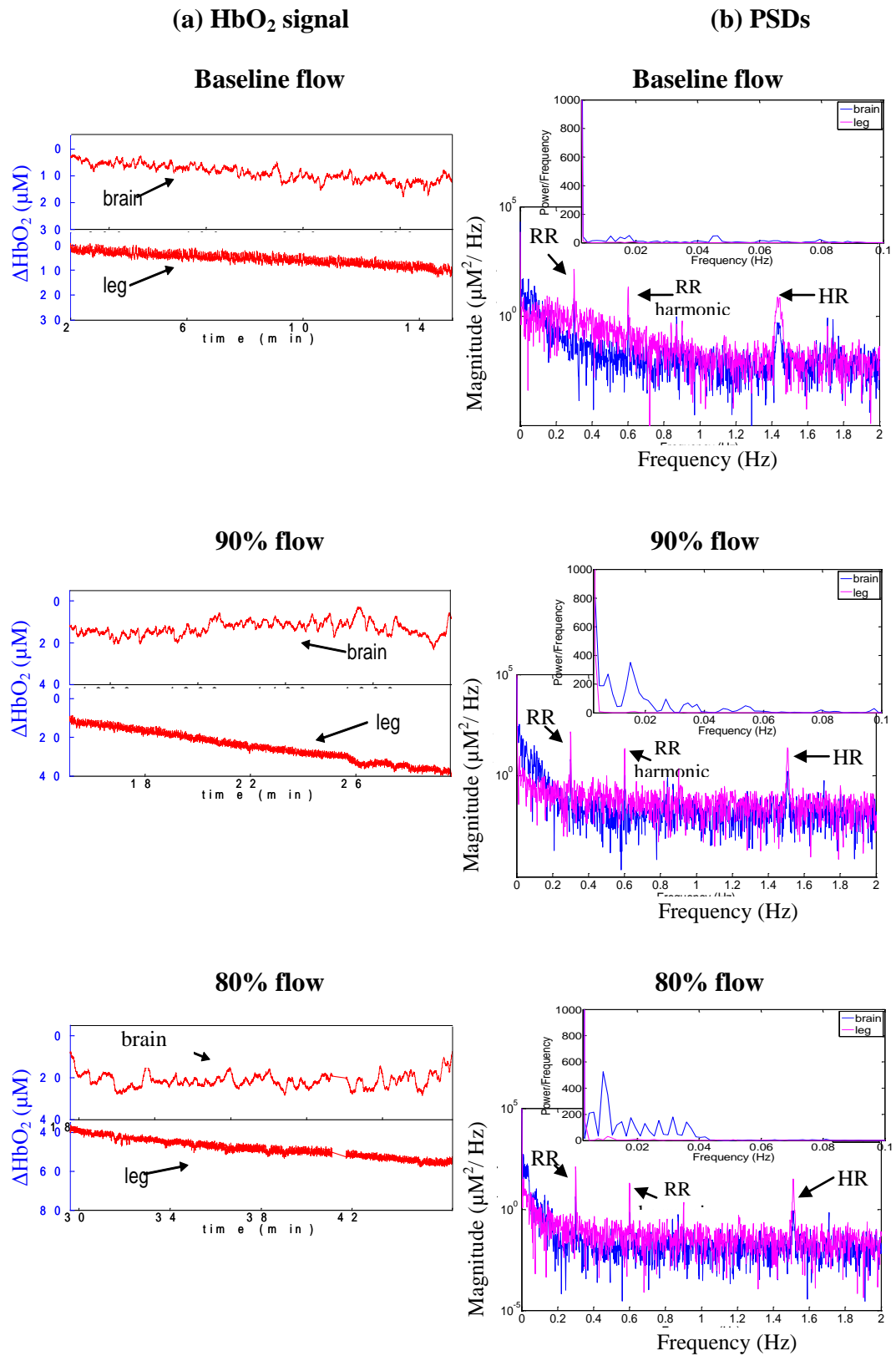


Figure 5.9: (a) HbO₂ data in the brain and leg for Patient D4 monitored during reductions in the ECMO flows. (b) Corresponding PSDs in the brain (blue) and leg (pink) showing the respiration rate (RR) and heart rate (HR). The inserts show the presence of a slow oscillation in the VLF range of the brain data.

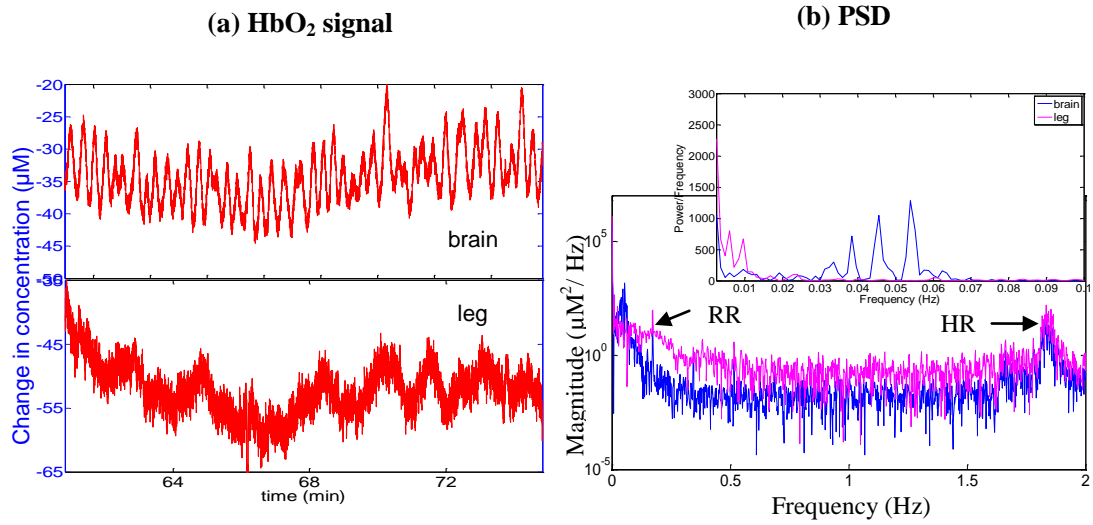


Figure 5.10: (a) HbO₂ data in the brain and leg for Patient D3. (b) Corresponding PSDs in the brain (blue) and leg (pink) showing the respiration rate (RR) and heart rate (HR). The insert shows the presence of slow oscillations in the VLF range.

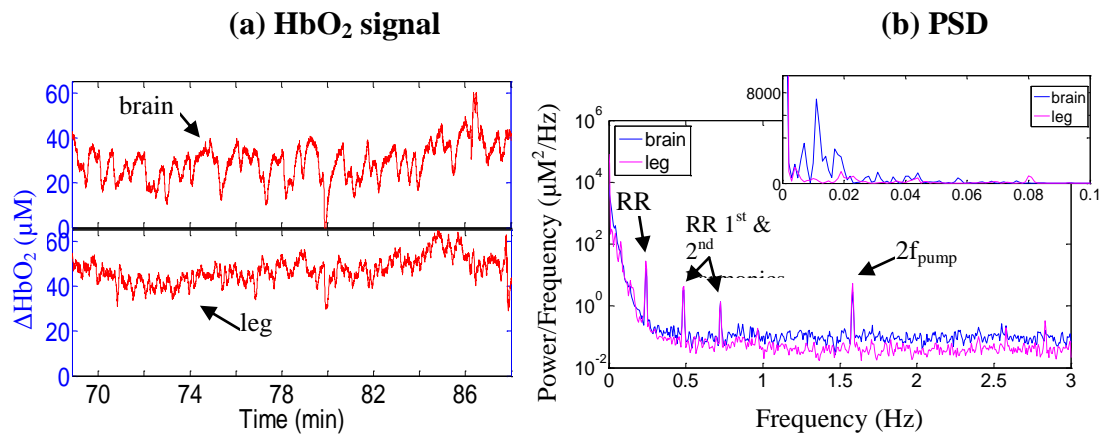


Figure 5.11: (a) HbO₂ data in the brain and leg for Patient D5. (b) Corresponding PSDs in the brain (blue) and leg (pink) showing the respiration rate (RR) and heart rate (HR). The insert shows the presence of slow oscillations in the VLF range present in the brain.

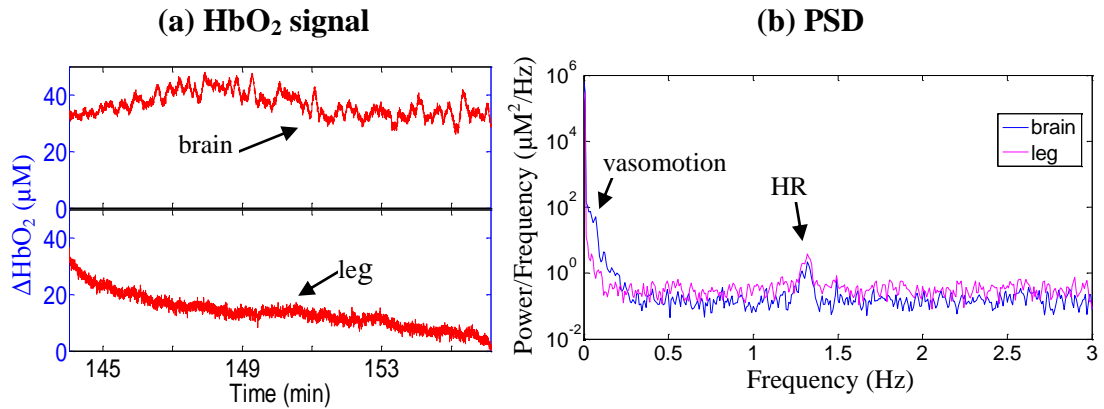


Figure 5.12: (a) HbO_2 data in the brain and leg for Patient D6. (b) Corresponding PSDs in the brain (blue) and leg (pink) showing the heart rate (HR) and vasomotion oscillations occurring in the brain.

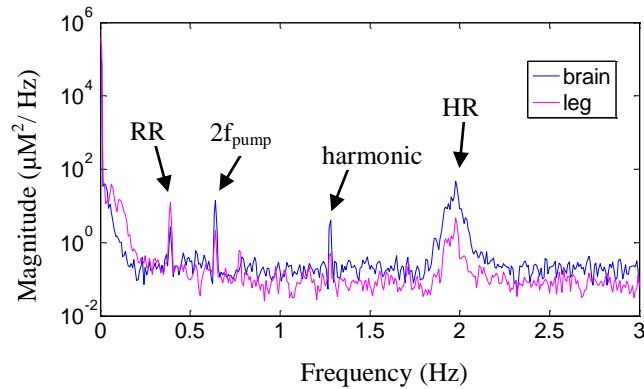


Figure 5.13: PSDs in the brain (blue) and leg (pink) of patient D7 showing the RR heart rate (HR) and pump frequency.

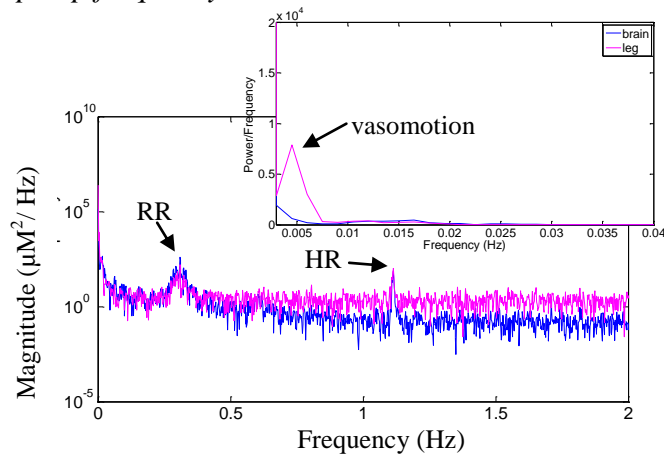


Figure 5.14: PSDs in the brain (blue) and leg (pink) of patient D2 showing the RR, heart rate (HR) and vasomotion oscillations occurring in the brain. The insert shows the presence of slow oscillations in the VLF range present in the leg.

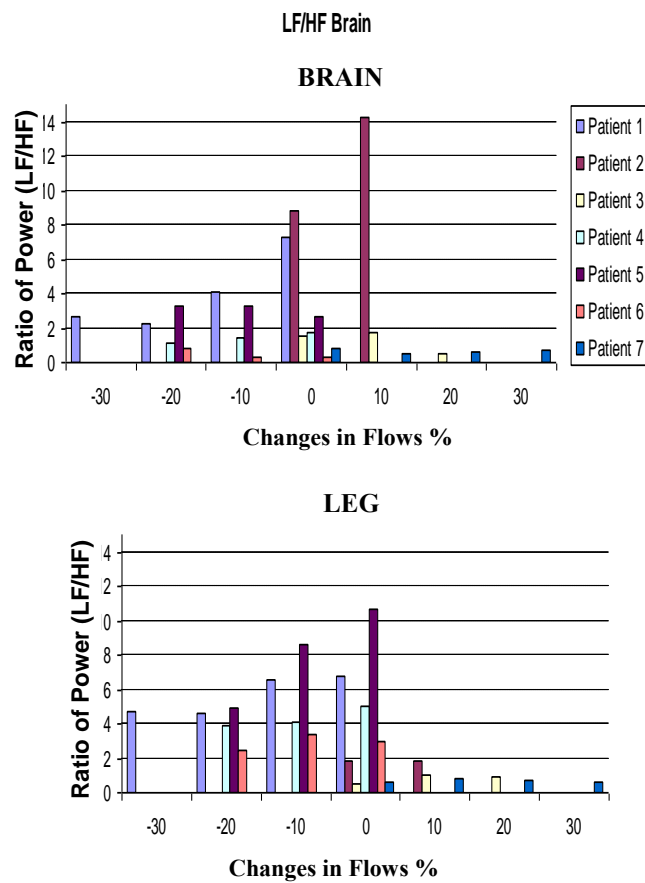


Figure 5.15: Power ratio as a function of ECMO flow in the brain and leg for the 7 ECMO patients.

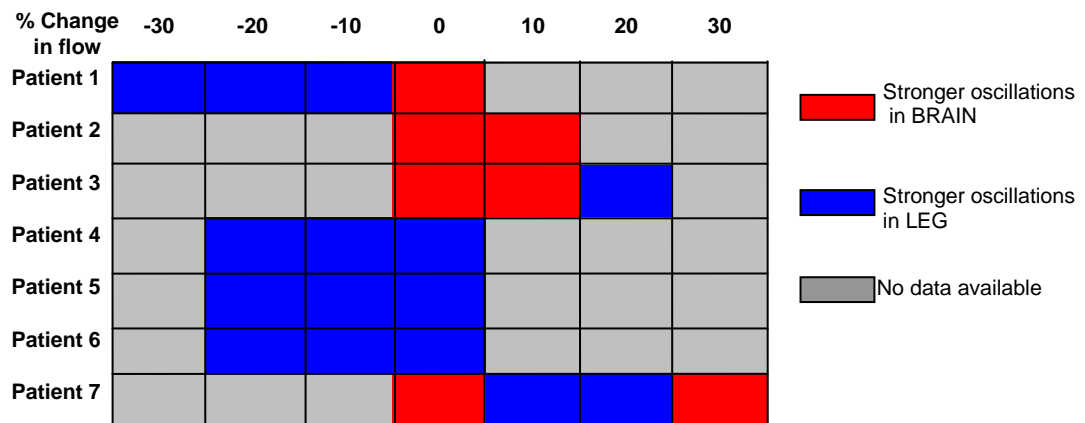


Figure 5.16: Comparison between the strength of oscillations in the brain and leg.

5.6.2 Coherence

5.6.2.1 Methods

One of the ECMO patients listed in table 5.1 had systemic and ECMO data collected simultaneously with NIRO data. The MAP was obtained by averaging the arterial waveform every 0.2s (equivalent to sampling frequency of 5Hz) and the NIRO 200 data were downsampled from 6Hz to 5Hz. The concordance between MAP and cerebral HbD (difference between HbO₂ and HHb) and MAP and peripheral HbD for this were quantified in a frequency specific manner using coherence function analysis. The signals were divided into sections representing each flow period and 9 minute epochs prior to decreasing (or increasing) the flow were analysed. The coherence describes the degree of correlation between the waveforms at a given frequency or frequency range. A coherence of 1 indicates perfect frequency specific correlation, and a coherence of 0 indicates complete lack of frequency specific correlation. Coherence scores were computed for each 9-minute epoch, representing a specific blood flow, for bandwidths covering the limits of the data sampling interval (0-0.01Hz, 0.01-0.25Hz, 0.25-0.5Hz, 0.5-1Hz, 1-2.5Hz for ultralow, very low, low, high, and very high frequency ranges, respectively). To obtain a measure of the coherence (COH) over a specific frequency band, the coherence function was averaged over that frequency band. By convention, COH values of ≥ 0.5 , are considered to represent significant concordance between the two waveforms (Kuo et al. 1998, Tsuji et al. 2000, Wong et al. 2008). High concordance between MAP and HbD, and therefore high COH values, can be anticipated when autoregulation is impaired, as in this circumstance CBF and oxygen delivery become pressure passive.

5.6.2.2 Results

Figure 5.17 illustrates the temporal variation in MAP and HbD in the brain and leg for a VA patient on a centrifugal pump undergoing manipulations in the ECMO circuit flows. The coherence function between cerebral HbD and MAP for the ECMO flow period A (baseline [100%] ECMO flow) is shown in figure 5.18. The

figure illustrates the variable COH indicating a high degree of concordance between the MAP and cerebral HbD in the ULF band ($\text{COH} > 0.5$) and low degree of concordance in the rest of the frequency bands. COH scores for the rest of the ECMO flow periods show a low degree of concordance in all frequency bands (table 5.2). A high coherence value between cerebral HbD and MAP is an indication that CBF is pressure passive and if this is maintained for a long period of time it can suggest that cerebrovascular autoregulation is impaired. The COH scores between peripheral HbD and MAP, and cerebral HbD and peripheral HbD for all ECMO flows are listed in Table 5.2. High COH scores between peripheral HbD and MAP are reported in the ULF band when the flows were increased from 80% of baseline back to 90% baseline and back to baseline. These high scores are not reflected in COH between cerebral HbD and MAP suggesting an intact cerebral autoregulation.

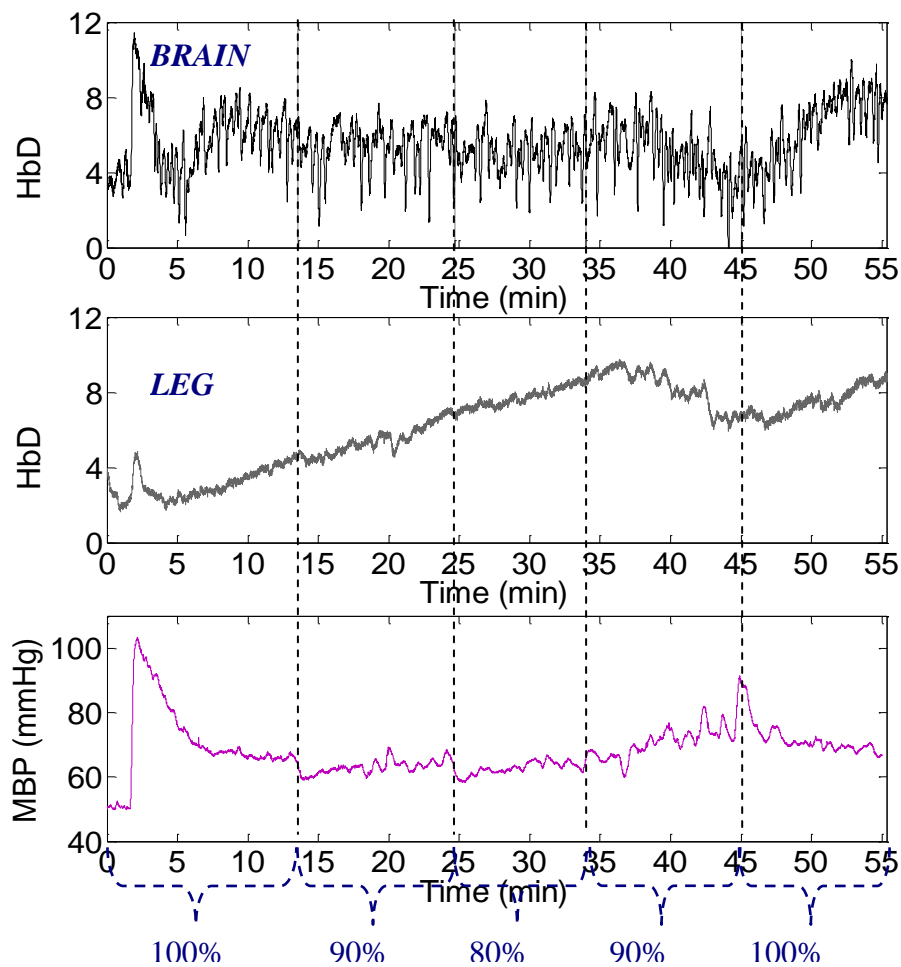


Figure 5.17: Temporal variation in cerebral HbD and peripheral HbD along with MAP for patient D8, a VA patient on centrifugal pump.

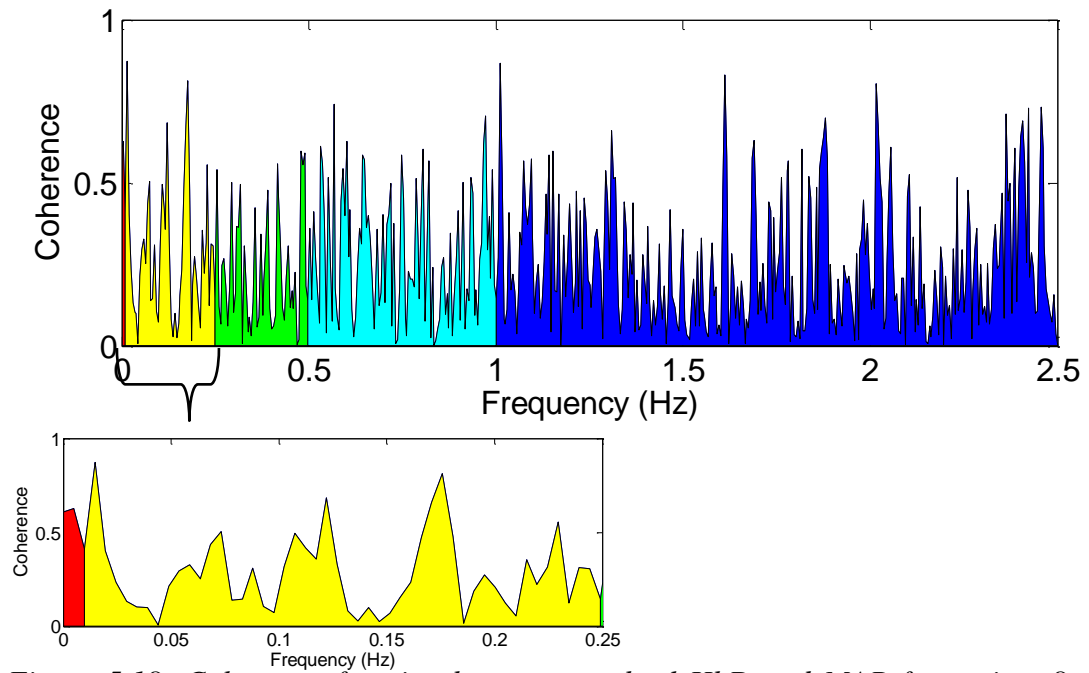


Figure 5.18: Coherence function between cerebral HbD and MAP for patient 8 at initial 100% ECMO flow, indicating high COH score (>0.5) in the ULF band (red), and low COH score in the VLF (yellow), LF (green), HF (cyan) and VHF (blue).

Table 5.2: COH scores for patient 19. High COH scores (≥ 0.5) are highlighted.

cerebral HbD Vs MAP	100% flow	90% flow	80% flow	90% flow	100% flow	
	ULF	0.57	0.25	0.09	0.19	0.37
	VLF	0.28	0.26	0.31	0.23	0.28
	LF	0.23	0.23	0.28	0.34	0.26
	HF	0.27	0.24	0.29	0.24	0.18
	VHF	0.24	0.24	0.23	0.25	0.21
peripheral HbD Vs MAP	100% flow	90% flow	80% flow	90% flow	100% flow	
	ULF	0.35	0.40	0.18	0.50	0.61
	VLF	0.28	0.35	0.28	0.28	0.23
	LF	0.23	0.23	0.22	0.27	0.21
	HF	0.24	0.22	0.23	0.26	0.27
	VHF	0.24	0.25	0.25	0.24	0.24
cerebral HbD Vs peripheral HbD	100% flow	90% flow	80% flow	90% flow	100% flow	
	ULF	0.48	0.29	0.66	0.18	0.31
	VLF	0.21	0.22	0.29	0.23	0.24
	LF	0.26	0.29	0.22	0.23	0.25
	HF	0.28	0.28	0.24	0.23	0.27
	VHF	0.22	0.26	0.26	0.24	0.21

Table 5.3: Oscillations in the ECMO patients

Patient ID	Type of ECMO	ECMO pump	HR	RR	Pump frequency	Vasomotion
1	VA	Roller	Yes	Yes	Yes	0.005Hz (leg)
4	VA	Centrifugal	Yes	Yes	-	0.005Hz (leg)
7	VV	Roller	Yes	Yes	-	0.005Hz (leg) 0.05Hz (brain)
8	VA	Centrifugal	Yes	Yes	-	0.015Hz (brain)
10	VA	Roller	-	Yes	Yes	0.01Hz (brain)
11	VA	Roller	Yes	Yes	Yes	0.05Hz (leg)
13	VA	Roller	Yes	-	-	0.05Hz (brain)

5.7 Discussion

In assessing the role of NIRS monitoring, it is important to emphasize its unique qualities, including non-invasive, continuous real-time measurement of regional tissue oxygen saturation. However, caution must be exercised in extrapolating regional measurements to global findings. A total of 8 patients were monitored using the dual channel system. This was a rather inhomogeneous sample, consisting of patients supported on both VA and VV ECMO, operating either on centrifugal or roller pumps and with a wide age range (from 1 day to 5 years). Varying baseline levels of tissue oxygenation index (TOI) were observed between individual patients. The range of TOI value in both the brain and leg of the patients varied between 55-80% with significant intersubject variability. In addition, variability in the trends of other NIRS parameters (HbO₂, HHb and HbT) were also observed. The small sample size in combination with the diverse population studied made it impracticable to formulate group observations by investigating trends or absolute changes in NIRS parameters.

The protocol was designed to include monitoring during routine ECMO procedures such as cannulation, weaning from ECMO (including the trial off period) and decannulation, and during interventions such as changes in the ECMO circuit

flow, temperature and carbon dioxide changes. Attempts were made to keep the full protocol with all patients. However, being the last on the list to have access on the unit it was particularly difficult to be present during non scheduled acute procedures such as cannulation, weaning and decannulation. NIRS data were obtained from one patient during cannulation and from another one during weaning and trial off period. Even though these are single data sets some interesting observations can be made. In the single dataset obtained with the dual channel NIRS system during the cannulation procedure, ligation of the RCCA was associated with a decrease in HbO₂ and an increase in HHb in the leg data and only a decrease in HbO₂ in the brain data. These changes were ~0.2 μM. In addition, TOI in the brain and leg decreased by ~3%. In the brain TOI returned back to baseline 3min after ligation while in the leg it was maintained in the decreased value until clamping the RIJV where it decreased by further 3%. TOI in the leg increased back to baseline value after all clamps were removed and the patient went on ECMO. An abrupt drop of ~7% in TOI was observed in the brain immediately after all clamps were removed and the patient went on ECMO and this was associated with abrupt drops in HbO₂, HHb and HbT. The values of all NIRS parameters in the brain remained lower than baseline values 15 minutes after ECMO support which was the end of the monitoring period. HbO₂ and HbT in the leg were higher than baseline values 15 minutes after ECMO support while TOI returned back to baseline value. Eijike et al. (2000) used the INVOS system with channels placed on the right and left frontal regions to monitor ECMO patients during cannulation. They report that the ligation of the right common carotid artery resulted in a 12-25% decrease in rSO₂ from baseline in the right frontal region for a duration ranging from 17 to 45 mins before returning toward baseline. No substantial change in the left frontal region was detected during cannulation. Following this depression in rSO₂ on the right there was a transient increase above baseline in rSO₂ in both hemispheres on initialising ECMO support. In a different study Van Heijst et al (2007) report a significant decrease in the concentration of oxyhaemoglobin and a significant increase in the concentration deoxyhaemoglobin in both cerebral hemispheres after RCCA ligation. RIJV ligation did not cause any significant changes in NIRS parameter. 60 min after ECMO initiation, the concentration of oxyhaemoglobin increased in both cerebral hemispheres, whereas the concentration of deoxyhaemoglobin decreased in both hemispheres.

The single patient dataset obtained during the trial off ECMO period showed interesting changes in the NIRS parameters during “flushing” of the cannulae. Each time the cannulae were “flushed” a sharp increase in HbO₂ and decrease in HHb and immediate in both brain and leg were observed. This was reflected as a sharp increase in TOI in both brain and leg. All NIRS parameters returned to their baseline values approximately 2 min after “flushing” the cannulae. This might be due to blood from the ECMO circuit rushing in the patient when unclamping the cannulae. Eijike et al. (2000) report that periods of trialing off ECMO were not related to any change rSO₂ in either hemisphere.

PSDs have been used to identify the presence of any oscillations occurring in the brain and leg of 7 ECMO patients undergoing flow manipulations. Table 5.3 summarizes the results of the PSD analysis. The RR and HR can be picked up in most of the patients and is present in both brain and leg. In addition to these oscillations, the presence of oscillations in the VLF band were identified. It is interesting that a low frequency oscillation (0.005Hz) was present in the leg data of 3 of the 7 patients studied (2 VA ECMO patients and 1 VV ECMO patient). Kvandal et al. report the presence of skin vasomotion oscillations in the interval 0.005-0.0095 Hz (Kvandal et al. 2006). One patient shows oscillations at 0.05Hz only in the leg. Four of the patients showed slow oscillations in the brain (~0.01 in Patient10, ~0.015Hz in Patient 8, ~0.05Hz in Patients 7 & 13), similar to those described by Obrig et al. (Obrig et al. 2000). Oscillations in the HF band appearing at twice the frequency of the ECMO pump were detected in brain and leg for 4 out of 5 VA patients operating on a roller pump.

The PSD analysis has shown an interesting distinction between the use of roller and centrifugal pumps. The roller pump was found to be associated with an oscillatory effect in the systemic and cerebral circulations, even though this does not reflect the pulsatile contour of blood pressure. In the absence of a roller pump the oscillations do not exist and systemic and cerebral circulations can be flat around the frequency of the arterial pressure. The discussion concerning pulsatile and non-pulsatile flow has been the subject of much research over the last three decades. It is argued that as long as the total blood flow is adequate, the presence of a pulse contour is not physiologically important (Van Meurs, Lally, Peek, & Zwischenberger

2005a). At low but less than adequate blood flow, the effects of hypoperfusion and acidosis are somewhat ameliorated by pulsatile flow. During ECMO, all management effort is placed on maintaining normal oxygen delivery. It is therefore argued that non-pulsatile perfusion does not have any deleterious effects. The kidney is the organ most sensitive to non-pulsatile flow. Even though the cardiac intensive care unit at GOS hospital has stopped using roller pumps in ECMO circuits within the last couple of years it would have been interesting to investigate the effect of the oscillations resulting from the use of a roller pump further.

Furthermore, coherence analysis was used to investigate the concordance between HbD and MAP. It has been shown previously that similar analysis can be used to detect cerebral autoregulation in premature newborns (De Smet et al. 2009, Morren et al. 2001, Soul et al. 2007, Tsuji et al. 2000). However, the monitoring period in previous studies was much longer than the monitoring period used in this study. Cerebral pressure passivity is not an all or none phenomenon but rather fluctuates over time (Soul et al. 2007). Since cerebral autoregulation is not a simple static system but rather a more complex rate-sensitive system, the total length of the signal analysed plays an important role in the concordance between CBF and MAP. Static and/or intermittent measurements of cerebral pressure autoregulation used in previous studies are likely to miss cerebral pressure passivity (Tyszczyk et al. 1998).

Furthermore, previous studies have confined the investigation of cerebral autoregulation to measurement of coherence only in the range 0-0.1Hz (ULF band). These frequencies correspond to changes occurring over several minutes. Changes in MAP increase in amplitude as frequency decreases (Parati et al. 1995). Because prolonged cerebral ischemia (e.g. several minutes to hours) is likely to be more injurious than transient (e.g. several seconds) reductions in CBF, prolonged correlations in CBF to these larger changes in MAP are more likely to be pathologically significant. These prolonged correlations are captured by ULF. However, in the case on ECMO patients our interest lays in higher frequencies since the ECMO machine itself induces oscillations driven by the circuit pump. It is in our interest to examine the impact of these higher oscillations, in addition to the lower oscillations, on cerebral blood flow and cerebral pressure autoregulation.

It is worth noting that such spectral analysis was not previously performed on ECMO patients. There is interest in investigating novel methods for analysing these data with a view to elucidating cerebral autoregulation mechanisms in ECMO patients. Further studies are required to more fully explore the relationship between oscillations arising in specific frequency bands and the type of ECMO procedures used in different patients.

Chapter 6

MULTICHANNEL NEAR INFRARED SPECTROSCOPY TO MEASURE REGIONAL CEREBRAL OXYGENATION IN INFANTS AND CHILDREN SUPPORTED ON ECMO

6.1 Introduction

In the current era of extracorporeal membrane oxygenation (ECMO), there are serious limitations with inadequate neuromonitoring, misleading neuromonitoring, or both, especially in the setting of hemodilution and nonpulsatile flow (Nollert et al. 1998). The implications of neurological monitoring with relevance to neurodevelopmental outcome have not been clearly delineated. As a result, there is equipoise about routine neuromonitoring, particularly with near-infrared spectroscopy (NIRS) and the relevance of data (Hirsch et al. 2010).

Near infrared spectroscopy (NIRS) has the advantage of monitoring cerebral oxygenation non-invasively and continuously by the bedside. To date, conventional NIRS uses single or dual channel systems with the optodes usually placed on the forehead of the patients providing information related to perfusion of only a small

area of the anterior cerebrum and therefore do not allow evaluation of the status of the cerebral circulation and oxygenation in the extended cerebral regions. NIRS was used on ECMO patients to study the effect of cannulation on cerebral oxygenation. Ligation of RCCA was associated with a decrease in HbO₂, an increase in HHb (Van Heijst et al. 2004) and a decrease in tissue oxygen saturation (TOS) (Ejike et al. 2006) while no changes were seen during IJV ligation. Also, an increase in HbO₂, a decrease in HHb and an increase in TOS was reported after ECMO was established compared to pre-cannulation values.

However, the fact that only regional information in cerebral oxygenation can be obtained from the current commercial NIRS systems in clinical use is considered a major limitation (Andropoulos et al. 2004b, Hirsch et al. 2010, Su and Undar 2010). Alterations in regional oxygen saturation may reflect local changes and not necessarily indicate global hypoperfusion.

This work aims at the development and induction of a multichannel near infrared spectroscopy system for use in the intensive care environment. With the specific application of the system to monitor ECMO patients and assess regional variations in cerebral oxygenation during different ECMO phases.

6.2 Methods

6.2.1 Instrumentation

The ETG-100 optical topography (OT) system was used to acquire multi-site HbO₂, HHb and HbT concentrations. The multichannel system does not give information on tissue oxygen saturation. The ETG-100 is a CW system with a maximum number of 18 optodes; 10 sources emitting at 730 nm and 810 nm and 8 avalanche photodiodes. The hardware configuration is described elsewhere (chapter 3). It is mainly designed for functional activation studies, and it has been used to study the activity of healthy brain and cerebral pathologies in adults, infants and newborns (Homae et al. 2006, Koizumi et al. 2003, Koizumi et al. 2005, Otsuka et al. 2007).

The Hitachi ETG-100 optical topography system has a software which allows the digitise NIRS signals to be shown on the monitor of the incorporated PC in real time. Also, depending on the operation mode, the software allows for a basic analysis of the stored data. However, the ETG-100 software is designed for functional activation studies and not for clinical use. Therefore, for the purpose of this study the software was only used in the “Measurement Operation” mode for displaying the signals in real time, collecting and storing the signals for off line analysis.

Before starting the data collection, the software performs a test to check whether enough light is reaching the detectors. During probe setting, a window appears displaying the positions of measurement channels and indicating the gain status of each channel. A green colour indicates optimal gain, red indicates over gain and yellow indicates under gain. If after placing the fibres on the patient most of the channels were over gained or under gained, the percentage gain threshold was changed accordingly. The percentage threshold gain is related to the A/D gain, i.e. 50% of 5V which is equivalent to 2.5V, means detection between -2.5V to 2.5V. Outside this region is under gain (yellow) or over gain (red). In other words, if the optical intensity was high, the gain threshold was increased.

Systemic data, arterial blood pressure (ABP), central venous pressure (CVP), end-tidal CO₂, heart rate (HR), respiration rate (RR), pulse, temperature and arterial oxygen saturation (SaO₂), were continually measured, recorded and displayed in real time at the bedside (Intellvue MP70, Philips Medical). ABP and CVP are obtained invasively, usually from radial artery and femoral vein respectively. SaO₂ is obtained from a pulse oximeter placed on the toe of the patients. ABP, CVP, RR and end-tidal CO₂ are recorded as continuous waveforms at a frequency of 125Hz (ABP and CVP) and 62.5Hz (RR and end-tidal CO₂). These four parameters are also collected as averaged values at 1Hz. HR, SpO₂, temperature and pulse are also collected at 1Hz. Software (Trendface, Ixellence GmbH, Germany) was used to collect and export the systemic data onto a PC for subsequent analysis.

Parameters related with the ECMO circuit were also collected continually at the bedside (M3 monitoring system, Spectrum Medical Ltd.). These included arterial oxygen saturation (SaO₂) and blood flow measured using probes placed on the arterial cannula, venous oxygen saturation (SvO₂) measured using a probe placed on

the venous cannula and haemotocrit. ECMO circuit parameters were collected with a random (or irregular) sampling rate and were stored in a S.D memory and exported to a PC.

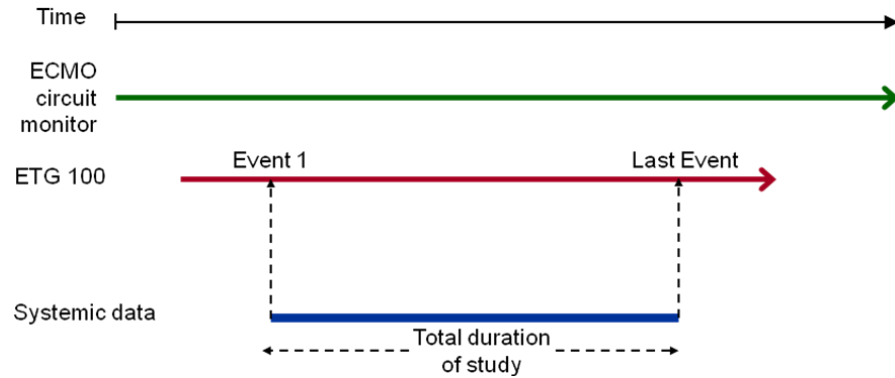


Figure 6.1: Illustrating the sequence followed for obtaining simultaneous collection of systemic, ECMO parameters and with optical parameters collected with ETG-100.

In order to proceed with data analysis synchronisation of the time base axes between the three monitors was addressed. Similar to the dual-channel system described in chapter 5, synchronisation between the ETG-100 data and systemic parameters was achieved by placing an event marker on the ETG-100 system at the time when the Trendface software started collecting the systemic data. For synchronising the ECMO circuit parameters with the physiologic parameters the clock stamps on the ECMO monitor and Trendface software were used. This sequence allowed data collection from the three monitors to be synchronised within $\pm 1s$. A MatLab script was written to synchronise the data from the three different files.

6.2.2 Neonatal cap design and construction

The ETG-100 optical topography system in our lab was previously used for functional activation studies in adults. Before we used it in a clinical neonatal environment, the optical fibres were changed from the adult probes to the much smaller neonatal probes. A neonatal cap was designed and constructed to house the neonatal fibres, hold them in place and maintain good contact with the patients' scalp.

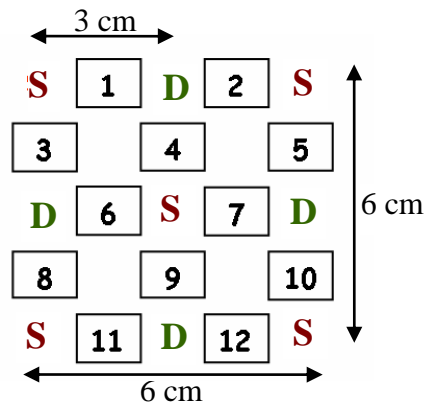


Figure 6.2: Source (S) – Detector (D) configuration used allowing measurements of haemoglobin concentration to be obtained from a total of 12 channels.

The source-detector configuration used is shown in figure 6.2. A 3x3 arrangement was used with source-detector separation set at 3cm and each laser emitting at 1.2 mW. A source-detector separation of 3cm was previously used in NIRS infant studies (Minagawa-Kawai et al. 2007). Taga et al (2007) report a good sensitivity and high signal-to-noise ratio when ETG-100 was used on 3 month old infants at S-D separation of 3cm and laser power at 1.2mW (Taga et al. 2007). The 3x3 arrangement placed centrally on the head of a newborn ECMO patient covers the largest area available taking into consideration that the occipital and part of the right temporal lobes cannot be accessed because the patient is lying down and has cannulae stitched above the right ear. This configuration allows data to be collected from a total of 12 channels.

The cap required to be flexible so as to fit different head shapes and sizes, due to the variability in head shapes of the newborn and wide age range of patients placed on ECMO. In addition, the cap needed to be made from a material that can be autoclaved (i.e. sterilised).

Fibre Holders

New holders to house the fibres were designed based on the original neonatal fibre holder designs obtained from Hitachi Medical Ltd. The holders are shown in figure 6.3. They are spring loaded with a very light spring that will allow the fibre tip to be kept in contact with the patient’s scalp. A rubber o-ring is placed at the bottom

of the holder to minimise the pressure applied on the scalp. Plastic connectors were also designed to connect the holders with each other, maintaining a distance of 3cm between them and keeping the desired array configuration.

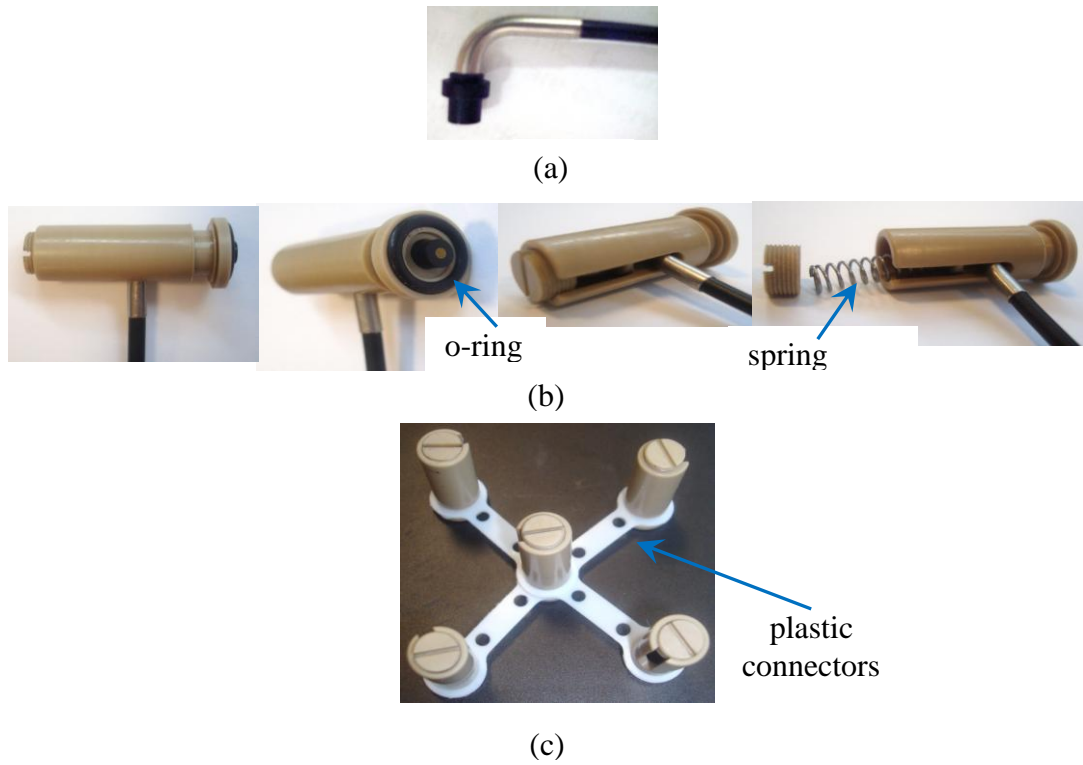


Figure 6.3: The neonatal optical fibres are L-shaped fibres (a) and they are housed in spring loaded plastic holders with an o-ring fitted at the bottom (b). The fibres are hold together in an array using plastic connectors (c).

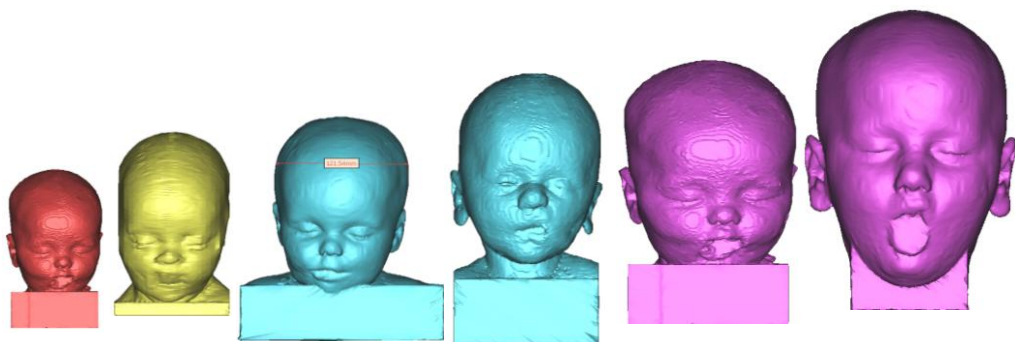


Figure 6.4: 3D reconstructions of MRI scans obtained from the radiology archives of GOS hospital courtesy of Claudio Capelli and Giovanni Biglino. Head circumferences from right to left: 51 cm, 47.5 cm, 43.5 cm, 41 cm, 37 cm and 33 cm.

Cap

A flexible light neonatal cap was constructed using room-temperature vulcanising (RTV) T30 high strength silicone mould rubber (Alec Tiranti Ltd.). Vulcanisation is a chemical process for converting rubber into more durable materials via the addition of sulphur or other equivalent “curative” agents. In its uncured state RTV T30 is a thick, white, sticky liquid. The inelastic deformation of the silicone rubber is due to its polymeric chemical structure. Polymer chains can move independently relative to each other, which enables the material to change shape. When RTV T30 is mixed with a curative agent, in a composition of 5% agent (by weight), it cures at room temperature to a solid elastomer. In other words, in its curable state RTV T30 is a flexible, strong, elastic solid. RTV remains flexible from -80 °C to +250 °C and is therefore autoclavable. Furthermore, RTV T30 can be moulded into any shape by pouring it into any container or by simply brush painting a surface.



Figure 6.5: ETG-100 neonatal cap on dummy head.

Six dummy heads were provided by rapid prototyping 3D image reconstructions of MRI scans of baby heads obtained from the archives of the radiology department in Great Ormond Street Hospital (with the help of Marina Hughes, Claudio Capelli, Giovanni Biglino, Martin Watmough). The six dummy heads were chosen to have different head circumferences to cover ages from 1 day to 5 years (figure 6.4). The cap base was made by brush painting three consecutive layers of RTV T30 mixed with black oil paint on a dummy head. This allows the cap to have the right curvature and therefore maintain good contact between the fibres and scalp. The silicon rubber was then peeled off from the dummy head and holes were cut out to fit the fibre holders in a 3x3 array. Straps were also made from silicon rubber reinforced with a net. The net allows for Velcro tapes to be sewed on the silicon rubber. A wide strap was attached to the base of the cap at the back of the head that goes around the periphery of the head and closes at the forehead using the Velcro tapes. Narrower straps were attached around the edges of the base so as when pulling them the cap fits the head of the patient. Figure 6.4 shows the neonatal cap on the dummy head and figure 6.5 shows the cap in use on an ECMO patient.

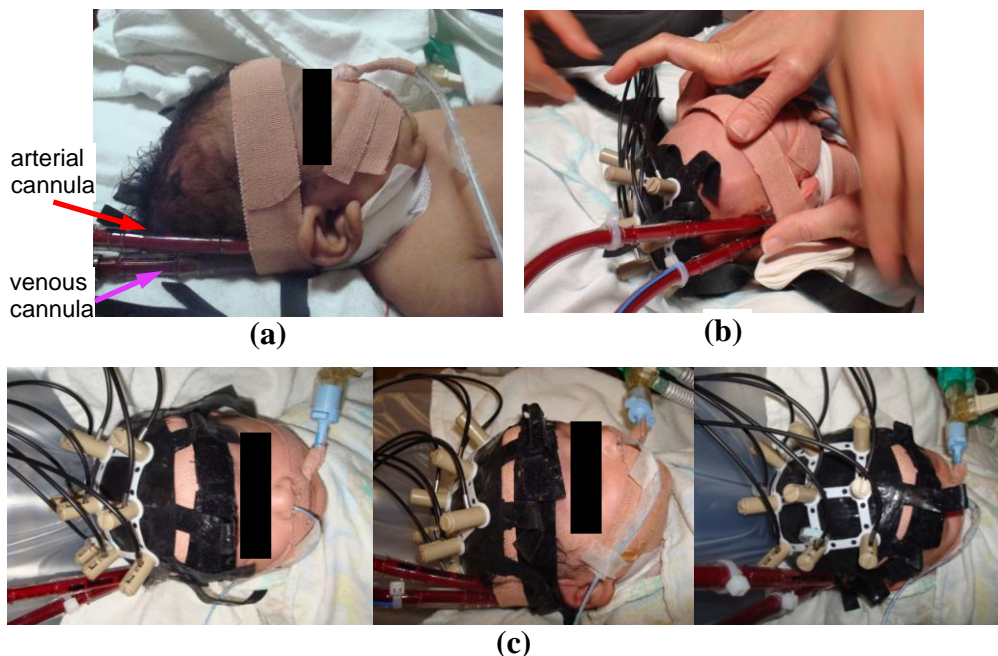


Figure 6.6: (a) Patient supported on ECMO with arterial and venous cannula shown. (b) Putting the neonatal cap on an ECMO patient and (c) the neonatal cap in use.

Note that prior to the *final cap* version, two earlier versions of the cap were made, *prototype1* and *prototype2*. *Prototype1* was designed before the fibre holders were constructed and was therefore susceptible to movement artefacts due to the fact that the fibres were not held stable. The design of *prototype2* was similar to the *final cap* design, however the base of the cap was obtained based on the curvature of a plastic hemispherical bowl as a result the cap did not fit so well on the patients head.

6.2.3 Protocol

The study protocol followed was similar to the one described in chapter 5. However, temperature and CO₂ interventions were omitted since preliminary results using the dual channel system showed practicality issues in performing those studies. Regional cerebral oxygenation was assessed during cannulation, decannulation, weaning from ECMO and changes in the ECMO circuit flows. Changes in the ECMO flows were carried out by successive reductions in the ECMO circuit flows by 10% of the baseline until 70 % of the baseline every 10-15 minutes and subsequently sequentially increasing it back to baseline flow.

6.2.4 Patients

A total of 12 VA ECMO patients were studied with age ranging between 1 to 25 days. One patient was monitored during weaning, one during cannulation and one during decannulation. Ten patients were monitored during ECMO flow changes. A full list of the subjects studied is shown in table 6.1. Parental consent was obtained prior to the start of each study.

6.2.3 Data rejection

Optical data collected at a sampling frequency of 5 Hz were resampled at 1 Hz and low pass filtered at 0.05 Hz to remove physiological noise. For the conversion of the optical attenuation changes to chromophore concentration changes a differential pathlength factor (DPF) of 4.99 was applied (Duncan et al. 1995). The recorded attenuation measurements for each data set were initially inspected and channels that

showed evidence of poor signal-to-noise ratio, mismatch in attenuation at the two wavelengths or saturation of the detector were rejected from further analysis.

6.2.4 Data analysis

During alterations in ECMO flows changes in HbO₂, HHb and HbT between phase I [from baseline flow (100%) to minimum flow (70%)] and phase II [from 70% flow back to baseline flow] were calculated from the differences in mean values over a 60-s period just before changing the flow. At weaning changes in HbO₂, HHb and HbT between the difference in mean values over 60-s period just before clamping the cannulae and around the minimum or maximum post clamping the cannulae were obtained. The results were analysed using a paired t-test ($p < 0.05$).

6.3 Results

A total of 12 VA ECMO patients were recruited in this study. One patient was monitored during cannulation, one during decannulation, one during weaning and 9 during alterations in the ECMO flows. Attempts were made to follow complete protocol and monitor each patient through all procedures as mentioned in the methods section above. However, it was particularly difficult to capture procedures such as cannulation, decannulation and weaning partly because they were usually taking place at inconvenient hours. Out of the 12 patients only 7 were used in the data analysis (6 patients monitored during flow changes and 1 during weaning). The 42% drop out is a result of a number of factors including: bad fitting of the cap especially in cases where the prototype versions of the cap were used; low signal-to-noise ratio due to very high or low light intensity reaching the detectors depending on the amount of hair and head transparency of the patients; and incomplete studies due to the critical condition of the patients. All the above are summarised in table 6.2 along with the number of channels used in data analysis after applying the data rejection criteria (see methods section above).

Table 6.1: Demographics of ECMO patients included in the study.

Patient ID	Age (days)	Type of ECMO	Cannulation sides	Type of pump	Type of study	Indication for ECMO	Clinical condition
1	4	VA	RCCA & IJV	Roller	Flow changes	Neonatal Respiratory failure	Neonatal hypoxaemic respiratory failure due to Left CDH
2	21	VA	chest cannulation	Centrifugal	Cannulation	Cardiac - post cardiac surgery	Post TAPVC repair
3	1	VA	RCCA&IJV	Centrifugal	Decannulation	Neonatal Respiratory failure	Neonatal hypoxaemic respiratory failure with PPHN and MAS
4	12	VA	RCCA & IJV	Centrifugal	Flow changes	Neonatal Respiratory failure	Neonatal hypoxaemic respiratory failure due to RSV infection post cardiac surgery
5	3	VA	RCCA&IJV	Centrifugal	Flow changes	Neonatal Respiratory failure	Neonatal hypoxaemic respiratory failure with PPHN and MAS
6	5	VA	RCCA & IJV	Centrifugal	Flow changes	Neonatal Respiratory failure	Neonatal hypoxaemic respiratory failure due to Left CDH
7	9	VA	RCCA&IJV	Centrifugal	Flow changes	Neonatal Respiratory failure	Neonatal hypoxaemic respiratory failure with PPHN and MAS
8	16	VA	RCCA&IJV & RA	Centrifugal	Flow changes	Cardiac - post cardiac surgery	Post Arterial Switch surgery
9	4	VA	RCCA&IJV	Centrifugal	Weaning	Neonatal Respiratory failure	Neonatal hypoxaemic respiratory failure with PPHN, sepsis
10	3	VA	RCCA&IJV	Centrifugal	Flow changes	Neonatal Respiratory failure	Neonatal hypoxaemic respiratory failure with PPHN and MAS
11	3	VA	RCCA&IJV	Centrifugal	Flow changes	Neonatal Respiratory failure	Neonatal hypoxaemic respiratory failure with PPHN and MAS
12	25	VA	RCCA&IJV	Centrifugal	Flow changes	Paediatric Respiratory failure	Paediatric hypoxaemic respiratory failure due to Pertussis

Table 6.2: List of patients included in the study showing useful channels after data rejection. Rejected channels are highlighted grey and active channels are highlighted green.

Patient ID	Type of study	Channel												Total # of channels	Cap	Comments	
		1	2	3	4	5	6	7	8	9	10	11	12				
1	Flow changes														0	Prototype1	No systemic and ECMO data collected. Unstable cap fitting leading to artefacts.
2	Cannulation														0	Prototype1	Lots of movement artefacts due instability in cap fitting.
3	Decannulation														0	Prototype1	Lots of movement artefacts due instability in cap fitting.
4	Flow changes														12	Prototype2	Patient has thick black hair. Channels undergain. Incomplete study due to the condition of the patient
5	Flow changes														3	Prototype2	
6	Flow changes														5	Prototype2	
7	Flow changes														8	Prototype2	
8	Flow changes														8	Prototype2	
9	Weaning														10	NeoFlexiCap	Too transparent. Channels overgain.
10	Flow changes														12	NeoFlexiCap	
11	Flow changes														8	NeoFlexiCap	
12	Flow changes														0	NeoFlexiCap	

6.3.1 Flow changes

Table 6.3: List of patients monitored during alterations in the ECMO flows. Green indicates useful data and grey indicated that the period was rejected due to noise.

Patient ID	ECMO period						
	A (100%)	B (90%)	C (80%)	D (70%)	E (80%)	F (90%)	G (100%)
4	Green	Green	Green	Green	Green	Green	Green
5	Green	Green	Green	Green	Green	Green	Green
7	Green	Green	Green	Grey	Grey	Green	Green
8	Green	Green	Green	Green	Green	Green	Green
10	Green	Green	Green	Green	Grey	Grey	Grey
11	Green	Green	Green	Green	Green	Green	Green

Table 3 lists the six patients monitored during flow changes and indicates the ECMO flow sequence followed for each patient. The ECMO periods used in the data analysis are highlighted green. Five patients were monitored during the complete flow changes sequence, i.e. flow periods A to G. However, for one of those patients (patient 10) only flow periods A to D were used in the data analysis the rest of the flow periods were rejected due to the presence of movement artefacts. In patient 7 ECMO flow was only decreased to 80% of the baseline and sequentially brought back to baseline. It was not possible to reduce the flow further to 70% because the patient presented a big drop in MAP, SpO₂ and SvO₂ when the flows were reduced to 80%.

Patient 4

Figure 6.6d shows concentration changes in HbO₂ (red), HHb (blue) and HbT (black) collected from the 12 channels during changes in ECMO flows in patient 4. The systemic variables (MAP, HR, SpO₂ and SvO₂) are shown in figure 6.6c. The channel configuration and ECMO flow sequence are shown by the schematics at the top left of figure 6.6. The vertical dotted lines in the concentration and systemic variables plots represent the time at which a change in flow was induced so that each section in the plots corresponds to a specific flow period. Sequential reduction in ECMO flows resulted in considerable increase in HHb and HbT in all 12 channels,

with moderate changes seen in HbO₂. Figure 6.7 shows the responses in the concentration changes (HHb and HbO₂) and systemic variables (MAP, HR, SpO₂ and SvO₂) during phases I (mean changes from baseline to minimum flow) and II (mean changes from minimum flow back to baseline). The range in the change of HHb concentration during phase I was from 9.7µM (channel 8) to 25.1µM (channel 10). In this patient a decrease in ECMO flow is associated with a decrease in SvO₂ (of 20%) and SpO₂ (of 8%) and an increase in HR (of 21 bpm) and MAP (of 5 mmHg). The effect is reversed when the flow is gradually increased back to baseline. Similar to the haemoglobin concentration data, these systemic and ECMO circuit parameters do not return to their baseline values by the end of the monitoring period.

Patient 5

The chromophore concentrations (HbO₂, HHb and HbT) data, along with the systemic variables (MAP, HR and SvO₂) during sequential changes in ECMO flow for patient 5 are shown in figure 6.8. The SpO₂ data were too noisy and are not shown here. This patient was monitored during the whole ECMO flow sequence from flow periods A to G as shown schematically in figure 6.8b. Unfortunately, the black hair of this patient did not allow collecting data from all channels and only channels 1, 2 and 3 were kept after the rejection criteria. The responses in the concentration data and systemic variables during phases I and II are shown in figure 6.9. In this patient sequential reduction in flows caused a decrease in HbO₂ between 8.7 µM (channel 3) and 2.2 µM (channel 2) and an increase in HHb between 2.3 µM (channel 2) and 1.7 µM (channel 3). In comparison to patient 4 the responses in patient 5 are not as big while the decrease in HbO₂ is greater than the increase in HHb. Reduction in flow from baseline to minimum was associated with a decrease in MAP (4.2 mmHg), decrease in HR (5.5 bpm) and a decrease in SvO₂ (6.4 %). Even though changes in HHb appear to be reversed during phase II changes in HbO₂ remain lower than baseline with the exception of channel 3. Also changes in SvO₂ are reversed while changes in MAP and HR remain lower than baseline values.

Patient 7

The results for patient 7 are presented in figures 6.10 and 6.11. Figure 6.10 shows the time course data of the chromophore concentrations and systemic variables during flow changes. The figure also shows the flow sequence followed by this patient (figure 6.10b). In this patient the flows were only reduced by a total of 20 %, i.e. they were only brought down to 80 % of baseline, and then sequentially increased back to baseline. Figure 6.11 shows the responses of the cerebral and systemic parameters during phases I (mean changes between baseline [A=100 % flow] and minimum flow [C=80 % flow]) and II (mean changes between minimum flow [C] and back to baseline [G]). Similar to patient 4, reduction in flows in patient 6 resulted in an increase in HHb and a smaller decrease in HbO₂ across all the channels. However, the changes seen in HHb ranged from 7.6 μ M (channel 9) to 3.1 μ M (channel 1) and are lower compared to those seen in patient 4. Responses during phase II indicate the changes are not reverse when the flow returns back to baseline. Reduction to minimum flow in this patient caused a decrease in SvO₂ of 14.6 % and a decrease in SpO₂ of 6.9 % while an increase in MAP (3.6 mmHg) and HR (0.6 bpm) were observed.

Patient 8

Time course data of chromophore concentrations and systemic variables during the complete ECMO flow changes sequence (from flow periods A to G) for patient 7 are shown in figure 6.12. The responses during phases I and II are shown in figure 6.13. In this patient the responses during phase I show that a decrease in flows is associated with a decrease in HbO₂ in all channels (ranging between 5.2 μ M in channel 1 and 2.2 μ M in channel 11). During phase II changes in HbO₂ are reversed in most channels and in some channels HbO₂ increases above baseline values. An increase in HHb is observed during phase I and most channels show an increase of HHb above baseline values during phase II. The increase in HbO₂ and HHb above baseline values during phase II could be due to the fact the MAP and HR increase above their baseline values during phase II. Reduction in flows during phase I cause a decrease in SpO₂ and SvO₂ by 0.2 % and 6 %, respectively.

Patient 10

The results of patient 8 are presented in figures 6.14 and 6.15. Figure 6.14 shows the time course data for cerebral parameters and systemic parameters during sequential reduction in ECMO flows (ECMO period A to D). Note that that in this patient data for ECMO periods E to F (increasing the flows back to baseline) are not shown due to the presence of movement artefacts. Consequently, figure 6.15 shows the responses in cerebral and systemic parameters during phase I. In this case, there is no evident trend in cerebral parameters and the changes are minor in relation to the previous patients. A decrease in SvO₂ of 6.7 % and SpO₂ of 3.4 % is observed. MAP and HR also decrease by 0.2 mmHg and 7.4 bpm, respectively.

Patient 11

Figures 6.16 and 6.17 show the results obtained for patient 10. Similar to patient 8, patient 9 shows minor changes in cerebral parameters during phase I. However, a decrease below baseline values is seen in both HHb and HbO₂ during phase II. In this patient reduction in flow is associated with drop in SvO₂ of 4.8 % and a drop in SpO₂ of 0.2 %.

6.3.2 Weaning

Figure 6.18 shows chromophore concentration data collected with the multichannel ETG-100 system for patient 9. This patient was monitored during weaning off ECMO and the data in figure 6.18 show the effect of clamping the cannulae on cerebral oxygenation. When the cannulae are clamped the patient goes off ECMO, i.e. the heart and lungs stop being dependent on the ECMO circuit. Clamping the cannulae causes a decrease in HbO₂ and an increase in HHb. The changes are reflected in all channels and are in the order of 5µM as shown in figure 6.19. A decrease in MAP and HR are also observed (figure 6.19b).

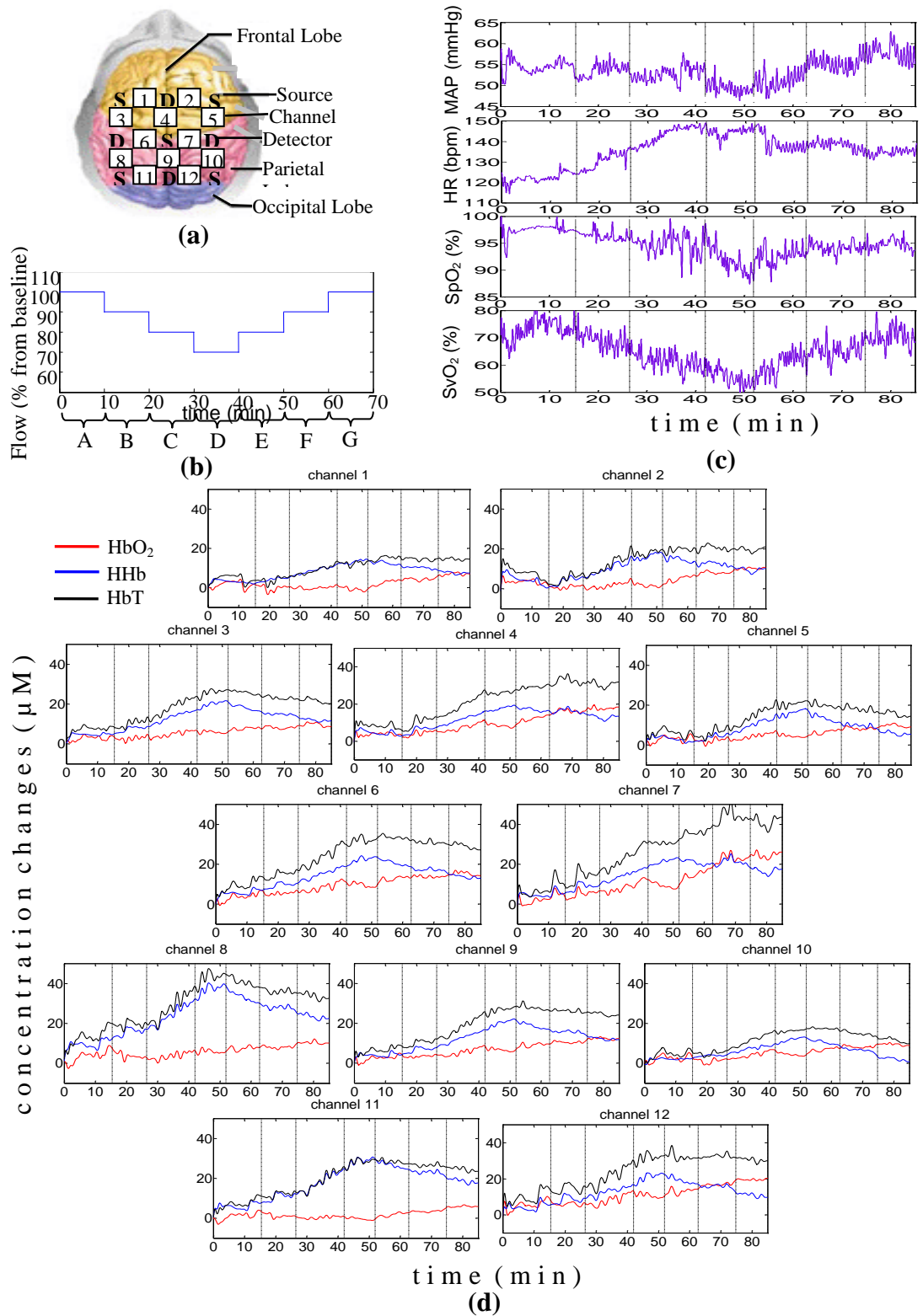


Figure 6.7: Multisite brain oxygenation and haemodynamics of **Patient 4** during flow changes. (a) Schematic of the 12-channel arrangement, (b) Sequence of flow changes indicating the different flow periods (A=100%, B=90%, C=80%, D=70%, E=80%, F=90%, G=100%), (c) Systemic parameters (MAP, HR, SpO₂ and SvO₂), (d) Multichannel NIRS parameters, HbO₂ (red), HHb (blue) and HbT (black). The vertical dotted lines split the plots into the different flow periods.

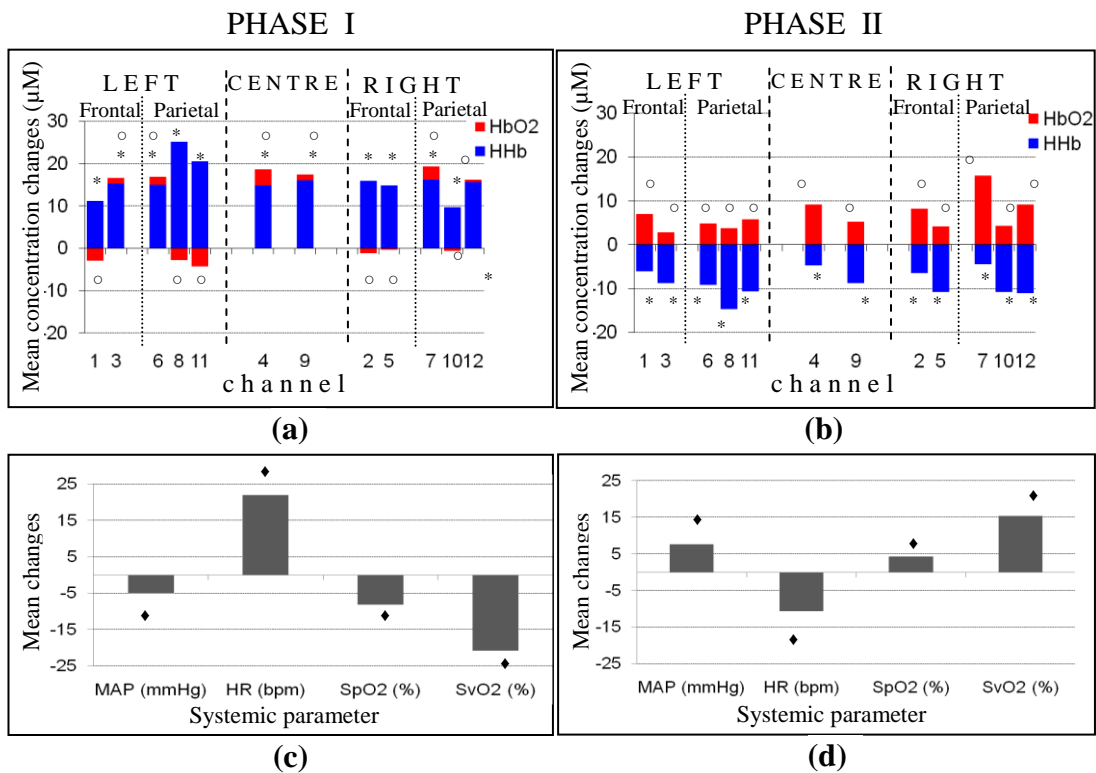


Figure 6.8: Mean absolute changes in haemoglobin concentrations across the 12-channels and systemic parameters during phases I (from baseline to minimum flow) and II (from minimum flow back to baseline) for **Patient 4**.

* Statistically significant differences in HHb ($p < 0.05$)

o Statistically significant differences in HbO₂ ($p < 0.05$)

♦ Statistically significant differences in systemic parameters ($p < 0.05$)

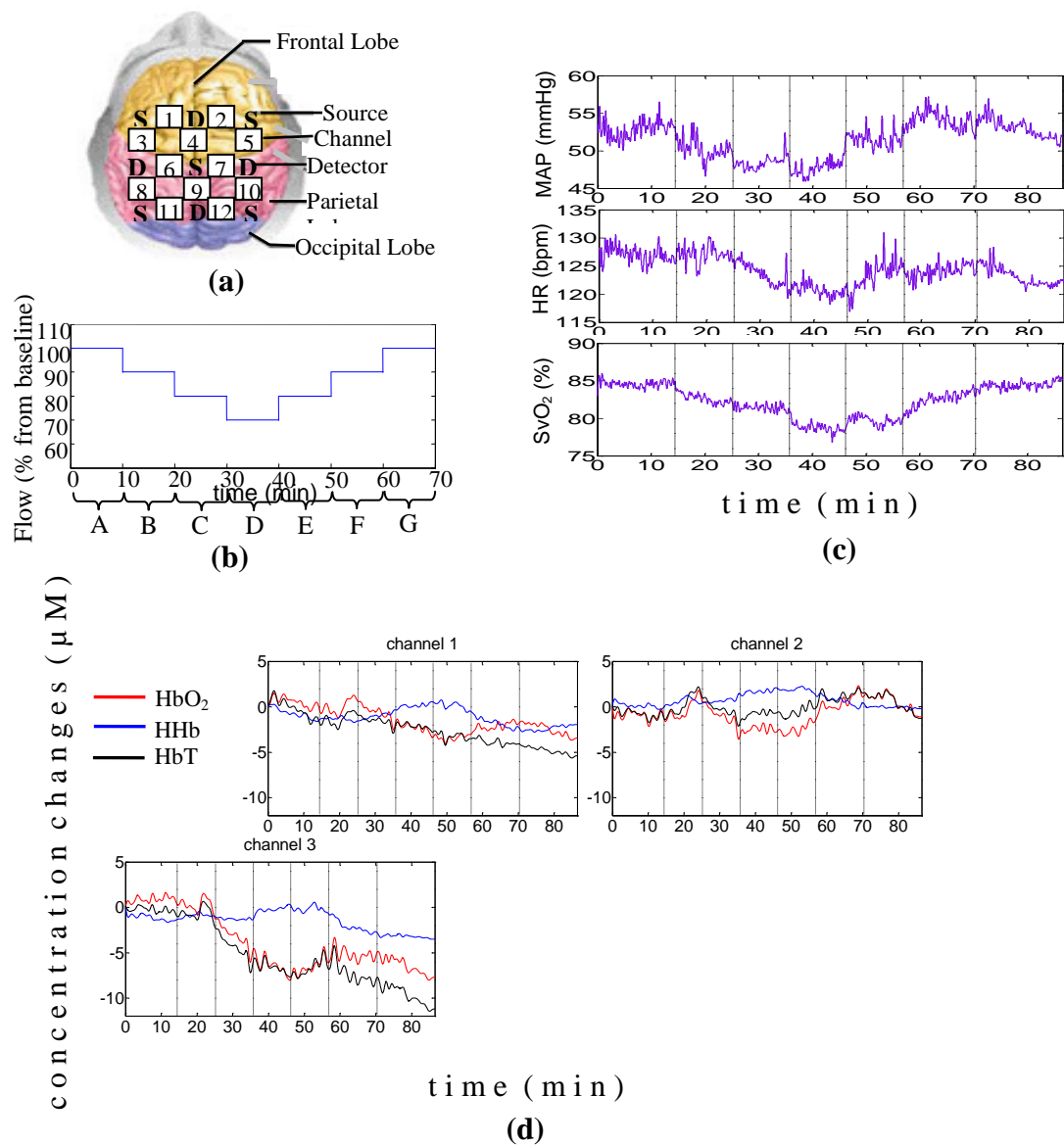


Figure 6.9: Multisite brain oxygenation and haemodynamics of **Patient 5** during flow changes. (a) Schematic of the 12-channel arrangement, (b) Sequence of flow changes indicating the different flow periods (A=100%, B=90%, C=80%, D=70%, E=80%, F=90%, G=100%), (c) Systemic parameters (MAP, HR, SpO₂ and SvO₂), (d) Multichannel NIRS parameters, HbO₂ (red), HHb (blue) and HbT (black). The vertical dotted lines split the plots into the different flow periods.

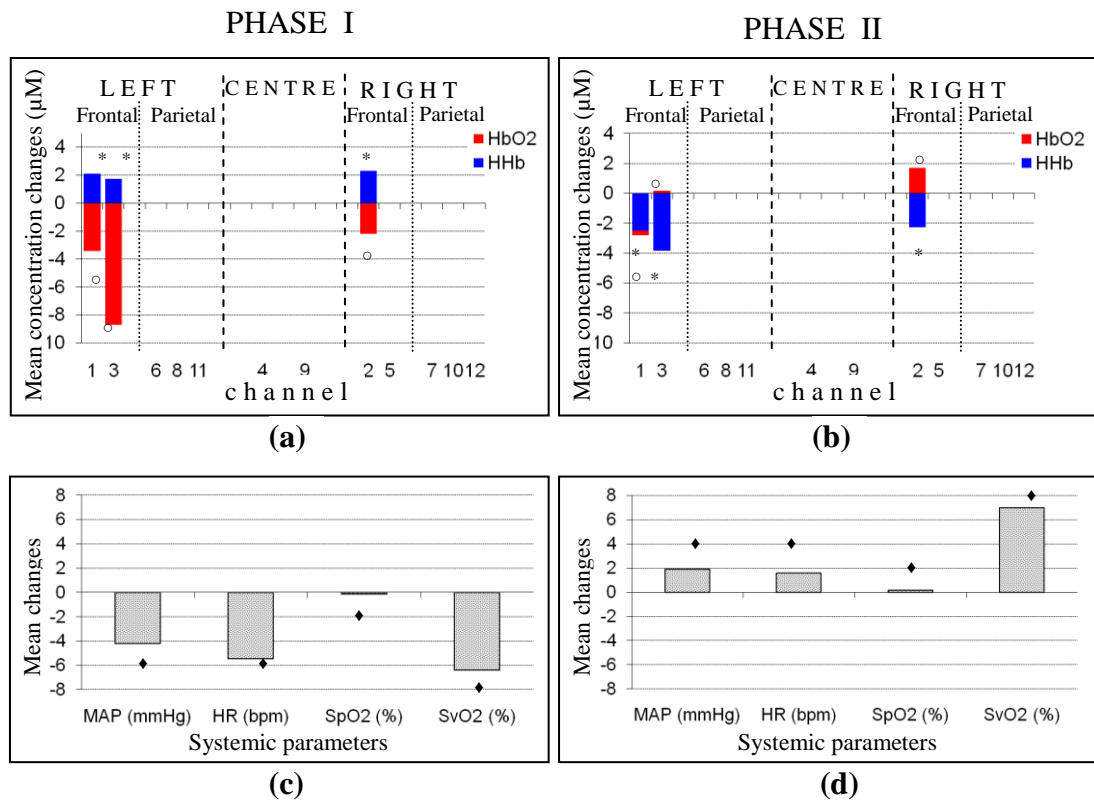


Figure 6.10: Mean absolute changes in haemoglobin concentrations across the 12-channels and systemic parameters during phases I (from baseline to minimum flow) and II (from minimum flow back to baseline) for **Patient 5**.

* Statistically significant differences in HHb ($p < 0.05$)

° Statistically significant differences in HbO₂ ($p < 0.05$)

♦ Statistically significant differences in systemic parameters ($p < 0.05$)

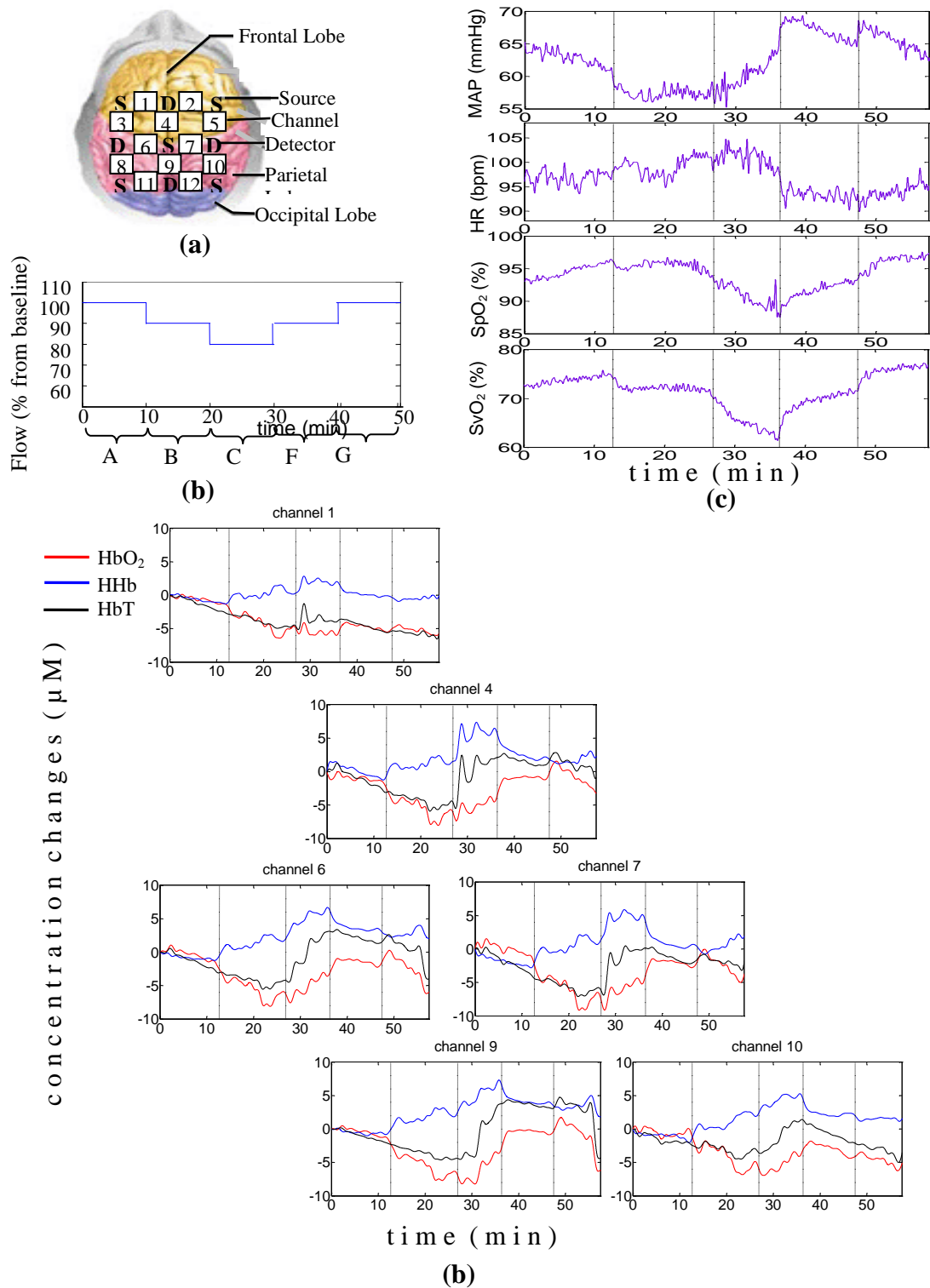


Figure 6.11: Multisite brain oxygenation and haemodynamics of **Patient 7** during flow changes. (a) Schematic of the 12-channel arrangement, (b) Sequence of flow changes indicating the different flow periods (A=100%, B=90%, C=80%, D=70%, E=80%, F=90%, G=100%), (c) Systemic parameters (MAP, HR, SpO₂ and SvO₂), (d) Multichannel NIRS parameters, HbO₂ (red), HHb (blue) and HbT (black). The vertical dotted lines split the plots into the different flow periods.

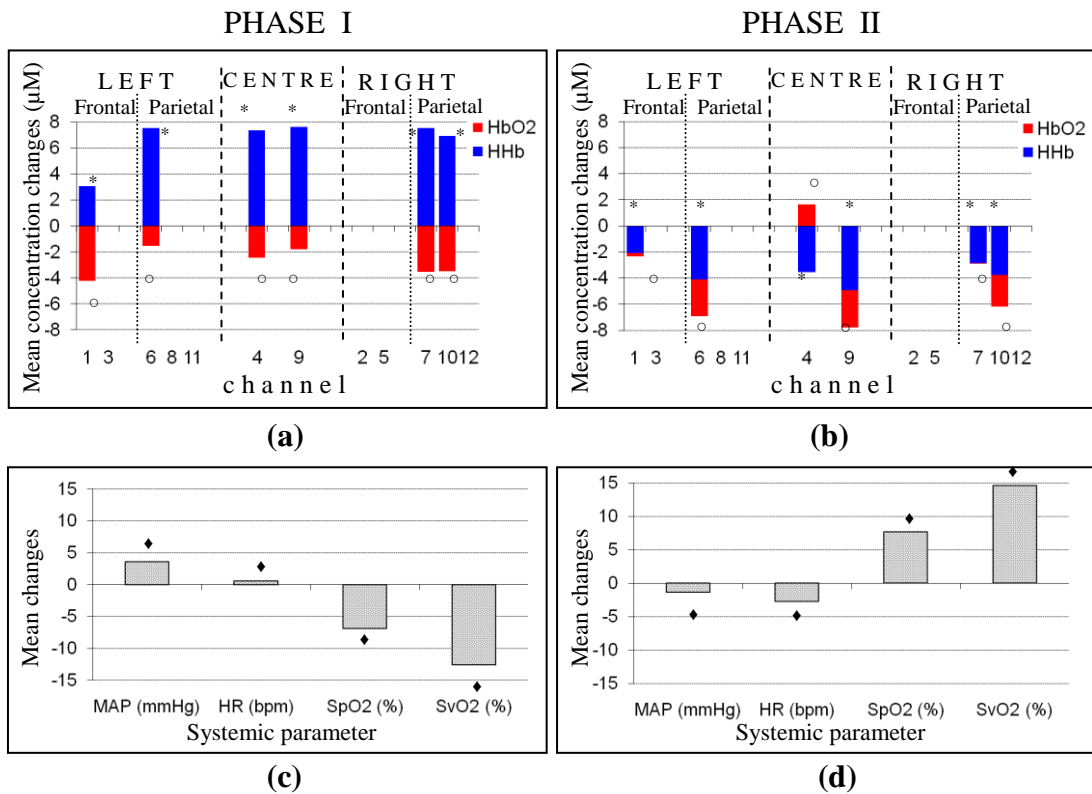


Figure 6.12: Mean absolute changes in haemoglobin concentrations across the 12-channels and systemic parameters during phases I (from baseline to minimum flow) and II (from minimum flow back to baseline) for **Patient 7**.

* Statistically significant differences in HHb ($p < 0.05$)

o Statistically significant differences in HbO₂ ($p < 0.05$)

♦ Statistically significant differences in systemic parameters ($p < 0.05$)

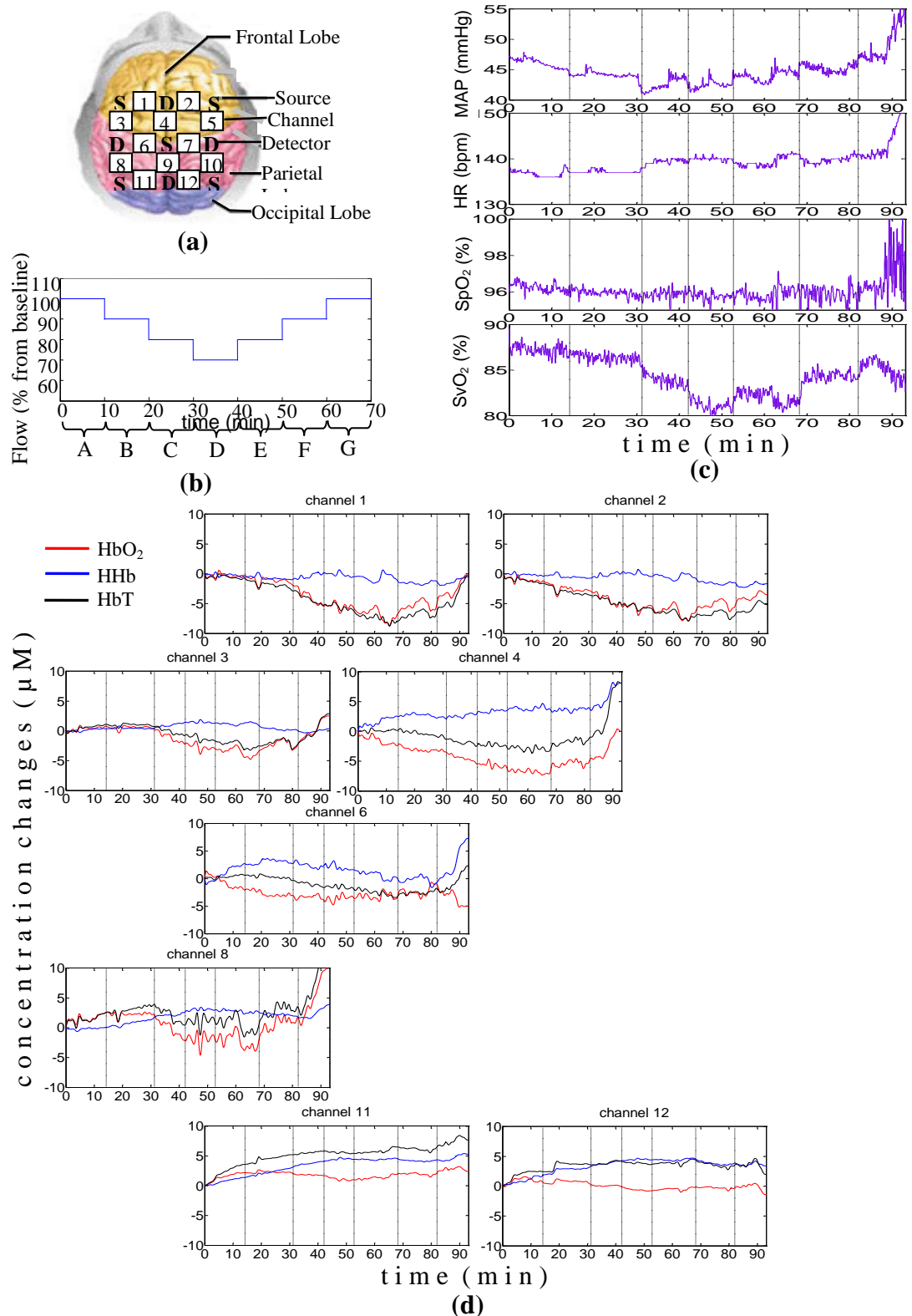


Figure 6.13: Multisite brain oxygenation and haemodynamics of **Patient 8** during flow changes. (a) Schematic of the 12-channel arrangement, (b) Sequence of flow changes indicating the different flow periods (A=100%, B=90%, C=80%, D=70%, E=80%, F=90%, G=100%), (c) Systemic parameters (MAP, HR, SpO₂ and SvO₂), (d) Multichannel NIRS parameters, HbO₂ (red), HHb (blue) and HbT (black). The vertical dotted lines split the plots into the different flow periods.

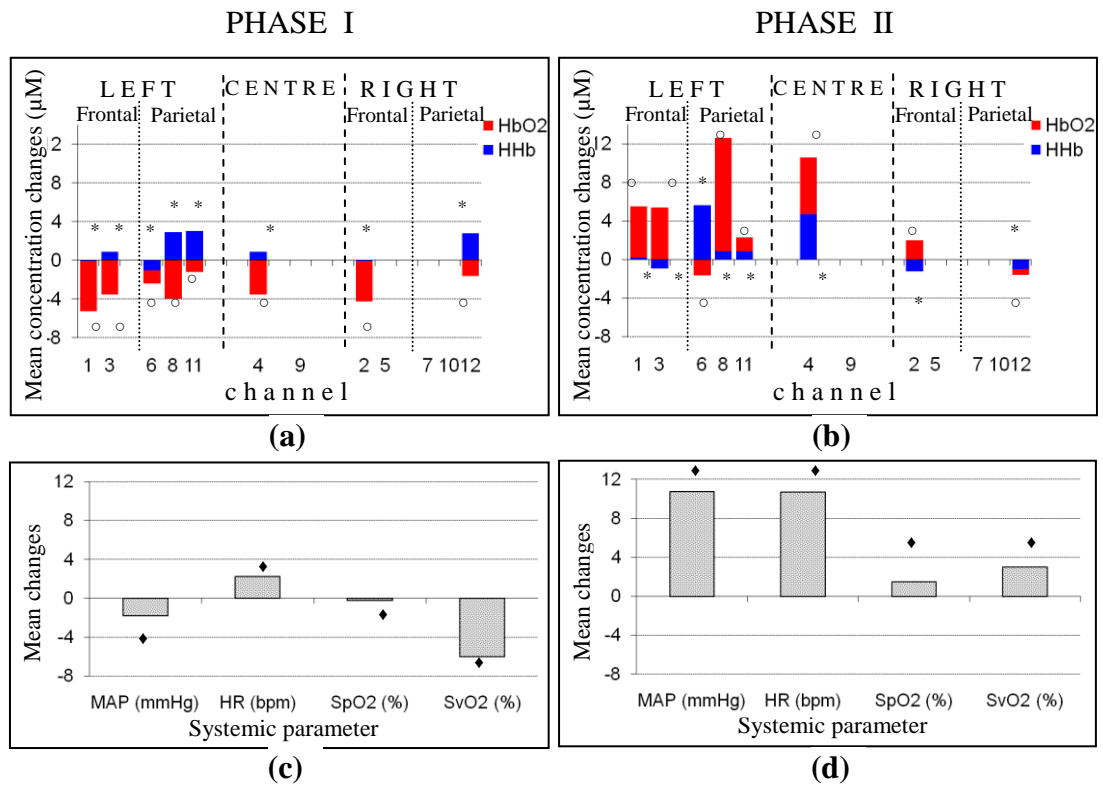


Figure 6.14: Mean absolute changes in haemoglobin concentrations across the 12-channels and systemic parameters during phases I (from baseline to minimum flow) and II (from minimum flow back to baseline) for **Patient 8**.

* Statistically significant differences in HHb ($p < 0.05$)

o Statistically significant differences in HbO₂ ($p < 0.05$)

◆ Statistically significant differences in systemic parameters ($p < 0.05$)

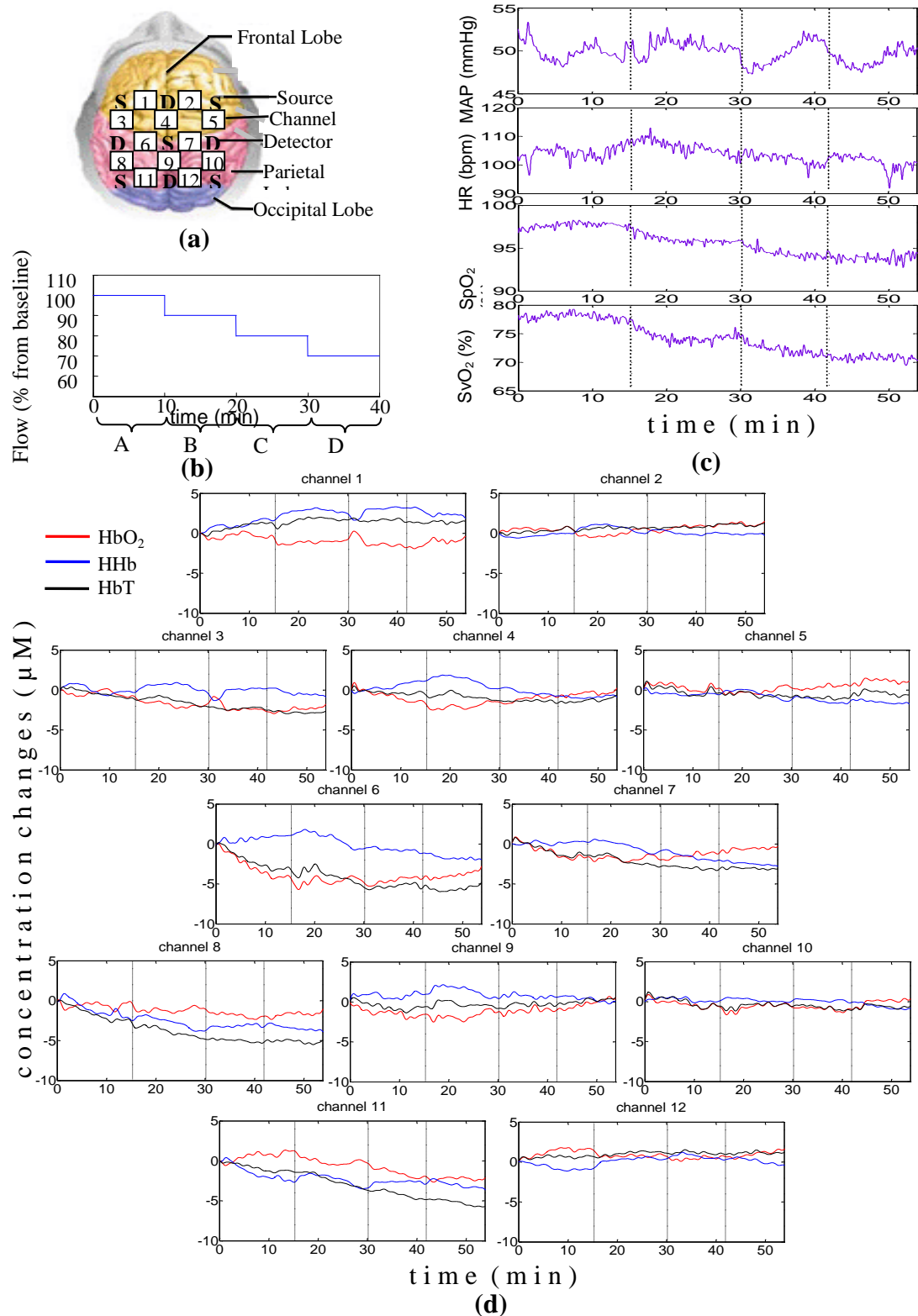
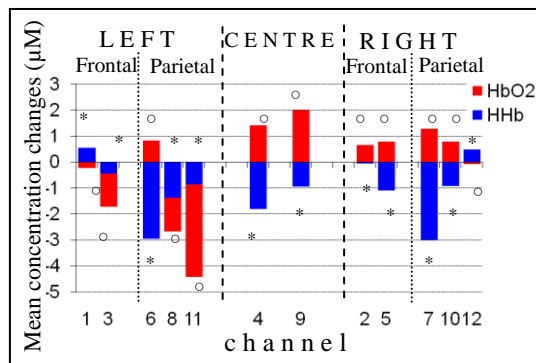
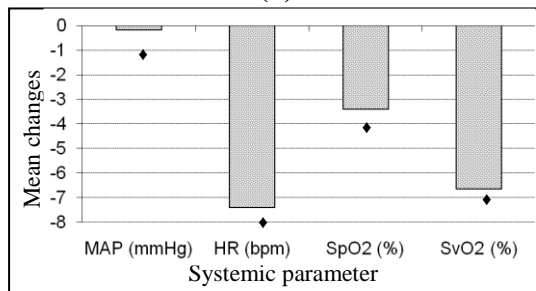


Figure 6.15: Multisite brain oxygenation and haemodynamics of **Patient 10** during flow changes. (a) Schematic of the 12-channel arrangement, (b) Sequence of flow changes indicating the different flow periods (A=100%, B=90%, C=80%, D=70%, E=80%, F=90%, G=100%), (c) Systemic parameters (MAP, HR, SpO₂ and SvO₂), (d) Multichannel NIRS parameters, HbO₂ (red), HHb (blue) and HbT (black). The vertical dotted lines split the plots into the different flow periods.

PHASE I



(a)



(b)

Figure 6.16: Mean absolute changes in haemoglobin concentrations across the 12-channels and systemic parameters during phases I (from baseline to minimum flow) and II (from minimum flow back to baseline) for **Patient 10**

* Statistically significant differences in HHb ($p < 0.05$)

◦ Statistically significant differences in HbO₂ ($p < 0.05$)

◆ Statistically significant differences in systemic parameters ($p < 0.05$)

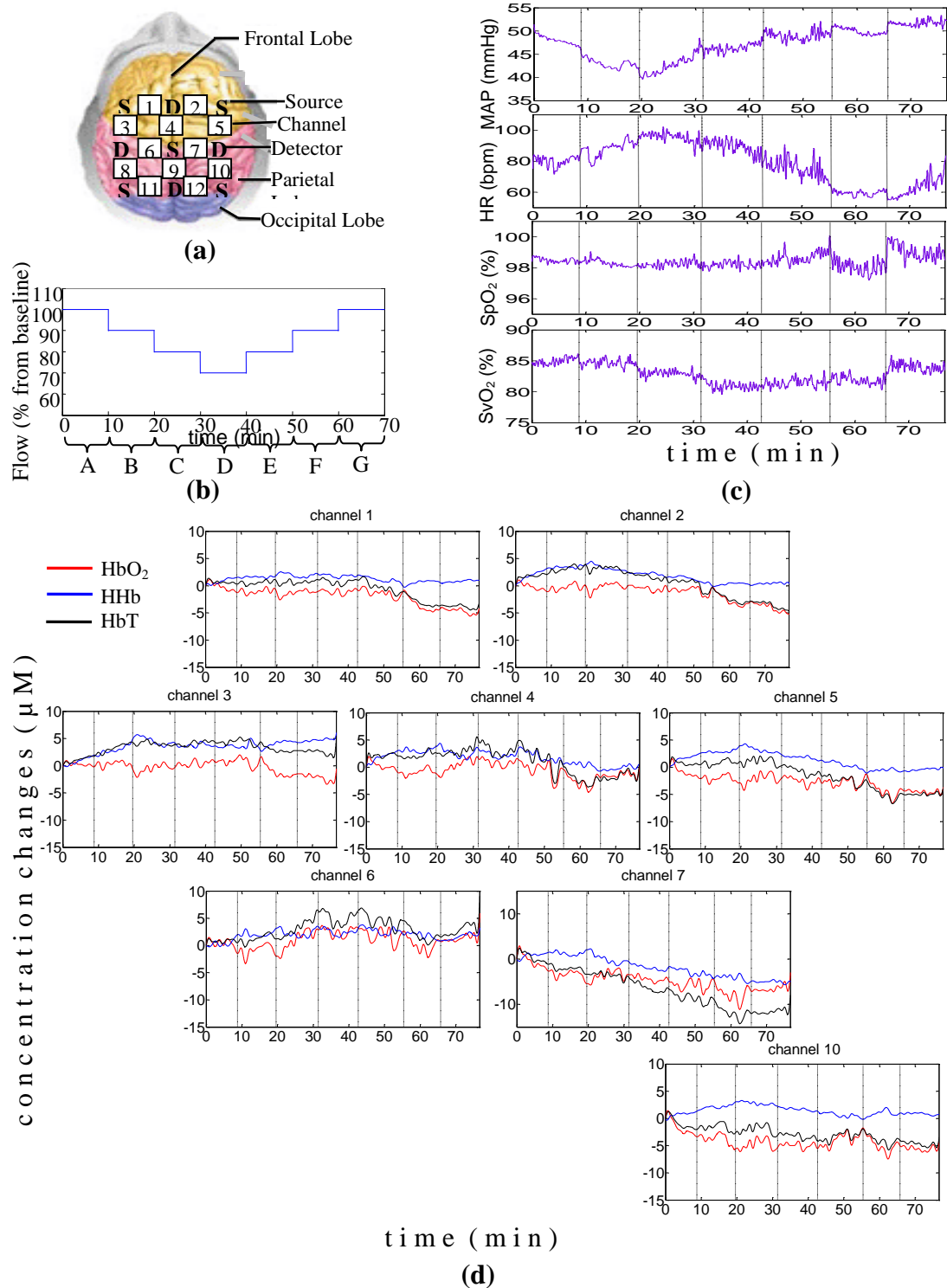


Figure 6.17: Multisite brain oxygenation and haemodynamics of **Patient 11** during flow changes. (a) Schematic of the 12-channel arrangement, (b) Sequence of flow changes indicating the different flow periods (A=100%, B=90%, C=80%, D=70%, E=80%, F=90%, G=100%), (c) Systemic parameters (MAP, HR, SpO₂ and SvO₂), (d) Multichannel NIRS parameters, HbO₂ (red), HHb (blue) and HbT (black). The vertical dotted lines split the plots into the different flow periods.

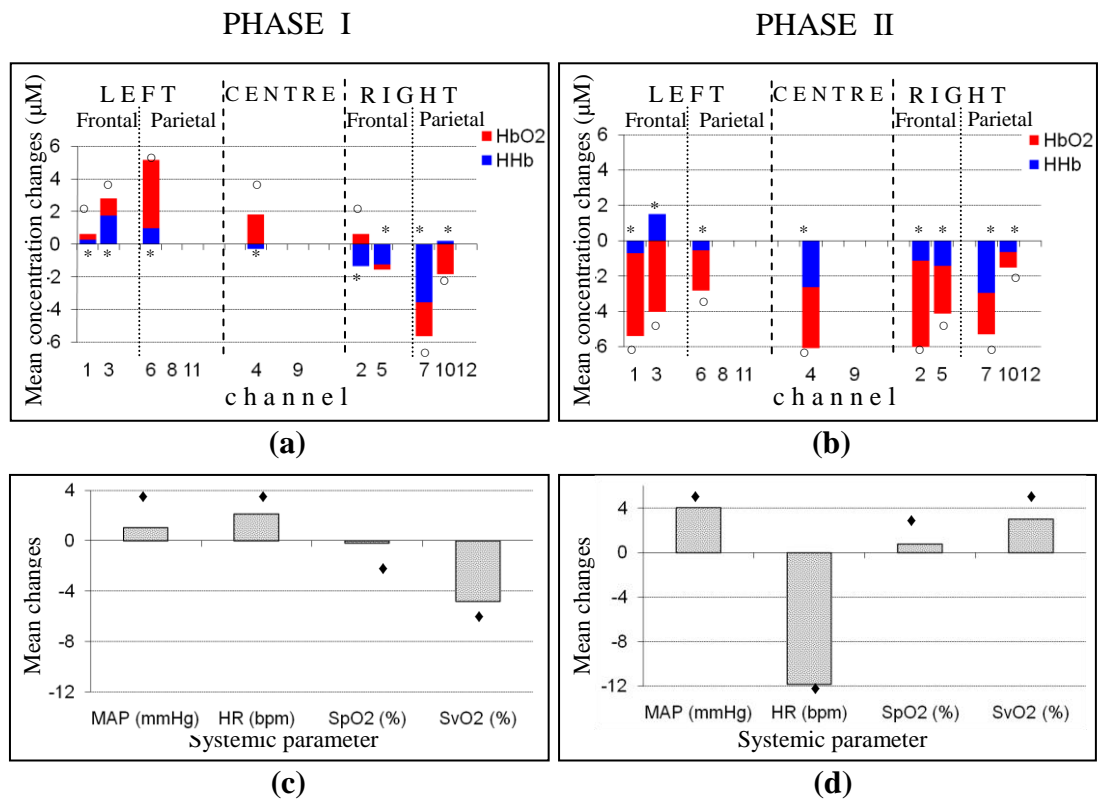


Figure 6.18: Mean absolute changes in haemoglobin concentrations across the 12-channels and systemic parameters during phases I (from baseline to minimum flow) and II (from minimum flow back to baseline) for **Patient 11**.

* Statistically significant differences in HHb ($p < 0.05$)

° Statistically significant differences in HbO₂ ($p < 0.05$)

♦ Statistically significant differences in systemic parameters ($p < 0.05$)

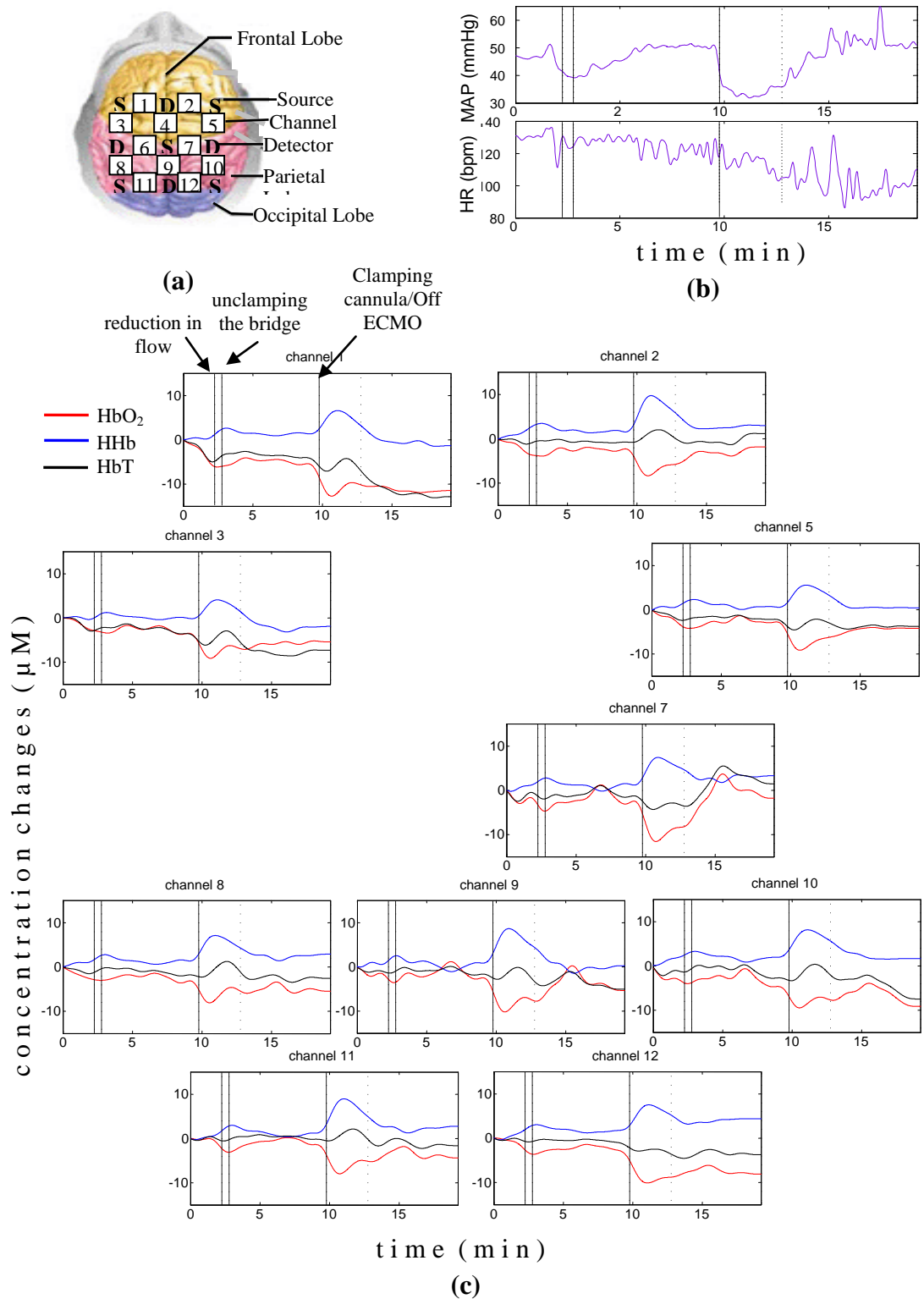
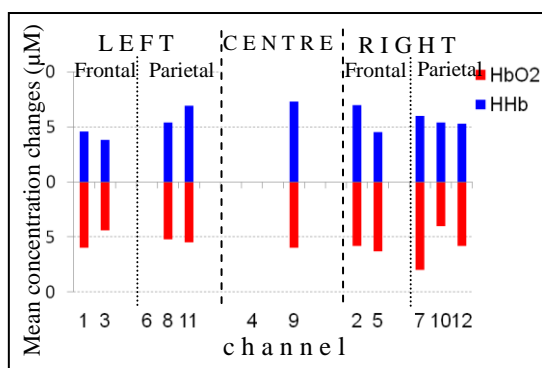
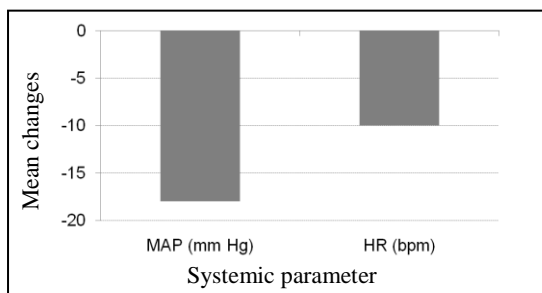


Figure 6.19: Multisite brain oxygenation and haemodynamics of **Patient 9** during **weaning**. (a) Schematic of the 12-channel arrangement, (b) Systemic parameters (MAP and HR), (d) Multichannel NIRS parameters, HbO₂ (red), HHb (blue) and HbT (black). The vertical dotted lines mark flow reduction, unclamping the bridge and clamping of the cannulae so that the patient is off ECMO, as indicated in channel 1.



(a)



(b)

Figure 6.20: Mean absolute changes in haemoglobin concentrations across the 12-channels and systemic parameters between prior to clamping the cannulae and at maximum/minimum after clamping the cannulae for **Patient 9** during weaning.

6.4 Discussion and Conclusions

The results indicate the effective use of the multichannel near infrared spectroscopy system to measure cerebral oxygenation on infants and children supported on ECMO.

Some general observations can be made for the 6 patients monitored during alterations in the ECMO flows. Significant changes in systemic oxygenation parameters and cerebral haemoglobin concentrations in response to changes in ECMO flows were observed.

In patients 4 and 5 a drop in SvO₂ in the order of 20% at minimum flows is observed. In these patients a reduction flow is associated with a higher increase in HHb than a decrease in HbO₂. A decrease in ECMO flow is associated with a decrease in oxygen delivery especially in the early course of ECMO treatment when the heart and lungs have not fully recovered. If ECMO flow is inadequate, there is a reduction in SvO₂ and a subsequent decrease in SpO₂. Consequently, in an effort to increase cardiac output, there is a compensatory increase in HR. The decrease in SpO₂ and SvO₂ seen in these patients suggest that lowering of ECMO flows has a similar effect to a hypoxemic challenge and the absence of decrease in HbO₂ in relation to increase in HHb could be explained by arterial dilation as a compensatory response to decreased blood flow due to decreased ECMO flows .

In particular, the changes seen in the total haemoglobin in patient 4 are relatively large compared to the suggested total cerebral blood volume in an infant of 2.2mL/100g (50µM) (Wyatt et al. 1990). Van Heijst et al. (2004) report changes in HbO₂ and HHb in the order of 1µmol/100g (10µM) 60 min after ECMO induction and suggest no interhemispheric differences. Eljike et al. (2006) report no relationship between ECMO flow and tissue oxygen saturation but changes in the individual HbO₂ and HHb parameters were not reported.

Minor changes in the haemoglobin parameters were observed in patients 8 and 10 possible due to the fact that in these patients a 30 % reduction in flows caused only minor reductions in venous (6.7% and 4.8%) and arterial (3.4% and 0.2%) saturations.

Multichannel optical topography can provide information on regional cerebral haemodynamics and oxygenation in ECMO patients. Simultaneous measurement of systemic and cerebral parameters can be used to characterise the response to changes in ECMO flows. Even though some interesting observations can be made by studying the trends in cerebral oxygenation parameters, it is difficult to address regional variations just by examining the absolute changes in these parameters. More sophisticated analytical tools are needed in order to identify patterns and investigate regional variation in cerebral circulation.

Chapter 7

WAVELET CROSS-CORRELATION TO INVESTIGATE REGIONAL VARIATION IN CEREBRAL OXYGENATION IN INFANTS SUPPORTED ON ECMO

7.1 Introduction

Extracorporeal membrane oxygenation (ECMO) has dramatically improved the survival rate of newborns with cardio-respiratory failure. The severity of illness that precipitates the initiation of ECMO, as well as the risks associated with the procedure itself, have raised concerns about morbidity among the survivors. Intracerebral complications are the largest cause of morbidity and mortality in these patients, with the reported frequency of abnormal neuroimaging ranging from 28-52% depending on techniques and methods of classification (Bulas and Glass 2005).

Initiation of ECMO involves cannulation of the major great vessels - right common carotid artery and internal jugular vein – which may cause lateralising cerebrovascular injury. Several studies noted an increase in injuries to the right hemisphere in infants who underwent ligation of the right carotid artery (Hahn et al. 1992, Hofkosh et al. 1991, Mendoza et al. 1991). Other studies however showed no selective or greater injury to the right hemisphere as compared with the left (Adolph

et al. 1990, Bulas et al. 1995, Graziani et al. 1997b). Furthermore, most ECMO infants suffer from hypoxia, asphyxia and hypercarbia, prior to the induction of ECMO. All these physiological changes can disrupt cerebral autoregulation leaving the cerebral microcirculation vulnerable to alterations in systemic blood pressure. Liam et al (1995) used near infrared spectroscopy and demonstrated increased cerebral blood volume and loss of autoregulation in patients supported on ECMO. Short et al (1993) evaluated the effect on cerebral autoregulation of exposure to VA ECMO in a lamb model. Exposure to VA ECMO for 1 hour in the healthy newborn lamb resulted in an alteration of cerebral autoregulation. Right to left blood flow differences were seen in this study when CBF decreased. In another study, Short et al (1994) exposed newborn lambs to 2 hours of severe hypoxia ($\text{SaO}_2 = 40\%$) with carotid artery and jugular vein ligation, simulating the hypoxia seen in patients pre-ECMO. Cerebral autoregulation was evaluated 1 hour after hypoxic insult and was found to be abnormal.

Cerebral autoregulation refers to the regulatory properties of the brain vascular bed to maintain constant cerebral blood flow (CBF) despite changes in blood pressure. Conversely, when changes in mean arterial pressure (MAP) result in concordant changes in CBF, the cerebral circulation is deemed 'pressure passive' and cerebral autoregulation is considered to be no longer intact. A MAP below the lower limit of pressure autoregulation increases the brain's vulnerability to ischemia while a MAP above the upper limit may result in cerebral oedema and haemorrhage. This has led to a body of literature attempting to assess the status of autoregulation by considering the relationship between spontaneous fluctuations in MAP and CBF surrogates either in the time or frequency domain. CBF surrogates include cerebral blood flow velocity (CBFV) measured using TCD and haemoglobin concentration parameters measured using NIRS (Czosnyka et al. 2009, van Beek et al. 2008).

Methods in the time domain include the calculation of linear Pearson's correlation between consecutive samples of averaged MAP and CBF determining a correlation index. For example, Czosnyka et al (1997) used the moving correlation coefficient between the MAP and ICP to obtain an index (pressure-reactivity index, PRx), which quantifies cerebrovascular reactivity with the strength of linear correlation between fluctuations in the two parameters (Czosnyka et al. 1997). A

positive PRx value signifies a positive correlation between MAP and ICP, implying a passive behaviour of a non-reactive vascular bed. A negative PRx signifies an absent or negative correlation, reflecting a normally reactive vascular bed. This index was reported to correlate with indices of autoregulation based on CBFV measurements using transcranial Doppler ultrasonography (Czosnyka et al. 1996, Lang et al. 2002). Similarly, a positive correlation between MAP and CBFV indicates disrupted autoregulation, while a negative correlation implies that autoregulation is intact. Brady et al used this method of moving linear correlation between MAP and tissue oxygen saturation (TOS) measured by NIRS to assess cerebral autoregulation in children undergoing cardiac surgery with cardiopulmonary bypass for correction of congenital heart defects (Brady et al. 2010b). The averaged correlation index values were sorted by MAP and an autocorrelation curve was constructed for each patient. Similar method was performed in adults undergoing CPB using both TCD and NIRS parameters (Brady et al. 2010a). The measures based on Pearson's correlation coefficient between the averaged values of the ABP and CBFV time series despite their appealing simplicity and proven clinical significance, are inherently incapable of taking into account non linear effects. In fact Giller and Mueller (2003) using four methods of comparison, conclude that there is strong evidence that cerebral autoregulation is nonlinear (Giller and Mueller 2003). Furthermore, Mitsis et al. not only concur in the findings regarding nonlinearity but also conclude that cerebral autoregulation is non stationary as well (Mitsis et al. 2004).

Typical frequency methods for investigating the regulation of cerebral haemodynamics include power spectral analysis under various physiological or pathological conditions (Papademetriou et al. 2010, Tachtsidis et al. 2004). However, large inter-subject variability are often found in these absolute measurements of power spectra, which makes statistical differences hard to achieve. Transfer function and coherence analysis have been developed as methods to quantify the frequency dependent covariation of MAP and CBF. These methods rely on the presence of oscillations in MAP and CBF surrogates. The regulation of CBF is effective in the low-frequency range of MAP fluctuations, i.e. respiratory waves (from 0.1 Hz to 0.4 Hz) and slow waves (<0.1 Hz), but not in the high frequency range, i.e. heart rate, because cerebral autoregulation acts primarily via active alteration of the diameter of

cerebral arterioles in time scales of a few seconds in healthy individuals (Czosnyka et al. 2009). Therefore, cerebral autoregulation functions like a high pass filter, allowing rapid MAP changes to be transmitted to CBF, whereas slow MAP changes are filtered (Van Beek et al. 2008).

The transfer function utilises cross spectral analysis and assumes that autoregulation mechanisms can be described by a linear dynamic system with arterial blood pressure as input and blood flow velocity as output. The transfer magnitude, or gain, quantifies the damping effect between the input and the output of the transfer function. A low gain indicates an efficient autoregulation, whereas an increase in gain represents a diminished efficiency of the dynamic process of cerebral autoregulation. The phase shift between the two signals is another parameter obtained from the transfer function analysis with a positive phase shift indicating an intact autoregulation. Transfer function analysis was used in premature infants to study the concordance between MAP and NIRS parameters (Soul et al. 2007, Tsuji et al. 2000). Wong et al used transfer function and coherence analysis to quantify the relation between MAP and NIRS parameters in the slow oscillations region ($<0.1\text{Hz}$) in preterm infants (Wong et al. 2008). The coherence function is describing the linearity of the relation between the input (MAP) and output (CBF) signals and ranges between 0 and 1 depending on the degree of correlation between the 2 waveforms. High coherence values can be anticipated when autoregulation is impaired.

Recent studies have emphasized that cerebral autoregulation is in fact a dynamic process (Giller & Mueller 2003, Mitsis et al. 2006, Panerai 1998, Panerai et al. 1999, Panerai et al. 2005). The transfer function analysis suffers from the big drawback of averaging out all the potential useful time information, hence treating cerebral autoragulation as a stationary, linear process. To overcome this drawback, it is natural to consider time-frequency analysis which combines the advantages of both time and frequency domain analysis. Unlike the Fourier Transform, the continuous wavelet transform (CWT) possesses to the ability to construct a time-frequency representation of a signal that offers very good time and frequency localisation. Latka et al (2005) used the complex Mortlet wavelet with the CWT to compute the instantaneous phase of the CBFV and ABP signals and a synchronisation index

between the two signals, defined as the standard deviation of the phase difference (Latka et al. 2005). Besides investigating the instantaneous phase difference, wavelet cross-correlation was introduced in Rowley et al (2007) as the cross correlation between CWT coefficients of two time series (Rowley et al. 2007). Compared to ordinary cross-correlation, wavelet cross-correlation is also a measure of similarity between two time series, but localised to different frequencies. This CWT-based technique was used by Rowley (2007) to analyse the coupling between oscillations in ABP and NIRS measured HbO₂ in both autonomic failure patients and age matched controls. They demonstrated that the frequency (wavelet scale) at where high correlation between MAP and HbO₂ occurs is posture dependent in patients but not in controls. Spectral analysis using wavelets provides a mathematical framework for analysis of both nonlinear and non-stationary effects in cerebral haemodynamics, thus overcoming the restrictions intrinsic to earlier methods.

To date, the focus of near infrared spectroscopy studies on ECMO patients have been concentrated on relative and absolute changes in the amplitudes of NIRS parameters during vessel ligation and alterations in the ECMO flows. Furthermore, single or dual channel systems have been used in these studies with optodes usually place on the forehead which monitor only a small area of the anterior cerebrum. In a previous study we have used a dual NIRS system and showed the presence of oscillations related to vasomotion, respiration rate and heart rate (Papademetriou et al 2010). Preliminary results using a multichannel NIRS system indicate regional variation in cerebral oxygenation responses during ECMO flow changes (Papademetriou et al. 2011). Here, we are investigating the use of wavelet cross-correlation as a method to study the concordance between multisite cerebral oxyhaemoglobin concentration measures and mean arterial pressure in order to assess regional variations in cerebral oxygenation in neonates supported on ECMO.

7.2 Methods

7.2.1 Subjects

The study was approved by the Institute of Child Health/Great Ormond Street Hospital Research Ethics Committee. A total of 12 veno-arterial (VA) ECMO patients, age range 1-25 days, were monitored during cannulation, decannulation, weaning from ECMO and alterations in the ECMO flows. The results from seven out of the twelve patients were used in the wavelet analysis described in this chapter. Data from the rest of the patients was rejected due to poor signal-to-noise ratio or movement artefacts. Six of these patients were monitored during alteration in ECMO flows and 1 during weaning. The demographics of the seven patients are shown in table 7.1. The chromophore concentration data along with the systemic variables for these patients are presented and discussed in chapter 6. Written informed parental consent was obtained from all participants prior to inclusion in the study.

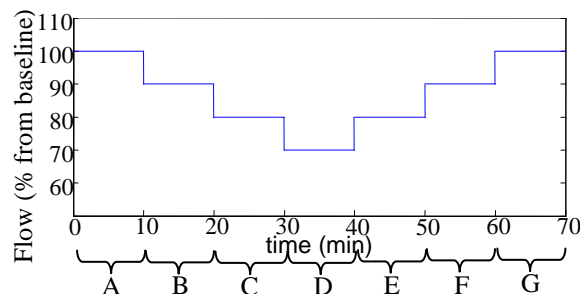


Figure 7.1: Schematic diagram showing the sequence followed during alterations in the ECMO flows. Flows were reduced sequentially by 10% from baseline approximately every 10 minutes and subsequently increase back to baseline. The letters at the bottom of the plot indicate the different flow periods (A=100%, B=90%, C=80%, D=70%, E=80%, G=90%, F=100%).

Alterations in the ECMO flows refer to successive decrease in the ECMO flow by 10% from the initial flow, approximately every 10 minutes, down to 70% of the initial flow followed by successive increase back to baseline (figure 7.1). Out of the six patients monitored during alterations in the ECMO flows four were monitored during the complete sequence (from flow periods A to G). One patient was

monitored from 100% down to only 80% of baseline and then sequentially back to baseline. For another patient only half sequence was used, i.e. reductions in flows only (periods A to D), the other half of the sequence was affected by movement artefacts.

7.2.2 Instrumentation

A multichannel continuous wave near infrared spectroscopy system (ETG-100, Hitachi Medical Ltd., Japan) was used to measure changes in oxyhaemoglobin (HbO₂), deoxyhaemoglobin (HHb) and total haemoglobin (HbT) concentrations using the modified Beer-Lambert Law. A differential pathlength factor (DPF) of 4.67 was used for the conversion of optical data to haemoglobin concentrations (Duncan et al. 1995). A novel neonatal cap was constructed to accommodate the optical sources and detectors in a 3 x 3 array (interoptode distance = 3 cm), allowing data to be collected from 12 channels. Alterations in ECMO flows and weaning were monitored at 5 Hz. Multimodal data were collected synchronously with the optical data that included systemic parameters (arterial blood pressure, heart rate [HR], and arterial oxygen saturation [SpO₂]) and ECMO circuit parameters (venous oxygen saturation [SvO₂], arterial saturation at the cannula [SaO₂], ECMO flows and hematocrit). Synchronisation between optical, systemic and ECMO circuit parameters is described in detail elsewhere (chapter 6).

7.2.3 Data Analysis

Spectral analysis using wavelets was performed on the multichannel HbO₂ data. Specifically, the wavelet cross-correlation (WCC) and synchronisation index, γ , were used as methods to investigate the relation between MAP and HbO₂.

The complex Morlet wavelet was used to calculate the continuous wavelet transform coefficients for each time series, MAP and HbO₂, using the MatLab (Mathworks,) wavelet toolbox function *cwt*.

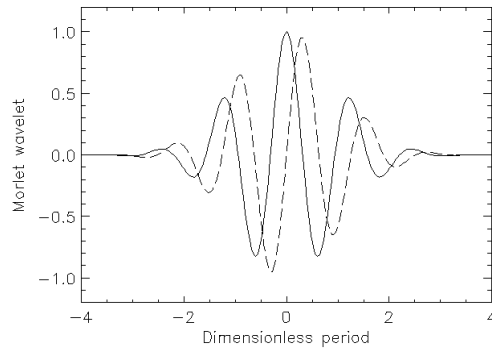
The continuous wavelet transform (CWT) of a signal $x(t)$ is defined as (Semmlow 2004):

$$W(\alpha, b) = \frac{1}{\sqrt{\alpha}} \int_{-\infty}^{\infty} x(t) \psi^* \left(\frac{t-b}{\alpha} \right) dt \quad (7.1)$$

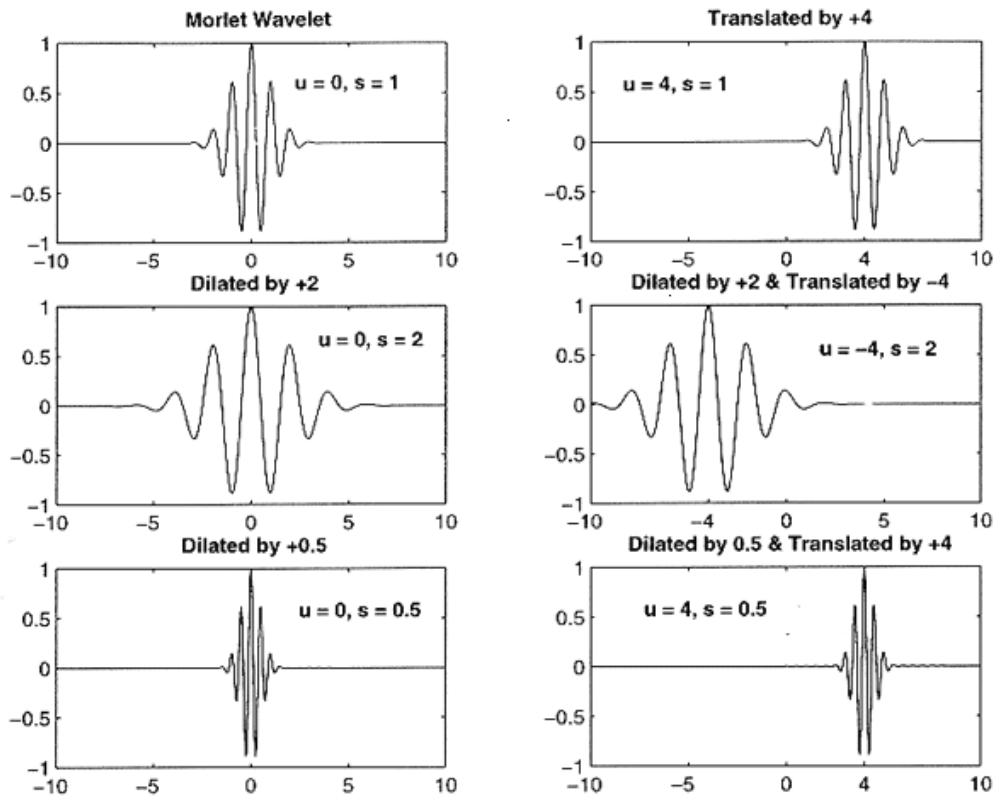
where $\psi(t)$ is a continuous function in both the time domain and the frequency domain called the mother wavelet and * represents operation of complex conjugate. Here, the complex Morlet wavelet was chosen as the mother wavelet which consists of a plane wave modulated by a Gaussian function (Torrence and Compo 1998):

$$\psi(t) = \frac{1}{\sqrt{\pi f_b}} e^{i2\pi f_c t} e^{-t^2/f_b} \quad (7.2)$$

where f_b is the bandwidth and f_c the wavelet centre frequency. The main purpose of the mother wavelet is to provide a source function to generate the daughter wavelets which are simply the translated and scaled versions of the mother wavelet. Hence, the variable b in equation 7.1 acts to translate the function across $x(t)$ and the variable α acts to vary the time scale of the probing function, ψ . If α is greater than one, the wavelet function, ψ , is stretched along the time axis, and if it is less than one (but still positive) it contracts the function. The normalising factor $1/\sqrt{\alpha}$ ensures that the energy is the same for all values of α . To be “admissible” as a wavelet, ψ must have zero mean and be localised in both time and frequency space (Torrence & Compo 1998). Hence, the centre frequency, f_c , was taken to be 1. The real and imaginary parts of the Morlet wavelet are shown in figure 7.2 along with some of its family members produced by dilation and contraction.



(a)



(b)

Figure 7.2: (a) Real and Imaginary part of the Morlet wavelet (b) the Morlet Wavelet with dilations, contraction and translations.(modified from Semmlow 2004)

While there is a general relationship between the scale α in the wavelet domain and frequency in the Fourier transform, no precise relationship exists. The translation from scale to frequency depends upon the particular choice of wavelet. However, an approximate relationship between wavelet scale and translated frequency, pseudo-frequency, f_a , can be computed as:

$$f_{\alpha} = \frac{f_c}{\alpha \cdot \delta t} \quad (7.3)$$

where f_c is the centre frequency and δt is the sampling period. This approximate relationship was previously used by (Latka et al. 2005, Rowley et al. 2007) to study similar physiological oscillations as reported herein.

Mean arterial pressure (MAP) was obtained by trapezoid integration of the arterial blood pressure waveform every 0.2 s, equivalent to sampling frequency of 5 Hz. The time series of MAP and HbO₂ were divided into sections representing each ECMO flow period. Each section of data was then high pass filtered using a fifth-order Butterworth filter with cut off frequency of 0.008 Hz to remove very slow variations and baseline shift and subsequently low pass filtered using a fifth-order Butterworth filter with a cut-off frequency of 1 Hz to remove variability in the signal due to the cardiac cycle. A scale range with unit spacing from 5 to 100, representing frequencies 0.008-1 Hz was use to obtain two complex time series, $W_{MAP}(a,t)$ and $W_{HbO_2}(a,t)$ for each flow period A to G (see figure 7.1) and across each of the 12 channels.

The wavelet cross-correlation (WCC) between MAP and HbO₂ in each channel and for each flow was obtained using the equation below (Rowley 2007):

$$\overline{WCC} = \frac{|R_{X,Y}(W_{MAP}, W_{HbO_2}, \alpha, \tau)|}{\sqrt{|R_{X,X}(W_{MAP}, \alpha, 0) \cdot R_{X,X}(W_{HbO_2}, \alpha, 0)|}} \quad (7.4)$$

in which $R_{X,Y}(s1, s2, a, \tau)$ denotes the cross-correlation of the wavelet coefficients of the series $s1$ and $s2$ at a scale a and for a relative time shift τ and $R_{X,X}(s1, a, 0)$ denotes the autocorrelation of the time series $s1$ for zero time shift. $WCC(a, \tau)$ represents the cross-spectral power in the two time series (shifted relative to each other by τ) as a fraction of the total power in the two time series. WCC ranges from 0 to 1. At a given wavelet scale, WCC=1 would indicate that the coefficients of the two wavelet transforms are related to each other by a simple scaling factor, suggesting strong synchronization at this frequency (Rowley et al. 2007). Figure 7.3 shows simulated data to demonstrate strong and weak synchronization between two signals.

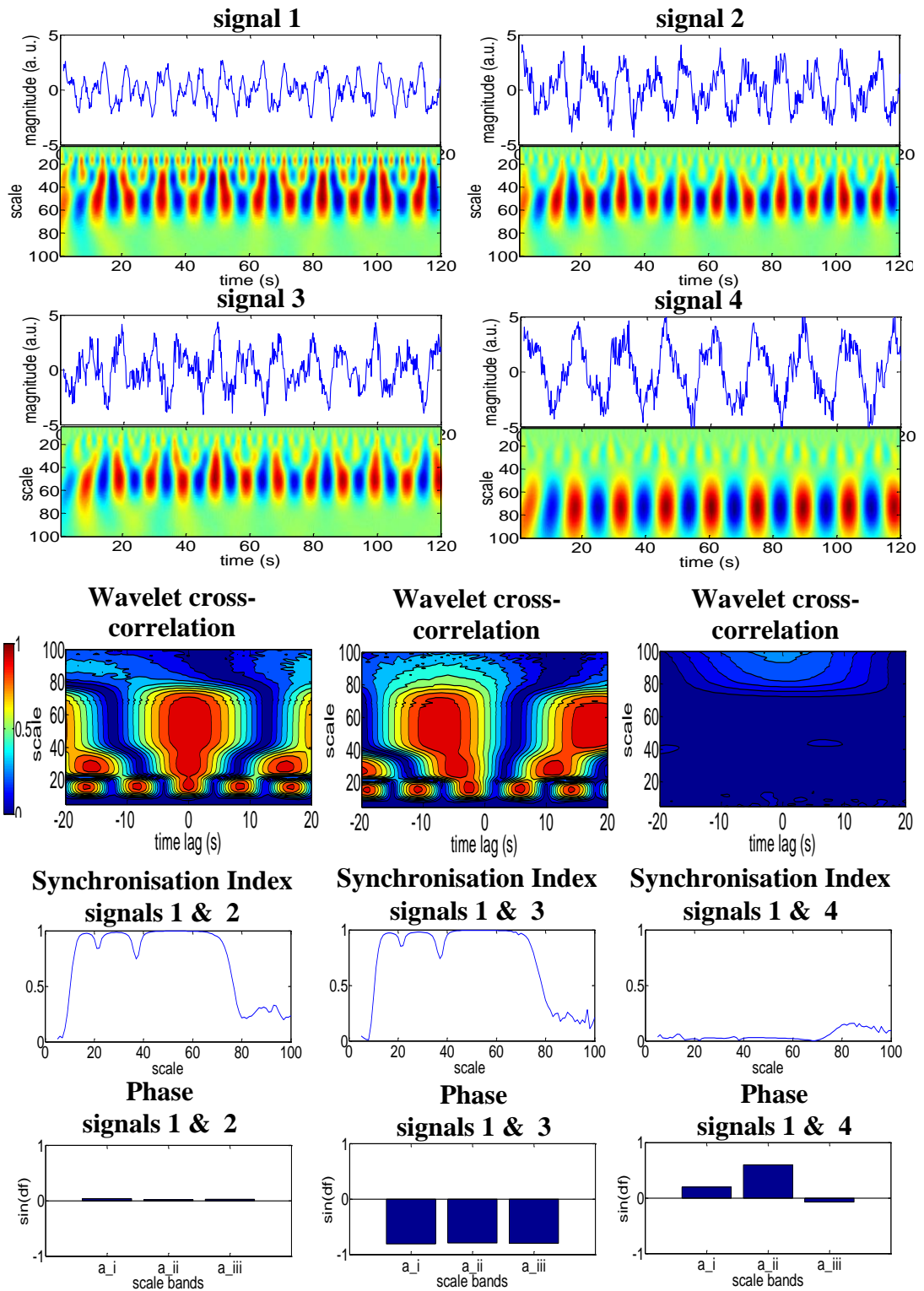


Figure 7.3: Wavelet cross-correlation and synchronisation index between signals with the same frequency content (signals 1 & 2), same frequency content but out of phase (signals 1 & 3), and signals with different frequency content (signals 1 & 4).

The synchronization index, $\gamma(\alpha)$, which is the inverse circular statistical mean analogue of variance was also calculated using (Rosenblum et al. 2001)

$$\gamma(\alpha) = \frac{1}{N} \left(\left[\sum_t \cos(\Delta\phi(\alpha, t)) \right]^2 + \left[\sum_t \sin(\Delta\phi(\alpha, t)) \right]^2 \right) \quad (7.5)$$

in which N is the number of points in the series and $\Delta\Phi(\alpha, \tau)$ is the instantaneous phase difference between the two signals. The instantaneous phase difference was calculated using

$$W_{MAP} \cdot W_{HbO2}^* = r \cdot e^{i\Delta\Phi} \quad (7.6)$$

The synchronization index varies from 0 to 1. Zero γ indicates uniform distribution of phase differences, so the time series are statistically independent of one another.

The phase difference between the two time series, Map and HbO2 was also calculated using the circular mean, $\overline{\Delta\Phi(\alpha)}$, of the phase difference over the duration of a test segment was the calculated using (Fisher 1995)

$$\overline{\Delta\Phi(\alpha)} = \tan^{-1} \left(\frac{\sum_t \sin(\Delta\phi(\alpha, t))}{\sum_t \cos(\Delta\phi(\alpha, t))} \right) \quad (7.7)$$

For each time series pair at each flow period and for each channel, the maximum value of $WCC(a, \tau)$ was found within three scale bands: $a_i = 5 < a < 20$ ($f_{ai} = 0.25 \text{ Hz} < f_a < 1 \text{ Hz}$), $a_{ii} = 20 < a < 40$ ($f_{a_{ii}} = 0.13 \text{ Hz} < f_a < 0.25 \text{ Hz}$), $a_{iii} = 40 < a < 80$ ($f_{a_{iii}} = 0.06 \text{ Hz} < f_a < 0.13 \text{ Hz}$). These bands were chosen to overlap with respiration rate (RR), ventilation rate (VR), and slow M-waves respectively. The maximum synchronization index, γ_{max} , and circular mean, $\Delta\Phi_{max}$, were also calculated within each scale band, for each flow period and each channel. Students; t-test was then used to analyse the statistical significance of the differences in the group mean of each of these variables between channels and within each flow period.

7.3 Results

Wavelet cross-correlation and synchronisation index were calculated for the patients listed in table 7.1. Group data were obtained for the six patients monitored during alterations in ECMO flows while individual data are presented for the one patient monitored during weaning. WCC was calculated for every flow period and every channel. The active channels and rejected channels and flow periods for the six patients are listed in table 7.2.

7.3.1 Wavelet cross-correlation (WCC)

7.3.1.1 Alterations in the ECMO flows

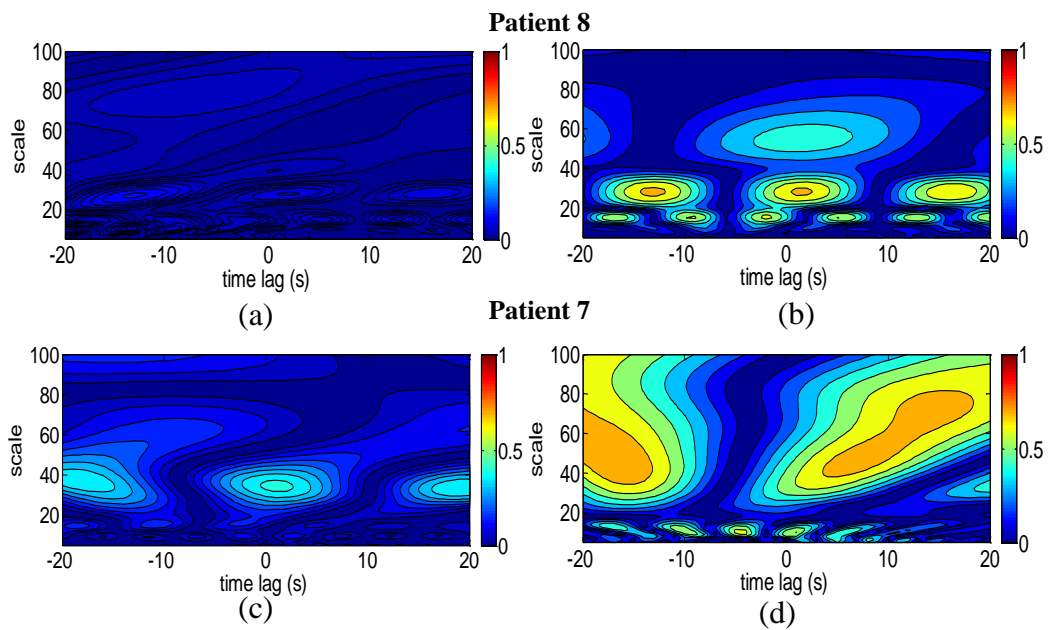


Figure 7.4: Wavelet cross-correlation between MAP and HbO₂ for two ECMO patients. Low correlation is shown at baseline ECMO flows (a and c) and high correlation around scales 16 and 30 for patient 1 at minimum flow (b) and around scales 16 and 40-80 for patient 2 (d) at minimum flow.

Figure 7.3 shows a set of typical wavelet cross-correlation contours obtained from two patients at baseline flow and minimum flow. For patient 8 WCC shows no distinct peaks at baseline flows indicating no correlation between MAP and HbO₂. At minimum flow, peaks in the WCC contours are shown at scales 15 ($f_a = 0.33$ Hz), 29 ($f_a = 0.17$ Hz) and a relatively weaker peak at scale 55 ($f_a = 0.09$ Hz). The wavelet

cross correlation contour for patient 7 at baseline flow shows a relatively weak peak at a scale 34 ($f_a = 0.15$ Hz). As with patient 8 correlation between MAP and HbO₂ becomes stronger at minimum flow with the peak at scale 34 spreading to higher Mayer-waves related scales and another peak occurring at scale 10 ($f_a = 0.5$ Hz). These peaks appear shifted from zero time lag. Rowley et al (2007) in their study of wavelet-cross correlation between MAP and HbO₂ also report a shift from zero time lag in WCC peaks in autonomic failure patients but not in healthy control subjects.

In general, wavelet cross-correlation between MAP and HbO₂ revealed three distinct peaks within three scale regions. The first peak typically occurs at a scale of around 14 (0.36 Hz), the second at a scale around 30 (0.16 Hz) and the third at a scale around 50 (0.1 Hz). These peaks could correspond to the respiration rate (RR), ventilation rate (VR) and Mayer-waves, respectively.

Figure 7.5c shows the group data for the mean of the maximum wavelet cross-correlation, WCC_{\max}^i , within scale band $a_i = 5 < a < 20$ ($f_a^i = 0.25 \text{ Hz} < f_a < 1 \text{ Hz}$) at each flow period and across the 12 channels. The channel arrangement is shown in figure 7.5a. The sequence of ECMO flow changes, with letters A to G representing the different flow periods, is shown in figure 7.5b. By convention a value of WCC below 0.5 indicates no correlation between MAP and HbO₂ (Latka et al. 2005, Latka et al. 2007, Rowley et al. 2007). A + sign is used to indicate that HbO₂ lags MAP, i.e. $\Delta\Phi > 0$, only for WCC greater than 0.5, i.e. strong correlation between the two signals. A – sign is used to indicate that HbO₂ is leading MAP, i.e. $\Delta\Phi < 0$, where $WCC > 0.5$. The following observations can be made:

- There are statistically significant differences ($p < 0.05$) in the mean WCC_{\max}^i across all flows between symmetrical channels most likely positioned on the right (channels 7, 10 and 12) and left (channels 6, 8 11) parietal lobes (figure 7.4d). WCC_{\max}^i for all flows in the three channels positioned on the left parietal lobe is below 0.5 suggesting no correlation between MAP and HbO₂ in these channels.
- Similarities are shown between symmetrical channels on the right (2 and 5) and left (1 and 3) frontal lobes. While for symmetrical channels 1 and 2 $WCC_{\max}^i > 0.5$ after minimum flow (period D) is reached, for symmetrical channels 3 and 5 $WCC_{\max}^i > 0.5$ for at flow periods.

- A general increase in WCC_{\max}^i was observed with decrease in flow across all channels. WCC_{\max}^i is highest either at flow period E or F.
- The group data showed that a_{\max}^i across flow changes for all channels ranges from 9 to 17 (0.29-0.56 Hz) (figure 7.4e). Most of the channels show a shift in a_{\max}^i to a lower scale when the highest WCC_{\max}^i is reached (flow period E) and a shift back to higher scales when the flow continues to increase back to baseline.

Figure 7.6 shows the group data for the mean maximum wavelet cross-correlation, WCC_{\max}^{ii} , within scale band $a_{ii} = 20 < a < 40$ ($f_{a_{ii}} = 0.13 \text{ Hz} < f_a < 0.25 \text{ Hz}$) for each flow period and across all 12 channels. The results obtained in the group analysis of the scale band a_{ii} are similar to those described above for scale band a_i :

- Statistically significant differences in mean WCC_{\max}^{ii} across flow periods are observed between symmetrical channels potentially placed on the right and left parietal lobes with channels on the right generally showing higher values of WCC_{\max}^{ii} than those on the left (figure 7.6d). Channels 6, 8 and 11 positioned on the left parietal lobe show no correlation ($WCC < 0.5$) between MAP and HbO₂ across all flow periods.
- The highest WCC_{\max}^{ii} occurs at flow period E for all channels.
- The group data of a_{\max}^{ii} , ranges from 15 to 32 (0.16-0.33 Hz) (figure 7.6e). A shift to higher scales is observed during decrease in flow, from flow periods A to D, and shift back to lower scales from flow periods D to F.
- In general values WCC_{\max}^{ii} are lower in this scale band than in a_i .

The group data for maximum wavelet cross-correlation, WCC_{\max}^{iii} , within scale band $a_{iii} = 40 < a < 80$ ($f_{a_{iii}} = 0.06 \text{ Hz} < f_a < 0.13 \text{ Hz}$) across flows periods and channels is shown in figure 7.7. Mean WCC_{\max}^{iii} across flow periods is higher on the right hemisphere than on the left, even though, with the exception of channels 5 and 3, these differences were not found to be statistically significant (figure 7.7d). Analogous to the other two scale bands, the strongest correlation between MAP and HbO₂ is observed at flow period E across all the channels. The scale at which WCC_{\max}^{iii} occurs, a_{\max}^{iii} , is shifted to lower scales as ECMO flow changes from flow period A to F (figure 7.7e).

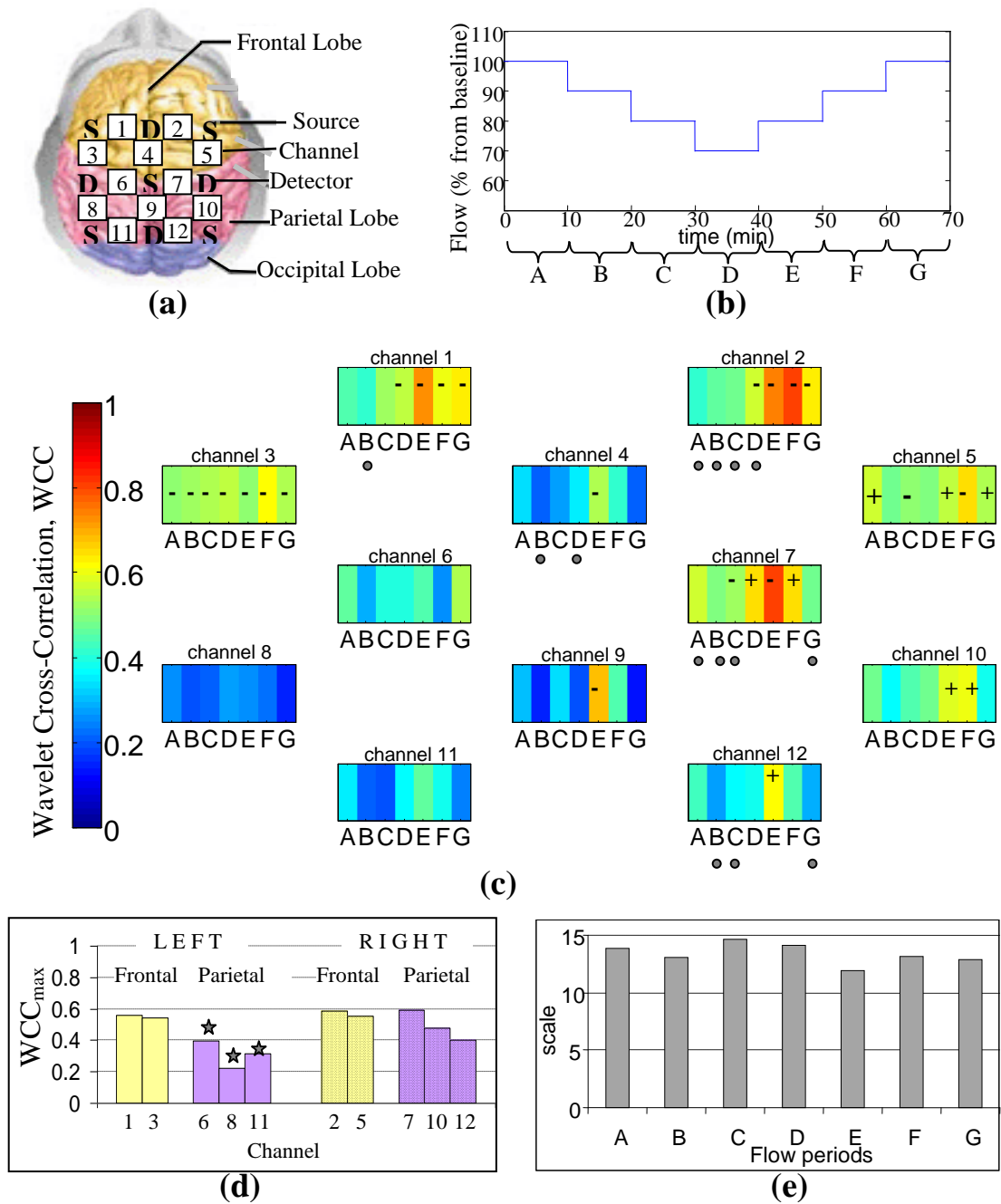


Figure 7.5: Group wavelet cross-correlation between MAP and HbO₂ within scale band $a_i = 5 < a < 20$ ($f_{ai} = 0.25 \text{ Hz} < f_a < 1 \text{ Hz}$): (a) Channel arrangement; (b) Sequence of flow changes (A=100%, B=90%, C=80%, D=70%, E=80%, F=90%, G=100%); (c) WCC_{max}^i at all flow periods across all channels; (d) mean WCC_{max}^i across all flow periods of channels on the right side and symmetrical channels on the left side; (e) mean of scale at WCC_{max}^i , a_{max}^i , for each flow period across all channels.

+/- denotes HbO₂ lagging/leading MAP for $WCC_{max}^i > 0.5$

◐ Statistically significant difference between flow period with highest WCC_{max}^i at each channel and the all the rest flow periods at the same channel ($p < 0.05$)

★ Statistical significant difference between symmetrical channels on right and left hemispheres ($p < 0.05$).

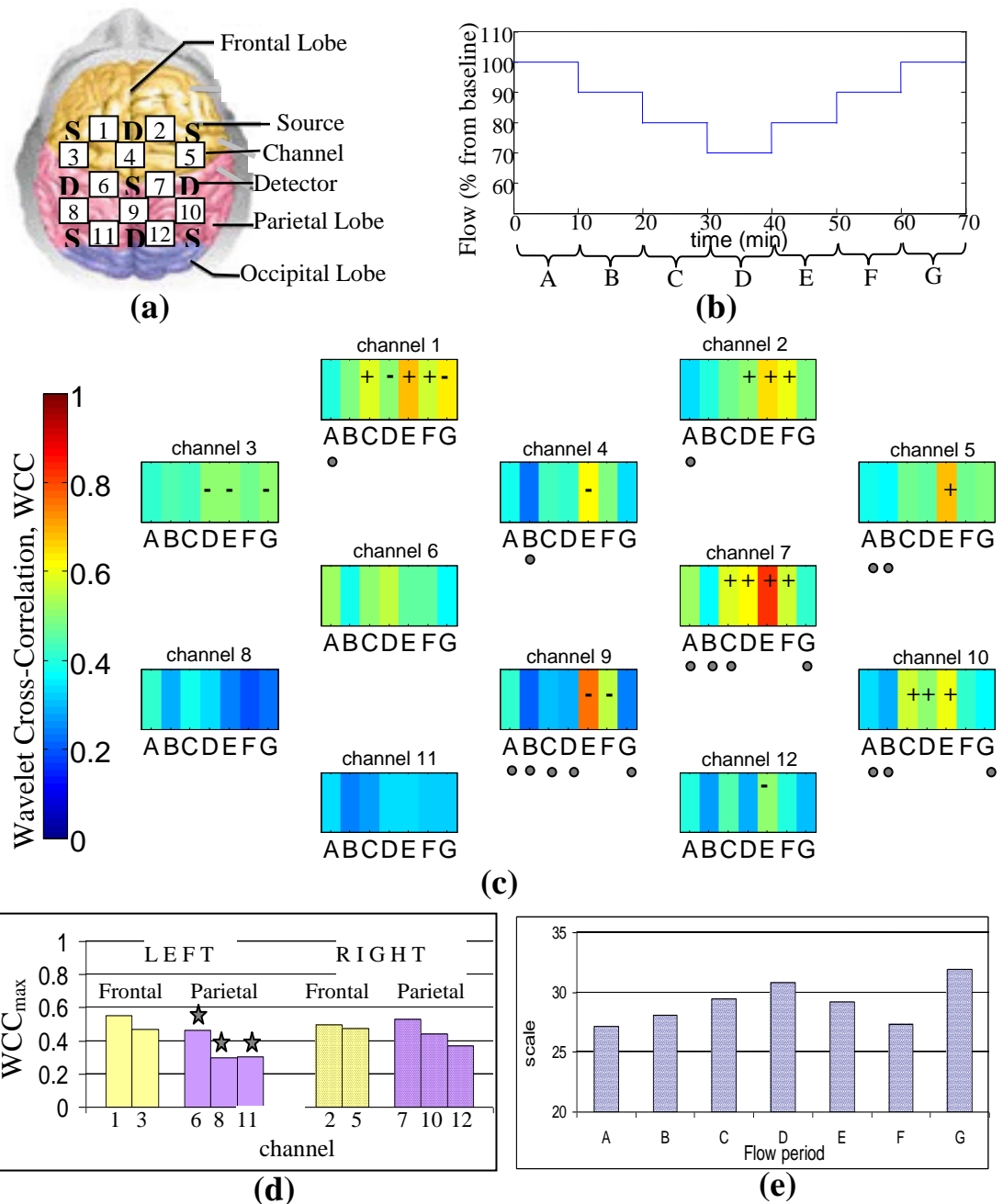


Figure 7.6: Group wavelet cross-correlation between MAP and HbO₂ within scale band $a_{ii} = 20 < a < 40$ ($f_{a_{ii}} = 0.13 \text{ Hz} < f_a < 0.25 \text{ Hz}$): (a) Channel arrangement, (b) Flow changes sequence (A=100%, B=90%, C=80%, D=70%, E=80%, F=90%, G=100%), (c) WCC_{max}ⁱⁱ at all flow periods across all channels, (d) mean WCC_{max}ⁱⁱ across all flow periods of channels on the right side and symmetrical channels on the left side, and (e) mean of scale at WCC_{max}ⁱⁱ, a_{max}^{ii} , for each flow period across all channels.

+ denotes HbO₂ lagging MAP for WCC_{max}ⁱⁱ > 0.5

- denotes HbO₂ leading MAP for WCC_{max}ⁱⁱ > 0.5

o Statistically significant difference between flow period with highest WCC_{max}ⁱⁱ at each channel and the all the rest flow periods at the same channel ($p < 0.05$)

★ Statistical significant difference between symmetrical channels on the right and the left hemispheres ($p < 0.05$).

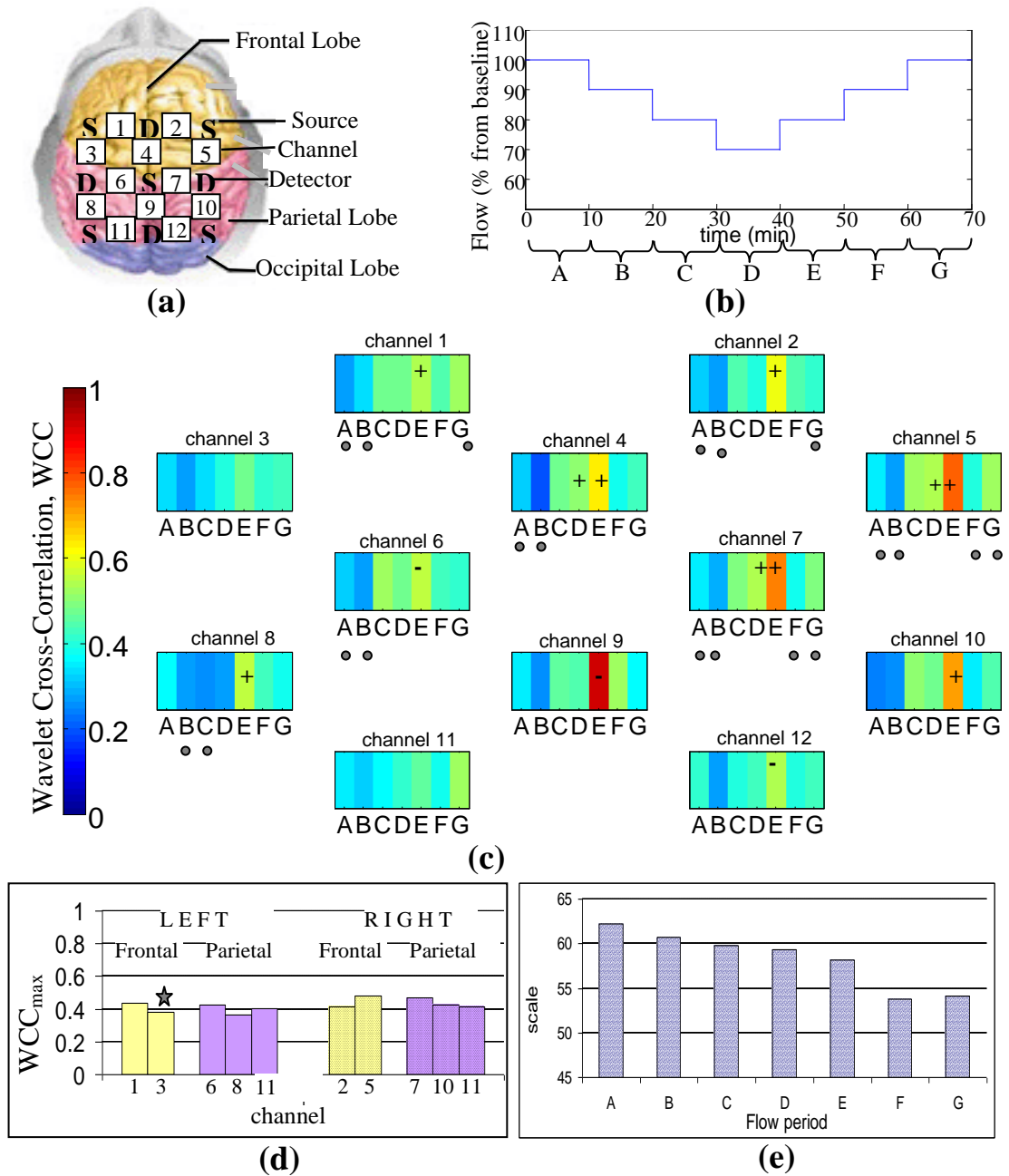


Figure 7.7: Group wavelet cross-correlation between MAP and HbO₂ within scale band $a_{iii} = 20 < a < 40$ ($f_{a_{ii}} = 0.06 \text{ Hz} < f_a < 0.13 \text{ Hz}$): (a) Channel arrangement, (b) Flow changes sequence (A=100%, B=90%, C=80%, D=70%, E=80%, F=90%, G=100%), (c) WCC_{max}ⁱⁱⁱ at all flow periods across all channels (d) mean WCC_{max}ⁱⁱⁱ across all flow periods of channels on the right side and symmetrical channels on the left side, and (e) mean of scale at WCC_{max}ⁱⁱⁱ, a_{max}^{ii} , for each flow period across all channels.

+ denotes HbO₂ lagging MAP for WCC_{max}ⁱⁱⁱ > 0.5

- denotes HbO₂ leading MAP for WCC_{max}ⁱⁱⁱ > 0.5

● Statistically significant difference between flow period with highest WCC_{max}ⁱⁱⁱ at each channel and the all the rest flow periods at the same channel ($p < 0.05$)

★ Statistical significant difference between symmetrical channels on the right and on the left hemispheres ($p < 0.05$).

7.3.1.2 Weaning

The results of the wavelet cross-correlation, WCC, within the three scale bands for the one patient monitored during weaning are shown in figures 7.8 to 7.10. As mentioned in the methods section above, here we compare maximum wavelet cross correlation values between MAP and HbO₂ within the three scale bands pre- and post- clamping the arterial and venous cannulae. Pre- clamping the cannulae the patient is still on ECMO but at minimum flows and when both arterial and venous cannulae are clamped the patient is off ECMO and the patient's own heart and lungs are entirely responsible for blood circulation and oxygenation.

Figure 7.8 shows multichannel results for WCC_{max} for scale band a_i . The channel configuration is shown in 7.8a and X and Y in 7.8b indicate results pre- and post clamping the cannulae, respectively. The scales at which WCC_{max} occurs pre- and post- clamping and across the 12 channels are shown in 7.8c. High correlation between MAP and HbO₂ is observed prior to clamping the cannulae across all channels with HbO₂ leading MAP, as indicated by the – sign on the plots. Interestingly, the low values of WCC obtained after clamping the cannulae suggest no correlation between MAP and HbO₂ when the patient goes off ECMO.

Similar results are obtained for the scale band a_{ii} . Strong correlation between MAP and HbO₂ is shown prior to clamping across all channels with correlation decreasing post-clamping. However, in contrast to the results of scale band a_i , in this band HbO₂ is lagging MAP prior to clamping and for most channels post-clamping correlation values are greater than 0.5 indicating that MAP and HbO₂ are still correlated. A shift in a_{max} to higher scales upon clamping the cannula is shown across all channels (figure 7.8c).

In contrast to the results obtained for scale bands a_i and a_{ii} , WCC results for scale band a_{iii} show no correlation between MAP and HbO₂ prior to clamping while the correlation increases above 0.5 for most channels after clamping the cannulae.

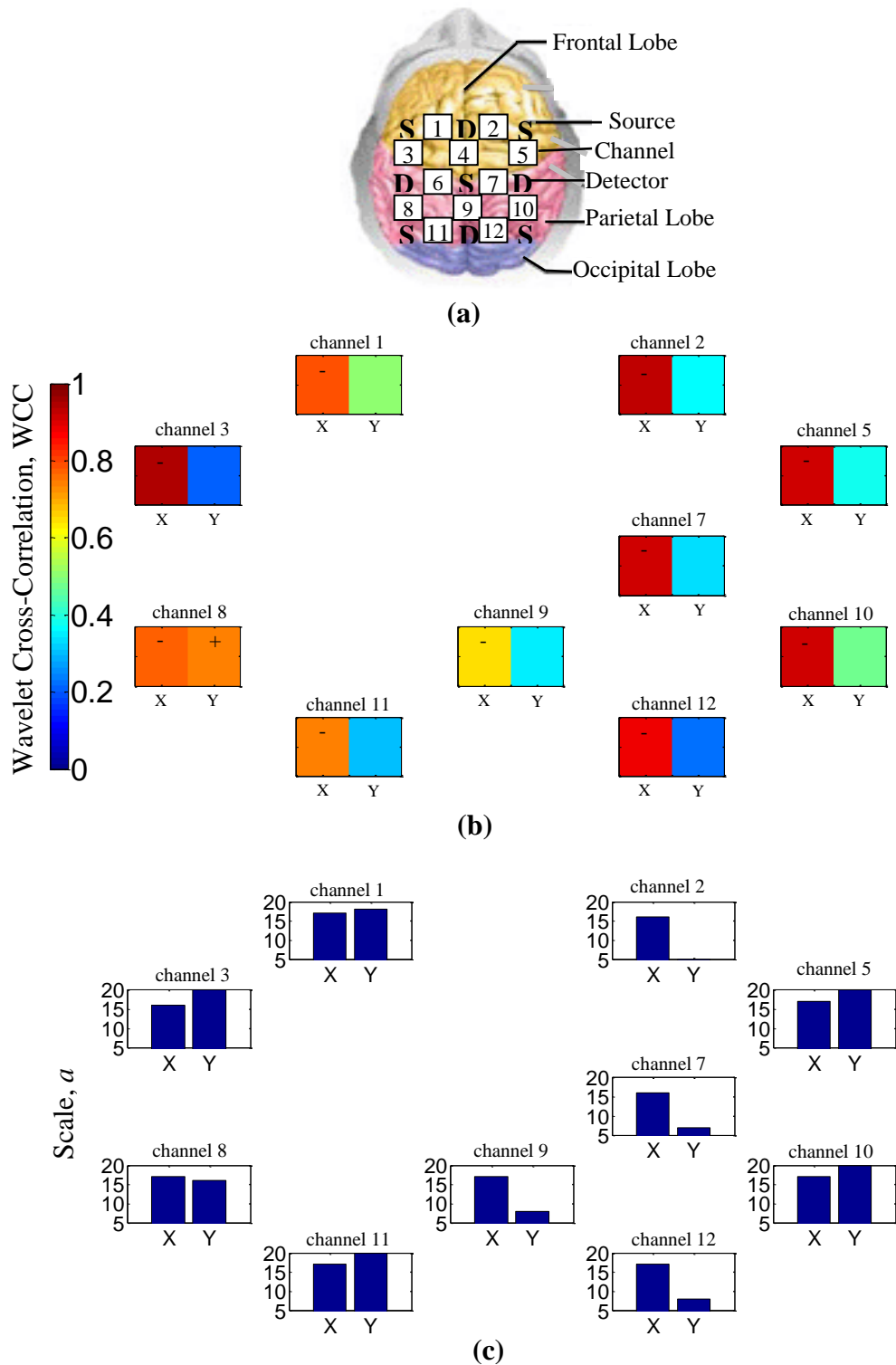


Figure 7.8: Wavelet cross-correlation between MAP and HbO₂ within scale band $a_i = 5 < a < 20$ ($f_{ai} = 0.25 \text{ Hz} < f_a < 1 \text{ Hz}$) for patient 9 during weaning (a) Channel arrangement, (b) WCC_{max}^i at pre-clamping the cannulae, X, and post-clamping the cannulae, Y, across all channels, (c) scale at WCC_{max}^i , a_{max}^i , pre- (X) and post- (Y) clamping across all channels.

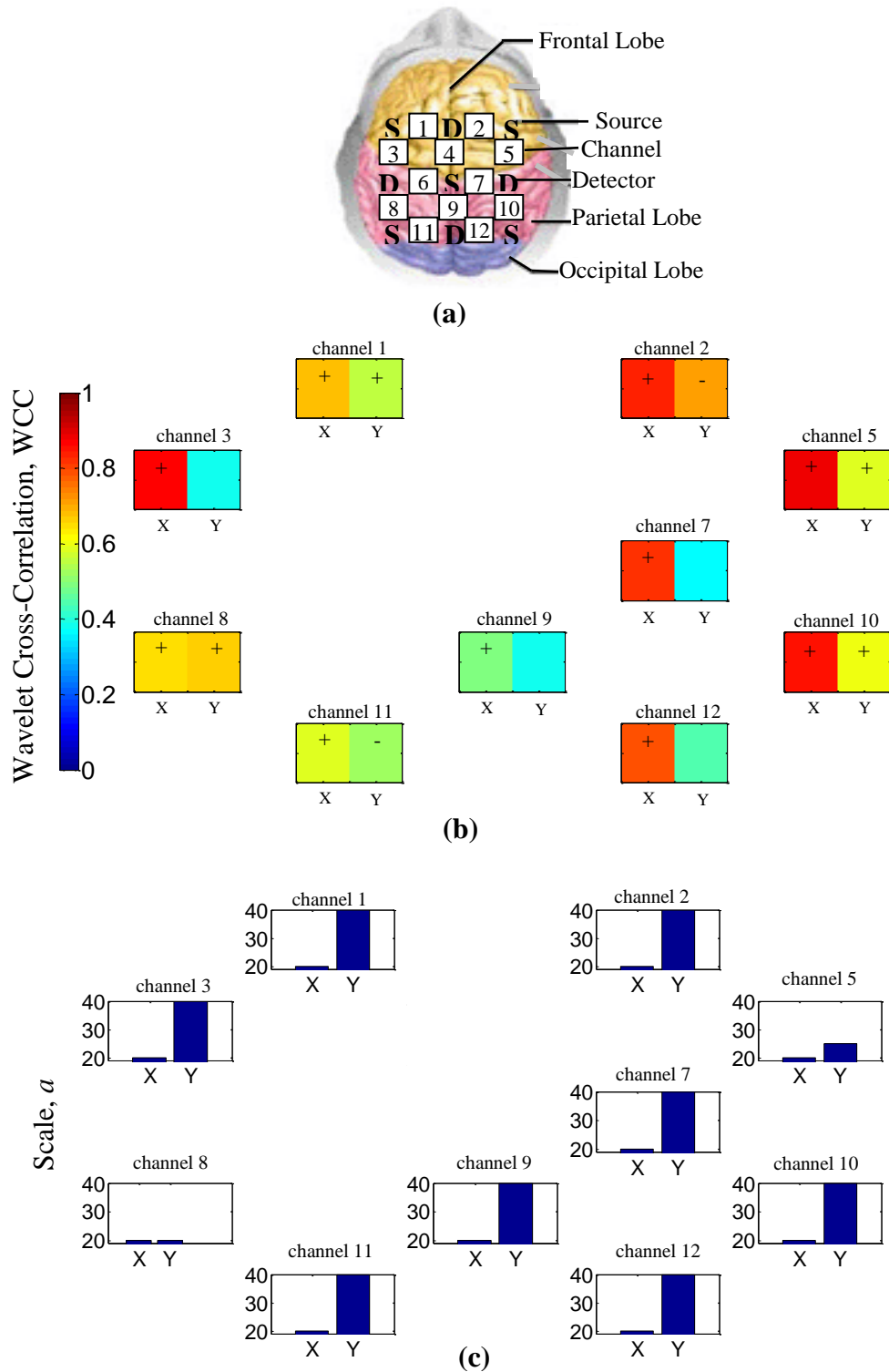


Figure 7.9: Wavelet cross-correlation between MAP and HbO₂ within scale band $a_{ii} = 20 < a < 40$ ($f_{a_{ii}} = 0.13 \text{ Hz} < f_a < 0.25 \text{ Hz}$) for patient 9 during weaning (a) Channel arrangement, (b) WCC_{max}^{ii} at pre-clamping the cannulae, X, and post-clamping the cannulae, Y, across all channels, (c) scale at WCC_{max}^{ii} , a_{max}^{ii} , pre- (X) and post- (Y) clamping across all channels.

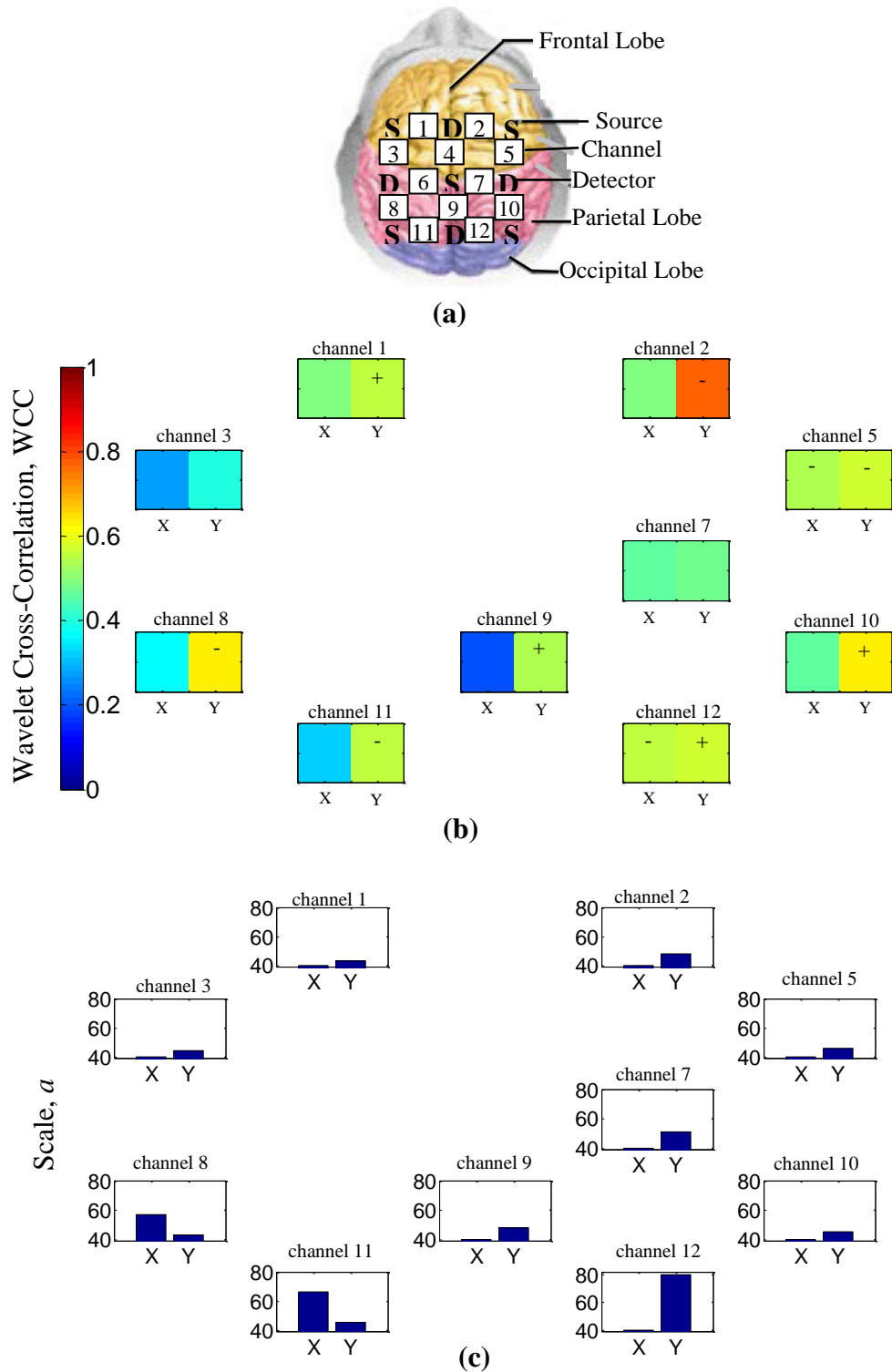


Figure 7.10: Wavelet cross-correlation between MAP and HbO₂ within scale band $a_{iii} = 40 < a < 80$ ($f_{a_{iii}} = 0.06 \text{ Hz} < f_a < 0.13 \text{ Hz}$) for patient 9 during weaning (a) Channel arrangement, (b) WCC_{max}^{iii} at pre-clamping the cannulae, X, and post-clamping the cannulae, Y, across all channels, (c) scale at WCC_{max}^{iii} , a_{max}^{iii} , pre- (X) and post- (Y) clamping across all channels.

7.3.2 Synchronisation index (γ)

7.3.2.1 Alteration in ECMO flows

Analogous to the wavelet cross-correlation analysis, the synchronisation index analysis showed three distinct peaks in scales around 14 (0.36 Hz) (RR), 30 (0.17 Hz) (VR) and 50 (0.1 Hz) (M-waves). The synchronisation index, γ , as function of scale at baseline and minimum flows for patients 8 and 7 are shown in figure 7.11. The three peaks corresponding to RR, VR and M-waves are clearly shown in the synchronisation index plot of patient 8, both at baseline and minimum flows (figure 7.11a). However, at baseline flow γ values are below 0.5 at the RR and M-wave peaks indicating weak synchronisation between MAP and HbO₂. At minimum flow the peaks become higher with an increase in γ value above 0.5 indicating strong synchronisation between MAP and HbO₂. The synchronisation index curve for patient 7 shows a broad but weak peak at a scale of 28 (0.18 Hz) on baseline flow (figure 7.11b). In this case, at minimum flow the peak becomes higher and is shifted to higher scales, spreading over to the Mayer-waves region.

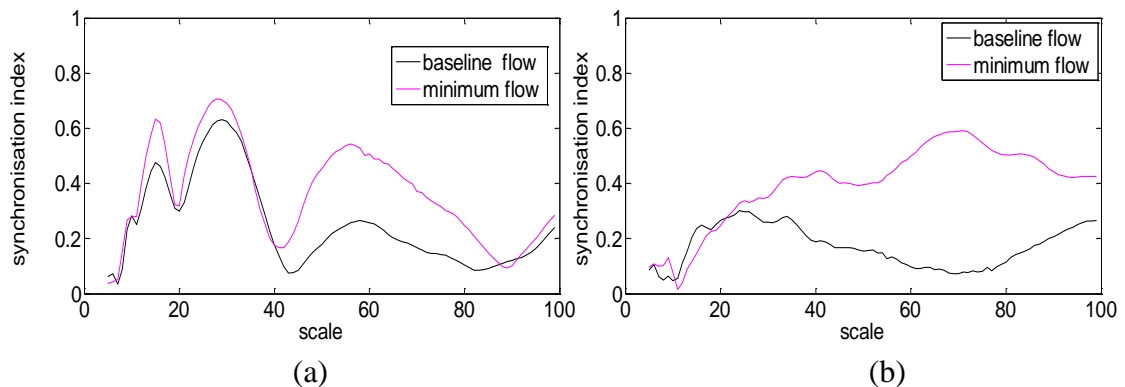


Figure 7.11: Synchronisation index, γ , as a function of scale at baseline and minimum flows for patient 8 (a) and patient 7 (b).

Group data for the maximum synchronisation index, γ_{\max}^i , within scale band a_i at each flow and across the 12 channels are shown in figure 7.12c. Statistical significant difference between the mean γ_{\max}^i across flow periods in the right and left hemispheres are observed (figure 7.12d). With the exception of channel 5, the

channels on the right hemisphere show higher γ values than the symmetrical channels in the left hemisphere. However, the synchronisation index, γ , appears to be greater than 0.5 only in channels 1, 2 and 3 (frontal lobe), and only when the flows are reduced to minimum (flow period D). In channels 1 and 2, which are symmetric, synchronisation continues to be strong when the flows are gradually increased back to baseline (flow periods E-G). The circular mean of the phase difference, $\Delta\Phi$, between the two signals is negative during these periods of high synchronisation suggesting that HbO₂ is leading MAP. The rest of the channels show weak synchronisation ($\gamma < 0.5$) across all flows. The group data of the scale at γ_{\max}^i , a_{\max}^i , across flow changes for all channels ranges from 10 to 16 (0.31 Hz to 0.5 Hz) (figure 7.12e). Similar to the wavelet cross-correlation analysis a shift in a_{\max}^i to lower scales at the highest γ_{\max}^i is observed.

For scale band a_{ii} the group data of the maximum synchronisation index, γ_{\max}^{ii} , across all events and for all channels are shown in figure 7.13c. Strong synchronisation between MAP and HbO₂ is shown only in channels 1, 2 and 5 at flow period E and channel 6 at flow period D. The circular mean of the phase difference was found to be positive in these flow periods indicating that HbO₂ is lagging MAP. Similar results were obtained for the group data of maximum synchronisation, γ_{\max}^{iii} , within the scale band a_{iii} with the difference that in this scale band channel 7 also appears to have high γ_{\max}^{iii} (> 0.5) at flow period E (figure 7.14).

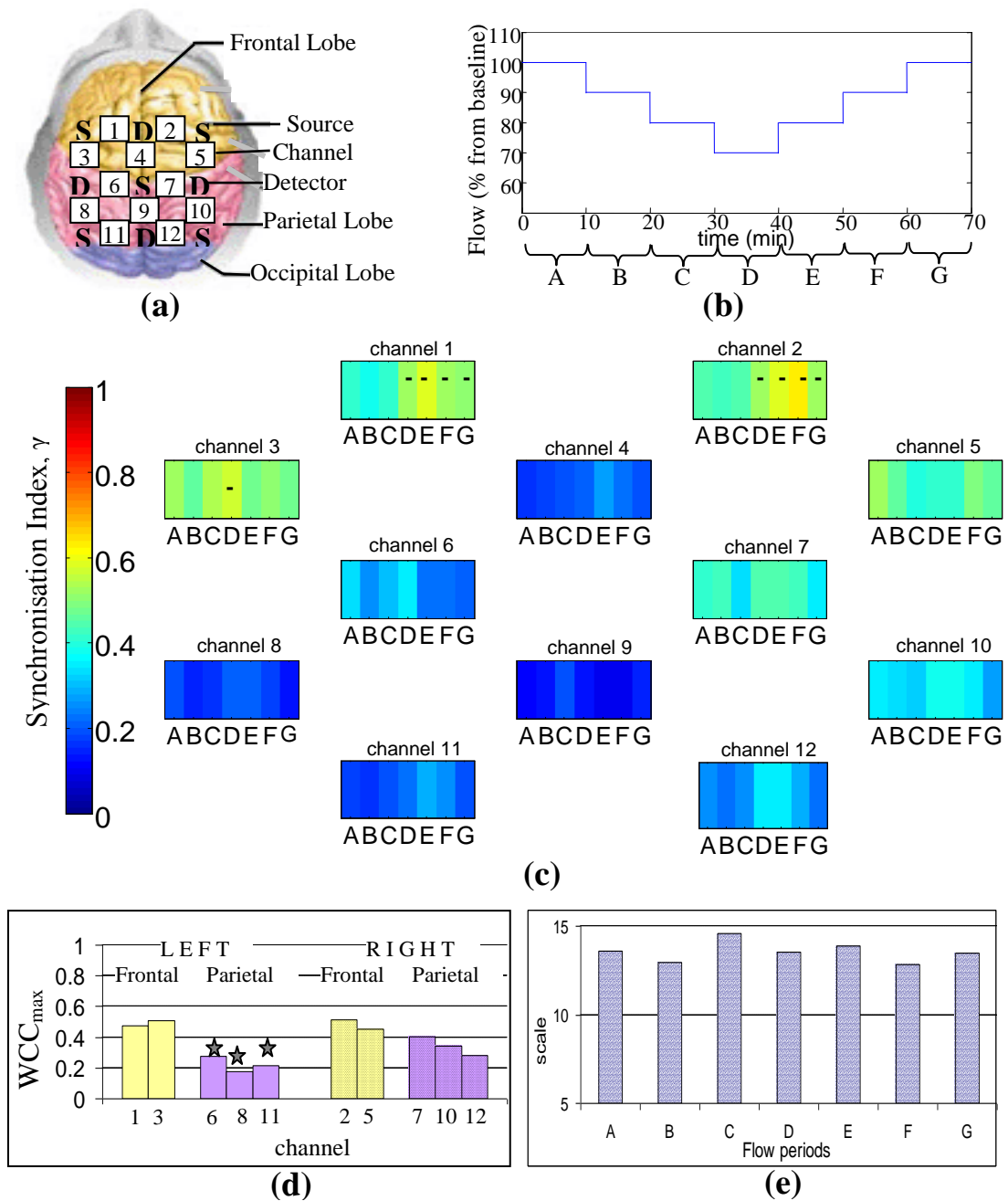


Figure 7.12: Group synchronisation index, γ , between MAP and HbO₂ within scale band $a_i = 5 < a < 20$ ($f_{ai} = 0.25 \text{ Hz} < f_a < 1.0 \text{ Hz}$): (a) Channel arrangement, (b) Flow changes sequence (A=100%, B=90%, C=80%, D=70%, E=80%, F=90%, G=100%), (c) γ_{max}^i at all flow periods across all channels and (d) mean of scale at γ_{max}^i , a_{max}^i , for each flow period across all channels.

+ denotes HbO₂ lagging MAP for $\gamma_{max}^i > 0.5$

- denotes HbO₂ leading MAP for $\gamma_{max}^i > 0.5$

⊙ Statistically significant difference between flow period with highest γ_{max}^i at each channel and the all the rest flow periods at the same channel ($p < 0.05$)

★ Statistical significant difference between mean γ_{max}^i across all flow periods of channels on the right side and symmetrical channels on the left side ($p < 0.05$).

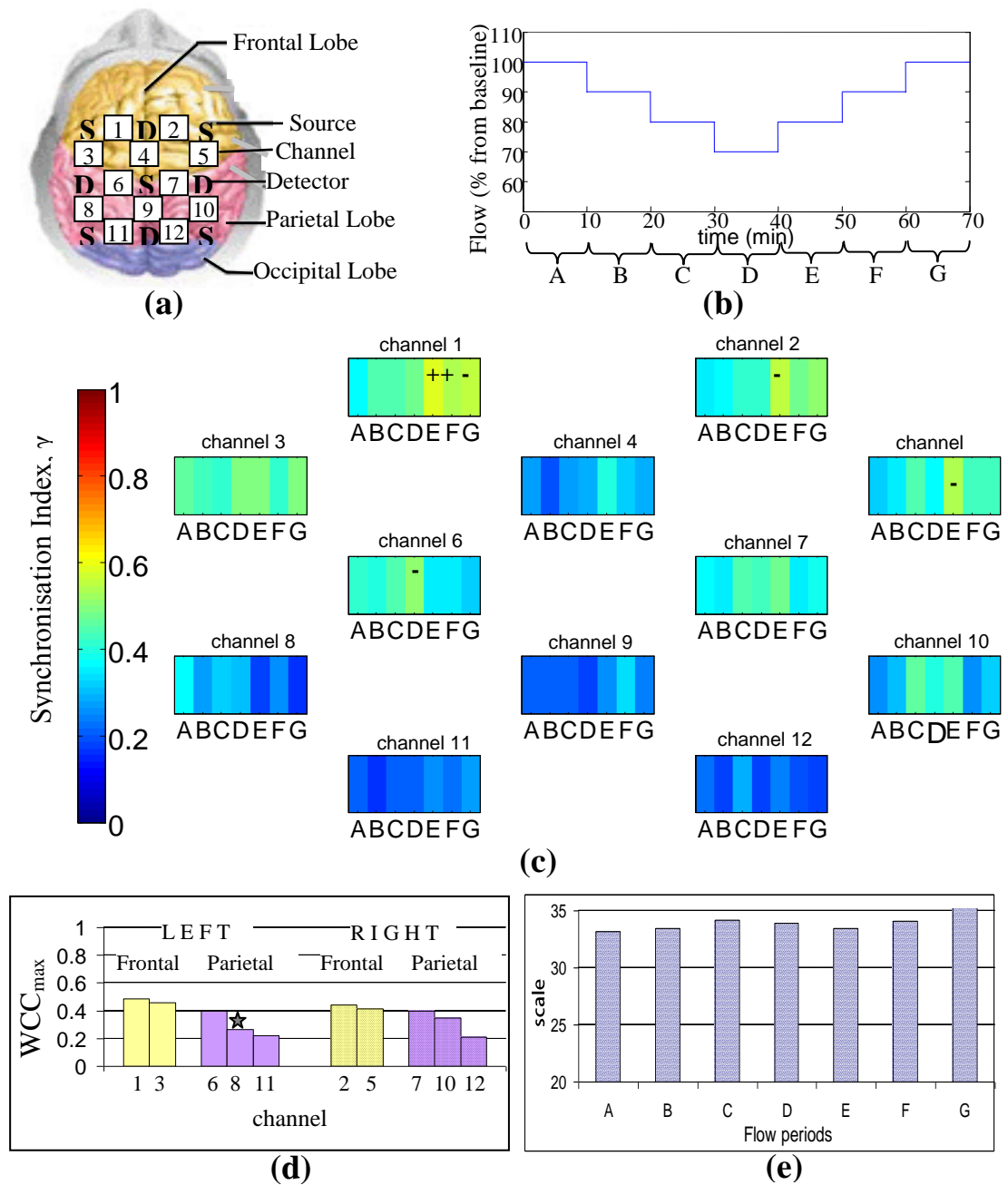


Figure 7.13: Group synchronisation index, γ , between MAP and HbO_2 within scale band $a_{ii} = 20 < a < 40$ ($f_{ai} = 0.13 \text{ Hz} < f_a < 0.25 \text{ Hz}$): (a) Channel arrangement, (b) Flow changes sequence (A=100%, B=90%, C=80%, D=70%, E=80%, F=90%, G=100%), (c) γ_{max}^{ii} at all flow periods across all channels and (d) mean of scale at γ_{max}^{ii} , a_{max}^{ii} , for each flow period across all channels.

+ denotes HbO_2 lagging MAP for $\gamma_{max}^{ii} > 0.5$

- denotes HbO_2 leading MAP for $\gamma_{max}^{ii} > 0.5$

⦿ Statistically significant difference between flow period with highest γ_{max}^{ii} at each channel and the all the rest flow periods at the same channel ($p < 0.05$)

★ Statistical significant difference between mean γ_{max}^{ii} across all flow periods of channels on the right side and symmetrical channels on the left side ($p < 0.05$).

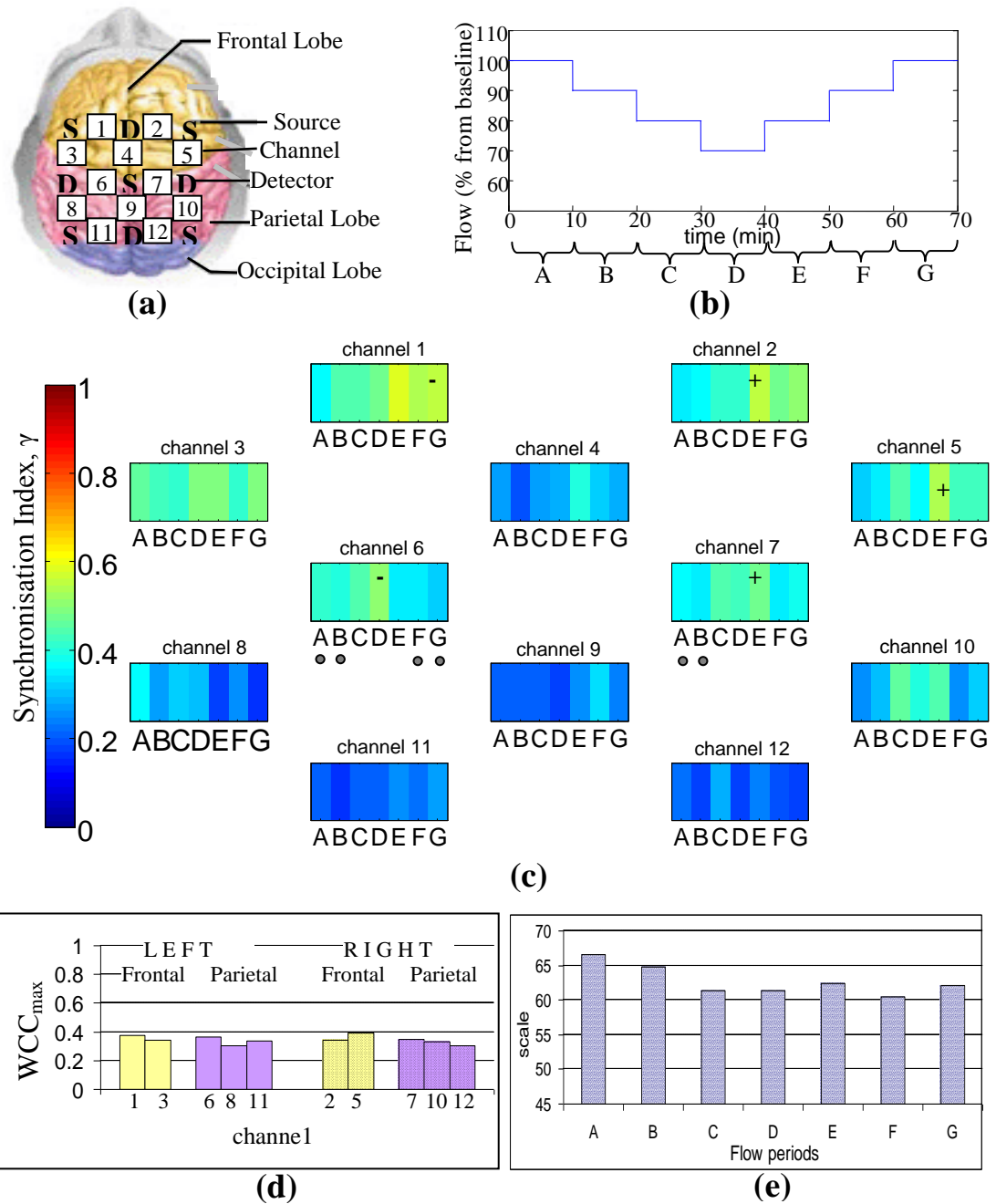


Figure 7.14: Group synchronisation index, γ , between MAP and HbO₂ within scale band $a_{iii} = 40 < a < 80$ ($f_{ai} = 0.06 \text{ Hz} < f_a < 0.13 \text{ Hz}$): (a) Channel arrangement, (b) Flow changes sequence (A=100%, B=90%, C=80%, D=70%, E=80%, F=90%, G=100%), (c) γ_{max}^{iii} at all flow periods across all channels and (d) mean of scale at γ_{max}^{iii} , a_{max}^{iii} , for each flow period across all channels.

+ denotes HbO₂ lagging MAP for $\gamma_{max}^{iii} > 0.5$

- denotes HbO₂ leading MAP for $\gamma_{max}^{iii} > 0.5$

● Statistically significant difference between flow period with highest γ_{max}^{iii} at each channel and the all the rest flow periods at the same channel ($p < 0.05$)

★ Statistical significant difference between mean γ_{max}^{iii} across all flow periods of channels on the right side and symmetrical channels on the left side ($p < 0.05$).

7.3.2.2 Weaning

The results of the synchronization index, γ , within the three scale bands for the patient monitored during weaning are shown in figures 7.15 to 7.17. The results for the synchronization index are similar to the ones obtained for the wavelet cross correlation.

Figure 7.15 shows multichannel results for γ_{\max} within scale band a_i . The channel configuration is shown in 7.15a and X and Y in 7.15b indicate results pre- and post clamping the cannulae, respectively. The scales at which WCC_{\max} occurs pre- and post- clamping and across the 12 channels are shown in 7.15c. High correlation between MAP and HbO₂ is observed prior to clamping the cannulae across all channels with HbO₂ leading MAP, as indicated by the – sign on the plots. Interestingly, the low values of WCC obtained after clamping the cannulae suggest no correlation between MAP and HbO₂ when the patient goes off ECMO.

Figure 7.16 shows the results for the synchronization index for the scale band a_{ii} . Strong correlation between MAP and HbO₂ is shown prior to clamping across all channels with correlation decreasing post-clamping. However, in contrast to the results of scale band a_i , in this band HbO₂ is lagging MAP prior to clamping and for most channels at post-clamping γ values are greater than 0.5 indicating that MAP and HbO₂ are still synchronized. A shift in a_{\max} to higher scales upon clamping the cannula is shown across all channels (figure 7.16c).

In contrast to the results obtained for scale bands a_i and a_{ii} , γ results for scale band a_{iii} show no synchronization between MAP and HbO₂ prior to clamping while the correlation increases above 0.5 for most channels after clamping the cannulae.

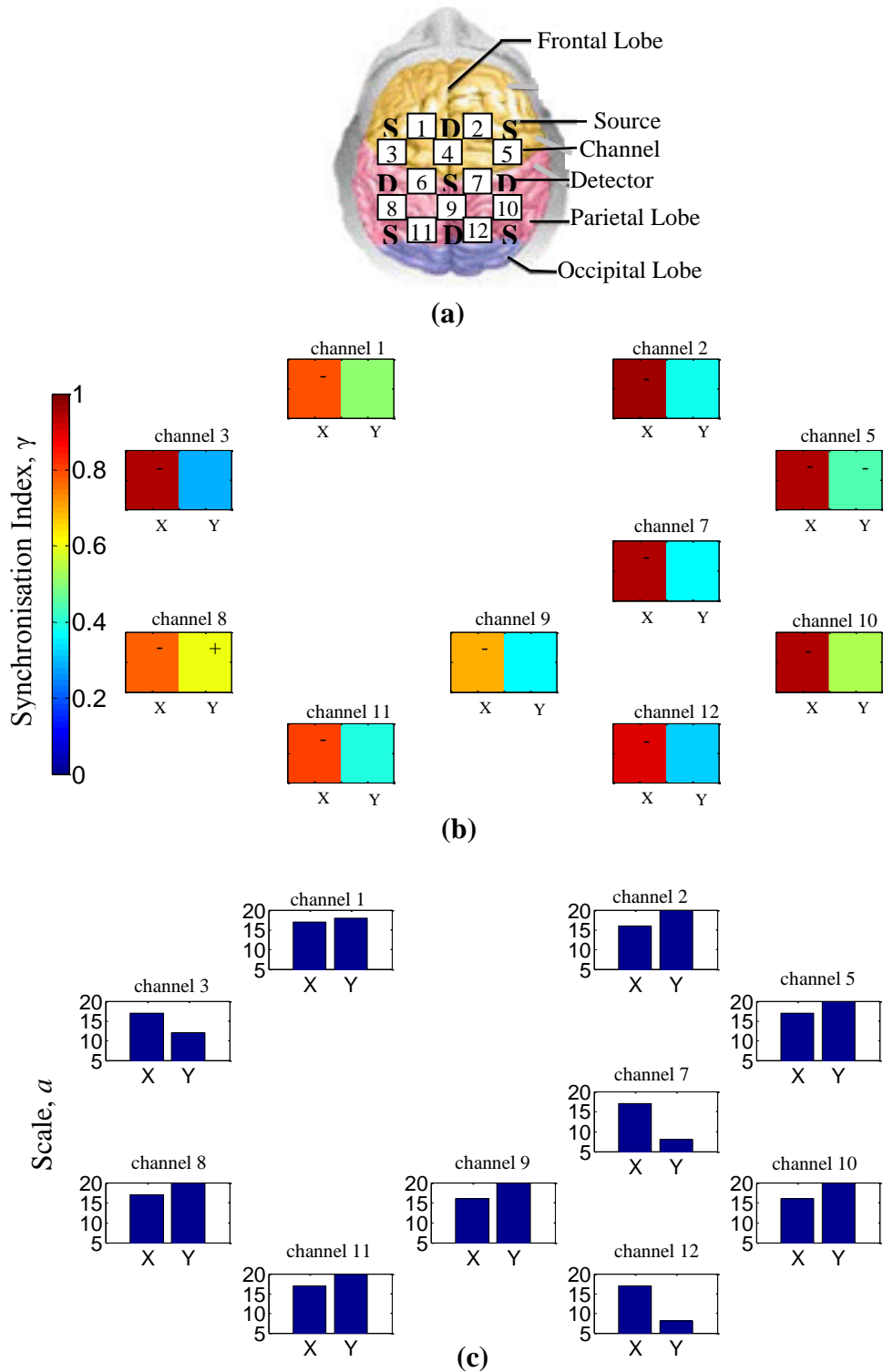


Figure 7.15: Synchronisation index between MAP and HbO_2 within scale band $a_i = 5 < a < 20$ ($f_{a_i} = 0.25 \text{ Hz} < f_a < 1 \text{ Hz}$) for patient 9 during weaning (a) Channel arrangement, (b) γ_{\max}^i at pre-clamping the cannulae, X, and post-clamping the cannulae, Y, across all channels, (c) scale at γ_{\max}^i , a_{\max}^i , pre- (X) and post- (Y) clamping across all channels.

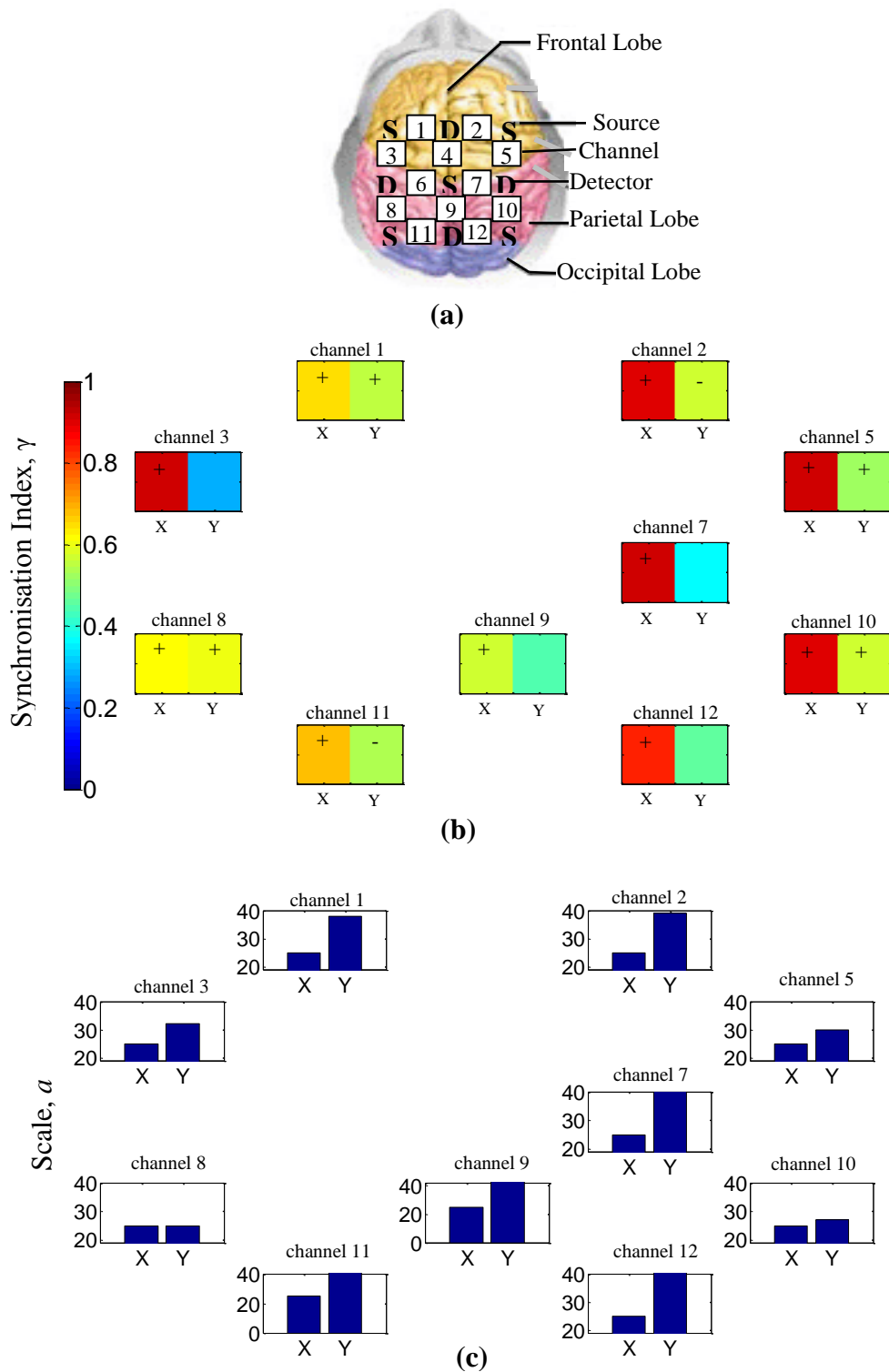


Figure 7.16: Synchronisation index between MAP and HbO₂ within scale band $a_{ii} = 20 < a < 40$ ($f_{ii} = 0.13 \text{ Hz} < f_a < 0.25 \text{ Hz}$) for patient 9 during weaning (a) Channel arrangement, (b) γ_{max}^{ii} at pre-clamping the cannulae, X, and post-clamping the cannulae, Y, across all channels, (c) scale at γ_{max}^{ii} , a_{max}^{ii} , pre- (X) and post- (Y) clamping across all channels.

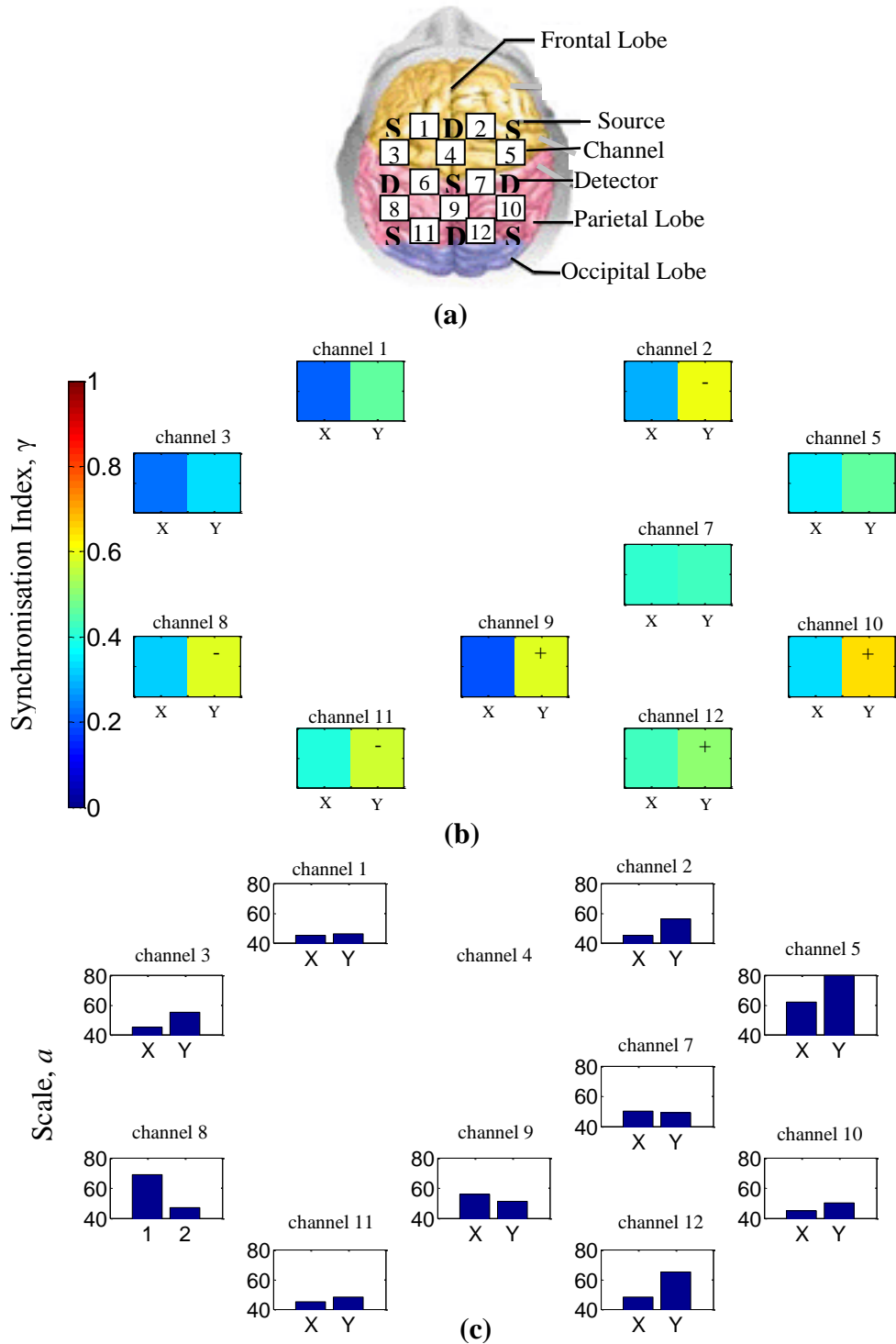


Figure 7.17: Synchronisation index between MAP and HbO₂ within scale band $a_{iii} = 40 < a < 80$ ($f_{iii} = 0.06 \text{ Hz} < f_a < 0.13 \text{ Hz}$) for patient 9 during weaning (a) Channel arrangement, (b) γ_{\max}^{iii} at pre-clamping the cannulae, X, and post-clamping the cannulae, Y, across all channels, (c) scale at γ_{\max}^{iii} , a_{\max}^{iii} , pre- (X) and post- (Y) clamping across all channels.

7.4 Discussion

Wavelet cross-correlation (WCC) between MAP and multisite cerebral HbO₂, across 12 channels, has been computed for 6 neonates supported on veno-arterial (VA) ECMO during sequential changes in the ECMO flow and one patient during weaning from ECMO. The wavelet cross-correlation (WCC) applied herein typically exhibits three peaks, the first at a scale corresponding to a frequency around 0.33Hz, the second at a frequency around 0.16 Hz and the third at a frequency around 0.1 Hz and could correspond respiration rate (RR), ventilation rate (VR) and Mayer-waves, respectively. Rowley et al. (2007) also applied WCC between MAP and HbO₂ in adult patients suffering from autonomic failure and age-matched controls and report peaks in WCC around 0.33 Hz and 0.1 Hz which they relate to respiration and M-waves, respectively. These findings are also in agreement with Latka et al (2005) where synchronisation index was obtained for healthy adult volunteers. Even though, these studies do not report a frequency around 0.16 Hz, in another study Latka et al (2007) used synchronisation index on adult patients with brain injuries and reported high variability of arterial blood pressure around 0.2 Hz as a direct consequence of mechanical ventilation.

The maximum wavelet cross-correlation, WCC_{max} , within three scale bands around the three frequency peaks were obtained for each ECMO flow period and each channel. Group data showed that WCC_{max} appears to be increasing with decreasing ECMO flow and peaks during flow period E, i.e. when the flow is brought back to 80% of the baseline from minimum flow. Even though a decrease in WCC is observed after flow period E, WCC is still typically higher than the baseline flows. High WCC (>0.5 by convention) indicates that any changes in MAP are mirrored in blood flow, i.e. cerebral blood flow is pressure passive, suggesting that cerebral autoregulation maybe impaired. In two out of the six patients monitored during alteration in the ECMO flows a drop in SpO₂ in the order of 20% was observed at minimum flows. Interestingly, these two patients showed the highest values in WCC compared to the rest of the patients. Regional variations in WCC were observed between channels potentially placed in the right parietal lobe and left

parietal lobes with channels on the right exhibiting higher values of WCC. Outcome and follow up of neonates treated with ECMO have shown that ECMO survivors are likely to have medical and developmental issues after discharge and tend to be at high risk for learning and/or behavioural problems in childhood (Glass and Brown 2005). Attention, memory and learning are described as “higher executive brain functions” and are localised in specialised regions of the brain known as the “association cortex” where much more complex information processing is conducted. The association cortex is part of the parietal lobes (Martini 2009). Further work could elucidate whether there is a robust link between the regions of the brain where altered WCC were observed and those regions associated with long term neurodevelopmental deficit.

A shift in the scale of maximum correlation across flow periods was also observed indicating that cerebral circulation is indeed challenged by changes in ECMO flows.

The synchronisation index, γ , was also calculated and also showed the presence of three peaks in agreement with WCC. The maximum synchronisation index within the three scale bands as a function of flow period and channel has revealed similar results to WCC analysis. However, in general γ_{\max} values appear to be lower than WCC_{\max} values. Rowley et al (2007) also used both methods, WCC and γ , to investigate the correlation between MAP and HbO₂ in autonomic failure patients and age matched controls during posture changes. They also report lower values in γ compared to WCC for both for both groups and at all postures.

Another observation that can be made is that generally correlation was highest in scale band a_i (RR) and lowest in a_{iii} (M-waves). WCC allows us to determine the dependency of the time series, in this case MAP and HbO₂, on multiple time scales and consequently determine the multiscale nature of the underlying dynamics. Our results suggest that the dependence of the fluctuations in MAP and HbO₂ time series is manifested differently in different scales. It is apparent that the interplay of the fluctuations of MAP and HbO₂ for high frequencies is different from that in the low frequency part of the spectrum. The strong reactivity of cerebral vessels to carbon dioxide arterial content might underlie the respiratory origin of the peak in scale band a_i . The origin of the low frequency, non respiratory oscillation in blood pressure still

remains controversial. Current evidence suggests that the baroreflex mechanisms substantially contribute to oscillations in this frequency range.

Other studies use coherence and transfer function between MAP and HbD (where $HbD = HbO_2 - HHb$) as a NIRS parameter to assess cerebral autoregulation (Tsuji et al. 2000, Wong et al. 2008). However, HbO_2 was previously used by Rowley et al (2007) when applying wavelet cross-correlation in patients suffering from autonomic failure and age matched controls. In addition, the previous work on spectral analysis using Fourier transforms on patients supported on ECMO, described extensively in chapter 5, showed that oscillations in HbO_2 are stronger than in other NIRS parameters (Papademetriou et al 2010). The presence of slow spontaneous oscillations may be more significant in the oxyhaemoglobin signal measured by NIRS than in the deoxyhaemoglobin or total haemoglobin signal (Elwell et al 1999; Orbig et al). It will be interesting however, to apply the method to other NIRS parameters and compare the results between them.

Wavelet cross-correlation (WCC) decomposes the MAP and HbO_2 signals into wavelet modes which are highly localised in frequency and allows investigation of which modes are most likely linearly related (Rowley 2007). Unlike other methods based on Fourier transforms, i. e. transfer function and coherence, WCC makes no assumption about the stationarity of the relationship between time series, and if other modes of oscillation in cerebral haemodynamics exist which are not driven by systemic variables these will show a low value of wavelet cross correlation. The Fourier transform of the signal yields a function that depends only on frequency, whereas the wavelet transform of that signal depends on both frequency and time. This distinction becomes important since the relation between MAP and HbO_2 signals is a non-stationary stochastic process, in which case the frequency spectrum of the signals changes over time. This time change is ill defined for a Fourier spectrum, but is well defined for a wavelet spectrum. Another important difference between the wavelet transforms and Fourier transforms is frequency resolution. The frequency resolution of a power density spectrum depends on the length of the sliding window in which the fast Fourier transforms (FFT) are applied (see chapter 6). The greater the length of the sliding window (higher number of samples) the higher the resolution but at the expense of lower signal to noise ratio (S/N). Consequently, the

length of the sliding window depends on the length and sampling frequency of the signal, i.e. number of sampling points. As a result a high sampling frequency and a long signal are required to resolve frequencies in the lower range which are of interest when studying cerebral autoregulation. Even if the frequency resolution is high enough it can still be difficult to capture frequencies in the lower range due to low S/N. In contrast to the Fourier transform, the Wavelet transform depends on scale which is inversely related to frequency. Consequently, there is a higher resolution at lower frequencies. Furthermore, wavelet cross-correlation is a measure of the level of similarity between two signals in a given frequency band and does not depend upon the power of those signals provided that the time series are compared for a sufficiently long time interval.

7.5 Conclusions

WCC between HbO₂ and MAP provides a useful method to investigate the dynamics of global and/or regional cerebral autoregulation. Cerebral autoregulation on ECMO is poorly studied, the most common reason being that there have been no easy non-invasive methods to study and interpret complex cerebral physiological process such as cerebral autoregulation. There are potential challenges to global and regional cerebral autoregulation whilst supported on ECMO starting from the time of cannulation when the great vessels (artery and vein) on the right side of neck are ligated for cannulation. Multichannel Near infrared spectroscopy (NIRS) offers the advantage of a continuous, non-invasive monitoring of regional cerebral oxyhaemoglobin concentration (HbO₂). The analysis presented in this chapter showed a relationship between WCC and ECMO flow in the grouped data of 6 patients. These differences were statistically significant between right and left hemispheres, especially when the flows were weaned sequentially by 10 and 20% of the baseline. Further more studies are necessary to elucidate this relationship and to understand regional differences in cerebral autoregulation during different clinical states on ECMO.

Chapter 8

CONCLUSIONS AND FURTHER WORK

8.1 Introduction

Infants and children placed on extracorporeal membrane oxygenation (ECMO) for cardiorespiratory failure are at risk of developing neurological injuries. The causes are multifactorial and are not yet fully understood. They can be associated both to pre-ECMO events and to the ECMO procedure itself. Most ECMO candidates suffer from hypoxemia, acidosis, hypercarbia and hypotension (Bulas & Glass 2005). Hypotension before or during ECMO may result in cerebral ischemia. Diminished pulsatility and blood pressure fluctuations affect cerebral blood flow. All these physiological changes can disrupt cerebral autoregulation leaving the cerebral microcirculation vulnerable to alterations in systemic blood pressure (Barlett 2006). Ligation of the major vessels in the neck-right common carotid artery and internal jugular vein-may cause lateralising cerebrovascular injuries.

The understanding of the origin and early detection of neurological dysfunction in this group of patients is highly significant. Near infrared spectroscopy offers a non-invasive, continuous real-time measurement of cerebral oxygenation. To date, there are only a few studies reporting of the use of this technology in this patient population. Moreover, all studies use commercially available single or dual channel NIRS systems and report only on absolute changes in haemoglobin concentrations or tissue oxygen saturation mainly during vessel ligation and induction of ECMO.

The work presented in this thesis describes the successful development and effective use of a multichannel NIRS system to monitor multisite cerebral oxygenation in patients supported on ECMO. Wavelet cross-correlation was generated as a novel method of analysis to investigate regional variations in cerebral oxygenation and assess cerebral autoregulation. The results of the work reported herein indicate that wavelet cross-correlation applied on multichannel NIRS can be used to investigate the dynamics of cerebral autoregulation during ECMO which may potentially have an important bearing on clinical outcome.

8.2 Summary and Concluding work on this thesis

The protocol was designed by the clinical team of the neonatal intensive care unit (NICU) in Great Ormond Street Hospital (GOSH) and included the use of NIRS to monitor all VA and VV ECMO candidates during routine ECMO procedures such as cannulation, weaning and decannulation and during interventions such as alterations in ECMO flows, CO₂ challenge and temperature challenge. ECMO candidates are critically ill and in fact the ECMO support is used as their last resort. While on ECMO these patients require intense bedside management with two specifically trained nurses per bed. Obtaining ethics approval was not trivial and also, obtaining parental consent was particularly challenging.

In the first instance, the intention was to investigate the feasibility of establishing this type of protocol. Hence, initially, a well clinically established NIRS instrument, the dual-channel NIRO-200, was used to obtain a series of pilot data. Even though the aim was to follow the complete protocol with every patient this was not

achievable in practice. The temperature and CO₂ challenges were attempted only once, on different patients. Due to the complex physiology of the ECMO circuit it was particularly difficult to induce changes in both these parameters and these two interventions were excluded from the protocol. In addition, being the last on the list to be informed and the last on the list to have access on the unit, it was difficult to be available for non scheduled acute procedures such as cannulation, weaning and decannulation. Furthermore, it was particularly difficult to single handle monitoring in such a busy intense environment.

The protocol also included multimodal data collection simultaneously with NIRS parameters which included systemic parameters (arterial pressure [ABP], central venous pressure [CVP], arterial saturation [SpO₂], end-tidal CO₂, heart rate [HR] and respiration rate [RR]) and ECMO parameters (venous saturation [SvO₂], arterial saturation measured at the arterial cannula [SaO₂], hematocrit and ECMO flow). The integration of the optical systems with established monitoring was not straight forward. The instrumentation used, especially the multichannel system, was not optimised for this setting and significant part of the work was spent in creating an environment where these measurements could be feasible.

The initial stage of the project involved the use of a dual-channel NIRS system (NIRO-200, Hamamatsu, Japan) to monitor cerebral and peripheral (calf muscle) tissue oxygenation. A total of 8 patients were monitored using the dual channel system. This was a rather inhomogeneous sample, consisting of patients supported on both VA and VV ECMO, operating either on centrifugal or roller pumps and with a wide age range (from 1 day to 5 years). Varying baseline levels of oxygenation (tissue oxygenation index) were observed between individual patients. In addition, variability in the trends of other NIRS parameters (HbO₂, HHb and HbT) were also observed. The small sample size in combination with the diverse population studied made it impractical to formulate group observations by investigating trends or absolute changes in NIRS parameters.

However, this pilot data from the dual channel system were used to investigate spectral analysis tools, using Fourier transforms, reported widely in the literature (De Smet et al 2009, Tachtsidis et al 2004, Tsuji et al 2000, Wong et al 2008). Power spectral density was used to investigate the presence of oscillations in cerebral and

peripheral circulations. PSD plots were obtained for the brain and leg data during changes in the ECMO flows and revealed the presence of oscillations in four frequency bands - (very low (VLF) 0.002-0.25 Hz, low (LF) 0.25-0.5 Hz, high (HF) 0.5-1 Hz and very high (VHF) 1-3 Hz). Oscillations within each of these frequency bands could correspond to skin vasomotion, respiratory rate, mechanical oscillation related to the roller ECMO pump and heart rate, respectively (Papademetriou et al. 2010). Coherence analysis was used to investigate the concordance between NIRS parameters and MAP as a means of assessing cerebral autoregulation. The intersubject variability found in the measurements of power spectra made it hard to obtain a direct comparison between the two measurement sites. In addition, analysis methods using Fourier transforms require high sampling frequency and a long signal in order to resolve frequencies in the lower range. Increasing the frequency resolution in both power spectra and coherence resulted in low signal-to-noise ratio making it difficult to obtain peaks in the frequency range of interest. Furthermore, the Fourier transform of the signal yields a function that depends only on frequency. This distinction becomes important since the relation between MAP and NIRS parameters (or CBF surrogates) is a non-stationary stochastic process, in which case the frequency spectrum of the signals changes over time. The coherence analysis suffers from the big drawback of averaging out all the potential useful time information, hence treating cerebral autoragulation as a stationary, linear process.

In assessing the role of NIRS monitoring, it is important to emphasize its unique qualities, including non-invasive, continuous real-time measurement of regional tissue oxygen saturation. However, caution must be exercised in extrapolating regional measurements to global findings. For example, alterations in regional oxygen saturation may reflect local changes and not necessarily indicate global hypoperfusion. The fact that only regional information in cerebral oxygenation can be obtained from the current commercial NIRS in clinical use is considered a major limitation by a number of review papers (Andropoulos et al. 2004b, Hirsch et al. 2010, Su & Undar 2010).

A multichannel NIRS system (Optical Topography, ETG-100, Hitachi Medical Ltd., Japan) was developed for clinical use. The specific instrument was designed for functional activation studies in adults. Adapting the instrument and software of the

system for use in a paediatric intensive care environment was not an easy task. Designing and constructing the multichannel neonatal cap was one of the biggest challenges of the project. Testing the cap in patients where access is restricted by the surgically positioned cannulae was particularly complex. Individual specific approach was required in these vulnerable patients in whom even a small head movement can be catastrophic. A novel flexible neonatal cap was designed and constructed to house a 3 x 3 array of sources and detectors (interoptode distance = 30 mm). This configuration allowed HbO₂, HHb and HbT concentrations to be collected from a total of 12 channels. The desirable fitting of the cap was achieved by the use of dummy heads obtained from informed MRI scans of real patients. A major limitation of this system was the fact that the intensity of the laser sources could not be controlled automatically as a result data were lost from patients with thick hair or too transparent.

Some general observations could be made for the 6 patients monitored during alterations in the ECMO flows. Significant changes in systemic oxygenation parameters and cerebral haemoglobin concentrations in response to changes in ECMO flows were observed. A major drop in SvO₂ (~20%) could be associated with a considerable increase in HHb and a moderate change in HbO₂ across all channels. Even though the trends in the NIRS haemoglobin concentration parameters might indicate variations in regional cerebral oxygenation, it was practically impossible to address them by simply relying on the absolute changes in the signals.

A novel method of analysis was generated to investigate regional variations in cerebral oxygenation and potentially assess cerebral autoregulation. Wavelet cross-correlation (WCC) between MAP and multisite cerebral HbO₂, across 12 channels, was computed for 6 neonates supported on veno-arterial (VA) ECMO during sequential changes in the ECMO flow. The wavelet cross-correlation (WCC) analysis showed the existence of three peaks, the first at a scale corresponding to a frequency around 0.33Hz, the second at a frequency around 0.16 Hz and the third at a frequency around 0.1 Hz which could correspond to respiration rate (RR), ventilation rate (VR) and Mayer-waves, respectively. The maximum wavelet cross-correlation, WCC_{max}, within three scale bands around the three frequency peaks were obtained for each ECMO flow period and each channel. Group data showed that

WCC_{max} appears to be increasing with decreasing ECMO flow. High WCC (>0.5 by convention) indicates that any changes in MAP are mirrored in blood flow, i.e. cerebral blood flow is pressure passive, suggesting that cerebral autoregulation may be impaired. Regional variations in WCC were observed between channels potentially placed in the right parietal lobe and left parietal lobes with channels on the right exhibiting higher values of WCC. Outcome and follow up of neonates treated with ECMO have shown that ECMO survivors are likely to have medical and developmental issues after discharge and tend to be at high risk for learning and/or behavioural problems in childhood (Glass & Brown 2005). Attention, memory and learning are described as “higher executive brain functions” and are localised in specialised regions of the brain known as the “association cortex” where much more complex information processing is conducted. The association cortex is part of the parietal lobes (Martini 2009). Further work could elucidate whether there is a robust link between the regions of the brain where altered WCC were observed and those regions associated with long term neurodevelopmental deficit.

8.3 Further work

The work presented in this thesis describes the successful development of a novel multichannel NIRS and multimodal protocol for providing regional measures of cerebral oxygenation and haemodynamics in intensive care units with the specific application in neonatal and paediatric patients supported on ECMO. Following the full clinical protocol, as designed originally, for each patient could potentially help to identify the causes of cerebrovascular injuries in this group of patients. It is worth considering monitoring these patients when admitted to the intensive care unit prior to ECMO induction as well as monitoring when the patient is removed from ECMO while still in recovery. Research nurses or clinical research fellows need to be recruited for this purpose. The restricted monitoring period and the fact that the intensity of the laser sources of the current system cannot be varied via the system’s software are limitations that need to be considered when extending the project further.

ECMO in the cardiac intensive care unit could be a surrogate model similar to a patient undergoing cardiac surgery during cardiopulmonary bypass. Therefore, the developed multichannel NIRS protocol can be extended for use in cardiac theatres. High rates of ischemic brain injury are the modern challenge to the perioperative congenital heart team (Andropoulos et al. 2004b). In the current era of advanced paediatric cardiac surgery for the treatment of congenital heart defects there are serious limitations with inadequate neuromonitoring, misleading neuromonitoring, or both (Nollert et al. 1998).

The wavelet cross-correlation generated as part of this work is based on the use of the continuous wavelet transform. As a result, the developed MatLab codes take a long time to generate the results. In addition, WCC is a bivariate method of analysis and in this case cerebral circulation was only compared with fluctuations in the MAP. However, cerebral circulation is much complex (Panerai et al. 1999). It has been suggested that the relation between synchronously measured spontaneous slow waves of perfusion pressure and CBF is vulnerable to confounding influences such as CO₂ changes (Czosnyka et al. 2009). The recently developed Maximal Overlap Discrete Wavelet Packet transform has the ability to calculate multivariate systems instantaneously and can be used as a method to assess dynamical changes in cerebral autoregulation continuously by the bedside (Peng 2008).

Continuous monitoring seems to be important as autoregulation status may change dynamically. The work presented in this thesis describes the development and establishment of a non invasive neuromonitoring system which has the prospects to assess regional variations in cerebral oxygenation in neonates supported on ECMO continuously by the bedside. For such a system to be useful in a clinical environment a threshold in the WCC index needs to be established to differentiate between patients with impaired and intact autoregulation. Establishing a threshold for such an index of autoregulation would appear to hold predictive value with special regard to favourable outcome. Consequently, the main objectives of brain monitoring are guiding therapeutic interventions, the prediction of outcome and the detection of ongoing secondary brain injury following the primary insult. Ideally, brain monitoring should prompt a timely and appropriate intervention and should be included in scheduled management protocols.

Continuous monitoring seems to be important as autoregulation status may change dynamically. The work presented in this thesis describes the development and establishment of a non invasive neuromonitoring system which has the prospects to assess regional variations in cerebral autoregulation in neonates supported on ECMO continuously by the bedside. For such a system to be useful in a clinical environment a threshold in the WCC index needs to be established to differentiate between patients with impaired and intact autoregulation. Establishing a threshold for such an index of autoregulation would appear to hold predictive value with special regard to favourable outcome. Consequently, the main objectives of brain monitoring are guiding therapeutic interventions, the prediction of outcome and the detection of ongoing secondary brain injury following the primary insult. Further development to assign such a threshold in the WCC index might aid clinical management of patients supported on ECMO.

REFERENCES

- Adolph, V., Ekelund, C., Starret, A., Falterman, K., & Arensman, R. 1990. Developmental outcome of neonates treated with extracorporeal membrane oxygenation. *J Pediatr Surg*, 25, 43-46
- Al Rawi, P., Smielewski, P., & Kirkpatrick, P. 2001. Evaluation of a Near Infrared Spectrometer (NIRO 300) for the detection of intracranial oxygenation changes in the adult head. *Stroke*, 32, 2492-2500
- An, H. & Lin, W. 2002. Cerebral venous and arterial blood volumes can be estimated separately in humans using magnetic resonance imaging. *Magn Reson Med*, 48, 583-588
- Andropoulos, D., Diaz, L., Fraser, C.J., McKenzie, E., & Stayer, S. 2004a. Is bilateral monitoring of cerebral oxygen saturation necessary during aortic arch reconstruction? *Anesth Analg*, 98, 1267-1272
- Andropoulos, D., Stayer, S., Diaz, L., & Ramamoorthy, C. 2004b. Neurological monitoring for congenital heart surgery. *Anesth Analg*, 99, 1365-1375
- Andropoulos, D., Stayer, S., McKenzie, E., & Fraser, C.J. 2003a. Novel cerebral physiologic monitoring to guide low flow cerebral perfusion during neonatal aortic arch reconstruction. *J Thorac Cardiovasc Surg*, 125, 491-499
- Andropoulos, D., Stayer, S., McKenzie, E., & Fraser, C.J. 2003b. Regional low flow perfusion provides comparable blood flow and oxygenation to both cerebral hemispheres during neonatal aortic arch reconstruction. *J Thorac Cardiovasc Surg*, 126, 1712-1717
- Arridge, S.R. 1995. Photo measurement density functions. Part I: Analytical forms. *Applied Optics*, 34, 7395-7409
- Arridge, S., Cope, M., & Delpy, D. 1992. The theoretical basis for the determination of optical pathlengths in tissue: temporal and frequency analysis. *Phys.Med.Biol.*, 37, 1531-1560
- Austin, E.e., Edmonds, H.J., Auden, S., Seremet, V., Niznik, G., & Sehic, A. 1997. Benefit of neurophysiologic monitoring for pediatric cardiac surgery. *J Thorac Cardiovasc Surg*, 114, 707-715
- Azokie, A., Muse, J., Gardner, M., Skidmore, K., Miller, S., & Karl, T. 2005. Cerebral oxygen balance is impaired in during repair of aortic contraction in infants and children. *J Thorac Cardiovasc Surg*, 130, 830-836
- Barlett, R. 2006, "Physiology of ECLS," *In Extracorporeal Cardiopulmonary Support in Critical Care*, K. Van Meurs et al., eds., pp. 5-27.

- Barlett, R., Gazzaniga, A., & Jefferies, M. 1976. Extracorporeal membrane oxygenation (ECMO) cardiopulmonary support in infancy. *Trans Am Soc Intern Organs*, 22, 80-93
- Bassan, H., Gauvreau, K., Newburger, J., Tsuji, M., Limperopoulos, C., & Soul, J. 2005. Identification of pressure passive perfusion and its mediators after infant cardiac surgery. *Pediatr Res*, 57, 35-41
- Beer, A. 1852. Bestimmung der Absorption des rothen Lichts in fabrigen Flussigkeiten. *Ann.Phys.Chem.*, 163, 78
- Bellinger, D.C., Wypij, D., DuPlessis, A.J., Rappaport, L.A., Jonas, R.A., Wernovsky, G., & Newburger, J.W. 2003. Neurodevelopmental status at eight years in children with dextro-transposition of the great arteries: The Boston Circulatory Arrest Trial. *Journal of Thoracic and Cardiovascular Surgery*, 126, 1385-1396
- Berens, R., Stuth, E., Robertson, F., Jaquiss, R., Hoffman, G., & Troshynski, T. 2006. Near infrared spectroscopy monitoring during pediatric aortic contraction repair. *Pediatr Anaesth*, 16, 777-781
- Brady, K., Joshi, B., Zweifel, C., Smielewski, P., Czosnyka, M., Easley, B., & Hogue, C.W.J. 2010a. Real-time continuous monitoring of cerebral blood flow autoregulation using near-infrared spectroscopy in patients undergoing cardiopulmonary bypass. *Stroke*, 41, 1951-1956
- Brady, K., Mytar, J.O., Lee, J.K., Cameron, D.E., Vricella, L.A., Thompson, W.R., Hogue, C.W.J., & Easley, B. 2010b. Monitoring cerebral blood flow pressure autoregulation in pediatric patients during cardiac surgery. *Stroke*, 41, 1957-1962
- Bulas, D. & Glass, P. 2005. Neonatal ECMO: Neuroimaging and neurodevelopmental outcome. *Semin Perinatol*, 29, 58-65
- Bulas, D., Glass, P., O'Donnell, R.M., Taylor, G.A., Short, B.L., & Veniza, G.L. 1995. Neonates treated with ECMO: Predictive value of early CT and US neuroimaging findings on short term neurodevelopmental outcome. *Radiology*, 195, 407-412
- Busija, D. W. 1993, "Cerebral Autoregulation," *In The regulation of cerebral blood flow*, J. Phillis, ed., Florida: CRC Press Inc., pp. 45-61.
- Busija, D.W. & Heistad, D.D. 1984. Factors involved in the physiological regulation of the cerebral circulation. *Reviews of Physiology Biochemistry and Pharmacology*, 101, 161-211
- Chakravarti, S., Srivastava, S., & Mittnacht, A. 2008. Near Infrared Spectroscopy (NIRS) in Children. *Semin Cardiothorac Anesth*, 12, 70-79
- Chakravarti, S.B., Mittnacht, A.J., Katz, J.C., Nguyen, K., Joashi, U., & Srivastava, S. 2009. Multisite near-infrared spectroscopy predicts elevated blood lactate level in children after cardiac surgery. *J Cardiothorac Vasc Anesth*, 23, (5) 663-667 available from: PM:19447648

- Chance, B., Zhuang, Z., UnAh, C., Alter, C., & Lipton, L. 1993. Cognition-activated low-frequency modulation of light absorption in human brain. *Proc.Natl.Acad.Sci.USA*, 90, 3770-3774
- Cheong, W., Pralh, S., & Welch, A. 1990. A review of the optical properties in biological tissues. *IEEE Journal of Quantum Electronics*, 26, 2166-2185
- Chow, G., Roberts, I., Edwards, A., Lloyd-Thomas, A., Wade, A., & Elliott, M. 1997a. The relation between pump flow rate and pulsatility on cerebral haemodynamics during paediatric cardiopulmonary bypass. *J Thorac Cardiovasc Surg*, 114, 568-577
- Chow, G., Roberts, I., Fallon, P., Onoe, M., Lloyd-Thomas, A., & Elliott, M. 1997b. The relation between arterial oxygen tension and cerebral blood flow during cardiopulmonary bypass. *European Journal of Cardio-thoracic surgery*, 11, 633-639
- Contini, D., Marteli, F., & Zaccanti, G. 1997. Photon migration through a turbid slab described by a model based on diffusion approximation I. *Theory Applied Optics*, 36, 4587-4599
- Cope, M. 1991. *The application of near-infrared spectroscopy to non-invasive monitoring of cerebral oxygenation in the newborn infant*. PhD (PhD Thesis). University College London.
- Czosnyka, M., Brady, K., Reinhard, M., Smielewski, P., & Steiner, L.A. 2009. Monitoring Cerebrovascular Autoregulation: Facts, Myths, and Missing links. *Neurocrit Care*, 10, 373-386
- Czosnyka, M. & Pickard, J.D. 2004. Monitoring and interpretation of intracranial pressure. *J Neurol Neurosurg Psychiatry*, 75, 813-821
- Czosnyka, M., Smielewski, P., Kirkpatrick, P., Laing, R.J., Menon, D., & Pickard, J.D. 1997. Continuous assessment of the cerebral vasomotor reactivity in head injury. *Neurosurgery* (41) 11-7
- Czosnyka, M., Smielewski, P., Laing, R.J., Menon, D., & Pickard, J.D. 1996. Monitoring of cerebral autoregulation in head-injured patients. *Stroke*, 27, 1829-1834
- Daubeney, P., Smith, D., Pilkington, S., Lamb, R., Monro, J., Tsang, V., Livesey, S., & Webber, S. 1998. Cerebral oxygenation during paediatric cardiac surgery: identification of vulnerable periods using near infrared spectroscopy. *European Journal of Cardio-thoracic surgery*, 13, 370-377
- De Smet, D., Vanderhaegen, J., Naulaers, G., & Van Huffel, S. 2009. New measurements for assessment of impaired cerebral autoregulation using Near Infrared Spectroscopy. *Adv Exp Med Biol*, 645, (273) 278
- Delpy, D. & Cope, M. 1997. Quantification in tissue near-infrared spectroscopy. *Philosophical transactions of the Royal Society of London Series B-Biological Sciences*, 352, 649-659

- Delpy, D., Cope, M., Van der Zee, Z., Arridge, S., Wray, S., & Wyatt, J. 1988. Estimation of optical pathlength through tissue from direct time of flight measurement. *Phys.Med.Biol.*, 33, 1433-1442
- Dent, C., Spaeth, J., Jones, B., Schwartz, S., Glayser, T., & Hallinan, B. 2006. Brain magnetic resonance abnormalities after the Norwood procedure using regional cerebral perfusion. *J Thorac Cardiovasc Surg*, 131, 190-197
- du Plessis, A., Newburger, J., Jonas, R., Hickey, P., Naruse, H., & Tsuji, M. 1995. Cerebral oxygen supply and utilisation during infant cardiac surgery. *Ann Neurol*, 37, 488-497
- Duncan, A., Meek, J.H., Clemence, M., Elwell, C.E., Tyszczuk, L., Cope, M., & Delpy, D.T. 1995. Optical pathlength measurements on adult head, calf, and forearm and the head of the newborn infant using phase resolved optical spectroscopy. *Phys Med Biol*, 40, 295-304
- Duncan, A., Whitlock, T., Cope, M., & Delpy, D. 1993. A multiwavelength, wideband, intensity modulated optical spectrometer for near infrared spectroscopy and imaging. *Proceedings of SPIE* (1888) 248-259
- Edvinsson, L. 1993, "Autoregulation: Arterial and intracranial pressure," *In Cerebral blood flow and metabolism*.
- Ejike, J., Schenkman, K., Seidel, K., Ramamoorthy, C., & Roberts, J. 2006. Cerebral oxygenation in neonatal and pediatric patients during veno-arterial extracorporeal life support. *Pediatr Crit Care Med*, 7, 154-158
- Elwell, C. 1995. *A practical users guide to Near infrared Spectroscopy* London, Hamamatsu Photonics.
- Elwell, C., Springett, R., Hillman, E., & Delpy, D. 1999. Oscillations in cerebral haemodynamics. Implications for functional activation studies. *Adv.Exp.Med.Biol.*, 471, 57-65
- Everdell, N.L., Gibson, A.P., Tullis, I.D.C., Vaithianathan, T., Hebden, J.C., & Delpy, D.T. 2005. A frequency multiplex near infrared optical topography system for imaging functional activation in the brain. *Rev Scient Instr*, 76, 093705
- Fallon, P., Roberts, I., Kirkham, F., Edwards, A., Lloyd-Thomas, A., & Elliott, M. 1994. Cerebral blood volume response to changes in carbon dioxide tension before and during cardiopulmonary bypass in children, investigated by near infrared spectroscopy. *European Journal of Cardio-thoracic surgery*, 8, 130-134
- Fallon, P., Roberts, I., Kirkham, F., Elliott, M., Lloyd-Thomas, A., & Maynard, R. 1993. Cerebral haemodynamics during cardiopulmonary in children using near infrared spectroscopy. *Ann Thorac Surg*, 56, 1473-1477
- Fenik, J. & Rais-Bahrami, K. 2009. Neonatal cerebral oximetry monitoring during ECMO cannulation. *J Perinatol*, 29, 376-381

- Fenton, K., Lessman, K., Glogowski, K., Fogg, S., & Duncan, K. 2007. Cerebral oxygen saturation does not normalise until after stage 2 single ventricle palliation. *Ann Thorac Surg*, 83, 1431-1436
- Ferrari, M., Mottola, L., & Quaresima, V. 2004. Principles, techniques and limitations of near infrared spectroscopy. *Can J Appl Physiol*, 29, 463-487
- Fisher, N.I. 1995. *Statistical analysis of circular data* Cambridge, Cambridge University Press.
- Franceschini, M. & Boas, D. 2004. Noninvasive measurement of neuronal activity with near-infrared optical imaging. *Neuroimaging*, 21, 372-386
- Franceschini, M., Joseph, D.K., Huppert, T.J., Diamond, S.J., & Boas, D.A. 2006. Diffuse optical imaging of the whole head. *Journal of Biomedical Optics*, 11, 054007
- Gannon, C., Kornhauser, M., Gross, G., Wiswell, T., Baumgart, S., Streletz, L., Graziani, L., & Spitzer, A. 2001. When combined early bedside head ultrasound and electroencephalography predict abnormal computerised tomography or magnetic resonance brain images obtained after extracorporeal membrane oxygenation treatment. *J Perinatol*, 21, 451-455
- Giacomuzzi, C., Heller, E., Mejak, B., You, J., Ungerleider, R., & Silberbach, M. 2005. Assessing the brain using near infrared spectroscopy during postoperative ventricular circulatory support. *Cardiol Young*, 15, 154-158
- Giller, C.A. & Mueller, M. 2003. Linearity and non-linearity in cerebral haemodynamics. *Med Eng Phys*, 25, 633-646
- Glass, P. & Brown, J. 2005, "Outcome and Follow-up of Neonates Treated with ECMO," *In ECMO Extracorporeal Cardiopulmonary Support in Critical Care*, 3rd ed. K. Van Meurs, ed..
- Goodman, M., Gringlas, M., Baumgart, S., Stanley, C., Desai, S., Turner, L., & Graziani, L. 2001. Neonatal electroencephalogram does not predict cognitive and academic achievement scores at early school age in survivors of neonatal extracorporeal membrane oxygenation. *J Child Neurol*, 16, 745-750
- Graziani, L.J., Baumgart, S., Desai, S., Stanley, C., Gringlas, M., & Spitzer, A.R. 1997a. Clinical antecedents of neurologic and audiological abnormalities in survivors of neonatal extracorporeal membrane oxygenation. *Journal of Child Neurology*, 12, (7) 415-422
- Graziani, L., Gringlas, M., & Baumgart, S. 1997b. Cerebrovascular complications and neurodevelopmental sequelae of neonatal ECMO. *Clin Perinatol*, 24, 655-675
- Graziani, L., Streletz, L., Baumgart, S., Cullen, J., & McKee, L. 1994. Predictive value of neonatal electroencephalograms before and during extracorporeal membrane oxygenation. *J Pediatr*, 125, 969-975

- Greeley, W.J., Ungerleider, R.M., Kern, F.H., Brusino, F.G., Smith, L.R., & Reves, J.G. 1989. Effects of cardiopulmonary bypass on cerebral blood flow in neonates, infants, and children. *Circulation*, 80, (3 SUPPL. I)
- Greeley, W., Bracey, V., & Ungerleider, R. 1991. Recovery of cerebral metabolism and mitochondrial oxidation state is delayed after hypothermic circulatory arrest. *Circulation*, 84, 400-406
- Hahn, J., Vaucher, Y., & Bejar, R. 1992. Electroencephalographic and neuroimaging findings in neonates undergoing extracorporeal membrane oxygenation. *Neuropediatrics*, 24, 19-24
- Hall-Craggs, E. 1995. *Anatomy as a basis for clinical medicine*, 3rd ed. Europe, Williams & Wilkins Waverly.
- Han, S., Kim, C., Bahk, J., & Park, Y. 2004. The effect of bloodless pump prime on cerebral oxygenation in paediatric patients. *Acta Anaesthesiol Scand*, 48, 648-652
- Hayashida, M., Kin, N., Tomioka, T., Orii, R., Sekiyama, H., & Usui, H. 2004. Cerebral ischemia during cardiac surgery in children detected by combining monitoring of BIS and near infrared spectroscopy. *Br J Anaesth*, 92, 662-669
- Hebden, J.C., Arridge, S.R., & Delpy, D.T. 1997. Optical Imaging in Medicine: I Experimental techniques. *Phys.Med.Biol.*, 42, 825-840
- Hillier, S., Burrows, F., Bissonnette, B., & Taylor, R. 1991. Cerebral haemodynamics in neonates and infants undergoing cardiopulmonary bypass and profound hypothermic circulatory arrest: assessment by transcranial Doppler sonography. *Anesth Analg*, 72, 723-728
- Hirsch, J., Charpie, J., Ohye, R., & Gurney, J. 2009. Near-infrared spectroscopy: What we know and what we need to know-A systematic review of congenital heart disease literature. *J Thorac Cardiovasc Surg*, 137, 154-159
- Hirsch, J., Charpie, J., Ohye, R., & Gurney, J. 2010. Near Infrared Spectroscopy (NIRS) Should Not be Standard of Care for Postoperative Management. *Semin Thorac Cardiovasc Surg Pediatr Card Surg Ann*, 13, 51-54
- Hofer, A., Haizinger, B., Geiselseder, G., Mair, R., Rehak, P., & Gombotz, A. 2005. Monitoring of selective antegrade cerebral perfusion using near infrared spectroscopy in neonatal aortic arch surgery. *Eur J Anaesthesiol*, 22, 293-298
- Hoffman, G. 2006. Neurological monitoring on cardiopulmonary bypass: what are we obligated to do? *Ann Thorac Surg*, 81, S2373-2380
- Hoffman, G., Stuth, E., Jaquiss, R., Vanderwal, P., Staudt, S., Troshynski, T., Ghanayem, N., & Tweddell, J. 2004. Changes in cerebral and somatic oxygenation during stage 1 palliation of hypoplastic left heart syndrome using continuous regional perfusion. *J Thorac Cardiovasc Surg*, 127, 223-233

- Hofkosh, D., Thompson, A., & Noza, R. 1991. Ten years of extracorporeal membrane oxygenation: neurodevelopmental outcome. *Pediatrics*, 87, 549-555
- Homae, F., Watanabe, H., Nakano, T., Asakawa, K., & Taga, G. 2006. The right hemisphere of sleeping infant perceives sentential prosody. *Neuroscience Research*, 54, 276-280
- Horan, M., Ichiba, S., Firmin, R.K., Killer, H.M., Edwards, D., Azzopardi, D., Hodge, R., Kotecha, S., & Field, D. 2004. A pilot investigation of mild hypothermia in neonates receiving extracorporeal membrane oxygenation (ECMO). *Journal of Pediatrics*, 144, 301-308
- Hudetz, A., Roman, R., & Harder, D. 1992. Spontaneous flow oscillations in the cerebral cortex during acute changes in mean arterial pressure. *J.Cereb.Blood flow Metab.*, 12, 491-499
- Hunter, C., Blood, A., Bishai, J., Hickerson, A., Wall, D., Peverini, R., Power, G., & Hopper, A. 2004. Cerebral blood flow and oxygenation during venoarterial and venobenuous extracorporeal oxygenation in the newborn lamb. *Pediatr Crit Care*, 5, 475-481
- Ingyinn, M., Evangelista, R., & Rais-Bahrami, L. 2002. Pulsatile ECMO maintains cerebral arterial endothelial function compared to non-pulsatile ECMO in newborn lambs. *Pediatr Res*, 51, 48A
- Jaggers, J. & Ungerleider, R. 2006, "Cardiopulmonary Bypass in Infants and Children," *In Critical Heart disease in Infants and Children*, D. Nichols et al., eds..
- Jobsis, F. 1977. Noninvasive, infrared monitoring of cerebral and myocardial oxygen sufficiency and circulatory parameters. *Science*, 198, 1264-1267
- Jones, T. & Elliott, M. 2004, "Perfusion Techniques," *In Surgery for congenital heart defects*.
- Karimova, A. & Goldman, A. 2006, "Paediatric Cardiac Mechanical Support," *In Surgery for Congenital Heart defects*, 3rd ed. J. Stark, M. De Leval, & V. Tsang, eds., John Wiley and Sons, Ltd, pp. 229-238.
- Karl, T., Kishbom, P., & Horton, S. 2006, "Mechanical Circulatory Support in Infants and Children," *In Critical Heart disease in Infants and Children*, 2nd ed. D. Nichols et al., eds., Philadelphia: Elsevier Mosby-Year Book Inc..
- Kaufman, J., Almodovar, M.C., Zuk, J., & Friesen, R.H. 2008. Correlation of abdominal site near-infrared spectroscopy with gastric tonometry in infants following surgery for congenital heart disease. *Pediatr Crit Care Med*, 9, (1) 62-68 available from: PM:18477915
- Kawaguchi, F., Ichikawa, N., Fujiwara, N., Yamashita, Y., & Kawasaki, S. 2001. Clinically available optical topography system. *Hitachi Review*, 50, 18-22

- Khan, A. & Lally, K. P. 2005, "Congenital diaphragmatic hernia and ECMO," *In ECMO extracorporeal cardiopulmonary support in critical care*, 3rd ed. K. Van Meurs et al., eds., pp. 297-306.
- Kilpack, V., Stayer, S., McKenzie, E., Fraser, C.J., & Andropoulos, D. 2004. Limiting circulatory arrest using regional low flow perfusion. *J Extra Corpor Technol*, 36, 133-138
- Koizumi, H., Maki, A., Yamamoto, T., Sato, H., Yamamoto, Y., & Kawaguchi, F. 2005. Non-invasive brain-function imaging by optical topography. *Trends in Analytical Chemistry*, 24, 147-156
- Koizumi, H., Yamamoto, T., Maki, A., Yamashita, Y., Sato, H., Kawaguchi, F., & Ichikawa, N. 2003. Optical topography: practical problems and new applications. *Applied Optics*, 42, 3054-3062
- Kumar, P., Gupta, R., Shankaran, S., Bedard, M., & Delaney-Black, V. 1999. EEG abnormalities in survivals of neonatal ECMO: its role as a predictor of neurodevelopmental outcome. *Am J Perinatol*, 16, 245-250
- Kuo, T., Chern, C., Sheng, W., Wong, W., & Hu, H. 1998. Frequency domain analysis of cerebral blood flow velocity and its correlation with blood pressure. *J Cereb Blood Flow Metab.*, 18, (3) 311-318
- Kurth, C., Steven, J., Montenegro, L., Watzman, H., Gaynor, J., & Spray, T. 2001. Cerebral oxygen saturation before congenital heart surgery. *Ann Thorac Surg*, 72, (187) 192
- Kurth, C., Steven, J., & Nicolson, S. 1995. Cerebral oxygenation during pediatric cardiac surgery using deep hypothermic circulatory arrest. *Anaesthesiology*, 82, 74-82
- Kurth, C., Steven, J., Nicolson, S., Chance, B., & Delivoria-Papadopoulos, M. 1992. Kinetics of cerebral deoxygenation during deep hypothermic circulatory arrest in neonates. *Anaesthesiology*, 77, 656-661
- Kurth, C., Steven, J., Nicolson, S., & Jacobs, M. 1997. Cerebral oxygenation during cardiopulmonary bypass in children. *J Thorac Cardiovasc Surg*, 113, 71-78
- Kuschinsky, W. 1996, "Regulation of cerebral blood flow: an overview," *In Neurophysiological basis of cerebral blood flow control: an introduction*, S. Mraovitch & R. Sercombe, eds..
- Kussman, B., Wypij, D., DiNardo, J., Newburger, J., Jonas, R., & Bartlett, j. 2005. An evaluation of bilateral monitoring of cerebral oxygen saturation during pediatric cardiac surgery. *Anesth Analg*, 101, 1294-1300
- Kvandal, P., Landsverk, S., Bernjak, A., Stefanovska, A., Kyernmo, H., & Kirkeboen, K. 2006. Low frequency oscillations of the Laser Doppler perfusion signal in human skin. *Microvascular Research*, 72, 120-127

- Lang, E., Mehdorn, H.M., Dorsch, N.W., & Czosnyka, M. 2002. Continuous monitoring of cerebrovascular autoregulation: a validation study. *J Neurol Neurosurg Psychiatry*, 72, 583-586
- Latka, M., Kolodziej, W., Turalska, M., Latka, D., Zub, W., & West, B.J. 2007. Wavelet assessment of cerebrospinal compensatory reserve and cerebrovascular reactivity. *Physiol Meas*, 28, 465-479
- Latka, M., Turalska, M., Latka, M.G., Kolodziej, W., Latka, D., & West, B.J. 2005. Phase dynamics in cerebral autoregulation. *Am J Heart Circ Physiol*, 289, H2272-H2279
- LeBlanc, J., Blackstock, D., Macnab, A., Gagnon, F., Gagnon, R., & Russell, J. 2000. Effects of propofol on cerebral oxygenation during cardiopulmonary bypass in children. *Can J Anaesth*, 47, 1082-1090
- Levick, J. 2003. *An introduction to cardiovascular physiology*, 4th ed. London, Arnold Publishers.
- Levy, M.N. & Pappano, A.J. 2007. *Cardiovascular Physiology*, 9th ed. Philadelphia, Mosby Inc.
- Li, J., Van Arsdell, G., Zhang, G., Cai, S., Humpl, T., & Caldarone, C. 2006. Assessment of the relationship between cerebral and splanchnic oxygen saturation measured by near infrared spectroscopy and direct measurement of systemic haemodynamic variables and oxygen transport after the Norwood procedure. *Heart*, 92, 1678-1685
- Li, J., Zhang, G., Holtby, H., Bissonnette, B., Wang, G., Redington, A., & Arsdell, G. 2008. Carbon dioxide-a complex gas in a complex circulation: Its effects on systemic circulation in neonates after the Norwood procedure. *J Thorac Cardiovasc Surg*, 136, (1207) 1214
- Liem, D., Hopman, J., Oeseburg, B., de Haan, A., Festen, C., & Kollee, L. 1995a. Cerebral oxygenation and hemodynamics during induction of extracorporeal membrane oxygenation as investigated by near infrared spectrophotometry. *Pediatrics*, 95, 555-561
- Liem, K.D., Kollee, L.A., Klaessens, J.H., Geven, W.B., Festen, C., De Haan, A.F., & Oeseburg, B. 1995b. Disturbance of cerebral oxygenation and hemodynamics related to the opening of the bypass bridge during veno-arterial extracorporeal membrane oxygenation. *Pediatr Res*, 38, (1) 124-129 available from: PM:7478790
- Liem, K.D., Kollee, L., Klaessens, J., De Haan, A.F., & Oeseburg, B. 1996. The influence of Extracorporeal Membrane Oxygenation on Cerebral Oxygenation and Hemodynamics in Normoxemic and Hypoxemic Piglets. *Pediatr Res*, 39, (2) 209-215
- Lissauer, T. & Clayden, G. 2001, "Cardiac Disorders," *In Illustrated textbook of Paediatrics*, T. Lissauer & G. Clayden, eds., pp. 285-306.

- Livera, L., Wickramasinghe, W., Spencer, S., Rofler, P., & Thernley, M. 1995. Cyclical fluctuations in cerebral blood volume. *Arch.Dis.Child*, 67, 62-63
- Lozano, S. & Mossad, E. 2004. Cerebral function monitors during pediatric surgery: can they make a difference? *J Cardiothorac Vasc Anesth*, 18, 645-656
- Marieb, E. 1998, "Blood," *In Human Anatomy and Physiology*, E. Marieb, ed., California: Benjamin/Cummings Science Publishing, pp. 626-655.
- Martini, F. 2006, "The heart," *In Fundamentals of Anatomy and Physiology*, F. Martini, ed., California: Pearson Education/Benjamin Cummings, pp. 451-494.
- Martini, F. 2009, "Blood vessels and Circulation," *In Fundamentals of Anatomy and Physiology*, F. Martini, ed., California: Pearson Education/Benjamin Cummings, pp. 708-762.
- Matcher, S., Kirkpatrick, P., Nahid, K., Cope, M., & Delpy, D. 1995. Absolute quantification methods in tissue near infrared spectroscopy. *Proceedings of SPIE*, 2389, 486-495
- Matcher, S., Nahid, K., Cope, M., & Delpy, D. 1996. Absolute SO₂ measurements in layered media. *OSA TOPS on Advantages in Optical Imaging and Photon Migration*, 3, 83-91
- McGahren, E.D., Mallik, K., & Rodgers, B.M. 1997. Neurological outcome is diminished in survivors of congenital diaphragmatic hernia requiring extracorporeal membrane oxygenation. *J Pediatr Surg*, 32, 1216-1220
- McQuillen, P., Barkovich, A., Hamrick, S., Perez, M., Ward, P., & Glidden, V. 2007a. Temporal and anatomic risk profile of brain injury with neonatal repair of congenital heart defects. *Stroke*, 38, 736-741
- McQuillen, P., Nishimoto, M., Bottrell, C., Fineman, L., Hamrick, S., Glidden, D., Azakie, A., & Adatia, I. 2007b. Regional and central venous saturation monitoring following pediatric cardiac surgery: Concordance and association with clinical variables. *Pediatr Crit Care Med*, 8, (154) 160
- Mendoza, J., Shearer, L., & Cood, L. 1991. Lateralisation of brain lesions following extracorporeal membrane oxygenation. *Pediatrics*, 88, 1004-1009
- Minagawa-Kawai, Y., Mori, K., Naoi, N., & Kojima, S. 2007. Neural attunement processes in infants during the acquisition of a language specific phonemic contrast. *J Neurosci*, 27, 315-321
- Mitsis, G.D., Poulin, M.J., Robbins, P.A., & Marmarelis, V.Z. 2004. Non linear modelling of the dynamic effects of arterial pressure and CO₂ variations on cerebral blood flow in healthy humans. *IEEE Trans Biomed Eng*, 51, 1932-1943
- Mitsis, G.D., Zhang, R., Levine, B.D., & Marmarelis, V.Z. 2006. Cerebral hemodynamics during orthostatic stress assessed by nonlinear modeling. *J Appl Physiol*, 101, 354-366

- Morimoto, Y., Niida, Y., Hisano, K., Hua, Y., Kemmotsu, O., & Murashita, T. 2003. Changes in cerebral oxygenation in children undergoing surgical repair of ventricular septal defects. *Anaesthesia*, 58, 77-83
- Morren, G., Lemmerling, P., Van Huffel, S., Naulaers, G., Devlieger, H., & Casaer, P. 2001. Detection of autoregulation in the brain of premature infants using a novel sub-space based technique. *EMBS, Proc.of the 23rd Annual Intern.Conf.of the IEEE* (2) 2064-2067
- Mott, A., Alomrani, A., Tortoriello, T., Perles, Z., East, D., & Stayer, S. 2006. Changes in cerebral saturation profile in response to mechanical ventilation alterations in infants with bidirectional superior cavopulmonary connection. *Pediatr Crit Care Med*, 7, 346-350
- Murayama, H., Tamaki, S., Usui, A., & Ueda, Y. 2006. Measurement of cerebral oxygenation status when commencing cardiopulmonary bypass in paediatric open-heart surgery. *Ann Thorac Cardiovasc Surg*, 12, 105-112
- Murphy, P.J. 2005. The fetal circulation. *Contin Educ Anaesth Crit Care Pain*, 5, 107-112
- Nagdyman, N., Fleck, T., Barth, S., Abdul-Khaliq, H., Stiller, B., Ewert, P., Huebler, M., Kuppe, H., & Lange, P. 2004. Relation of cerebral tissue oxygenation index to central venous oxygen saturation in children. *Intensive Care Med*, 30, 468-471
- Nagdyman, N., Fleck, T., Bitterling, B., Ewert, P., Abdul-Khaliq, H., & Stiller, B. 2006. Influence of intravenous sildenafil on cerebral oxygenation measured by near infrared spectroscopy in infants after cardiac surgery. *Pediatr Res*, 59, 462-465
- Nagdyman, N., Ewert, P., Peters, B., Miera, O., Fleck, T., & Berger, F. 2008. Comparison of different near-infrared spectroscopic cerebral oxygenation indices with central venous and jugular venous oxygenation saturation in children. *Paediatr.Anaesth*, 18, (2) 160-166 available from: PM:18184248
- Nellhaus, G. 1968. Head circumference from birth to eighteen years: Practical composite international and interracial graphs. *Pediatrics*, 41, 106-114
- Nollert, G., Shin'oka, T., & Jonas, R.A. 1998. Near Infrared Spectrophotometry of the brain in cardiovascular surgery. *Thorac Cardiovasc Surg*, 46, 167-175
- O'Brien, J., Butterworth, J., & Hammon, J.e.a. 1997. Cerebral emboli during cardiac surgery in children. *Anesthesiology*, 87, 1063-1069
- Obrig, H., Neufang, M., Wenzel, R., Kohl, M., Steinbrink, J., Einhaupl, K., & Villringer, A. 2000. Spontaneous Low Frequency Oscillations of Cerebral Hemodynamics and Metabolism in Human Adults. *Neuroimage*, 12, 623-639
- Oda, I., Wada, Y., Takeuchi, S., Konishi, I., & Tzunazawa, Y. 2003. Near Infrared Imager with a flexible source detector arrangement and a new detection gain control. *Optical Review*, 10, 422-426

- Otsuka, Y., Nakato, E., Kanazawa, S., Yamaguchi, M.K., Watanabe, S., & Kakigie, R. 2007. Neural activation to upright and inverted faces in infants measured by near infrared spectroscopy. *Neuroimage*, 34, 399-406
- Panerai, R.B. 1998. Assessment of cerebral pressure autoregulation in humans - a review of measurement methods. *Physiol Meas*, 19, 305-338
- Panerai, R.B., Dawson, S.L., & Potter, J.F. 1999. Linear and nonlinear analysis of human dynamic cerebral autoregulation. *Am J Physiol*, 277, H1089-1099
- Panerai, R.B., Moody, M., Eames, P.J., & Potter, J.F. 2005. Cerebral blood flow velocity during mental activation: interpretation with different models of the passive pressure-velocity relationship. *J Appl Physiol*, 99, 2352-2362
- Papademetriou, M.D., Tachtsidis, I., Leung, T.S., Elliott, M.J., Hoskote, A., & Elwell, C.E. 2010. Cerebral and Peripheral tissue oxygenation in infants and children supported on ECMO for cardio-respiratory failure. *Adv Exp Med Biol*, 662, 447-453
- Papademetriou, M.D., Tachtsidis, I., Banaji, M., Elliott, M.J., Hoskote, A., & Elwell, C.E. 2011. Regional cerebral oxygenation measured by multichannel near infrared spectroscopy (optical topography) in an infant supported on veno-arterial Extracorporeal Membrane Oxygenation. *J Thorac Cardiovasc Surg*, 141, e31-33
- Parati, G., Saul, J., Di Rienzo, M., & Mancia, G. 1995. Spectral analysis of blood pressure and heart rate variability in evaluating cerebrovascular regulation: a critical appraisal. *Hypertension*, 25, 1276-1286
- Patterson, M., Chance, D., & Wilson, B. 1989. Time resolved reflectance and transmittance for the non-invasive measurement of tissue optical properties. *Applied Optics*, 28, 2331-2336
- Peng, T. 2008. *Signal Processing methods for the analysis of cerebral blood flow and metabolism*. PhD University of Oxford.
- Phelps, H., Mahle, W., Kim, D., Simsic, J., Kirhbom, P., Kanter, K., & Maher, K. 2009. Postoperative cerebral oxygenation in hypoplastic left heart syndrome after the Norwood procedure. *Ann Thorac Surg*, 87, 1490-1494
- Pigula, F., Gandhi, S., Siewers, R., Davis, P., Weber, S., & Nemoto, E. 2001. Regional low flow perfusion provides somatic circulatory support during neonatal aortic arch surgery. *Ann Thorac Surg*, 72, 401-406
- Pigula, F., Nemoto, E., Griffith, B., & Siewers, R. 2000. Regional low-flow perfusion provides cerebral circulatory support during neonatal aortic arch reconstruction. *J Thorac Cardiovasc Surg*, 119, 331-339
- Purves, M. 1972. *The physiology of the cerebral circulation* Cambridge, Cambridge university press.

- Rais-Bahrami, K., Rivera, O., & Short, B. 2006. Validation of a non-invasive neonatal optical cerebral oximeter in a veno-venous ECMO patient with a cephalad catheter. *J Perinatol*, 26, (628) 635
- Ramaekers, V.T., Caaer, P., Daniels, H., & Marchal, G. 1990. Upper limits of brain blood flow autoregulation in stable infants of various conceptional age. *Early human development*, 24, 249-258
- Ramamoorthy, C., Tabbutt, S., Kurth, C., Steven, J., Montenegro, L., & Durning, S. 2002. Effects of inspired hypoxic and hypercapnic gas mixtures on cerebral oxygen saturation in neonates with univentricular heart defects. *Anaesthesiology*, 96, 283-288
- Redlin, M., Koster, A., Huebler, M., Boettcher, W., Nagdyman, N., Hetzer, R., Kuppe, H., & Kuebler, W.M. 2008. Regional differences in tissue oxygenation during cardiopulmonary bypass for correction of congenital heart disease in neonates and small infants: relevance of near-infrared spectroscopy. *J Thorac Cardiovasc Surg*, 136, (4) 962-967 available from: PM:18954637
- Roberts, I., Fallon, P., Kirkham, F., Cooper, C., & Elliott, M. 1998. Measurement of cerebral blood flow during cardiopulmonary bypass with near infrared spectroscopy. *J Thorac Cardiovasc Surg*, 115, 94-102
- Roche-Labarbe, N., Wallois, F., Ponchel, E., Kongolo, G., & Grebe, R. 2007. Coupled oxygenation oscillation measured by NIRS and intermittent cerebral activation on EEG in premature infants. *Neuroimage*, 36, 718-727
- Rodriguez, R., Cornel, G., Semelhago, L., & el al 2000. Cerebral vascular effects of aortovenous cannulations for pediatric cardiopulmonary bypass. *Ann Thorac Surg*, 69, 1229-1235
- Rosenblum, M., Pikovsky, A., Kurths, J., Schafer, C., & Tass, P. A. 2001, "Phase synchronisation from theory to data analysis," *In Handbook of biological physics*, F. Moss & S. Gielen, eds., Elsevier Science.
- Rowley, A.B., Payne, S.J., Tachtsidis, I., Ebdon, M.J., Whiteley, J.P., Gavaghan, D.J., Smith, M., Elwell, C.E., & Delpy, D.T. 2007. Synchronisation between arterial blood pressure and cerebral concentration investigated by wavelet cross-correlation. *Physiol Meas*, 28, 161-173
- Sakamoto, T., Kurosawa, H., Shin'oka, T., Aoki, M., & Isomatsu, Y. 2004. The influence of pH strategy on cerebral and collateral circulation during hypothermic cardiopulmonary bypass in cyanotic patients with heart disease: Results on a randomised trial and real-time monitoring. *J Thorac Cardiovasc Surg*, 127, 12-19
- Schmidt, F. 1999. *Development of a time-resolved optical tomography system for neonatal brain imaging*. PhD (PhD Thesis). University College London.
- Semmlow, J. L. 2004, "Wavelet Analysis," *In Biosignal and biomedical Image processing. MATLAB based applications*, J. L. Semmlow, ed., New York: Marcal Dekker Inc..

- Shaaban, A., Harmer, M., Elliott, M., Thomas, A., & Kirkham, F. 2004. A pilot study of evaluation of cerebral function by S100beta protein and near infrared spectroscopy during cold and warm cardiopulmonary bypass in infants and children undergoing open-heart surgery. *Anaesthesia*, 59, 20-26
- Short, B.L., Bender, K., Walker, L.K., & Traystman, R.J. 1994a. The cerebrovascular response to prolonged hypoxia with carotid artery and jugular vein ligation in the newborn lamb. *Journal of Pediatric Surgery*, 29, 887-891
- Short, B.L., Walker, L.K., & Traystman, R.J. 1994b. Impaired cerebral autoregulation in the newborn lamb during recovery from severe, prolonged hypoxia, combined with carotid artery and jugular vein ligation. *Critical Care Medicine*, 22, 1262-1268
- Short, B., Walker, L., Bender, K., & Traystman, R. 1993. Impairment of cerebral autoregulation during extracorporeal membrane oxygenation in newborn lambs. *Pediatric Research*, 33, (3) 289-294
- Skov, L. & Greisen, G. 1994. Apparent cerebral cytochrome aa3 reduction during cardiopulmonary bypass in hypoxaemic children with congenital heart disease. *Physiol Meas*, 15, 447-457
- Smith, J. J. & Kampine, J. P. 1990a, "Circulation to special regions," *In Circulatory Physiology: The essentials*, 3rd ed. J. Smith & J. Kampine, eds., William and Wilkins, pp. 181-222.
- Smith, J. J. & Kampine, J. P. 1990b, "Pressure and flow in the arterial and venous systems," *In Circulatory Physiology: The essentials*, 3rd ed. J. Smith & J. Kampine, eds., William and Wilkins, pp. 140-159.
- Soul, J.S., Hammer, P.E., Tsuji, M., Soul, J.P., Bassan, H., Limperopoulos, C., Disalvo, D.N., Moore, M., Akins, P., Ringer, S., Volpe, J.J., Trachtenberg, F., & du Plessis, A. 2007. Fluctuating pressure passivity os common in the cerebral circulation of sick premature infants. *Pediatr Res*, 61, 467-473
- Srinivasan, C., Sachdeva, R., Morrow, W.R., Gossett, J., Chipman, C.W., Imamura, M., & Jaquiss, R.D. 2009. Standardized management improves outcomes after the Norwood procedure. *Congenit.Heart Dis*, 4, (5) 329-337 available from: PM:19740187
- Stebor, A. & Short, M. 2005. Basic principles of non-invasive BP measurement in infants: Understanding BP values. *Advances in Neonatal Care*, 5, 252-261
- Steiner, L.A. & Andrews, P.J.D. 2006. Monitoring the injured brain: ICP and CBF. *Br J Anaesth*, 97, 26-38
- Stolar, C.J. 1996. What do survivors of congenital diaphragmatic hernia look like when they grow up? *Semin Pediatr Surg*, 5, 275-279
- Stump, D., Jones, T., & Rorie, K. 1999. Neurophysiologic monitoring and outcomes in cardiovascular surgery. *J Cardiothorac Vasc Anesth*, 13, (5) 600-613

- Su, X.W. & Undar, A. 2010. Brain Protection during Pediatric Cardiopulmonary bypass. *Artif Organs*, 34, E91-E102
- Suzuki, S., Takasaki, S., Ozaki, T., & Kabayashi, Y. 1999. A tissue Oxygenation monitoring using NIR spatially resolved spectroscopy. *Proceedings of SPIE*, 3597, 582-592
- Tachtsidis, I. 2005. *Experimental measurements of cerebral haemodynamics and oxygenation and comparisons with a computational model: a near infrared spectroscopy investigation*. PhD (PhD Thesis). University College London.
- Tachtsidis, I., Elwell, C.E., Leung, T.S., Lee, C.W., Smith, M., & Delpy, D.T. 2004. Investigation of cerebral haemodynamics by near infrared spectroscopy in young healthy volunteers reveals posture-dependent spontaneous oscillations. *Physiol Meas*, 25, 437-445
- Tachtsidis, I., Tisdall, M., Delpy, D., & Elwell, C. 2008. Measurement of cerebral tissue oxygen oxygenation in young healthy volunteers during acetazolamide provocation: a transcranial Doppler and near-infrared spectrascopy investigation. *Adv Exp Med Biol*, 614, 389-396
- Tachtsidis, I., Tisdall, M., Leung, T., Cooper, C., Smith, M., & Elwell, C. 2007. Investigation of in-vivo measurement of cerebral cytochrome-c-oxidase redox changes using near-infrared spectroscopy in patients with orthostatic hypotension. *Physiological Measurements*, 28, 199-211
- Taga, G., Homae, F., & Watanabe, H. 2007. Effects of source-detector distance of near infrared spectroscopy on the measurement of the cortical haemodynamic response in infants. *Neuroimage*, 38, 452-460
- Taga, G., Konishi, Y., Maki, A., Tachibana, T., Fujiwara, M., & Koizumi, H. 2000. Spontaneous oscillation of oxy- and deoxy- hemoglobin changes with a phase difference through the occipital cortex of newborn infants observed using non-invasive optical topography. *Neuroscience Letters*, 282, 101-104
- Takami, T., Yamamura, H., Inai, K., Nishikawa, Y., Takei, Y., & Hoshika, A. 2005. Monitoring of cerebral oxygenation during hypoxic gas management in congenital heart disease with increased pulmonary blood flow. *Pediatr Res*, 58, 521-524
- Tasker, R. C. 2006, "Cerebral function and heart disease," *In Critical heart disease for infants and children*, D. Nichols et al., eds..
- Taylor, R.H., Burrows, F.A., & Bissonnette, B. 1992. Cerebral pressure-flow velocity relationship during hypothermic cardiopulmonary bypass in neonates and infants. *Anesthesia and Analgesia*, 74, 636-642
- Thibodeau, G. & Patton, K. 2007a, "Anatomy of the Cardiovascular System," *In Anatomy and Physiology*, G. Thibodeau & K. Patton, eds., Philadelphia: Elsevier Health Sciences, pp. 677-731.

- Thibodeau, G. & Patton, K. 2007b, "Physiology of the cardiovascular system," *In Anatomy and Physiology*, G. Thibodeau & K. Patton, eds., Philadelphia: Elsevier Health Sciences, pp. 471-514.
- Tobias, J., Russo, P., & Russo, J. 2009. Changes in near infrared spectroscopy during deep hypothermic circulatory arrest. *Annals of Cardiac Anaesthesia*, 12, 17-21
- Toet, M., Flinterman, A., Laar, I., Vries, J., Bennink, G., Uiterwaal, C., & Bel, F. 2005. Cerebral oxygen saturation and electrical brain activity before, during, and up to 36 hours after arterial switch procedure in neonates without pre-existing brain damage: its relationship to neurodevelopmental outcome. *Exp Brain Res*, 165, 343-350
- Torrence, C. & Compo, G.P. 1998. A Practical guide to wavelet analysis. *Bulletin of the American Meteorological society* 61-78
- Tortoriello, T., Stayer, S., Mott, A., McKenzie, E., Fraser, C.J., & Andropoulos, D. 2005. A non invasive estimation of mixed venous oxygen saturation using near infrared spectroscopy by cerebral oximetry in pediatric cardiac surgery patients. *Pediatr Anaesth*, 15, 495-503
- Trittenwein, G., Plenk, S., Mach, E., Mostafa, G., Boigner, H., Burda, G., Hermon, M., Golej, J., & Pollak, A. 2006. Quantitative electroencephalography values of neonates during and after venoarterial extracorporeal membrane oxygenation and permanent ligation of right common carotid artery. *Artif Organs*, 30, 447-451
- Tsuji, M. & du Plessis, A. 1998. Near infrared spectroscopy detects cerebral ischemia during hypotension in piglets. *Pediatric Research*, 44, 591-595
- Tsuji, M., Saul, J.P., du Plessis, A., Eichenwald, E., Sobh, J., Crocker, R., & Volpe, J.J. 2000. Cerebral intravascular oxygenation correlates with mean arterial pressure in critically ill premature infants. *Pediatrics*, 106, 625-632
- Tyree, K., Tyree, M., & Digeronimo, R. 2009. Correlation of brain tissue oxygen tension with cerebral near infrared spectroscopy and mixed venous oxygen saturation during extracorporeal membrane oxygenation. *Perfusion* available from: PM:19948748
- Tyszczyk, L., Meek, J., Elwell, C., & Wyatt, J. 1998. Cerebral blood flow is independent of mean arterial pressure in preterm infants undergoing intensive care. *Pediatrics*, 102, 337-341
- Van Beek, A., Claassen, J., Rikkert, M., & Jansen, R. 2008. Cerebral autoregulation: an overview of current concepts and methodology with special focus on the elderly. *J Cerebr Blood Flow & Metab* 1-15
- Van Bel, F., Zeeuwe, W., Dorrepaal, C., Benders, M., Van de Bor, M., & Hardjowijono, R. 1996. Changes in cerebral haemodynamics and oxygenation during hypothermic cardiopulmonary bypass in infants and children. *Biol Neonate*, 70, 141-154

- Van der Zee, P. 1992. *Measurement and modelling of the optical properties of tissue in the near-infrared*. PhD University College London.
- Van Heijst, A., Liem, D., Hopman, J., van der Staak, F., & Senders, R. 2004. Oxygenation and hemodynamics in left and right cerebral hemispheres during induction of veno-arterial extracorporeal membrane oxygenation. *J Pediatr*, 144, 223-228
- Van Heijst, A., Liem, D., van der Staak, F., Klaessens, J., Festen, C., Haan, T., Geven, W., & van der Bor, M. 2001. Hemodynamic changes during opening of the bridge in venoarterial extracorporeal membrane oxygenation. *Pediatr Crit Care Med*, 2, 265-270
- Van Meurs, K., Lally, K.P., Peek, G., & Zwischenberger, J.B. 2005a. *ECMO extracorporeal cardiopulmonary support in critical care*, 3rd ed. Extracorporeal Life Support Organisation, Ann Arbor, Michigan.
- Van Meurs, K. P., Hintz, S. R., & Sheehan, A. M. 2005b, "ECMO for neonatal respiratory failure," *In ECMO Extracorporeal Cardiopulmonary support in critical care*, 3rd ed. K. P. Van Meurs et al., eds., pp. 273-295.
- Versmold, H.T., Kitterman, J.A., Phibbs, R.H., Gregory, G.A., & Tooley, W.H. 1981. Aortic blood pressure during the first hours of life in infants with birth weight 610 to 4,220 grams. *Pediatrics*, 67, 607-613
- Von Allmen, D. & Ryckman, F.C. 1991. Cardiac arrest in the ECMO candidate. *Journal of Pediatric Surgery*, 26, 143-146
- Walker, L., Short, B., & Traystman, R. 1996. Impairment of cerebral autoregulation during venovenous extracorporeal membrane oxygenation in the newborn lamb. *Critical Care Medicine*, 24, (12) 2001-2006
- Walters, F.J.M. 1998. Intracranial pressure and cerebral blood flow. *Physiology*, 4, (8) 1-4
- Wardle, S., Yoxall, C., & Weindling, A. 1998. Cerebral oxygenation during cardiopulmonary bypass. *Arch Dis Child*, 78, 26-32
- Weber, T.R., Kountzman, B., Coran, A.G., & Bagwell, C.E. 1996. The effects of venous occlusion on cerebral blood flow characteristics during ECMO. *Journal of Pediatric Surgery*, 31, 1124-1127
- Welch, P. 1967. The use of Fast Fourier Transform for the Estimation of Power Spectra: A Method Based on Time Averaging of Short Modified Periodograms. *IEEE Trans.Audio and Electroacoustics*, AU-15, (2) 70-73
- Whitcher, B., Cragmille, P.F., & Brown, P. 2005. Time varying spectral analysis in neurophysiological time series using hilbert wavelet pairs. *Signal Process*, 85, 2065-2081

- Williams, G. & Ramamoorthy, C. 2007. Brain Monitoring and Protection During Pediatric Cardiac Surgery. *Semin Cardiothorac Anesth*, 11, 23-33
- Wolf, M., Ferrari, M., & Quaresima, V. 2007. Progress of near infrared spectroscopy and topography for brain and muscle applications. *Journal of Biomedical Optics*, 12, 062104
- Wong, F.Y., Leung, T.S., Austin, T., Wilkinson, M., Meek, J.H., Wyatt, J.S., & Walker, A.M. 2008. Impaired autoregulation in preterm infants identified by using spatially resolved spectroscopy. *Pediatrics*, 121, e604-611
- Woodard, H. & White, H. 1986. The composition of body tissues. *British Journal of Radiology*, 59, 1209-1219
- Wyatt, J.S., Cope, M., Delpy, D.T., Richardson, C.E., Edwards, A.D., Wray, S., & Reynolds, E.O.R. 1990. Quantitation of cerebral blood volume in human infants by near infrared spectroscopy. *Appl Physiol*, 68, 1086-1091
- Wypij, D., Newburg, J., & Rappaport, L. 2003. The effect of deep hypothermic circulatory arrest in infant heart surgery neurodevelopment: The Boston circulatory arrest trial. *J Cardiovasc Surg*, 126, 1397-1403
- Yamashita, Y., Maki, A., & Koizumi, H. 1999. Measurement system for noninvasive dynamic optical topography. *Journal of Biomedical Optics*, 4, 414-417
- Zhang, R., Zuckerman, J., Giller, C., & Levine, B. 1998. Transfer function analysis of cerebral autoregulation in humans. *Am.J.Physiol.*, 274, H233-H241
- Zwischenberger, J. & Barlett, R. 2005, "Extracorporeal Life support: overview," *In Extracorporeal Cardiopulmonary support in Critical Care*, K. Van Meurs et al., eds., pp. 1-4.